A study on inverse problems of realistic heat transfer systems

Submitted in partial fulfillment of the requirements

of the degree of

Doctor of Philosophy

by

Meenal Singhal

(Roll No. 901711004)

Supervisors

Dr. Kavita

Dr. Rohit Kumar Singla

THAPAR INSTITUTE
OF ENGINEERING & TECHNOLOGY
(Deemed to be University)

School of Mathematics
Thapar Institute of Engineering and Technology,
Patiala-147004, INDIA

(February 11, 2021)

Certificate

I hereby certify that the work, which is being presented in the thesis, entitled, **"A study on inverse problems of realistic heat transfer systems"**, in partial fulfillment of the requirements for the award of the degree of **Doctor of Philosophy** and submitted to the institution is an authentic record of my own work carried out during the period **July 27, 2017 to February 11, 2021** under the supervision of **Dr. Kavita**, Assistant Professor, School of Mathematics and **Dr. Rohit Kumar Singla**, Assistant Professor, Mechanical Engineering Department, Thapar Institute of Engineering and Technology, Patiala.

Date: 03/09/2021

Meenal.

(Meenal Singhal)
Candidate

It is certified that the above statement made by the candidate is correct to the best of my knowledge.

Date: 03/09/2021

Kavita

Dr. Kavita
Supervisor

Date: 03/09/2021

Dr. Rohit Kumar Singla
Supervisor

Dedicated to

Almighty

and my family

Acknowledgments

Completion of a journey cannot be marked without thanking and paying gratitude to the persons involved. During my research journey, it felt the events were predefined in an unusual sense, so firstly, I would like to thank the Marvelous Creator for giving me knowledge and wisdom to work with efficient people and in a professional environment. I am thankful for the invisible hand of God and the blessings.

"*The best teachers know how to bring out the best from their students.*" I extend profound gratitude and sincere thanks to my supervisors, *Dr. Kavita*, Assistant Professor, School of Mathematics and *Dr. Rohit Kumar Singla*, Assistant Professor, Mechanical Engineering Department, TIET, Patiala, for their immense encouragement and valuable guidance. The knowledge and the freedom given to me in carrying out research is beyond words. I feel extremely lucky to have the best mentors. I am highly thankful to Dr. Rohit Singla, as he is always approachable and helpful. His observations towards research and continuous efforts always inspired me to work hard. The constant support and motivation received from both of them is remarkable. I feel grateful to be a part of their research team. Dr. Kavita had been the role model for me, since the very first day. Not only her research, but her teaching style has motivated me. Her vision towards research, and quality education, not only elevated my professional growth, but also enhanced my personality in general. I am extremly thankful to you both.

"*Plans fail for lack of counsel, but with many advisers they succeed*". I am thankful to TIET, Patiala authorities for providing me the necessary facilities for the smooth completion of my Ph.D. I would like to give special thanks to my dissertation committee members: Dr. Sapna Sharma, Dr. A. K. Lal and Dr. Neeraj Grover for their insightful comments, enthusiasm and encouragement, but also for the meaningful questions which motivated me to widen my research from various perspectives. A special thanks to Dr. Satish Kumar Sharma, Head of the Department, Dr. A. K. Lal, former Head of the Department for their support and for providing all the necessary facilities in the department. Their support and sincere attitude towards department have always been encouraging and helped me pave my way for the dissertation. I express my gratitude to all the faculty members and staff of the School of Mathematics, TIET Patiala, for their support.

I am thankful to Dr. Deepak Jain, Assistant Professor, TIET, Patiala, for his valuable suggestions and inputs. It gives me great pleasure in acknowledging the help from Dr. Prashant Singh Rana, Assistant Professor, TIET, Patiala. He has been a great source of knowledge and inspiration. Thank you for always being so helpful. Discussions with Dr. Anuj Kumar, Assistant Professor, TIET, were enlighting and motivating. I appreciate the support of Ms. Gurwinder Kaur, Assistant Professor, Khalsa College Patiala, who during my post graduation instilled the

research seed. I would also like to thank the anonymous reviewers and editors of our papers for their useful and enriching suggestions.

"*Best research is produced when researchers and communities work together.*" I feel grateful to be a part of a wonderful research team. I would like to thank Dr. Rohit Kumar Singla for this. I am also thankful to Mr. Sarvjeet Singh, for stimulating discussions, believing and exploring the research subject together. I would like to thank Dr. Deepika Sharma, for providing an excellent research path to follow. I am also thankful to my friends Navjot Kaur, Manpreet Kaur, Nikita Madaan, Gagandeep Kaur, Madhu Aneja, Jagbir Kaur and Shahid. Discussions with Dr. Pali Rosha were the most fruitful of all. I am grateful to the lab members, Dr. Ramanpreet Kaur and Dr. Abdullah Al-Qudaimi for valuable discussions. I would also like to thank Avirup Baral for showing me the righteous way. I also acknowledge all the lab members at TIET, who were available instantaneously for any help. During the journey of Ph.D., I learnt various things from persons I met, but I cannot mention each one here, so please accept my humble thanks.

"*Family is the most important in a person's life.*" I am thankful for the blessings of my elders particularly, my grandparents. I would like to express the heartiest gratitude to my parents for loving, caring and what not. Without their constant will, efforts and endless love, I would not be anywhere near today. I thank my mother, *Mrs. Vineeta* for having unconditional faith in me and my father, *Mr. Amit Kumar* for being the ultimate guide. I would like to express appreciation and thanks to my dearest sister, *Malika Singhal*, for finding joy and companionship in every aspect of life. The constant support, encouragement and love received from my brothers *Mahesh Garg* and *Naman Garg*, is enormous and I am thankful to both of them.

Meenal Singhal

Abstract

This thesis aims to contribute towards the optimization of energy requirements. This is achieved by finding the solution of inverse problems in the heat transfer setting. To enhance the performance efficiency of a thermal system, the controlling parameters should be tuned. This is realized for composite walls, where performance is marked through efficiency. Besides, to have deeper information about a practical system, various important thermal parameters are to be estimated. This is procured by performing real-time experiments on fins, where the time-dependent heat flux is retrieved. Marking the presence of tumor through inverse detection of blood perfusion rate demonstrates the versatility of the process. Apart from the retrieval of parameters, the current work focuses on the different techniques for inversion.

With the presence of a large number of inversion algorithms for Inverse heat transfer problems (IHTPs) and non-IHTPs, a need for review to have a holistic view is seen. To accomplish the task, an exhaustive literature review, based on regularization techniques and methods to find the solution of inverse problems is performed. With the motivation of selection of the inversion technique best fit for a given problem, the comparison was made for a general inverse problem. Having the exact solution is necessary, to compare the numerical solutions, of a non-linear problem. In this purview, the Adomian decomposition method is established for non-linear heat transfer in double-layered walls. The closed-form of temperature is obtained, with a maximum efficiency of 98.32% for the specific thermal parameters. The contribution of this analysis is seen through its application in an industrial furnace.

In the subsequent analysis, the non-suitability of gradient-based algorithms is identified. For the IHTPs, complexity increases due to the presence of several temperature-dependent properties, thus evolutionary algorithms were recognized suitable for the solution of IHTPs. Unlike the steady-state analysis of composite walls, the transient-state retrieval of the functional form of heat flux in pin fin is obtained. An experimental setup with thermocouples of the fin is selected, and experiments are performed to obtain the temperature profile of the fin. A mathematical model with temperature-dependent thermal parameters is solved using Matlab's pdepe toolbox. GSSM is implemented for retrieval of time-dependent single parameter. To contribute towards the performance of the fin, the effect of measurement errors on the retrieval is depicted. The acceptable measurement errors in temperature are reported as 3%, 2%, and 2% with a maximum error of 6.8%, 9.6%, and 14% respectively for the constant, triangular and realistic case study. Moreover, for the measurement errors due to uncertainty of thermocouples, the temperature profile at $V = 80$V, 60V, 70V and $I = 0.027\text{A}, 0.018\text{A}, 0.022\text{A}$ is known to have 5%, 6% and 2% reconstruction error. The proposed procedure illustrating an error bound is useful to determine the auto-cut for various devices for their efficient working.

After the successful retrieval of a single parameter, multiple critical parameters of the fin are obtained based on sensitivity analysis. For this inverse estimation, an algorithm capable to handle every kind of non-linearity is sought in literature, whose absence laid the foundation of the next objective. The main research question, "Is there a technique that works globally for every inverse problem?", is asked prior to, "What if the available techniques were not utilized to an extent that they should?" is posed. In lieu of this gap, a general comparative framework is developed, such that an efficient technique is selected, based on the total minimum error. To mitigate the associated ill-posedness, regularization by modification in the objective function is proposed. A suitable objective function out of least squares, Tikhonov/Ridge regularization, lasso estimators and elastic net techniques is selected by comparing the total relative error and the CPU time. Elastic net regularization ($\lambda = 0.9$) is selected with an error of 0.39 and CPU time of 34s for fin. The regularization parameter $\alpha = 10^{-4}$ is selected based on the minimum total relative error (3.87). TOPSIS analysis is implemented to compare among evolution-based (DE), swarm-based (PSO, WOA), nature-based (WCA, BOA), physics-based (ASO) and hybrid (GWOCS) optimization algorithms for parameter estimation. Inculcating the pdepe-based temperature profile, the best algorithm, along with their performance parameter is obtained in the order BOA (0.77), WOA (0.75) and WCA (0.74), respectively. However, WOA (0.78) works best when experimental temperature profile was utilized, suggesting the robustness of WOA, with elastic net regularization ($\lambda = 0.9$, $\alpha = 10^{-4}$) for fins. This developed framework could easily be implemented in any other inverse problem for parameter estimation. The proposed procedure designed for comparison enriches the effectiveness in the working of existing inversion methods.

To test the applicability of the proposed framework, an inverse bio-medical problem to detect tumor in the human brain is studied. The best inversion algorithm, WOA, obtained previously, together with a hybrid GWOCS are utilized. Pennes model is used for the formulation of heat transfer within the human brain. Using inverse analysis, the unknown blood perfusion rate ω_i is retrieved in the regularized environment. The current research reported that at positions where tumor cells are present, the temperature rises. Moreover, with an increase in time, temperature of the cancer cells increases, whereas no change in the temperature of tissue without tumor is seen. This observation marks the presence of tumor. Elastic net regularization ($\lambda = 0.1$, $\alpha = 10^{-2}$) for WOA and ($\lambda = 0.9$, $\alpha = 10^{-4}$) for GWOCS shows the least RE. After regularization, the perfusion rate is retrieved. A clear distinction of two tumors from the brain tissue is observed. The obtained perfusion rate is used to reconstruct temperature profile. An excellent matching of reconstructed temperature field and the exact field is obtained, even when the forward data contain measurement errors. The obtained set of perfusion rate is appropriate for tumor detection, up to 7% error in the measured data. Thus, the proposed comparative procedure is found suitable for the bio-heat transfer problem. In future, real-time experimental temperature data could be utilized for the detction of tumor through thermal images.

Table of Contents

Nomenclature

A	surface area of the fin, [m^2]
a, l, p, r	random numbers
$a_1,\ a_2,\ a_3$	vectors
A_{cs}	cross sectional area of the fin, [m^2]
$b,\ b_1,\ c_1$	vectors
b^T	transpose of vector b
Bi	Biot number
C	Crossover probability
c	sensor modality in BOA
c_p	specific heat [J (kg. K)$^{-1}$]
c_λ	linear functionals
c_{w1}, c_{w2}	confidence weight vectors
CR	crossover rate in DE
d	diameter of the fin, [m]
DS	Data smoothing operator
e	error

F	scaling factor in DE
f	input model parameter
F_i	interaction force in ASO
F_α	filter function
g	slope of thermal conductivity-temperature curve [K^{-1}]
G_i	constraint force in ASO
h	heat transfer coefficient [$Wm^{-2}K^{-1}$]
h_b	initial heat transfer convection coefficient [$Wm^{-2}K^{-1}$]
H_1, H_2	Hilbert spaces
I	stimulus intensity in BOA
J	objective function
j	iteration count for which restarting is required
$J_\delta \tilde{m}$	Mollified noisy data function
k	thermal conductivity [$Wm^{-1}K^{-1}$]
$K^\dagger$	pseudo inverse of K
k_1, k_2, k_3	coefficients of thermal conductivity
k_a	thermal conductivity at ambient temperature
L	Total length [m]
M	Mutation probability
m	output parameter
n	exponent for variable heat transfer coefficient
N_c	dimensionless convection-conduction parameter
N_g	Gaussian distribution
N_r	dimensionless radiation-conduction parameter
N_{br}	radiation parameter at boundary

N_{pop}	Number of raindrops in WCA
N_{sr}	Numbers of rivers and sea
o	direction of descent
P	perimeter of the fin, [m]
Q	heat generation [W/m^3]
q	Heat flux [W/m^2]
R	positive definite matrix
r	radius of the fin, [m]
r_1, r_2	random numbers
R_α	regularization operators
ra, rb	random numbers between 0 and 1
s	regularization order
$S(f)$	constriants
S_i^+, S_i^-	separation measures in TOPSIS
T	Temperature [K]
t	time coordinate [s]
$T(f)$	estimated values of temperature
T_a	ambient/arterial temperature, [K]
T_b	base temperature, [K]
T_e	Total relative error
T_∞	ambient temperature [K]
u	temperature profile
u_t	partial derivative of temperature w.r.t. t
u_x	partial derivative of temperature w.r.t. x
v_i	velocity of i^{th} particle

V_j^+, V_j^-	ideal best and worst respectively
w	inertia weight vector
X	dimensionless axial length
x	space co-ordinate
x_g	global best position in PSO
x_i	position of i^{th} particle
Y	population vector in WCA, WOA, GWOCS, ASO
y	position vector
$\tilde{m}$	noisy output parameter
$\dot{q}$	Volume internal heat generation rate [Wm^{-3}]
$\tilde{T}$	measured values of temperature
z	search step size

Greek Symbols

α	regularization parameter
α_1	non-dimensional thermal conductivity coefficient
β	constant, describing the variation of thermal conductivity
χ	kernel in mollification
δ_1, δ_2	coefficients of emissivity-temperature curve [K^{-1}, K^{-2}]
δ_{ij}	Kronecker's delta
η	thermal conductivity coefficient [K]
η_{eff}	Efficiency
γ	constant, describing the variation of heat transfer coefficient
γ_1, γ_2	dimensionless coefficients of emissivity-temperature curve
λ	mixing parameter
μ_1, μ_2	heat flux functions representing boundary

ω	blood perfusion rate, [s^{-1}]
Φ	dimensionless heat flux
ϕ	temperature at initial time
ψ_λ	family of orthogonal wavelets and Lagrange multiplier
ρ	density [kg/m^3]
σ	5.67×10^{-8} called Stephan's Boltzmann Constant
τ	final time
θ, θ_o	dimensionless temperature
θ_a	dimensionless ambient temperature
$\tilde{\theta}$	guessed dimensionless temperature
υ	slope of thermal emissivity-temperature curve [K^{-1}]
ε	surface emissivity
φ	unit impulse function
ξ	dimensionless length of fin
ζ	dimensionless junction length of walls

Subscripts

a	ambient, artery
b	fin base, blood
C	Convection
i	inner wall, different layers
ini	initial
L	left of internal wall
m	metabolic
n	normal
o	outer wall

R	Radiation
r	ratio

List of Figures

List of Tables

Chapter 1

Introduction

In our day-to-day life we are constantly dealing with inverse and ill-posed problems. We can solve such problems quickly and effectively, provided good mental and physical state. For example, consider our visual insight. It is known that at any given instant, our eyes can recognize visual information from only a limited number of points in its vicinity. Then why do we have an impression to see and locate everything around us? The reason is that our brain, like a computer, completes the recognized image by interpolating and extrapolating the visual data obtained from the finite number of points. The actual three-dimensional image can be adequately retrieved from various points only if we are accustomed to the image, i.e., if we previously saw most of the objects in it. Thus, although the problem of retrieving the image of an object and its surroundings is ill-posed (i.e., there is no uniqueness or stability of solutions), the human brain can solve it rather quickly. This is due to the brain's capability to utilize its extensive previous experience (a priori information). A glance at a person is sufficient to determine if the person is a child or an adult, but it is usually not enough to determine the person's age with an error of at most five years. To understand a substantially complex phenomenon and solve a problem such that the probability of error is high, we usually arrive at an unstable (ill-posed) problem Kabanikhin (2008). Ill-posed inverse problems are everywhere in our daily lives. Indeed, everyone realizes how easy it is to make a mistake when reconstructing the events of the past from several facts of the present. For example,

1. To imagine and to redraw a crime scene based on the existing direct and indirect evidence.

2. To determine the cause of a disease based on the available results of a medical test.

The same is true for tasks which involve predicting the future. For example,

1. To predict the occurrence of a natural disaster.

2. To produce by prediction a one-week weather forecast report.

3. To identify the inaccessible zones to explore their structure. For example,

    - Subsurface exploration in geophysics.

    - Examine a patient's brain using tomography.

In forward problems (often known direct problems), the aim is to find the exact or approximate functions or solutions. These unknowns usually describe many physical phenomena such as the propagation of sound, heat, seismic waves, electromagnetic waves, etc. In such problems, the equation coefficients or the initial state of the process or its properties on the boundary, representing the media properties are assumed to be known and parameters such as speed, pressure etc. are evaluated. However, in reality, these media properties go missing or are unknown. This results in the formulation of inverse problems, where it is required to estimate the equation coefficients from the measured data about the solution of the direct problem. Majority of such problems are ill-posed in nature, i.e., unstable with respect to measurement errors. The unknown equation coefficients represent important media properties such as density, electrical conductivity, heat conductivity, design (shape) etc. Finding the solution to inverse problems can also lead to determining the location, shape, and geometry of intrusions, defects, sources (of heat, waves, potential difference, pollution), and so on. Given such a large variety of applications, which we shall see in detail ahead, it is no surprise that the theory and application of inverse and ill-posed problems have become one of the most rapidly developing areas of modern science since its emergence.

1.1 What are inverse problems?

For making conclusions about a specific problem at hand, a physical phenomenon under consideration, for example, earth for geologist, matter and energy for the physicist, seismic signals for a seismologist etc., can be modeled by first identifying the parameters, which completely describe the problem, then a forward model is constructed for its study, Tarantola (2005).

Forward problem: For the known values of the input parameters, making estimations about the output parameters (or physical laws) is a forward problem. If $\mathbf{f}$ represents model parameters, $\mathbf{K}$ denotes the operator (linear or nonlinear) which arises during the process and $\mathbf{m}$ represents output values obtained after the process, then the forward problem is to find $\mathbf{m}$ by applying $\mathbf{K}$ on $\mathbf{f}$, i.e.,

$$\mathbf{f} \longrightarrow \mathbf{Kf} = \mathbf{m}.$$

Inverse problem: The inverse of the forward problem is to find $\mathbf{f}$ from $\mathbf{Kf}$

$$\mathbf{m} = \mathbf{Kf} \longrightarrow \mathbf{f}.$$

Here we have $\mathbf{m}$ (output parameters) and we need to find the actual model parameters $\mathbf{f}$ from it. Thus, an inverse problem is to infer the actual parameters (i.e., the original signal, clear images

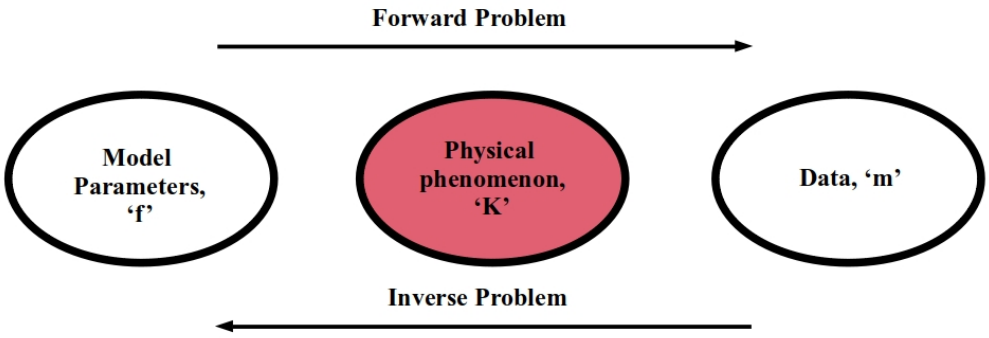

Fig. 1.1 Two-way diagram for Inverse Problems

etc.) by using the values of observed parameters, obtained easily for example when signals get mixed with noise or blurred images, Tarantola (2005). The process can be visualized in the Fig.(1.1).

The phenomena such as scanning the brain, geophysical processes, heat transfer, acoustic, electromagnetic, etc. which involves the solution of the forward problem requires more thinking and making inferences from the observed values. On the other hand, more of mathematics is involved in evaluating the solution to the inverse problem, which makes it quite rigorous as compared to the forward problem.

Classification of inverse problems

Linear inverse problems

In a linear inverse problem, $\mathbf{Kf} = \mathbf{m}$, the operator $\mathbf{K}$ gives linear relation between model parameters and observed results and is a matrix.

If matrix $\mathbf{K}$ is singular, then surely, $\mathbf{K^{-1}}$ cannot be calculated. If matrix $\mathbf{K}$ is non singular, then condition number for $\mathbf{K}$ is checked. Condition number basically measures how much the output $\mathbf{m}$ changes with small change in input $\mathbf{f}$ and is calculated using the formula $\|\mathbf{K^{-1}}\|.\|\mathbf{K}\|$. If the condition number of $\mathbf{K}$ is small, then $\mathbf{Kf} = \mathbf{m}$ is well-conditioned but if condition number is high, which usually is the case, $\mathbf{Kf} = \mathbf{m}$ is ill-conditioned and its inverse cannot be calculated.

Non linear inverse problems

In non linear inverse problems, $\mathbf{Kf} = \mathbf{m}$, the operator $\mathbf{K}$ provides a non linear relationship between $\mathbf{f}$ and $\mathbf{m}$. In most of the problems operator $\mathbf{K}$ is an ill-posed operator (See definition 1.1.1) and various techniques are required to find solution of inverse problems.

Definition 1.1.1 ***[Hadamard (1902, 1923)] Ill posedness and Well posedness:*** *Let* $\mathbf{K}$ *:* $H_1 \longrightarrow$

H_2, where H_1 and H_2 are any vector spaces. An operator equation

$$\mathbf{Kf} = \mathbf{m},$$

*is said to be **Well posed** if it satisfies the following conditions:*
*1. **Existence:** For each $\mathbf{m} \in H_2$, there exists $\mathbf{f} \in H_1$ called a solution which satisfies the operator equation.*
*2. **Uniqueness:** The solution $\mathbf{m}$ is unique.*
*3. **Stability:** The solution is stable w.r.t. perturbations in $\mathbf{m}$. This means if $\mathbf{K}\bar{f} = \bar{\mathbf{m}}$ and $\mathbf{Kf} = \mathbf{m}$ then $\mathbf{f} \longrightarrow \bar{\mathbf{f}}$ whenever $\mathbf{m} \longrightarrow \bar{\mathbf{m}}$.*
*An operator which does not satisfy any of the above is termed as **Ill posed**.*

The very simple examples of the well and the ill-posed problem is that of multiplication and division involved in arithmetic. Multiplication by a small number 'd' $df = g$ is well-posed problem. Whereas division by a very small number 'd', $f = d^{-1}g, \quad d \ll 1$ is ill-posed problem. Another example is found in algebra, where multiplication by a matrix (K), $Kf = q$ is well-posed. Whereas finding the inverse in $f = K^{-1}q$, where K is ill-conditioned, degenerate or $m \times n$ degenerate matrix, is an ill-posed problem.

1.2 The emergence of inverse problems

In 1823, N. H. Abel for the very first time raised a mechanical problem, in which an unknown path is to be determined when some material object moved from rest along it, in a specified amount of time. This was one of the first inverse problems. Another occurrence of the inverse problem was again seen in 19^{th} century when the most remote planet known at the time was Uranus. The disturbances on Uranus brought about by Jupiter and Saturn were noted, which did not agree with the observed movement of the orbit of Uranus. Thus, Le-Verrier in 1844, encouraged by Arago used these observations and calculated the characteristics like mass, position, etc. of some conjectured planet responsible for such irregular disturbances. Thus, in August 1846, a new planet named 'Neptune' was discovered. Until now, researchers were finding the solutions of inverse problems without actually knowing the fact. To address the problem of finding unknowns in geophysics, the term inverse problem was coined in the 1960s, through input-output experiments or cause-effect experiments. In the 1970s, Backus and Gilbert (1967, 1968) explored the mathematical working behind inverse problems and developed various methods for data analysis in geophysics. Soon, mathematicians, physicists and engineers lost their interest in the solution of inverse problems as it was believed that the solution to such a problem would be meaningless if the concerned problem was ill-posed, thereby it lost its practical importance. This myth was shattered when excellent work by Russians like Tikhonov (1943), Tikhonov and Arsenin (1977b), Ivanov (1962), Lavrentiev (1959) and more recently Tikhonov's students, Badeva and Morozov (1991) on the solution of ill-posed inverse problems came in appearance. Another group of researchers worked on inverse problems during the second world war with multiple aims in mind. These were inverse scattering problems where information

about detailed images and locations of targets was required. Radar and sonar appeared as a consequence for reconstruction purposes. Numerous research areas like biomedical imaging, atmospheric profile inversions, non-destructive testing were developed using this motivation. This leads to the development of various tools and techniques since the 1980s with the emergence of newer ideas and concepts. In the field of scattering and tomography, many techniques for reconstruction have been given in the 1980s and 1990s with important methods involving quality Engl *et al.* (1996), Kirsch (1996).

Holschneider (1991) gave an exact inversion technique for the inverse problem, where information regarding Radon transformation was found. Radon transform is an integral transformation, which provides information regarding projections received from tomographic data. Mathematically, it is a line integral of a function over a straight line in 2-D space. Since 2000, new regularization strategies have been devised, with an expanded interest in the treatment of sparsity. These days the enhanced approach and advancements made in computation and technology has made it conceivable to assess and process an extensive volume of data for finding adequately precise solutions of practical inverse problems.

Lately, interest has been developed in the theory and applicability of IHTPs. It is found in almost every domain of science. People involved in mechanical, aviation, chemical, mathematical and astroscience are altogether keen regarding this subject, each sub-group with a variety of applications. IHTPs come under the category of ill-posed problems, whereas its direct counterpart is well-posed. One of the earlier work was to analyze the inner surface of a gun barrel, due to Giedt (1955). Whereas Stolz (1960) provided a way to retrieve surface temperature and heat flux from the known temperature profile, taken at the surface of the heating body. The theory and methods for IHTP can be found in books (Alifanov *et al.* (1995), Beck and Arnold (1977), Dulikravich and Martin (1996), Goldberg (1989), Morozov (1984), Özışık (1994), Sabatier (1978), Tikhonov and Arsenin (1977b).

1.3 Areas where the inverse problem arises, apart from IHTP

There are many areas which directly or indirectly involve inverse problems. Some areas illustrated below give various problems relating to different fields.

1. **Linear algebra:** Consider the system of linear equations, represented as, $Kf = m$, where K is a $n_1 \times n_2$ matrix, m and f are n_1 and n_2-dimensional vectors, respectively. Let the rank of K be $\min(n_1, n_2)$. For $n_1 < n_2$ the system may have many solutions. For $n_1 > n_2$ there may be no solution. For $n_1 = n_2$, the system has a unique solution. For the unique solution, an inverse operator (matrix) K^{-1} exists. It is bounded since it is a linear operator in a finite-dimensional space. Thus, all three conditions of Hadamard are satisfied. This results in the well-posedness of the inverse problem.

2. **Geometry**: Consider a body in three-dimensional space that is illuminated by a light source from many directions. The associated direct problem, if the shape of the body is known, is to find the shape of its shadow. This problem is well-posed. Whereas, the inverse problem is to reconstruct the shape of the body, given its projections (shadows) on several planes. Aristotle was the first to formulate and provide solution of this inverse problem. Observing the shadow cast by the Earth on the moon, he reported that the Earth is spherical in shape.

3. **Astronomy**: In 1846, the astronomer Urbain Le Verrier predicted the position of the planet Neptune for the first time. Unknowingly, he solved an inverse problem. He used the recorded observations about the position of Uranus in its orbit and predicted the presence of the hypothetical eighth planet in the solar system by noting the effects it made on the Uranus's orbit.

4. **Integral geometry, Radon inversion, X-ray tomography**: Inverse problem in computerized tomography is to reconstruct a function of two variables q(x,y) from the observed data of integrals

$$\int_{L(p,\varphi)} q(x,y)\,dl = f(p,\varphi),$$

along various straight lines $L(p,\varphi)$ in the plane (x, y), where p and φ represent the line parameters. Tomography is an efficient way to detect the anomalities found in geophysics, medicine, metallurgy, radiology, biology, astrophysics, seismology and in many other branches of science. The details of tomography can be found in Mueller and Siltanen (2012)

5. **Differential Equation**: In differential equations, a very famous problem of radioactive decay is studied. According to the observations, the rate of decay is proportional to the amount of the radioactive substance present at any instant of time. Here the constant q_1 is called the decay constant. The process of radioactive decay is described by the solution of the Cauchy problem for an ordinary differential equation

$$\frac{du}{dt} = -q_1 u(t), \qquad t \geq 0, \tag{1.1}$$

$$u(0) = q_0, \tag{1.2}$$

where $u(t)$ is the amount of the substance at a given instant of time and q_0 is the amount of the radioactive substance at the initial instant of time. The direct problem is, given the constants q_0 and q_1, determine how the amount of the substance $u(t)$ changes with time. This problem is obviously well-posed. Moreover, its solution can be written explicitly as follows:

$$u(t) = q_0 e^{-q_1 t}, \qquad t \geq 0. \tag{1.3}$$

The inverse problem consists in determining the coefficient q_1 in equation (1.1) and the initial condition q_0 from the additional information about the solution to the direct problem $u(t_k) = f_k$, $k = 1,2,...,N$, where the decay constant q_1 and the initial amount of the radioactive substance q_0 are unknown, but the amount of the radioactive substance $u(t)$ for certain values of t could be measured.

6. **Partial differential equation (PDE)**: We can see inverse problems in PDEs. Let q(x) be continuous and $\varphi(x)$ be continuously differentiable for all $x \in \mathbb{R}$. Then the following Cauchy problem is well-posed:

$$u_x - u_y + q(x)u = 0, \qquad (x, y) \in \mathbb{R}^2, \tag{1.4}$$

$$u(x, 0) = \varphi(x), \qquad x \in \mathbb{R}. \tag{1.5}$$

Consider the inverse problem of reconstructing q(x) from the additional information about the solution to the problem (1.4), (1.5)

$$u(0, y) = \psi(y), \qquad y \in \mathbb{R}. \tag{1.6}$$

7. **Geophysics**: In geophysics, an acoustic wave is sent from the surface of the earth, for a different range of frequencies. Thereafter, the scattered wave is collected. To find the irregularities caused due to the inhomogeneities is the inverse problem. This irregularity can be an oil deposit, a cave or a mine in case of geophysics, in medicine it can be a tumor or some abnormality in the human body, and in the field of metallurgy, it can be a hole in the metal.

8. **Acoustics**: The inverse problem here is to find out the shape, structure and the material properties of the obstacle from the observed acoustic scattered field. Such problems are significant in the identification of flying objects (for example, aeroplanes, missiles etc.), objects immersed in water (for example, submarines, paces of fishes etc.) and in many other situations, Goyal and Mehra (2012).

9. **Seismology**: The inverse problem in seismology is to detect the behavior of elastic waves propagating through the earth, to gain information about the earth's interior structure. Earthquakes, and other sources (e.g., tsunamis), produce different types of seismic waves which travel through rock, and provide an effective way to image both sources and structures deep within the surface of earth and cannot be measured directly.

10. **Share market**: European options are contracts that give the owner the right, but not the obligation, to buy or to sell the underlying security at a specific price known as the strike's price, on the option's expiration date. To obtain some parameters which are not available

directly in the European options is an inverse problem. Here most of the parameters involved are obtained directly but not all are known beforehand Papiol *et al.* (2017).

11. **RADAR based imaging**: It is done by transmitting and receiving the high power microwaves using antennas and to extract and interpret useful information from the received microwaves. The transmitting and receiving of microwaves is done via appropriate hardware devices, whereas extracting information from the received signals is mathematically more complicated and is an inverse problem.

12. **Signal processing**: The inverse problem in signal processing involve the retrieval of high resolution and high-quality signals and images from partial and noisy measurements. Its applications are found in medical imaging to analog and digital conversions, from seismic exploration to a high definition video display. Measurements are modeled through the forward analysis, with a linear operator applied to the input signal but this operator usually is not invertible. Thus, a strong prior information on the signal is required to retrieve a precise signal of interest, Mallat (2008).

In this thesis, we will focus on inverse problems from heat transfer. In the next sections, we shall see what are IHTPs, the associated gaps and motivation for the thesis.

1.3.1 Inverse heat transfer problems (IHTP)

The analysis for IHTPs requires estimation of heat flux or other material properties when the measured value of temperature at certain points of the domain is available. For example, in the case of a conduction-convection problem, the following mathematical model, governs the phenomenon

$$c\rho u_t = (ku_x)_x - hu + G, \qquad 0 < x < L, \quad 0 < t < \tau, \tag{1.7}$$

$$hu|_{(0,t)} - ku_x|_{(0,t)} = \mu_1(t), \qquad 0 \le t \le \tau, \tag{1.8}$$

$$hu|_{(L,t)} - ku_x|_{(L,t)} = \mu_2(t), \qquad 0 \le t \le \tau, \tag{1.9}$$

$$u(x,0) = \varphi(x), \qquad 0 \le x \le L, \tag{1.10}$$

where equation (1.7) models the conduction-convection with equations (1.8-1.9) as the boundary condition and equation (1.10) as the initial condition. Such a model represents various heat transfer phenomena found in various processes involving heat transfer. The material of the system is characterized by c (heat capacity coefficient), k (heat conduction coefficient), h (heat convection coefficient), G (heat generation from source). The direct problem here is to obtain the temperature profile $u(x,t)$ from the known material properties (c, ρ(density), k_1, k_2, h_1, h_2 (thermal conductivity constant and heat transfer coefficient for left and right boundaries respectively.), μ_1, μ_2 (heat flux functions representing the boundary), and φ (temperature profile at initial time). Inverse problem arises when temperature is measured at various locations of the system, say bar, either by using thermocouples or is found by forward analysis, with few

material properties to be determined (for e.g., heat conduction coefficient 'k'), with all other parameters in (1.7) - (1.10) known beforehand.
IHTPs can be classified as follows:

- In terms of dimensions as one, two, three dimensional.
- As linear and non-linear.
- In terms of mode of heat transfer, i.e. conduction, convection (forced or natural), radiation or any combination of these processes, Özışık and Orlande (2000).
- Based on the characteristics (or parameter) to be retrieved, like boundary conditions, initial conditions, geometry/shape/design, thermal or physical properties of the material involved.

The main goal of moving in the direction of inverse heat transfer, is to contribute towards the minimization of energy consumption. One way to achieve this goal is by increasing the overall performance of a product. This is usually done by tuning the thermal parameters accordingly. Another way is to design a certain product keeping in mind the output required. For example, the current trend is to create small devices with increased technology. In doing so, more power is utilized resulting in more heat production. Thus, for efficient working of the device, a maximum amount of heat should be removed from a specified amount of area. In addition to that, IHTPs belong to a class of ill-posed problems whereas the direct heat transfer problems are well-posed. Thus, the solution of inverse problem is very sensitive towards measurement errors in the output data.

1.4 Motivation for the current work

Literature review suggests that various inverse methods are compared in the articles, Beck *et al.* (1996a), Colaco *et al.* (2006), Deb *et al.* (2014), Iwan *et al.* (2012), Krejsa *et al.* (1996), Lilla *et al.* (2013), Marcos *et al.* (2011), Muniz *et al.* (1999), Park and Chung (1999). For the thermal domain, reviews such as Goldstein *et al.* (2005, 2006) are available providing a complete literature review of heat transfer until 2002 and 2003 respectively. Whereas the only reviews available for inverse problems in heat transfer cover a very particular domain involving conduction problems, as in Sharma *et al.* (2014), Chang *et al.* (2018) and radiation problems in McCormick (1992). With such a limited review at hand, there is the much-awaited need for a review, which not only discusses what had been done but also the available and known methods for estimating the solution. Hitherto, a different set of regularization techniques could be found in Hansen (1994), Orlande (2012) and review for optimization methods, have been done in Colaco *et al.* (2006). A review again, particularly on the Bayesian approach (relating to modeling issues) is provided by Kaipio and Fox (2011), which is not sufficient for the current scenario. Such a comparison is problem-specific, which varies from problem to problem and is

not suitable for general purposes. Hence there is a need to compare the existing methods and see whether these could be compared on a more general problem. If these cannot be compared, then can we move towards some hybrid techniques? Right now no method is available, which can be applied to all types of the inverse problem. Hence, there is a need which motivates us to study in this direction.

Many problems like double-wall heat conduction problem, Torabi and Zhang (2015), heat transfer problem in fins, Singh *et al.* (2016), Singla and Das (2014, 2017) are available in the literature, having applications in various industries. To study the heat transfer, the closed form of solutions is required as identified above. Moreover, in Torabi and Zhang (2015) and Singh *et al.* (2016), only forward analysis is done and in Singla and Das (2014, 2017), an inverse analysis is done but only the thermal conductivities of the material are considered temperature-dependent. Instead for more practical method, heat transfer coefficient and internal heat generation should be time-dependent (which changes more frequently with time). Such problems are previously solved by making some assumptions either regarding the material involved or the process involved. Sometimes properties of a particular material are taken as time-independent or constant. But in actual practice, i.e., when the process occur, all processes like conduction, convection, radiation, internal heat generation, involving loss or gain of heat occurs simultaneously and to achieve the correct and near to reality solutions, one must consider a more general problem at hand. So, there is a need to apply the above-sorted technique to the same problem but with a wider set of parameters and properties, which no doubt increases the complexity of the problem but is essential to obtain results near to reality.

Further, in the race of improving the solutions for inverse problems, despite the presence of multiple algorithms, is there any technique which can be implemented on every kind of nonlinear inverse problem for parameter estimation? If not, could some procedure be developed which enhance the inversion process in IHTP? Right now no method is available, which can be applied to all types of inverse problems. Thus, there is a need to develop a procedure for inverse problems which enhances the overall computational efficiency of any system, in particular IHTP.

1.5 Objectives of the Ph.D. thesis

The purpose of the present work is to explore the best methods and their extensions for solving inverse problems. The complete objectives of the work are summarized as below:

1. Selection of inverse technique best fit for a given problem.
2. Implementation of above selected technique on realistic problems taken from heat transfer systems.
3. Formulation and theoretical aspects of new technique for solving inverse problems.

1.6 Organization of the thesis

This thesis consists of seven chapters and is organized as follows:

Chapter 1 provides an overview and introduction to the topic of inverse problem with the basics and the necessary preliminaries. Then we have discussed the ill-posed nature of inverse problems with their classifications. Thereafter, the emergence of inverse problems is discussed starting from the year when N. H. Abel raised his famous problem to determine the unknown path in the given time. Inverse problems can be found in different domains. The brief description in various fields has been explored and discussed. Then the need to work in inverse heat transfer has been stated, with the required preliminaries. Then the associated gaps and motivation for working in this direction has been defined. The complete objectives of the Ph.D. thesis, with the overall structure and contribution, are defined at the end of this chapter.

Chapter 2 is a comprehensive literature review on the present methods for the solution of inverse problems. The need for regularization with details about regularization techniques is presented in chapter 2. This classification is novel and defines the available techniques classified within natural regularization, regularization based on modification in the objective function, modification in data, modification in both and the iterative regularization. Further, the methods to solve IHTP are classified with the latest literature on IHTP. The main categories include the analytic methods, methods based on minimization and without minimization. As the available analytical methods are limited to linear inverse problems, methods involving minimization come into the light. These include gradient-based and heuristic methods. After analyzing the pros and cons of each algorithm, it has been concluded that both the gradient-based and nature-based methods are application-specific. The wavelet methods for both denoising and reconstruction has also been explored.

Chapter 3 includes steady-state heat transfer in double-layered walls, with temperature-dependent properties like thermal conductivity, internal heat generation, surface emissivity and convection coefficient. In the present context, problem is solved by Adomian Decomposition Method (ADM) using Matlab. The literature on heat transfer in composite walls reveals the usage of Differential Transformation Method (DTM) to deal with the nonlinear terms present but comparing both methods, ADM turns out to be a more efficient method in terms of handling additional non-linearity. The boundary conditions are solved using Newton's Raphson Method for better convergence of the solution. The efficiency of the system is calculated and a particular application of furnace is modeled. In addition to furnaces, these composite walls found applications in many areas, for example in the insulation of buildings under extreme weather conditions, as walls of refrigerator, micro hotplates, cold and hot water storage tanks etc. in which the heat exchange is to be minimized. Lastly, an inverse analysis of these composite walls is performed. The

internal heat generation in both walls, along with the thermal conductivity ratio are estimated. Such estimation is required when a suitable material is to be selected for furnace construction.

Chapter 4 investigates the performance of transient, nonlinear, longitudinal circular pin fin with all temperature-dependent thermal parameters. The developed mathematical model with non-linear equations was solved with the MATLAB based tool Pdepe. An experiment has also been performed on the test rig to obtain the temperature profile of the surface of the fin. The study investigates the effect of various parameters on the temperature distribution of the longitudinal circular pin fin. Using the inverse analysis, transient, non-linear heat flux has been retrieved. This retrieval of heat flux as a function of time has been accomplished using the golden section search method. A case study is made under static and dynamic conditions for cases when heat flux is assumed to be constant, linear triangular and non-linear realistic. The recovered heat flux is compared with its expected value. The computed and experimental trend of heat flux has been observed. Further, the study results in finding the tolerance limits for heat flux and change in output with added error is seen. The overall impact reconstruction error has, on parameters is reported, which determines the performance of the model.

Chapter 5 demonstrates the developed novel comparison procedure to compare and select the best algorithm for IHTP. The proposed procedure is useful in the sense that no particular algorithm is suitable to solve the inverse problem from every domain. This is explained using no free lunch theorem, which states that no optimization algorithm works for every set of problem. Thus, the proposed comparative procedure could be applied to any domain involving estimation of parameters using inverse analysis. Based on the literature survey revealing the presence of a large number of inversion algorithms, the new inverse formulation involves a combination of best forward, regularization and hybrid optimization techniques. The forward analysis utilizes Matlab based pdepe for the computation of surface temperature. The regularization is proposed by the modification in the objective function. The objective functions lasso, Tikhonov and elastic net were proposed for the purpose instead of the traditional least-squares. Whereas for minimization, several optimization algorithms were picked from different categories, namely, evolution-based Differential Evolution (DE), swarm-based (Particle Swarm Optimization (PSO), Whale Optimization Algorithm (WOA)), nature-based (Water Cycle Algorithm (WCA), Butterfly Optimization Algorithm (BOA)), physics-based (Atom Search Algorithm (ASO)) and a hybrid (Grey Wolf Optimization and Cuckoo Search (GWOCS)). These methods are efficient and thus can be tailored according to the needs of the problem. The decision for the efficient algorithm was made using TOPSIS, where the top three algorithms were reported for IHTP. This methodology thus provides a robust procedure for comparing and selecting the best inversion technique in IHTP and the procedure can be easily imple-

mented to any domain of interest.

Chapter 6 provides an application of the proposed methodology given in chapter 5, for the detection of tumor in human brain tissue. The best algorithms were selected based on the TOPSIS method of chapter 5 and their implementation is seen for the non-invasive diagnosis of tumor. Based on the temperature response of skin by the thermal exchange between skin and surroundings, the inversion techniques, such as PDEPE-WOA and PDEPE-GWOCS are proposed for the detection of tumor. The temperature profile for the bioheat transfer problem in one-dimension is obtained for the human brain tissue using Pennes model. The associated inverse heat transfer problem is ill-posed, thus Tikhonov, lasso and elastic net regularizations are applied. There $\lambda = 0.1$, $\alpha = 10^{-2}$ for WOA and $\lambda = 0.9$, $\alpha = 10^{-4}$ for GWOCS regularization parameters are observed optimal based on the total relative error. A study on the effect of control parameters of WOA and GWOCS have been conducted, where the number of search agents reported optimal are 30 for minimum CPU time and objective function value. To retrieve the blood perfusion rate, the minimum objective function is of order O(10^{-2}) for WOA and O(10^{-4}) for GWOCS. The lower value of perfusion rate (0.0005 s^{-1}) in second and fourth layer indicate clearly the presence of multiple tumors. Moreover, the presence of multiple tumors is detected quite effectively for exact temperature distribution. Further, an error analysis with noise, $e = 1\%, 2\%, 3\%, 4\%, 7\%$ and 10%, has also been performed to retrieve blood perfusion rate.

Chapter 7 deals with the overall conclusions of this study. The available inversion methods have been classified into different categories. The major outcomes of the thesis revolve around finding the solution of inverse problems in the heat transfer setting. The retrieval of boundary condition (heat flux), thermophysical properties (thermal conductivity, heat transfer coefficient, conduction-convection, conduction-radiation) and biological tissue properties (blood perfusion rate) has been satisfactorily performed. The efficiency of the composite walls and the maximum loss of heat in the extended surface has been studied. Moreover, the detection of tumor by observing the temperature profile and by the estimated value of blood perfusion rate indicates the regions of malignancy. The usability of various algorithms in IHTP, starting from golden section search method, for retrieval of a single parameter, to the regularized versions of inversion technique, for retrieval of multiple parameters with uncertainty, strengthen the computational domain of IHTP. The procedure for comparing and selecting the best inversion algorithm has been developed, which can be used in any field of interest. Lastly, a brief direction on the scope of future work is presented.

To select which inversion algorithm best suits a given problem, let us start with the literature review in the next chapter.

Chapter 2

Literature Review

Given an ill-posed problem, its solution can be obtained by a combination of a regularization technique and a solution technique. In this chapter, we shall describe the available regularization techniques, followed by the available inversion techniques. An exhaustive literature survey is simultaneously listed corresponding to each technique discussed in this chapter.

2.1 Regularization Techniques

As already discussed in Chapter 1, an inverse problem is finding '**f**' from the measured data

$$\mathbf{Kf} = \mathbf{m}. \tag{2.1}$$

However, when data values '**m**' are measured experimentally, a certain amount of error or noise 'e' is incorporated in the measurements. Therefore, we have $\mathbf{Kf} = \mathbf{m} + \mathbf{e}$, which is to be solved for '**f**. Hence in the process of finding a solution, one must get rid of the e first. The error or noise can be removed via denoising or filtering, explained in section 2.2.3. Once the error is removed, the next step is to invert the operator '**K**' in the equation $\mathbf{Kf} = \mathbf{m}$ to find the unknown '**f**'. However, in most of the situations, the operator '**K**' cannot be inverted as it is ill-conditioned (i.e., the matrix associated with '**K**', let us call it **K** again, is having a high condition number $||\mathbf{K}||\,||\mathbf{K}^{-1}||$.) To handle the ill-conditioned operators, we have regularization techniques as saviour. The problem in inverting the matrix associated with operator **K** is either the high condition number of K or its singularity which is caused due to rank deficiency. Most of the inverse heat transfer problems are ill-posed because the solution does not depend continuously on the input. To make an ill-posed inverse problem as well-posed, regularization is needed to be done. Further, if a large number of parameters are required to be calculated, the corresponding problem becomes unstable and challenging to solve. Thus, to make it stable, one must regularize it. To overcome the problem of rank deficiency and ill-posedness, several regularization techniques are used, Vogel (2002). Broadly, these regularization techniques are classified as shown in Fig.(2.1). Whenever regularization occurs while the evaluation of the

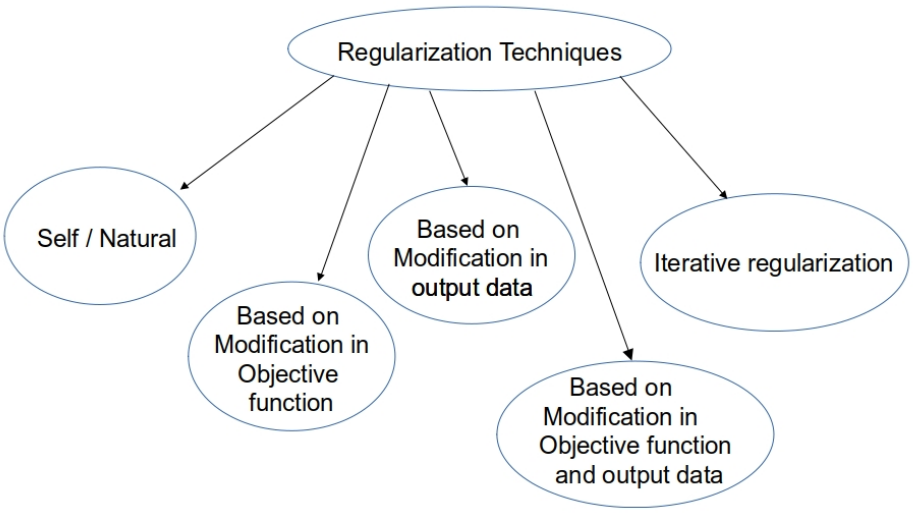

Fig. 2.1 Classification of regularization techniques.

solution, it is termed as self regularization. Furthermore, one can modify the objective function or modify the given data by making it smooth or can modify both. For a good regularization method, consistency (i.e., the obtained regularized solution should tend towards the original solution of the inverse problem) and stability (i.e., the obtained regularized solution should depend continuously on the data) conditions should be satisfied, (Woodbury (2002), chapter-4). The necessary practical requirement thus remains to check whether small changes in the regularization parameters should produce small changes in the obtained regularized solution, in the case, when no error (for consistency) or a fixed amount of error (for stability) is present in the data. Most of the regularization techniques can be classified as shown in Fig.(2.1), details of which are given below.

2.1.1 Self / Natural regularization

This kind of regularization is achieved by the application of inversion methods, which within the process of obtaining the solution, regularizes the ill-posed problem and thus obtain a solution which is near to exact one. Regularization in principle is achieved by modifying one or more parameter required for computation, for example, the step size involved or the number of terms involved, when the corresponding function is approximated by an infinite series. Regularization of such kind provides control over the nearness of the approximated solution to that of exact solution (Alifanov (1994), chapter-2). This approach of obtaining the solution is usually simpler and hence is widely employed. Methods like Truncated singular value decomposition, stochastic methods (like Monte Carlo method) compute the solution of inverse problems by regularization built within the process and without the explicit implementation of regularization algorithm. Wang and Zabaras (2004), used Hierarchical Bayesian models, for parameter estimation of boundary heat flux. Moreover, heat source reconstruction using Markov Chain,

Monte Carlo simulations were conducted for the associated inverse problem.

2.1.2 Modification in the objective function

In this category, the objective function is modified such that there is a minimal deviation of approximated solution from the exact one. **Tikhonov regularization** is regarded as the most popular and widely used regularization technique for linear inverse problems, Alifanov (1994), Alifanov *et al.* (1995), Beck and Arnold (1977), Morozov (1984), Özışık and Orlande (2000), Tikhonov and Arsenin (1977b). This method regularizes the problem by modifying the least-squares objective function, in which the primary goal is to minimize the error between the experimental and guessed values of the unknowns, $||Kf - m||^2$. In Tikhonov regularization, the solution of the equation $m = Kf + e$ is given by,

$$T_\alpha(m) = BD_\alpha^\dagger A^T m, \tag{2.2}$$

where $K = ADB^T$ is the SVD of K (refer footnote [1]) and $D_\alpha^\dagger$ is given as

$$D_\alpha^\dagger = diag\Big(\frac{d_1}{d_1^2+\alpha}, \cdots\cdots, \frac{d_{min(k,n)}}{d_{min(k,n)}^2+\alpha}\Big) \in \mathbb{R}^{n\times k}. \tag{2.3}$$

In the variational terminology, a vector $T_\alpha(m) \in \mathbb{R}^n$ is regarded as a Tikhonov regularized solution if it is evaluated using

$$T_\alpha(m) = \underset{z\in\mathbb{R}^n}{\operatorname{argmin}} \left\{ \|Kz - m\|^2 + \alpha\|z\|^2 \right\}. \tag{2.4}$$

It means that such a $T_\alpha(m) \in \mathbb{R}^n$ is to be evaluated which minimizes

$$\|KT_\alpha(m) - m\|^2 + \alpha\|T_\alpha(m)\|^2.$$

Here $\alpha > 0$ is the regularization parameter. The first term reduces the amount of error involved in the solution and the second term provides regularization by adding a certain amount

[1] For the operator **K** : $H_1 \longrightarrow H_2$ defined in equation (2.1) Let **K** $\in \mathbb{R}^{m\times n}$ be a rectangular or square matrix associated with operator **K** and assume m is greater than or equal to n. Then the following is the **SVD of K**,

$$K = ADB^T = \sum_{i=1}^{n} a_i d_i b_i^T,$$

such that

$$a_i^T a_j = \delta_{ij}, \quad b_i^T b_j = \delta_{ij},$$

and

$$Kb_i = d_i a_i, \quad K^T a_i = d_i b_i,$$

are satisfied. Here δ_{ij} denotes Kronecker delta, which takes value 1 when i=j and zero otherwise. Also $A = (a_1, \ldots, a_n) \in \mathbb{R}^{m\times n}$, $B = (b_1, \ldots, b_n) \in \mathbb{R}^{n\times n}$ and the non negative diagonal entries $d_1 \geq d_2 \geq \cdots \geq d_n \geq 0$ in non increasing order (decreasing order) forms the elements of matrix D = diag(d_1, …, d_n). The number 'd_i' represents the i^{th} singular value, of matrix K, whilst the i^{th} singular vectors are denoted by a_i and b_i, satisfying $A^T = A^{-1}$ and $B^T = B^{-1}$.

of penalty and hence called the penalty term. The known methods for choosing 'α' are the Morozov discrepancy principle and the L-curve method, Mueller and Siltanen (2012), although none of these results in an optimal value of α. The method tries to create an equilibrium such that a small residual of $KT_\alpha(m) - m$ is obtained in addition to a lower L^2-norm for solution $T_\alpha(m)$. The lower L^2-norm is responsible for providing a unique solution as many solutions would be available which create a small residual value. This method usually retrieves the solution providing smooth results, thus ignoring the edges with sharp features. Further, a priori information is included in this method, as these are available easily sometimes like the known properties of the solution. A numerical solution of non-linear IHCP was solved by Alifanov and Artyukhin (1975) using the implicit difference scheme. Their problem involved moving boundaries, where regularization was done in Tikhonov manner. Shen (1999) used BEMs, namely collocation and weighted methods, where regularization has been done in the Tikhonov's sense. A numerical study using collocation and TSVD was also discussed. Time independent heat transfer coefficient has been determined experimentally in Chantasiriwan (2000). Use of unstructured meshes, using a control volume method has been used for irregularly shaped bodies by Duda and Taler (2000), to find the solution of non-linear IHCP. Throne and Olson (2001), compared newly developed generalized eigensystem with that of the Tikhonov method, with earlier comparisons being made, knowing the true solution to fix regularization parameters. To overcome this difficulty of collecting a priori information regarding the material, a sensor sensitivity method had been proposed. Hon and Wei (2004), build a meshless numerical scheme, without involving integrals, utilizing the principal solution as a radial basis function. Both Tikhonov and the L-curve method had been applied for stability. This method of the fundamental solution provided an efficient universal scheme for IHCP. An algorithm for regularization has been put forward by Ling *et al.* (2006), using a blend of Tikhonov method, the sequential function specification method in addition to eigenvalue reduction and self regularization method. A physical interpretation of equations was given by the method and it shows the diverse applicability of the proposed algorithm. A heat source problem had been solved in 2008, where Yan *et al.* (2008) used a meshless technique, making use of fundamental solution along with Tikhonov regularization, with parameter chosen according to cross-validation criterion. A numerical approach to solve IHCP utilized various algorithms using Newton's method as illustrated by Kang *et al.* (2010). The solutions were regularized by using Tikhonov regularization, with the implementation of Newton-Tikhonov and Newton-implicit iterative methods, which largely minimizes the computing costs. Unknown non-linear boundary transient heat transfer coefficient has been recovered numerically by Slodička *et al.* (2010), by the implementation of BEM. Tikhonov regularization has been implemented to make the problem well-posed. Theoretical aspects like existence and uniqueness were also presented. To predict transient heat source, Yang and Fu (2010), used a simplified version of Tikhonov regularization to solve the ill-posed inverse problem. An error estimate is provided along with numerical examples justifying the technique. Reeve and Johansson (2013) used method of fundamental solutions, along

with Tikhonov regularization, to handle ill-posedness of transient 2-D Cauchy heat conduction problem. Some data was initially known at the boundary in terms of derivatives. This method did not require any a priori information relating to initial condition and can work in a multiply connected domain with singular functions as well, proving its versatility. Tikhonov regularization was implemented by Dubot *et al.* (2016) to estimate space-dependent functions using boundary measurements. An improved version of Tikhonov regularization was introduced by Cheng and Ma (2016), to solve IHCP, with boundary located at $x = 0$ only. The solution was required in (0,1]. Conditional stability was proved, making use of Hölder's inequality. An estimate of error was also calculated. Variation of stability and accuracy was studied by using the application of Tikhonov regularization to retrieve heat flux on the surface of the plate. To consider a more realistic situation, random errors were added to the obtained temperature measurements. Yang and Xiong (2018), used Tikhonov regularization to determine the heat source in IHCP, where the stability of the solution was assured by the optimal control method. Hazanee *et al.* (2019), took a population model from mathematical biology, where a transient source was identified for IHTP, with a non-local nature of boundaries. Tikhonov regularization was imposed, with regularization parameter selected using the discrepancy principle and generalized cross-validation criterion. BEM was used for forward analysis and generalized Fourier method was used to prove uniqueness.

Other than the famous Tikhonov regularization, there are other regularization techniques in this category, which are discussed ahead. For equation (2.1), given K a monotone operator, then the objective function could be modified as

$$Kf + \alpha B^s F = m^\delta,$$

where B is linear, unbounded, self-adjoint, densely defined, and strictly positive definite operator, δ is the noise in data m and m^δ is the perturbed data. To compute f_α^δ, by the solution of the above-regularized algorithm, is called the method of **Lavrentiev regularization in the Hilbert scales**. This method proves to be better over Tikhonov regularization because of simpler and faster numerical computations as the natural evolutionary structure remains preserved, Janno and Tautenhahn (2003).

The objective function can also be modified statistically, using the Bayesian approach. In **Bayesian regularization**, the objective function becomes

$$\alpha_1 \sum (Kf - m)^2 + \alpha_2 \sum (w^2), \tag{2.5}$$

where α_1 and α_2 are regularization parameters, chosen iteratively, such that the corresponding objective function is minimized, depending on which inverse method is applied along with the regularization. For example, Deng and Hwang (2006), used this regularization in combination with neural networks. The choice of α_1 and α_2 is crucial because if α_1 is large, underfitting may occur and if α_2 is large, overfitting may occur. w here represents the corresponding network

weights, which are random numbers following Gaussian distribution and adjusted during the inversion process. Maniatty and Zabaras (1994) used Bayesian statistical theory to inverse elasticity problems. The authors compared the effect of regularization parameters and the error in the initial data. Wang and Zabaras (2004) used Bayesian inference for the solution of IHCP. Markov Chain Monte Carlo algorithm was used to determine unknown heat flux. To determine the heat source in radiation, the Bayesian approach was used by Wang and Zabaras (2005). Emery (2008) showed the use of a least-squares method and Bayesian Inference to tackle errors in inverse problems.

A different classification of regularization was given by Beck *et al.* (1985). According to him, regularization by modification in the objective function is achieved using two approaches namely the whole domain regularization method and the sequential regularization method. The first one includes the estimation of the unknown at all time steps (assuming a time discretization has been done) simultaneously. This approach is termed as **whole domain regularization method**. The method was developed for IHCPs for different time steps, with multiple sensors. The zeroth-order formulation when single sensor is involved, is obtained by minimizing the objective function with respect to $\mu_i,\ i = 1, 2, \ldots, n$ as follows,

$$J = \sum_{i=1}^{n} (\tilde{T}_i - T_i(\mu))^2 + \alpha \sum_{i=1}^{n} \mu_i^2. \tag{2.6}$$

Here again α is the regularization parameter and μ is the unknown heat flux. If $\alpha \to 0$, then exact matching of $\tilde{T}_i$ and $T_i(\mu)$ is achieved, i.e., the exact and measured temperature values coincide. Note here the unknown f is heat flux, represented by μ. When time steps are decreased, then the second term in equation (2.6) becomes large, dominating the solution, which may lead to unstable procedures. It is interesting to note here that in the case of well-posed problems, mainly done by various numerical techniques, small-time steps usually increase the accuracy whereas, for ill-posed problems, small-time steps lead to unstable solutions. For large α, μ_i's are reduced to zero. Thus, proper selection of α is mandatory. The objective function reduces to

$$J = \sum_{i=1}^{n} (\tilde{T}_i - T_i(\mu))^2 + \alpha \sum_{i=1}^{n} (\mu_{i+1} - \mu_i)^2,$$

for first-order regularization and to

$$J = \sum_{i=1}^{n} (\tilde{T}_i - T_i(\mu))^2 + \alpha \sum_{i=1}^{n} (\mu_{i+2} - 2\mu_{i+1} + \mu_i)\mu_i^2,$$

for second-order regularization. For the first order, $\alpha \to 0$ leads again to exact matching and large α results in constant μ_i. For second-order, large α leads to an approximation of μ by a straight line with two unknowns. Another category is **sequential regularization method**. Most of the regularization methods work, using the whole domain approach. The sequential method provides approximately the same results but the computation involved is greatly reduced, as this

method utilizes sequential computation of unknowns at future time steps. If $\mu_1, \mu_2, \ldots, \mu_{M-1}$ represent the heat flux components which need to be estimated, assuming all heat flux after $M-1$ are zero. Then the temperature at j^{th} space position and $m+i-1$ time position is given as

$$T(\mu)_{j,m+i-1} = \hat{T}(\mu)_{j,m+i-1}|_{\mu_M=.....=\mu_{M+i-1}=0} + \mu_M \Delta\varphi_{j,i-1} + ... + \mu_{M+i-1}\Delta\varphi_{j,0}.$$

For the zeroth-order regularization, the objective function is modified as,

$$J = \sum_{i=1}^{n} (\tilde{T}_i - \hat{T}_i(\mu)|_{\mu_M=0} - \mu_M \Delta\varphi_j)^2 + \alpha\mu_M^2.$$

Minimization of 'J' with respect to μ_M gives an estimator for heat flux as follows,

$$\hat{\mu}_M = \sum_{j=1}^{J} Q_{1j}(\tilde{T}_i - \hat{T}_i(\mu)|_{\mu_M=0}), \text{ with } Q_{1j} = \Delta\varphi_{j_0}(\alpha + \sum_{k=1}^{J} \Delta\varphi_{k_0}^2)^{-1}.$$

If the regularization parameter $\alpha \to 0$, the above equation provides heat flux estimate for a single time step, whereas for $J = 1$, in addition, results in exact matching, when the single temperature sensor is involved. For a significant regularization, the regularization parameter should either be larger than or equal to the order of the square of the largest $\Delta\varphi_{k_0}$. Another mathematical interpretation of sequential regularization was given by Lamm (1995). Generalizing Beck's ideas, the author provides sequential regularization for Volterra equation of the first kind and gave theoretical proofs for convergence, with application to IHCPs. Lamm suggested that the structure of the underlying operator remains preserved, with sequential regularization. A solution to IHCP using a numerical implementation of methods was provided by Bass (1980), where FEM and Beck's non-linear estimation procedure was implemented, to determine the temperature and heat flux in the direct and inverse analysis respectively. Weiland and Babary (1988), introduced a time marching numerical method for non-linear IHCP, whose main aim was to reduce the limit set for stabilizing parameters. Flach and Özışık (1989), evaluated simultaneously thermal conductivity, which varied in space and heat capacity numerically. Reinhardt (1991) extended Beck's sequential method to solve IHCP in 2-D space. Ruperti *et al.* (1996), used an already available space marching technique, this time for the solution of IHTP including convection and radiation, and provided a generalized version of it. A non-iterative semi numerical approach to determine the surface heat flux was presented by Taler (1996), where no initial temperature was required, with the only requirement of previous and next data with respect to time. An initial valued IHCP was solved in 1997, by Eldèn (1997) using the method of lines. The advantage in the utilization of earlier proposed space marching schemes was the reduction of sensitivity using perturbation in the data. Also for regularization, an additional term was required to be added, for obtaining a stable solution. The current approach approximates the equation instead of altering it, hence proved better. The authors further reported the use of Runge-Kutta numerical methods for stability in various contexts. Osman *et al.* (1997) used

a sequential method for time-variable along with the regularization technique. Xu and Chen (1998), solved 2-D, steady IHCP whereas an experimental analysis has been suggested by Ji and Jang (1998), using Kalman filter.

2.1.3 Modification in output data

Most of the time, data in the form of output parameters is available either from the experiments or using direct analysis. Such data is associated with random errors. Without knowing the kind of errors involved, the task remains is to extract the components of noise (another term used for error) from it. Elimination or minimization of error is important as the inverse problem is ill-posed, which causes the unknown parameter f to deviate quite away from the exact solution. For this, data is firstly modified or smoothed prior to the calculation of the solution. This could be achieved either using some filter function like convolution or by making use of suitable bases to retrieve the solution. Wavelet bases are one such kind, using which a **method of wavelet shrinkage** is obtained which provides smoothing to the noisy data. The major aim of this method is to suppress or shrink the individual coefficients obtained when expanded in a wavelet series. Then after filtering, data is smoothed by reconstructing the remaining coefficients. Another way to smooth the given data is by using the **Mollification method**. In this method, the given noisy data is convolved by a suitable mollifier. A mollifier is itself a smooth function, which, when convolved with non-smooth function results in a smooth function. In other words, sharp or irregular features are flattened or smoothed with minimal loss of original data properties. Mathematically, this could be understood as follows, with the aim to minimize $||m - J_\delta \tilde{m}||$. Let $\delta > 0$, $p > 0$, then

$$A_p = \Big(\int_{-p}^{p} e^{-s^2}\, ds \Big)^{-1}.$$

The δ-mollification of an integrable function is based on the convolution with Gaussian kernel

$$\chi_{\delta,p}(x) = \left\{ \begin{array}{ll} A_p \delta^{-1} e^{\frac{-x^2}{\delta^2}}, & \text{for } |x| \leq p\delta \\ 0, & \text{for } |x| > p\delta \end{array} \right\}.$$

Here $\chi_{\delta,p}$, a non-negative function called mollifier, satisfying $\int_{-p\delta}^{p\delta} \chi_{\delta,p}(x)\, dx = 1$. Assuming that kernel is independent of p, then the δ-mollification by the convolution operator is given as

$$J_\delta \tilde{m}(x) = (\chi_\delta * m)(x) = \int_{-\infty}^{\infty} \chi_\delta(x-s) m(s)\, ds = \int_{x-\chi\delta}^{x+\chi\delta} \chi_\delta(x-s) m(s)\, ds.$$

2.1.4 Modification in the objective function and output data

Regularization by modification in objective function after smoothing the data is another way to achieve regularization. This could be done by the two-step methods, which could be thought of as the implementation of the composition of data smoothing operator and one or more regularization operator. The need for such kind of regularization lies in the fact that when Tikhonov or Landweber regularization methods are applied, they over smooth the solution, missing out the

critical information hidden in the edges of the reconstructed solution. To overcome this over smoothing and damping of the data, the filter functions of Tikhonov and Landweber iterations are altered. Thus, wavelet shrinking methods are utilized for pre-smoothing of the data. For ill-posed problem, equation (2.1), the first step is smoothing of the data to obtain noise-free, better estimate $\tilde{m}$ by the operator. Then the obtained estimate is regularized either by modification in the objective function (e.g. Tikhonov regularization) or by the construction of iterative regularization operators R_α as discussed ahead in the text. Refer Klann and Ramlau (2008), Cohen *et al.* (2004), Klann (2006), Klann *et al.* (2006) for more details. Let $K = ADB^T$ represents the SVD see footnote[1], then

$$R_\alpha m = \sum_{d_n>0} F_\alpha(d_n)\, d_n^{-1} < m, b_n > a_n, \tag{2.7}$$

represents regularization by the application of filter function F_α, with α as the regularization parameter and $< ., . >$ represents the inner product of vectors. The fractional filter function F_α^ξ, where $\xi \in [0, 1]$ is the exponent of the filter function F_α, then replaces F_α in equation (2.7) and the associated method is called a fractional filter method. If $\xi > \frac{1}{2}$, the optimality of the method is maintained while modifying Tikhonov and Landweber method, where $\xi \leq \frac{1}{2}$, optimal results are obtained by using wavelet shrinkage methods for adapted pre-smoothing.

2.1.5 Iterative regularization

There is another class of regularization, namely iterative regularization, which provides self regularization while modifying the objective function too. In a very general sense, regularization here means approximating the operator $\mathbf{K^{-1}}$ by a family of stable operators R_α, i.e., instead of obtaining $\mathbf{m} = \mathbf{K^{-1}f}$, we obtain $\mathbf{m}_\alpha = \mathbf{R}_\alpha(\mathbf{f})$ in such a way that in the limiting case $R_\alpha = \mathbf{K}^{-1}$. R_α are called the regularization operators and α as the regularization parameter. This kind of regularization is a multistep process because the next iterative approximation depends not only on the previous one but on all other approximations obtained thereof. The major limitations in using such iterative methods (such as the steepest descent method, Conjugate gradient method, etc.), involves, a) calculation of the gradient of the objective function; b) Choice of regularization parameter; c) requirement of a priori information. Despite these limitations, sometimes, the problem is formulated in the form of an extremal of the objective function, which then needs to be minimized. Regularization of such kind is called **Total Variation regularization**. The earlier used Tikhonov regularization method provides a solution which is smooth and less approximate. But in many practical situations, one expects a solution which is more elaborate in the sense that sharp features and edges are retrieved for a better approximation of the unknowns and hence provides an additional approach, Chan and Shen (2005), Scherzer *et al.* (2009), Vogel (2002). By sharp features, the authors mean enhanced significant details about the solution. Total variation (TV) regularization was first given by Rudin *et al.* (1992). The variational representation in Tikhonov regularization involved l^2-norm which provides smooth reconstructions whereas TV regularization use l^1-norm which allows piecewise reconstructions

yielding more useful information about the solution. The target was to find a function $z \in \mathbb{R}^n$ such that

$$\|Kz - m\|_2^2 + \alpha \sum_{j=1}^{n} |(Lz)_j|, \tag{2.8}$$

is minimized, with L as the finite difference matrix. The second term defined in the expression (2.8) regularizes the least square norm in the variational sense.

Hào and Reinhardt (1998), solved the IHCP using the variational approach to estimate initial condition and heat flux. To regularize the problem, an iterative approach of CGM was utilized, where gradient used in variation was provided by adjoint equations. Geng and Lin (2009), employed variational iterative method (VIM) to determine heat source. As no discretization was required, thus no numerical errors were added to the solution. VIM proved itself as a satisfactory technique for transient IHTP.
One way to generalize Tikhonov regularization for the indirect measurement $m = Kf + e$ is to consider the minimization problem

$$T_\alpha(m) = \underset{z \in \mathbb{R}^n}{\operatorname{argmin}} \left\{ \|Kz - m\|_2^2 + \alpha \|Lz\|_p^p \right\}, \tag{2.9}$$

The parameter $1 < p < \infty$ in (2.9) is related to the l^p-norm defined for vectors $g \in \mathbb{R}^n$ by

$$\|g\|_p = \left(\sum_{j=1}^{n} |g_j|^p \right)^{\frac{1}{p}}. \tag{2.10}$$

Note that taking $p = 2$ in formula (2.9) leads to **generalized Tikhonov regularization**, which strongly favors smooth reconstructions over discontinuous case. For $p = 1$ the method is referred as **total variation regularization**, which allows piecewise constant reconstructions. The norm simplifies to

$$\|g\|_1 = |g_1| + \ldots \cdots + |g_n|.$$

Beck and Murio (1986), developed a procedure for regularization consisting of sequential function specification method and the regularization method given by Beck and Tikhonov respectively. The obtained values of unknown parameters differ slightly when the combined technique was applied but the method was efficient computationally. A paper by Scott and Beck (1989), extended the sequential regularization method earlier proposed by Beck and Murio. They studied the effects of regularization parameters and order of regularization. Here regularization terms $\left(\alpha \sum_{s=0}^{2} R_s\right)$ were added to the ordinary least squares objective function, where 'α' represents the regularization parameter and 's ' the regularization order. They concluded that decreasing α leads to an increase in random errors and decrease in bias errors, whereas on increasing order of regularization, a decrease in bias errors was observed. Hansen (1994), provided a Matlab tool, which proved a boon for researchers working on ill-posed problems. Various regularization techniques had been covered for the discrete problems, with methods

suggesting the choice of regularization parameter.
Artyukhin and Nenarokomov (1984), developed an iterative computational algorithm, which they used to determine the set of coefficients of the inhomogeneous quasi-linear heat conduction equation by applying iterative regularization. Alifanov and Nenarokomov (1999), solved three-dimensional boundary IHCP for regular co-ordinates. Yang (1998) used a linear least square error method, which they applied on a linear model, where heat source was represented as a linear combination of unknown coefficients to be determined. The method worked on the linear domain where computations were to be performed once but according to the authors, the technique could be extended to various shapes on the spatial domain. Iterative regularization was performed by Nenarokomov *et al.* (2004) to regularize the ill-posedness of a specimen in a high-enthalpy dust-loaded flow. The corresponding convective heat flux was determined using the adjoint method. Su and Hewitt (2004), retrieved time-varying heat transfer coefficient in a heater tube. Alifanov's regularization had been applied for well-posedness where the temperature was measured using thermocouples. Conjugate Gradient Method (CGM) had been applied to minimize the error involved. A gradient of functional and direction of descent was obtained by solving adjoint and sensitivity problem respectively. The authors concluded that given the experimental values from any physical system, this type of inverse analysis was capable to retrieve heat transfer coefficient. Okamoto (2005) during his Ph.D., worked on Inverse Heat Conduction Problems (IHCP) and inverse solidification problems, with techniques like SVD, Tikhonov regularization and Levenberg-Marquardt method. He also studied methods to choose regularization parameters. Alifanov *et al.* (2004, 2008, 2009) studied the multilayer thermal insulation having application to thermal control systems of spacecraft. A new iterative method was then suggested to retrieve thermal parameters in the system. To determine the geometrical shape, an inverse technique using the variational approach along with the finite element method has been implemented by Wu (2009), where the temperature and heat flux on the surface were known. Lesnic and Mohsin (2012) applied a meshless method of fundamental solutions (MFS) to estimate inner boundary and surface heat transfer coefficients. The modified Helmholtz equation for a fin is a geometric inverse problem, which is stabilized by adding regularization terms in the non-linear objective function. Deolmi and Marcuzzi (2013), solved a parabolic inverse convection-diffusion-reaction problem, arising while estimating water and air pollution. The authors used Projected Damped Gauss-Newton (PDGN) and adaptivity for the cases when source location was known (a well-posed case) and when it was unknown (an ill-posed case) respectively. To eliminate ill-posedness, McMasters (2014) used regularization involving derivatives. Here time derivatives of measured data and sensitivity coefficients were used in pre-conditioning matrix, making the problem unbiased, unlike additive regularization. However, this regularization suffered from larger estimated errors, decreasing advantages of unbiasedness. Yang and Fu (2014) picked an inverse problem of determining space-dependent heat source and to make it well-posed, they proposed a mollification regularization method with Gauss kernel. Further 'a posteriori' parameter choice rule was also suggested for good error es-

timates. Tapaswini *et al.* (2015) gave a numerical solution using the concept of a fuzzy number together with the variational iterative method. Wróblewska *et al.* (2016), made use of Fourier transform to regularize IHCP. Two methods were presented, first one mimics TSVD, in which certain components of the Discrete Fourier Transform (DFT) were reduced and the second one regularized the solution using Tikhonov regularization in DFT domain. The authors observed that better results were obtained in a case when DFT was used, as the number of oscillations of the solution decreased significantly and a regularization parameter could be chosen optimally for this domain. Yu *et al.* (2017), introduced a new technique depending on BEM for inverse analysis of boundary conditions on the inner wall of the furnace. Usually in an iterative process, during inverse, the direct method is solved many times, decreasing the productivity and usefulness of technique whereas the current method involves direct computations only once while evaluating the inverse. Least-square-error method is employed to calculate the inverse. Numerical results found by Sarabadan *et al.* (2018), included solving 1-D and 2-D IHCP by applying Landau's transformation followed by satisfier function. In the two-dimensional case, the collocation method was applied, with regularization being done using Landweber's iterative method. The properties of polymers mainly composites were studied by Dmitriev and Zhivenkova (2018), where thermal conductivity and heat transfer coefficient were determined. The numerical method introduced an iterative algorithm, which converts a differential equation to the integro-functional equation. Vikulov and Nenarokomov (2019), explored the problem of identifying mathematical heat exchange models using a modified variational method of iterative regularization.

2.2 Inverse solution techniques

Having discussed the regularization techniques, there are plenty of solution techniques available which can be associated with regularization techniques. We are discussing mainly the three categories of these methods. A quick look at the classification of methods used to solve inverse problems is given in Fig.(2.2).

2.2.1 Analytical Methods

The exact solution to IHTP is called an analytical solution. Having a handful of analytical methods is necessary for any particular kind of problem because such methods provide a characteristic insight into the problem. As closed-form expressions are obtained, which behave as standard for other numerical methods. For IHTP, few attempts were made to find the exact solutions. Situations with only the effect of heat conduction were considered, with the further assumption that the temperature sensors are placed at random positions. Burggraf (1964) developed the very first exact solution. He gave the solution in terms of an infinite series of temperature function. He assumed that the information about temperature and heat flux both were available at those points where the temperature sensors were located. He also concluded that by the presence of temperature sensors at the center of a solid cylinder or sphere, heat flux becomes zero everywhere. The detailed solution could be found in a book by Beck *et al.* (1985),

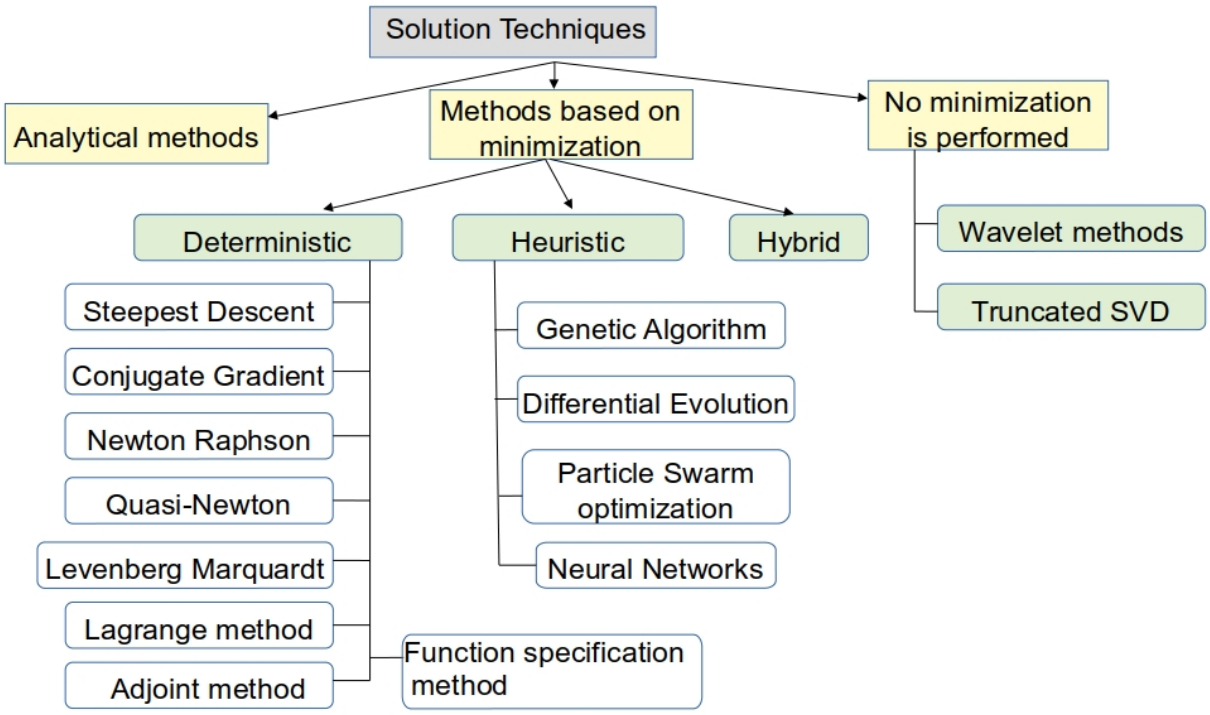

Fig. 2.2 Classification of methods to solve inverse problems

(chapter-2). The approach used in the analysis cannot be used for two-dimensions or where the temperature sensor present in the interior of the surface is more than one. Furthermore, the direct problem and higher-order derivatives must be calculated using numerical methods, which again introduces error. Along with these limitations, this analytical solution cannot be applied to problems involving temperature-dependent properties. Similar work by Langford (1967) was done. Thereafter, Koveryanov (1967) worked to determine heat flux, by differentiating the obtained temperature field. Imber and Khan (1972) used Laplace transform to evaluate the exact solution when the temperature measurements were obtained at different sensor locations. Hsieh and Kassab (1986), derived exact solution by separation of variables technique for the inverse problem of heat conduction when different boundary conditions were specified. The authors have also proved the uniqueness, convergence, stability and consistency of the obtained solution using the derived method. Zabaras and Mukherjee (1987) used boundary element method together with time-dependent Green's functions and convolution integrals to evaluate the motion of the solid-liquid interface in the solidification problem. Zabaras *et al.* (1988) used boundary element method together with Beck's sensitivity analysis for IHCP involving phase changes. Authors developed an Integral method to solve inverse problems, including design of casting processes. In 1989, an unknown heat source has been discovered Malyshev (1989) using integral transform technique. Yan *et al.* (1993) gave an exact solution of a two-layered composite structure in three-dimensions. The authors used Green's function to determine temperature using partitioning in time. Aviles-Ramos *et al.* (1998) gave an analytical series solution in case

of composite material made up of two layers, one orthotropic and other isotropic. According to the authors, the difficulty in the determination of heat flux at the surface in the conduction problem is due to the presence of singularities. To satisfy the nonhomogenous boundary conditions, a differentiable auxiliary function is introduced, which removes these singularities. Lesnic and Elliott (1999), solved IHCP using the Adomian decomposition method in conjunction with Fourier transformation. Thus, an exact solution is only available for IHCP, having constant properties. For calculation, infinite order derivatives of experimental data need to be calculated, which should on the first hand exist. Moreover, using small time steps, higher-order derivatives may dominate and thus give a misleading result. Laplace transform was utilized by Monde *et al.* (2003) to provide an analytical solution to IHCP, where direct measurements of temperatures were evaluated using the Spline method of third-order. The same approach had previously been applied to one-dimensional problems. A hybrid of two numerical procedures had been given by Chen and Wu (2007) where "finite difference-Laplace transform" and "experimental temperatures-least square method" was used to recover surface conditions. Temperature-dependent properties were used, where Taylor series was used to remove nonlinearity. Authors Chen and Wu (2008) again utilized this hybrid approach to estimate the heat transfer coefficient for the transient case in the two-dimensional domain. Authors Frąckowiak *et al.* (2015), took a Cauchy problem for the Laplace equation and solved the corresponding Poisson equation, to determine source function. The problem was converted from multiply to simply connected region.

2.2.2 Optimization Methods (based on minimization)

Various optimization methods are found in literature ranging from deterministic methods to stochastic/evolutionary methods. All such methods iteratively converge when the desired unknowns are obtained for which the objective function reaches the optimal value. The main goal here is to minimize the objective function

$$J = \|\tilde{T} - T(f)\|^2 = [\tilde{T} - T(f)]^T[\tilde{T} - T(f)], \tag{2.11}$$

where, '$\tilde{T}$' is the measured values of temperature (in case of heat transfer problems), '$T(f)$' is the estimated value of temperature (obtained from inverse analysis), 'f' is a random vector with known mean 'μ'.

Deng *et al.* (2008) found the radiative coefficient as a solution to IHCP by using a semi-discrete technique, which enlightened the theoretical aspects of 1-D inverse problems. The results for its existence, uniqueness and stability were proved in their work. Diligenskaya and Rapoport (2016) applied the method of minimax optimization to find the coefficient in the Neumann boundary condition for coefficient IHCP.

Type I: Deterministic Methods

Deterministic methods are the ones where a unique output is obtained corresponding to a given set of input variables. These methods are iterative in nature and are applicable to non-linear

minimization problems. These methods converge surely to the minimum of the objective function. Let 'f' denote vector of unknown parameter, 'z' be the search step size, 'o' be the direction of descent, 'j' is the iteration count, then the iterative formula, as stated in Alifanov (1994), Alifanov *et al.* (1995), Beck and Arnold (1977), Belegundu and Chandrupatla (1999), Dennis and Schnabel (1983), Fletcher (2000), Jaluria (1998), Stoecker (1989) is given by

$$f^{j+1} = f^j + z^j o^j, \tag{2.12}$$

where $f^{(0)}$ is the initial guess, which is decided according to the situation at hand. The sequence (2.12) converges to a unique solution, provided certain conditions are satisfied. Those methods in which direction of descent is using the gradient direction, are called gradient methods. The advantage of these methods over stochastic methods is that these methods are computationally faster and are based on a strong mathematical basis. However, in practice, one usually got stuck around a local minimum near initial guess.

Note:

1. An iteration step is acceptable if $J^{j+1} < J^j$, where J^j denotes the value of the objective for J at j^{th} term.

2. A gradient method of such kind is accepted if 'o' forms an angle greater than 90° with the gradient direction and 'o' generates an acceptable step iff there exists a matrix 'R' (positive definite) such that $o = -R\nabla J$, Bard (1974), ∇J is the gradient of the objective function to be minimized.

Convergence of gradient method: The convergence of a gradient method is guaranteed if the said objective function has no stationary points (a point where $\nabla J = 0$) and the method itself reaches some stationary point.

Assuming different procedures for finding the direction of descent 'o', various methods are discussed as follows:

(a) *Steepest Descent Method*

This is the most basic deterministic method. One usually tries to locate minimum such that least iterations should be performed, in a direction with a maximum change. One such available direction is that provided by negative of the gradient of the objective function Colaco *et al.* (2006). Thus, to locate minimum, the search direction is chosen as

$$o^j = -\nabla J(f^j). \tag{2.13}$$

However, being an obvious choice for the descent direction, the method is not that efficient. Initially, when the method starts, the rate of convergence is fast taking a large change in the descent direction, but once the solution approaches minimum, the rate of convergence becomes

small. Some classical techniques to choose 'z' (search step size), for unimodal function are Dichotomous Search, Fibonacci Search, Golden Search, Cubic interpolation, etc. If it is not unimodal, then exhaustive search method or technique based on exhaustive interpolation is used. Although the method seems quite easy to implement with an assured minimum, it may not be global and may mislead in some cases. The algorithm for the steepest descent method is given in Fig.(2.3).

Péneau *et al.* (1995) devised a shape identification method by minimization of the objective function using descent methods to determine heat flux at the boundary of IHCP. According to the authors, the prime difficulty in the application of the algorithm lies in the calculation of the matrices involved and their sensitivity due to the presence of the measurement errors. Huang *et al.* (2003) solved an inverse problem in imaging where the heat transfer coefficient was required to be determined for the plated, finned tube heat exchanger's surface, in the three-dimensional space. The inverse analysis has been done using the steepest descent method, where the temperature measurements were made using infrared thermography. Authors concluded that no 'apriori' information regarding the unknown parameter was required and the obtained estimates were satisfactory.

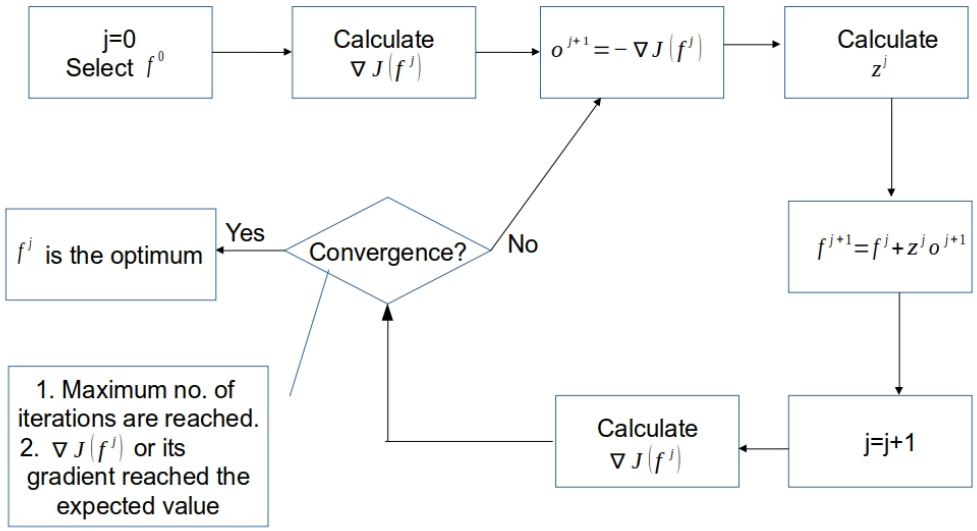

Fig. 2.3 Flowchart for Steepest Descent Method.

(b) ***Conjugate Gradient Method (CGM)***

In this method the descent direction is selected as a linear combination of gradient directions and search direction 'o' from the previous iteration Alifanov (1994), Alifanov *et al.* (1995), Belegundu and Chandrupatla (1999), Jaluria (1998), Özışık and Orlande (2000), Stoecker (1989) as

$$o^j = -\nabla(f^j) + \gamma_1^j o^{j-1} + \gamma_2^j o^i, \tag{2.14}$$

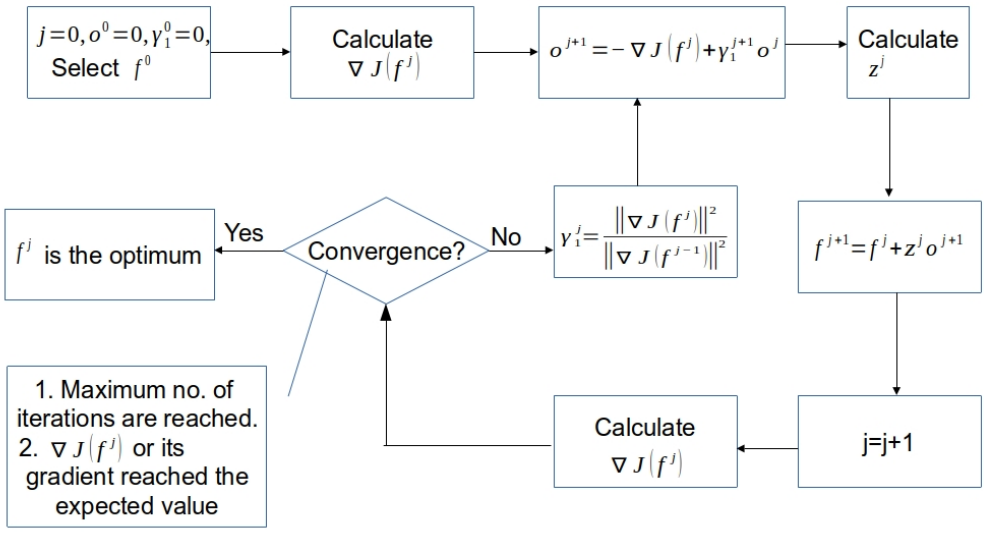

Fig. 2.4 Flowchart for Fletcher Reeves version of Conjugate Gradient Method.

where γ_1^j, γ_2^j are called conjugate coefficients, 'i' represents the iteration number where restarting strategy is required. The advantage of this method over the steepest descent method is its faster convergence rate. Based on different γ_1^j, γ_2^j, different conjugate gradient methods are available.

1. Fletcher Reeves Version
   The method was introduced in Fletcher (2000), Fletcher and Reeves (1964) and here we take

$$\gamma_1^j = \frac{\|\nabla J(f^j)\|^2}{\|\nabla J(f^{j-1})\|^2}, \quad \gamma_1^0 = 0, \qquad j = 1, 2, \ldots,$$

$$\gamma_2^j = 0, \qquad j = 0, 1, \ldots, \tag{2.15}$$

   where $\|.\|$ is the Euclidean norm. Flowchart for Fletcher Reeves version is shown in Fig.(2.4).

2. Polak-Ribiere Version
   This method was introduced in Polak (1971), with

$$\gamma_1^j = \frac{[\nabla J(f^j)]^T[\nabla J(f^j) - \nabla J(f^{(j-1)})]}{\|\nabla J(f^{j-1})\|^2}, \quad \gamma_1^0 = 0,$$

$$\gamma_2^j = 0, \qquad j = 0, 1, \ldots. \tag{2.16}$$

3. Powell-Beale's Version

This method was given by Beale (1972) and Powell (1977), with

$$\gamma^j = \frac{[\nabla J(f^j)]^T[\nabla J(f^j) - \nabla J(f^{(j-1)})]}{[o^{j-1}]^T[\nabla J(f^j) - \nabla J(f^{(j-1)})]}, \quad \gamma^0 = 0,$$

$$\gamma_2^j = \frac{[\nabla J(f^j)]^T[\nabla J(f^{i+1}) - \nabla J(f^i)]}{[o^i]^T[\nabla J(f^{i+1}) - \nabla J(f^i)]}, \quad \gamma_2^0 = 0, \qquad j = 1, 2, \ldots . \tag{2.17}$$

Colaco and Orlande (1999) compared all the CGM methods, namely Fletcher-Reeves, Polak-Ribiere and Powell-Beale. They analyzed cooling of continuously cast slabs using sprays, by recording directly the temperature in the plate, with known physical properties, initial conditions, boundary conditions, heat transfer coefficients. Cooling occurred by convection, where thermal conductivity and heat flux were assumed to be temperature-dependent. Obtaining temperature from direct analysis, the dimensionless heat transfer coefficient was determined by all the three methods, for comparison and it was reported that Powell-Beale's version is the best among others.
Note: Restarting is required and is done by making $\gamma_2^j = 0$, when gradients at forthcoming iterations become

- either non orthogonal (which measures non linearity of the problem) and is checked by

$$|[\nabla(f^{j-1})]^T\nabla(f^j)| \geq 0.2\|\nabla(f^j)\|^2, \tag{2.18}$$

- or when 'o' is not sufficiently downhill, which is identified by

$$[o^j]^T\nabla(f^j) \leq -1.2\|\nabla(f^j)\|^2, \tag{2.19}$$

$$[o^j]^T\nabla(f^j) \geq -0.8\|\nabla(f^j)\|^2. \tag{2.20}$$

Algorithm for CGM: For $j \geq 1$, steps of the algorithm are as follows:

1. Test the inequality (2.18), If true, set $i = j - 1$
2. Compute γ^j
3. If $j = i + 1$, set $\gamma_2^j = 0$
   If $j \neq i + 1$, compute γ_2^j
4. Compute o^j using (2.14)
5. If $j \neq i + 1$, test (2.19),(2.20). If either is true, set $i = j - 1$ and $\gamma_2^j = 0$. Then again calculate search direction using (2.14).

The conjugate gradient method reduces to steepest descent method if $\gamma^j = \gamma_2^j = 0$.

Huang and Yan (1996) worked on a nonlinear problem of determining heat capacity per unit volume, depending on temperature. Use of CGM, without any prior information, solved the purpose. Prud'homme and Nguyen (1998) used CGM as a regularization tool to find the solution to IHCP and determined transient flux at the boundary. The authors observed that CGM acted as a filter to random noises, with the iteration count as a regularization parameter, providing the basic higher frequency components at a later stage. Huang and Tsai (1998) utilized CGM, which was based on the Boundary Element Method (BEM) to retrieve time-dependent boundary heat flux in an irregular, multidimensional domain, regularizing the problem iteratively. The method remains stable even when fewer sensors were used, which in turn increased the measurement errors. Huang and Wang (1999) solved a three-dimensional IHCP, again to deduce heat flux at the boundary. This time the domain was 3-D, where CGM was applied in conjunction with a commercial code namely CFX4.2 (which generally are used to solve fluid and thermal problems, where communication between two occurs via data transportation). The authors used CFX4.2 code as a subroutine to CGM. Dowding and Beck (1999) used a sequential approach to solve IHCP, where CGM has been used, using adjoint equations and Tikhonov regularization is implemented, including prior information to stabilize the solution. Khachfe and Jarny (2000) solved two-dimensional non-linear problem using finite element method for direct analysis and CGM for inverse analysis. Regularization is done using iterative principle. To design the shape of the surface containing heating element, Cheng *et al.* (2003) used CGM. The steady-state conduction equation for solid has been solved in 2-D space, where the medium was considered homogeneous and isotropic. To determine the surface temperature, optimization tools such as direct problem solver, direct differentiation sensitivity analyzer and numerical grid generator were used in succession. Cheng and Chang (2003) used CGM to estimate the geometry, involving shape and location, with known temperature measurements, obtained using installed thermocouples. The task has been accomplished by using tools like curvilinear grid generation scheme, direct problem solver, redistribution method and CGM, tested on five different shapes, i.e., outer(o) ellipse-inner(i) ellipse, o ellipse-i eccentric ellipse, o ellipse-i circle, o circle-i rectangle and o-circle-i circle. Saker and Orlande (2004) solved the problem of estimating heat and mass transfer coefficients using CGM, where the function needs to be estimated at the surface of a drying-capillary porous body. Kim and Daniel (2004) used a gradient method to study 1-D heat conduction for nanoscale structures. The Boltzmann transport equation was used for modelling. One boundary was exposed to known conditions, other to unknown temperature. The authors used the sensitivity and adjoint equations, along with the discrepancy principle to fix the regularization parameter. The solution to hyperbolic IHCP was calculated using CGM by Huang and Wu (2006) where time-dependent heat flux at the boundary was required to be estimated. Results showed that CGM performs better as it was not sensitive to measurement errors and phase errors. Hào *et al.* (2009) formulated a transient, multidimen-

sional IHCP using a variational approach to determine the initial conditions. CGM along with splitting method was used for the solution, where no additional regularization was required to be done, showing a faster convergence. Lu *et al.* (2012), solved the time-dependent 3-D IHCP again using a combination of CGM and Tikhonov regularization. Fazeli and Mirzaei (2012) detected the location, size and shape parameters of defects in a solid using CGM. The forward analysis used the finite element method. Defects like porosity, poor cure and crack were identified using iterations, till an exact shaped was recovered. An adjoint optimization method based inverse analysis has been done by Ferlauto (2014) to design cooling passages of the turbine blade. The obtained results have been compared with theoretical (analytical), experimental data (obtained from literature) and numerical data (using finite element). Cui *et al.* (2014) proposed a modified Conjugate Gradient Method (MCGM) to retrieve temperature-dependent thermal conductivity. Complex variable differentiation method (CVDM) is used for sensitivity analysis. This altered version allows CGM to work independent of forward analysis, which reduces a considerable amount of computations, showing its effectiveness. An algorithm based on CGM and discrepancy principle was applied by Chen *et al.* (2014) on a hyperbolic IHCP to determine flux, used in 2-D cylindrical pin fins. Determination of time-dependent as well as steady convective boiling heat transfer coefficient by Farahani *et al.* (2014) of nanofluid in a rectangular channel. The direct analysis was done using the finite element method, and inverse using the sequential CGM scheme. Haghighi *et al.* (2015), evaluated pressure and heat flux in functionally graded cylindrical shells, as a function of both space and time using CGM with discrepancy principle. The recent work includes Jolly and Autrique (2016), who used a semi-analytic CGM, Farzad and Mathieu (2016) for evaluation of conductivity, flux and heat transfer coefficient in the three-dimensional domain, Mohebbi *et al.* (2017) to estimate thermal conductivity, as a linear function of temperature. Moftakhari *et al.* (2017) predicted heat flux and heat transfer coefficient using CGM, where the direct problem was solved using the differential quadrature method. The transient IHCP involved functionally graded multilayered cylinders, where formulation being done using non-Fourier heat transfer. A steady-state IHTP of irregular fins made of functionally graded material was solved by Chen *et al.* (2017a) for unknown heat flux again using CGM and the discrepancy principle, with known temperature values, obtained from forward analysis. Nenarokomov *et al.* (2018) studied the effects of elastic thermal protection of non-linear acoustic using CGM. Nenarokomov *et al.* (2019) solved a geometric inverse problem of radiative heat transfer to determine the angles of orientation of a spacecraft. Authors used CGM for minimization.

(c) *Newton Raphson Method*

This method uses the second derivative of the objective function 'J' (i.e., computing the Hessian matrix, 'D^2J'), while the previous methods (SD, CG) used gradients (∇J) of 'J'. The advantage of this method over others is its faster convergence rate (quadratic specifically). But at the same time, this method is computationally costly as the calculations involved in evaluat-

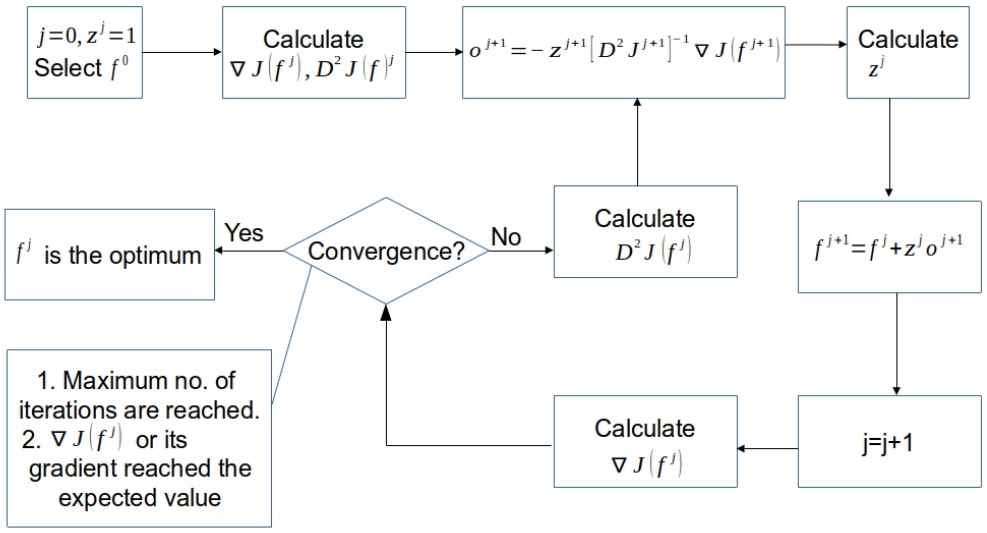

Fig. 2.5 Flowchart for Newton-Raphson Method.

ing Hessian matrix are expensive. Let us consider a twice differentiable objective function 'J'. Writing the Taylor series of J at $f^j + e$, with e as a small increment,

$$J(f^{j+1}) = J(f^j + e) = J(f^j) + \nabla J(f^j)^T e + \frac{1}{2} e^T D^2 J(f^j) e + \mathcal{O}(e^3). \tag{2.21}$$

On rearrangement,

$$\nabla J(f^j + e) = \nabla J(f^j) + D^2 J(f^j) e. \tag{2.22}$$

For an objective function to be minimized, the gradient should vanish necessarily, i.e., $\nabla J(f^j + e) = 0$. Hence $e = -[D^2 J(f^k)]^T \nabla J(f^k)$ and the vector that optimizes $J(f)$ is

$$f = f^j - [D^2 J(f^j)]^{-1} \nabla J(f^j). \tag{2.23}$$

The search direction is taken as $o^j = -z^j [D^2 J(f^j)]^{-1} \nabla J(f^j)$. Newton's method guarantees to converge to the extreme point of J disregarding the fact, that it is a maximum, minimum or a saddle point. The method is described in Beck and Arnold (1977), Jaluria (1998), Belegundu and Chandrupatla (1999), Broyden (1965), Broyden (1967). The flowchart for Newton-Raphson method is shown in Fig.(2.5) below. A non-linear time-dependent IHCP, involving radiative heat transfer at the boundary was studied by Mehta (1984) using finite differences and Newton-Raphson, Regula-Falsi numerical iterative methods.

(d) *Quasi-Newton Method*

Due to high computational costs involved in Newton's method, and still higher cost when the problem under consideration is large, a method was needed which could decrease these costs but reduces the rate of convergence obtained using Newton's method. Thus, Newton's method was modified by approximating the inverse of Hessian matrix using first derivatives as $G^j =$

$[D^2J(f^j)]^{-1}$ and subsequently search direction becomes $o^{j+1} = -G^j \nabla J(f^j)$. G is recursively calculated as

$$G^j = G^{j-1} + M^{j-1} + N^{j-1} \qquad \text{for } j = 1, 2, \ldots \quad \& \, G^j = I, \quad \text{for } j = 0. \tag{2.24}$$

Based on different values for M and N, various methods are discussed as follows:

1. Davidson-Fletcher Powell Method

$$M^{j-1} = z^{j-1} \frac{o^{j-1}(o^{j-1})^T}{(o^{j-1})^T Y^{j-1}}, \tag{2.25}$$

$$N^{j-1} = -\frac{[G^{j-1}Y^{j-1}][G^{j-1}Y^{j-1}]^T}{[Y^{j-1}]^T G^{j-1} Y^{j-1}}, \tag{2.26}$$

where $Y^{j-1} = \nabla J(f^j) - \nabla J(f^{j-1})$. The limitation of this method is that some errors are propagated as G is calculated iteratively and method requires a restart after certain iterations. Another weak point of the method is that it is very sensitive to the choice of z, because M depends on z.

Tervola (1989) investigated temperature-dependent thermal conductivity, given measured temperature profiles, constant density and temperature-dependent specific heat in a homogeneous material. The problem was solved in 1-D space as time-dependent, where the finite element with predictor-corrector was implemented for forward and Davidson-Fletcher Powell Method for inverse analysis.

2. Broyden-Fletcher-Goldfarb-Shanno (BFGS) Method
The advantage of using this method is that it is less sensitive to the choice of 'z' and thus is often used in computations. This method was introduced by Fletcher and Powell (1963), Broyden (1965, 1967). The flowchart showing BFGS Quasi-Newton algorithm is shown in Fig.(2.6) ahead.

$$M^{j-1} = \left[\frac{1 + (Y^{j-1})^T G^{j-1} Y^{j-1}}{(Y^{j-1})^T o^{j-1}}\right]\left[\frac{o^{j-1}(o^{j-1})^T}{(o^{j-1})^T o^{j-1}}\right], \tag{2.27}$$

$$N^{j-1} = -\frac{o^{j-1}(Y^{j-1})^T G^{j-1} + G^{j-1} Y^{j-1}(o^{j-1})^T}{(Y^{j-1})^T o^{j-1}}. \tag{2.28}$$

To locate global optimum, Li *et al.* (2012) developed a filled function method in unison with the BFGS algorithm to solve IHCP. Further, Tikhonov regularization was implemented, where the efficiency of the proposed technique was ensured by numerical simulations. A generalized objective function was also proposed here. In ultrasonic welding to avoid defects and to maintain quality, convection heat transfer coefficient and transient heat generation were found by Ngo *et al.* (2015) using the BFGS method. They have compared their method with the previous CGM and its simplified version. Associated forward problem was solved using a hybrid spline

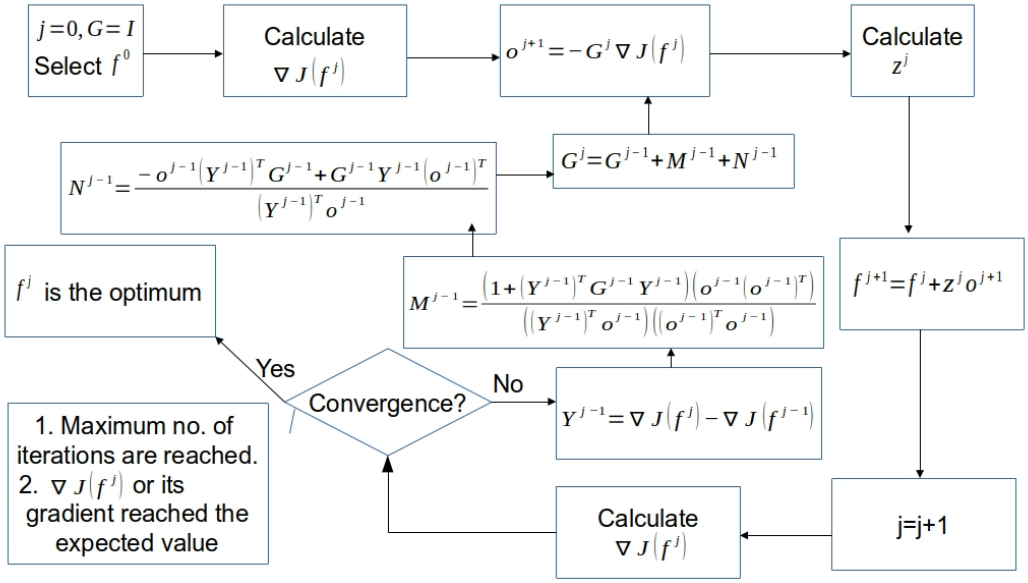

Fig. 2.6 Flowchart for BFGS version of Quasi-Newton Method.

difference method. Hematiyan *et al.* (2015) displayed another numerical inverse method to identify six segments of a thermal conductivity tensor with a self-assertive shaped body in a 3-D anisotropic domain, using BEM for forward calculations and damped Gauss-Newton technique was embraced for the inverse analysis with numerical examples ensuring trustworthy solutions with estimations, which were quite different from correct solutions. To investigate the evolution of unknown boundary heat flux, Mobtil *et al.* (2018) used the quasi-Newton method along with Variable Metric Method (VMM) for the circular fin used in the staggered finned tube exchanger assembly. An experimental study has been done, the direct problem to determine temperature was solved by applying finite element for space variable and Crank-Nicholson for time variable.

(e) *Levenberg-Marquardt (LM) Method*

Marquardt (1963) modified Levenberg's method, Levenberg (1944) to build a technique which tends to steepest descent method in the vicinity of initial guess and to the Gauss method in neighbourhood of ordinary least square term. This method converts G (a matrix that approximates to Hessian) into a positive definite matrix (say matrix B), then the search direction is given by

$$o^j = -(B^j + \lambda^j P^j)^{-1} \nabla J(f^j),\ z^j = 1. \tag{2.29}$$

Here P is a diagonal matrix having elements as the absolute value of diagonal elements of B. This method is based on the observation that, if B is positive definite, then $B + \lambda P$ is positive definite for sufficiently large 'λ', Bard (1974).

Levenberg Marquardt method was implemented to determine temperature-dependent thermal conductivity and heat capacity in 1995 by Sawaf *et al.* (1995). A paper by Taler (2007), displayed two procedures namely, LM and SVD to estimate the heat transfer coefficient taken as

a function of space variable on the boundary of a smooth tube. The authors concluded that the two methods provide approximately the same results. For LM, initial parameter selection was difficult and computation required huge time, but the method could be applied to the diversified problem. In contrast, SVD saved computational time. Another limitation in the use of LM is non-availability of a general technique for precisely computing sensitivity coefficients except the available numerical differentiation strategies. Cui *et al.* (2016a) proposed a modified LM method where a complex variable differentiation method had been suggested for sensitivity coefficients. A time-dependent, non-linear IHCP was studied to investigate various parameters of boundary flux. The outcome demonstrated that altered method was better in terms of accuracy and effectiveness. Cui *et al.* (2017) presented a new algorithm, relating the damping factor specifically to the objective function. Efficiency and convergence were influenced by the damping factor and hence played a vital role in inverse computations. Temperature-dependent conductivities were determined precisely and the method proved to be robust for easily calculating damping factors. A combination of the weighted least square method and LM method was provided by Wang *et al.* (2017) to recover heat transfer coefficient for continuous casting, using temperature measurements, which usually contained large measurement errors. Recent literature includes work by Hafid and Lacroix (2018) where parameters like flux and conductivities (temperature-dependent) were evaluated inside melting furnaces. Inverse algorithm LM in conjunction with Broyden method was introduced for the solution, which provided accurate results compared to the classical LM method. Besides, location and installation of sensors were also suggested.

(f) *Lagrange Method*

To minimize or maximize an objective function, subject to equality constraints, Lagrange multipliers are used. Let $f = [f_1, f_2]^T$ represents an unknown solution to the following optimization problem.

$$\begin{aligned} &\text{Minimize } J(f) \\ &\text{subject to } S(f) = 0 \end{aligned} \tag{2.30}$$

One way to solve for f is by reducing it to one variable, provided f_2 is a function of f_1 or vice-versa. In such a case, the problem reduces to 'Minimize $J(f_1, f_2(f_1))$'. If there is no such explicit relation between the unknowns, then the other way is to reformulate the problem as 'Minimize $\mathscr{L} = J(f, \psi) = J(f) - \psi S(f)$', where ψ is a constant called Lagrange's multiplier, Woodbury (2002). The next task is then to determine all the stationary points (points where $d\mathscr{L} = 0$) of $\mathscr{L}$, and to inspect what point corresponds to the minimum J. To determine the stationary points of the Lagrangian $\mathscr{L}$, one must find

$$\nabla \mathscr{L} = \left(\frac{\partial \mathscr{L}}{\partial f_1}, \frac{\partial \mathscr{L}}{\partial f_2}, \frac{\partial \mathscr{L}}{\partial \psi} \right) = 0.$$

Determine $\psi,\ f_1,\ f_2$ by solving three algebraic equations,

$$\frac{\partial \mathscr{L}}{\partial f_1} = 0,\ \frac{\partial \mathscr{L}}{\partial f_2} = 0,\ \frac{\partial \mathscr{L}}{\partial \psi} = 0.$$

Non-linear IHCP was solved by El Bagdouri and Jarny (1987) to determine heat flux. The problem was formulated as a minimization problem where CGM was used to minimize the associated Lagrangian. Badrinarayanan and Zabaras (1996) performed a sensitivity analysis for the optimal design of metal-forming processes. Here, the process conditions were selected for the design state and the geometry of the product, initial workpiece conditions, material state were known a priori. The process used was minimization of Lagrangian. Agazzi *et al.* (2014) applied Lagrangian in conjunction with conjugate gradient method to determine the fluid temperature for cooling system design in injection moulding.

(g) *Adjoint Method*

This method is a generalization of Lagrange's method in which the number of unknowns to be detected and the number of constraints is high. In this case, the Lagrangian is a function of both the input and output parameters unlike Langrange's method, where the Lagrangian depends only on the input parameter. Adjoint method neither depends on the mathematical models nor on the unknown variable to be determined. Suppose the constraints in f and m be n algebraic equations. Let $S[m, f]$ denote the vector consisting of all the equality constraints. Now, the Lagrangian

$$\mathscr{L}(m, f, \psi) = ||Kf - m||^2 - < \psi, S(m, f) > .$$

As the Lagrangian is a function of m and f both, therefore, these are considered independent variables inside Lagrangian. For a case when output parameter m depends on f, i.e. $m(f)$, then the Lagrangian equivalent to the Least Square criterion.

$$\mathscr{L}(m(f), f, \psi) = ||Kf - m(f)||^2 - < \psi, S(m(f), f) >= W(f),$$

where

$$W(f) = ||Kf - m(f)||^2.$$

Then constant ψ is calculated such that the derivative of the Lagrangian is zero.

$$\begin{aligned} d\mathscr{L} &=< \nabla_m W, \Delta m > - < \psi, [\nabla_m S^T]^T \Delta m + [\nabla_f S]^T \Delta f > \\ &=< \nabla_m W - [\nabla_m S^T]\psi, \Delta m > - < [\nabla_f S^T]\psi, \Delta f > . \end{aligned}$$

Let ψ be such that it is the solution of the linear equation,

$$\nabla_m W - < [\nabla_m S^T]\psi, \Delta m >= 0,$$

$$\text{or } < [\nabla_m S^T]\psi, \Delta m >= -2(Kf - m).$$

This equation is called the adjoint equation. The stationary condition of the Lagrangian i.e., $d\mathscr{L} = 0$ is reduced to

$$< [\nabla_f S^T]\psi, \Delta f >= 0 \quad \forall\, \Delta f,$$

which also determines the gradient in the gradient equation. Thus the stationary points are the points which are then obtained by solving the following (2n+p) algebraic equations, with p representing the number of constraints.

$$\begin{aligned} S[m(f), f] &= 0, \\ [\nabla_f S^T(m(f), f)]\psi &= 0, \\ [\nabla_m S^T(m(f), f)]\psi &= -2(Kf - m(f)). \end{aligned}$$

Furthermore, the solution of the above equations could be calculated using various gradient algorithms discussed above. For a detailed discussion, one can refer books by Woodbury (2002) and by Özışık and Orlande (2000). A multidimensional IHCP was solved by Jarny *et al.* (1991) using adjoint equation coupled with CGM. No a priori information was required about the unknown heat flux. Samai *et al.* (1993) used adjoint equation for the estimation of heat flux for the identification of solidification location. Neto and Özişik (1992) solved a two-dimensional inverse heat conduction problem using a combination of conjugate gradient method and adjoint equations. The authors estimated time-varying strength of a line heat source, where no a priori information was available. Kang and Zabaras (1995) used Conjugate gradient method in conjunction with adjoint method to calculate boundary cooling conditions in two-dimensional solidification processes. Huang and Jan-Yuan (1995) implemented the adjoint method in conjunction with the conjugate gradient method to retrieve temperature-dependent conductivity and heat capacity. Bailleul *et al.* (2003) used adjoint equation in combination with CGM to monitor temperature variations in the composite materials. Adjoint Method together with Modal Identification Method was implemented on IHCP by Favennec *et al.* (2006) to obtain reduced models. Nenarokomov *et al.* (2016) developed a heat flux sensor for ablative thermal protection of spacecrafts using the adjoint method. Nenarokomov *et al.* (2017) again studied the radiative heat transfer in a multilayer thermal insulation of a spacecraft where authors determined radiative heat transfer by conducting experiments and computation was done the using adjoint method.

(h) *Function specification method*

The method was initially given for IHCP, where the unknown to be determined was heat flux. The method is named so, as the functional form of unknown to be determined is assumed. The assumed function could be defined as a sequence of constant pieces, straight-line segments. These could also be polynomials (degree greater than one) or exponentials as a function of time. To determine the unknown, the remaining task is to retrieve these values at certain predefined time steps. One way to do is to calculate unknown at all time steps simultaneously, which is the whole domain approach. Another way involves the determination of unknowns sequentially in

time. First one involves the determination of the assumed function at one stretch whereas, in second case small portions are calculated for the initial time and the successive pieces are then determined, marching forward in time. According to Beck *et al.* (1985), a sequential method is computationally faster as fewer calculations are performed for each time step.

Frank (1963) and Davies (1966) gave a whole domain estimation to solve IHCP, where they assumed heat flux as a polynomial function of temperature and used least squares estimation method. The sequential approach was given by Beck (1970). Beck (1979) provided a ground for comparison of methods for inverse analysis, where accuracy, stability and errors were the comparison parameters. For linear IHCP, the procedure involves the assumption of the functional form of heat flux for time steps greater than t_M. For time steps previous to t_M, heat flux values were known a priori. Thereafter, the least-squares objective function between measured and exact temperatures is constructed, which need to be minimized for the assumed functional form. The process of minimization returns heat flux at t_M time step. The process is then repeated for M replaced with $M + 1$ until all heat flux components are determined. Alifanov and Nenarokomov (2001) solved boundary IHCP using spline approximation and iterative regularization. To retrieve heat source in IHTP, a numerical technique has been devised in Fatullayev (2002), using over specified data, which estimates, heat sources using linear polygon pieces, which were evaluated continuously from the minimization problem. Alifanov *et al.* (2012) estimated thermal and thermokinetic properties of certain advanced materials having application to inflatable spacecraft structure. The unknown temperature-dependent properties were assumed to be a function of cubic B-splines. Again, simultaneous estimation of temperature-dependent thermal conductivity, heat capacity and integral emissivity was done by Nenarokomov *et al.* (2012). The unknown functions were assumed to be represented in cubic B-splines. The solution was found for insulating materials and the corresponding regularization was iterative in nature.

Type II: Heuristic Methods

Heuristic algorithms are those which learn by themselves. Evolutionary algorithms are the one among the pool of heuristic algorithms. Evolutionary methods are nature-inspired methods based on biological evolution. These algorithms mimic the natural processes like the behaviour of birds or ants, evolution in species or changes in genes, resulting in the best solution ultimately. The solution taken initially improves itself in each iteration (also termed as a generation) stochastically by applying certain random changes. These changes would be good or bad. The best solutions with desired characteristics are kept, discarding the bad ones. This selection is done by constructing an objective function (also called fitness function). The solutions or candidates having higher fitness improve the population leading gradually towards the best solution (called global optimum) among all. Unlike deterministic methods, evolutionary methods do not evaluate the gradient of the objective function and hence are not based on a strong mathematical basis.

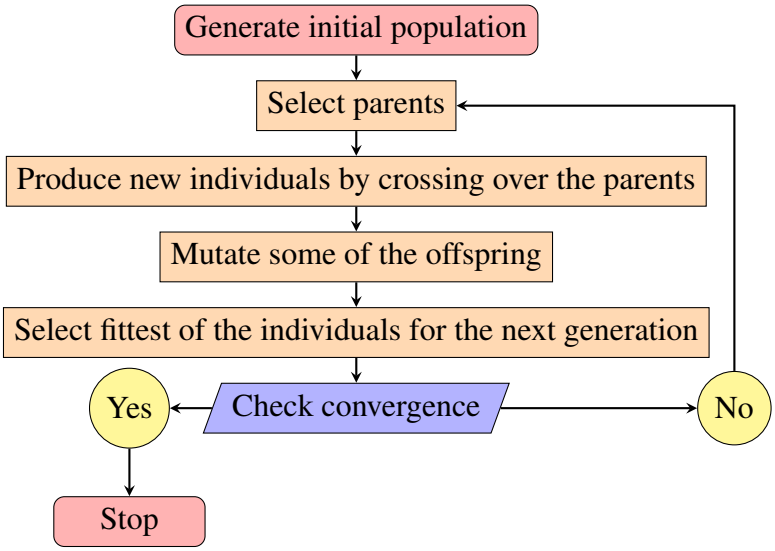

Fig. 2.7 Evolutionary process

Suram and Bryden (2004), developed an evolutionary algorithm, which did not require any additional regularization parameter, instead the authors worked on the stability by altering the fitness criteria, using minimization in variance of unknown temperature. In the manufacturing process involving laser, Kumar *et al.* (2019) developed a heuristic algorithm to find the thermal conductivity, heat transfer coefficient and absorptivity of the material. The most important stochastic methods, namely genetic algorithm, differential evolution and particle swarm optimization will be discussed ahead. The basic algorithm used in any evolutionary process for the determination of minimum is summarized in the chart 2.7.

(a) *Genetic algorithm*

Genetic algorithm is one of the first and most basic of the evolutionary algorithm developed by Holland (1992), De Jong (1975). The basic idea involved in its working is based solely on Charles Darwin's work on biological evolution, involving natural selection based on genes. The process of crossing over genes followed by mutation and selection is replicated by this algorithm in a form to find the best of individuals (or solutions) by repeated application of crossover, mutation and selection operators defined uniquely for different problems.

The algorithm starts by creating an objective function $J(f) = (f_1, f_2, .., f_d)$, a d-dimensional vector which needs to be minimized. This function defines the fitness of each solution, each of which is stored as a set of strings often called chromosomes. Then an initial population is created with a size P, selected such that its range usually varies from 40 to 200. Larger values of P mean that more evaluations and hence large computational cost whereas smaller P either leads population towards extinction, as lesser evolution occurs or a local optimum is obtained instead of the global one. Two solutions, (or parents) are then selected from the population. This selection could either be random or solutions with higher fitness are selected. These so-

lutions are operated with crossover operator, replacing parts of solution with another solution, such that, a new blended solution along with mixed convergence is created. For a crossover, a crossover probability 'C' is defined with an optimal range of 0.7-1. For effective evolution, a large crossover is required for faster convergence as with lower 'C' values, evolution will occur at dispersed locations. Once a new solution is obtained, the mutation operator is applied, which is responsible for changing a particular part of the solution. The need for such an operator is to diversify the solution and to help avoid local minimum. For faster evolution, mutation at multiple-step is performed but large mutations may be a hurdle for convergence. A mutation probability 'M' is defined as a number in the range 0.001-0.05. If a large 'M' is selected, then the solution might jump to and fro rapidly and may not reach a minimum in a due course of time. As a new solution is mutated, selection between parent and offspring (new solution) is done based on the fitter solution. A solution with lesser objective value (in case of minimization) is labelled fit to be retained in the population, thus completing the first iterative step. The process again repeats itself for many generations of solutions until a global minimum is reached.

Raudenský *et al.* (1995) illustrated the use of GA in estimating the solution of IHTP. Their report answered every question relating to the application of GA on IHTP and to know the basics of the method, one is recommended to go through the report. Liu (2008) developed the modified GA which reduced the computation time as compared to the classical GA. Here cost function was also added which enhances the computational efficiency, which in turn chooses the best genes for newer generations. Czèl and Gróf (2012) used GA to determine the temperature-dependent conductivity of a solid material. In this work, authors, modified GA as previously done by Liu and rearranged the entities to make a total of three algorithms, each of which gave better convergence and accuracy in comparison to the traditional GA. Pourgholi *et al.* (2014) estimated the unknown boundary condition in the IHCP by using parallel real-valued GA using the sequential and multicore approach. Crank Nicholson scheme has been used in the direct calculation and numerical results were presented with no requirement to add regularization terms. Singla and Das (2014), used GA in combination with Adomian Decomposition Method (ADM) to study the effects of conduction, convection and radiation in a moving fin, to determine heat transfer coefficient, thermal conductivity and velocity of moving fin. Their method was compared with the simplex search method and simulated annealing. He *et al.* (2015) investigated the steady-state thermal conductivity. A multi-objective optimization problem is then solved using radial basis functions (RBF) in association with Non-dominated Sorting GA (NSGA-II), which increases the efficiency and robustness of the solution.

(b) *Differential Evolution*

The most popular stochastic method, Differential Evolution (DE) is one of the most reliable algorithms used by researchers which is based on the idea of evolution in species. Given in 1997 by Storn and Price (1997), this algorithm is an imitation of the natural process of evolution working on "Survival of the fittest". Out of a whole lot of the population, few individuals

with different characteristics are selected at random and are allowed to mate, resulting in the formation of a newer generation of individuals having entirely different properties as their parents. The newly generated individuals may be good or bad, depending on the characteristics they randomly inherit from their parents. The offspring with good characteristics are kept and are again allowed to mate to produce even better individuals of the second generation. This process continues until the best possible characteristics of the individual are obtained, which were required. The main outline of the algorithm involves keeping these good or fit individuals from the population by the application of three operators namely Mutation, Crossover and Selection.

In IHTP required temperature is obtained either by measuring the values experimentally or are calculated by forward analysis with approximate values of unknowns. All unknown quantities (say n in number) are expressed in a single vector. The algorithm aims to minimize the objective function

$$J = \sum_{i=1}^{I} (T_i - \tilde{T}_i), \tag{2.31}$$

where $\tilde{T}$ is the available temperature with errors or exact value of temperature obtained either experimentally or by forward analysis. T is the temperature with a guessed value of unknowns.

The first step is to generate a large population (say 100 times of the previous) of all possible solutions, of length n for the given problem. These solutions can either be guessed or can be generated randomly, using any of uniform, exponential, binomial or normal distribution. For a particular vector in the population (say a_1) called the parent vector, three vectors (say $a_2,\ a_3,\ a_4$) from the population are chosen randomly. Then the mutation operator is performed on these three vectors. The modified vector or the mutant (say b_1) is obtained using the expression

$$b_1 = a_2 + F(a_3 - a_4), \tag{2.32}$$

where F is called the scaling factor, chosen randomly. F$\in$ [0,2] in theory, but in practice F$\in$ (0,1), in fact (0.7,0.9) is a good choice for beginners. DE is more sensitive to the value of 'F' than 'C' defined ahead. The operation, discussed above, is the most common mutation operation, although different kinds of mutant vectors can be used here. On a closer look at mutation operator reveals that the difference of two vectors is involved in the calculation. This difference eventually decreases as DE evolves over generations because initially in the search space of possible solutions, generated randomly, the magnitude of the difference vector is large. As DE evolves, better solutions are obtained in successive iterations (or generations) resulting in the lower magnitude of the difference vector. Hence the name differential is justified as is evolutionary.

Next step is to apply the crossover operator. Here, the next generation vector (often called

offspring or child) is generated via crossover operation defined as

$$c_1 = \begin{cases} b_1 & : \text{if } r \leq C \\ a_1 & : \text{if } r > C \end{cases} \tag{2.33}$$

here 'r' is the random number in (0,1) and 'C' is the crossover factor (probability)$\in$ [0,1], which decides in what proportion the characteristics of the original vector (parent vector) are retained in the formation of the new offspring vector. The most common usage is C=0.5, although [0.1,0.8] is a good range to choose. Once the crossover is done, selection between parent and offspring is made on the basis of their fitness. The one with higher fitness (lower value of the objective function) is retained or selected to be a member of the new generation. Selection operator is

$$c_1 = \begin{cases} a_1 & : \text{ if } J(a_1) \leq J(c_1) \\ c_1 & : \text{ if } J(a_1) > J(c_1) \end{cases} \tag{2.34}$$

One generation vectors are obtained as explained above. Many generations can now be generated iteratively, using the newly selected vector, until a maximum predefined number of iterations is crossed (which means that we are happy with that particular minimized objective function evolved in the specified number of generations) or a minimum tolerance (say of the order of 10^{-6}) is defined for better convergence. In other words, when the least value of the objective function is obtained, we stop. The flow chart of DE is seen in Fig.(2.8) below.

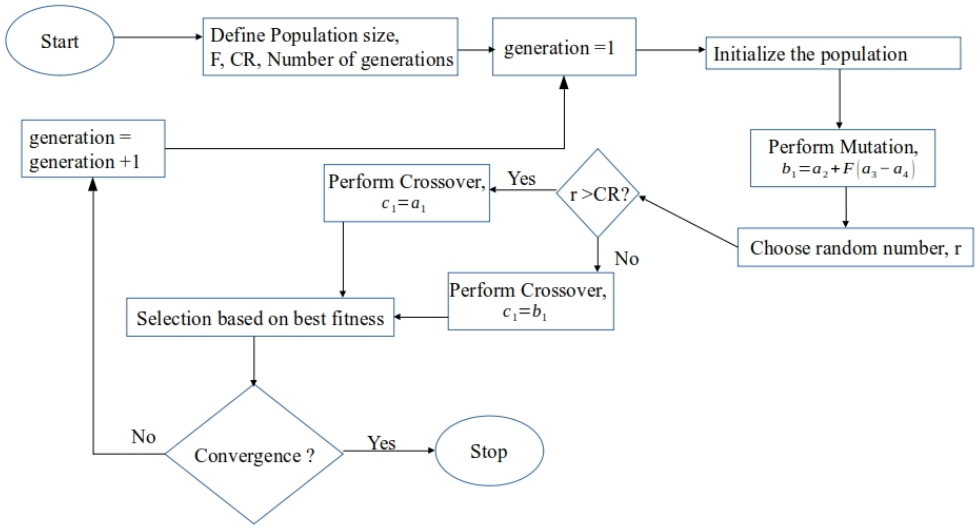

Fig. 2.8 Flow chart of the Differential Evolution optimization algorithm.

The advantage of using this method over others is that it gives a global optimum. Further, no gradients are required to implement it, thus non-differentiable and complex objective functions

could be solved easily using DE and person with less mathematical knowledge can also apply it easily. Moreover, it is easy to implement as few control parameters are involved. DE differs from GA in that it moves to a new position (vector) after checking its fitness, i.e., first mutation followed by crossover, whereas in GA crossover occurs before mutation. The only disadvantage is that in some problems, many generations (iterations) are needed to obtain a satisfactory optimum, which can increase the overall computing cost.

Work done using DE involved Bhowmik *et al.* (2013b), who used DE in conjunction with the Adomian Decomposition Method (ADM) to find the dimensions and hence the shape of an annular fin. The authors used ADM to determine the temperature profile using direct analysis, which in turn is used by DE for the inverse analysis. The authors concluded that unknown parameters are related and thus, multiple combinations are available which satisfy the given temperature profile. Das and Singla (2014) worked on a non-linear inverse problem of a porous fin having applications in cooling of gas turbine blades. A hybrid method consisting of DE and non-linear programming (NLP) was used to determine porosity, permeability, length and thickness of the fin. This hybrid method proved to be better than the corresponding NLP and DE algorithms. Das and Prasad (2015) used DE to determine porosity and thermal diffusivity of a porous fin. The method has been compared with LM, Simulated Annealing, GA and showed better results for the current problem. Singla and Das (2018) took a highly non-linear problem in which the fin parameters are to be determined, such that maximum heat is dissipated from the heating surface. Here, radiation and convection are temperature-dependent. DE is used here for the inverse analysis of parameter estimation in the case of stepped fins.

(c) *Particle Swarm Optimization (PSO)*

Russel Eberhart, an electrical engineer and James Kennedy, a social psychologist Kennedy and Eberhart (1995), Naka *et al.* (2001) worked together in 1995 and formed another class of stochastic algorithm, namely PSO. The method works by balancing the social and individual behaviour of certain solutions (measured in terms of global and personal best position), which leads to an optimal solution. This algorithm uses the swarm behaviour found in birds, looking for the best place to construct their nest and similar behaviour is seen in fishes. While locating the best, the basic idea suggests if the individuality of the particle increases, the particle would look for more places and hence would explore more choices. In doing so, particle (bird) may end up with no best solution (or best home). While if the sociability becomes high the particle may settle down for the first minima, getting influenced by the best position discovered by other particles. Thus, a typical balance between the two is created to reach the global optimum.

Tian *et al.* (2011) used Quantum Particle Swarm Optimization (QPSO) for an approximation of unknown heat source function in IHCP. The authors used Tikhonov regularization, to make the problem well-posed. Further, the method had been validated against CGM. Liu (2012) improved the classical PSO, namely MPSO by modifying the velocities using Gaussian mutations, in

which velocity was updated using $v_i^{j+1} = N_g v_{max}$, N_g was the Gaussian distribution with zero mean and variance 1. According to the author, despite showing a faster convergence such a modification was required for PSO to move out of local optimum and hence the operator increased the diversity of the particle, which in turn increased the chances for local escape. Ding (2012) gave yet another version of improved PSO and MPSO for the inverse solution of the convective problem, overcoming its premature convergence. Earlier, according to writers either the velocities were large or very small for each particle, which causes each particle to leave the search space or get trapped in the local optimum. Enhanced Particle Swarm Optimization (EPSO) works in such a manner so as to maintain an optimum velocity along with improving the local position for particles. EPSO thus overpowers the classical PSO, when it comes to larger dimensions of unknowns. Ding and Sun (2015) again used EPSO, this time to estimate the time-dependent heat source within a complex domain. Bangian-Tabrizi and Jaluria (2018) used PSO to solve inverse natural convection problem. Here, the heat source's location and strength were to be estimated, which were approximated first individually and then in combination where both location and strength of heat source were unknown.

The main steps followed during the process include evaluation of the present position, followed by comparison (either with personal (x_p) or with global best (x_g)), leading to modification in the solution. Each particle update itself using position, current velocity, the distance between the current position with x_p and x_g. Using the following iterations with j as the iteration count for a 'd' dimensional position vector:

$$v_i^{j+1} = w v_i^j + c_{w1}(ra)_i(x_p - x_i^j) + c_{w2}(rb)_i(x_g - x_i^j), \tag{2.35}$$

$$x_i^{j+1} = x_i^j + v_i^{j+1} \qquad (i = 1, 2, ..., d), \tag{2.36}$$

where x_i and v_i represent position and velocity for i^{th} individual. Here for $j = 0$, x_i^0 is chosen/guessed initially and $v_i^1 = 0$. Here $(ra)_i$ and $(rb)_i$ are random numbers between 0 and 1 following uniform distribution, 'w' is the inertia weight vector between 0 and 1, 'c_{w1}' and 'c_{w2}' represent the confidence weight vectors. The algorithm could be tailored for different problems by choosing large 'w' for enhanced global search ability whilst lower 'w' value results in increased local search abilities. How much confidence a particle shows on itself and on its neighbour can be varied by constants 'c_{w1}' and 'c_{w2}'. If both are tuned to zero, no inertia is shown and the particles will keep on moving at their current velocity until they hit the boundary. For $c_1 = 0$ and $c_2 > 0$ (or $c_2 = 0$ and $c_1 > 0$), the particles are not bothered about their own findings (particles are not influenced by their neighbour's findings) resulting in maximum sociability (individuality). The iterative algorithm for PSO is explained in Fig.(2.9).

(d) ***Neural Networks***

The above mentioned evolutionary or swarm algorithms are applied mostly to multi-dimensional problems, where a global optimum is desired from the domain of interest. Random processes are popular when little information about the system is available. The neural network recog-

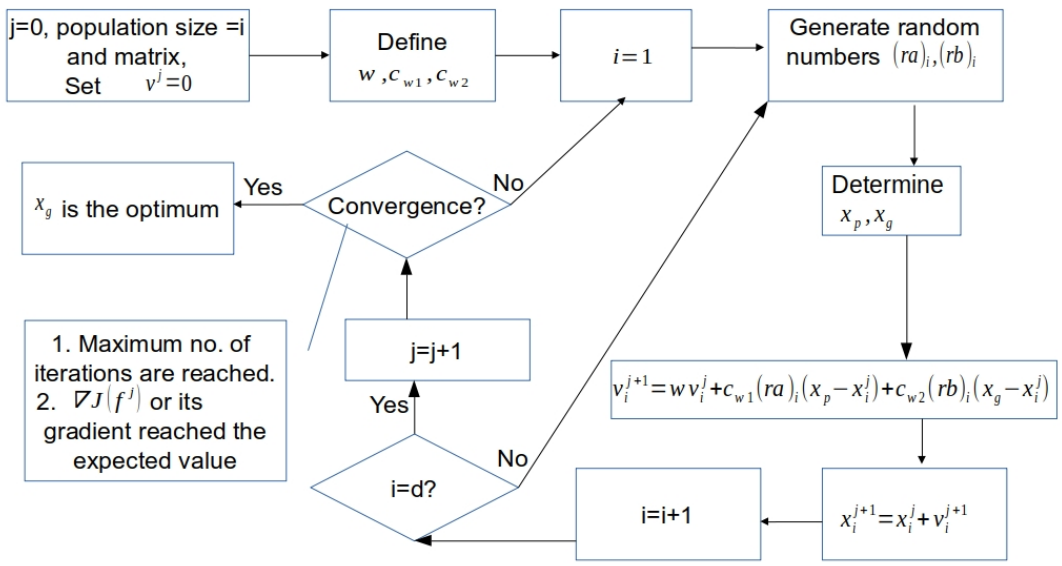

Fig. 2.9 Flowchart for Particle Swarm Optimization.

nizes the solution in terms of various patterns. Neural networks mimic a human brain and each working unit in such a network is thus termed as a neuron. The main component of the neural network involves input, hidden and output layers, each connected either by direct or weighted connections. Data flows through the network from the input layer to the output layer, with one or multiple hidden layers in between. Different circles represent different nodes, whose number can vary according to the number of unknowns to be recovered. Different weights are assigned in terms of weighing matrix, which define the "knowledge" of the network. The solution is then predicted by training the model with previously available estimates of the solution. When the network is trained, corresponding weights are modified so that the error defined by the least-squares sum is minimized. Usually, during the training, a neuron travels back and forth several times. Backward movement is termed as backpropagation. An activation function like linear, sigmoid, etc. can be applied, which judges the activation of neurons for different weights, during the backpropagation. A complete review of the working of neural networks in IHTP is found in Kamble *et al.* (2014).

Krejsa *et al.* (1999) compared Whole History Mapping (WHM) approach and Sequential Approach using neural networks in IHCP. The authors concluded that none of the approaches could match the traditional methods, but instead is useful when the associated problem is quite complex to handle. Berdnik and Mukhamedyarov (2003) solved the coefficient inverse problem using neural networks. They observed that the magnitude of error decreases and tend towards the fitting characteristics of the fitting method by increasing the number of neurons. Furthermore, the method is suitable for the identification of unknowns in real-time as the speed of estimation of unknowns by this method is quite high. Shiguemori *et al.* (2004) used two dif-

ferent neural networks, namely multilayer perceptron neural network (MP-NN) and radial base function neural network (RBF-NN) for the estimation of heat flux at the boundary when only heat conduction occurs. These authors concluded that RBF-NN performed better than MP-NN. Deng and Hwang (2006) implemented continuous-time analogue Hopfield neural network for forward analysis in IHCP, along with backpropagation neural (BPN) network to determine the unknown heat flux at the boundary. Also, Bayesian regularization is applied, in which the objective function is modified by adding a regularization term, whose parameters are selected randomly. Cortés *et al.* (2007) used artificial neural networks (ANN) in IHTP involving the internal heat generation, where the network was feedforward with backpropagation algorithm. The method used was compared with the Levenberg-Marquardt Method and was concluded that ANN improves the results obtained with the Levenberg-Marquardt method. Czél *et al.* (2014) determined temperature-dependent volumetric heat capacity and thermal conductivity simultaneously using artificial neural networks consisting of multiple layers. The authors concluded that the applied method is quite efficient to determine temperature profile non-iteratively. Heidari and Garshasbi (2015) retrieved heat flux at the boundary in IHCP using backpropagation neural networks. According to the authors, non-linear problems could easily be solved using neural networks. Mirsepahi (2017) used an artificial neural network in combination with a genetic algorithm in radiative problems of furnace or dryer body.

The optimum found in each of the above-discussed algorithms is assured for correctness by using the statistical tests such as t-test, Analysis of variance (ANOVA), Chi-square test, etc.

Type III: Hybrid Methods

Deterministic methods perform computations quickly than the evolutionary algorithms, although convergence is usually to its local optimum. Whereas for the stochastic methods, the only harm in the usage, resulting in non-practicality, is due to higher costs of computation requiring thousands of evaluations. Taking advantage of faster convergence and robustness of deterministic as well as stochastic methods respectively, hybrid algorithms came into play. The main focus of such algorithms is to utilize characteristics of stochastic methods, to quickly identify where the global optimum would be and then using deterministic one for faster convergence, Colaco *et al.* (2006). These methods are efficient and thus can be tailored according to the needs of the problem. Several comparisons are made in this direction. The inverse problem of parameter estimation has been taken by Neto and Soeiro (2003) and hybrid approach was then applied, yielding good estimates of global minimum, with a lower computational time. Two pairs Simulated annealing-Levenberg Marquardt and GA-Levenberg Marquardt of the deterministic and stochastic algorithms were then applied on IHCP yielding better results with increased convergence. Vakili and Gadala (2013) used evolutionary GA and PSO methods to find a solution to IHCP, making use of surrogate models. These models can reduce the high computational cost of stochastic methods by using inexact evaluations and could be five times faster. Various surrogate models have been discussed. Another optimization method namely Ant Colony Optimization

(ACO) had been applied in Zhang *et al.* (2013), for the solution of IHTP involving effects of radiation and conduction. To estimate cooling of "Steel continuous casting machine", Bertelli *et al.* (2015) used stochastic techniques, namely GA, improved ranking stochastic strategy, and with that of the Cauchy distribution. Udayraj *et al.* (2015) compared ACO, PSO and Cuckoo search algorithms. According to the authors, ACO leads followed by PSO and Cuckoo search algorithm for IHTP, the comparison is made based on computational time. Hence, boundary condition involving time-dependent heat flux was estimated. Lee and Kim (2015) compared PSO with GA to find the surface temperature and emissivities for the inverse surface radiation problem. The authors concluded that Repulsive Particle Swarm Optimization (RPSO) and PSO are better in computation as they have higher convergence, accuracy and speed as compared to the Hybrid Genetic Algorithm (HGA). Zhang *et al.* (2016) estimated the thermal and physical properties in time-dependent heat conduction, where the data was captured using the infrared camera. Another evolutionary algorithm, namely Social Spider Optimization (SSO), was utilized by Sun *et al.* (2017b) to solve IHTP, involving radiation and conduction and in Sun *et al.* (2017a) to retrieve properties of a phase-changing material. A scaled boundary finite element method (SBFEM) which handles singularities of the problem with ease has been used in conjunction with a hybrid GA-SQP (Genetic Algorithm-Sequential quadratic programming), an evolutionary-deterministic pair, which has been put forward by Mohasseb *et al.* (2017), to find the heat flux in IHCP. The combination lowers the computational time, taking global search advantage of GA and SQP's contribution in higher accuracy and SBFEM, as a meshless solver.

2.2.3 Methods where no minimization is performed

(a) *Wavelet Methods*

What are wavelets? Realistic information in terms of signals and data, most of the time shows patterns and trends which change gradually over time, whereas sharpness and discontinuities are shown by edges. These features form an important part of the data. To capture such characteristics, the Fourier transform was used, which decompose a signal into a combination of sine and cosine waves. Such a decomposition does not adapt itself to the signal and hence provide less accurate data. Wavelet transform was then utilized, as it formed a class of functions which were confined in space and time. Thus, to break down signals and image data with unexpected variations, wavelets play a superb role.

Quickly changing wave-like movement is termed as a wavelet. Existing for a limited span (i.e., having a compact support), wavelets vanish after some time (i.e., have zero mean). Available in various shapes and sizes, few of which are Morlet wavelet (1984) Grossmann and Morlet (1984), Daubechies wavelet (1992), Coiflets (1991), Biorthogonal (1992), Mexican Hat (1994), Symlets (1992), Diffusion wavelets (2006), curvelets (2006) and Spectral graph wavelets (2011). In addition to the above-mentioned wavelets, one can construct his/her own wavelet according to the specific needs of the problem involved. Such an extensive variety of wavelets strengthen the subject area. Gradual changes in signals can be noted by stretching and compressing the wavelet by a known process of scaling, whereas the whole length of the signal

could be covered by displacing the fundamental wavelet using shifting.

Wavelets in inverse problems

The wavelet theory got started almost 35 years back and find its applications in numerous fields of mathematics, physics, computer science and engineering. These applications are a result of large properties of wavelets. Wavelets allow decomposition of an object into multiple scales, thereby providing better resolution. Wavelets allow one to study the local and detailed features of the object due to its localization in both time as well as frequency. They have an excellent data compression capacity (for example, wavelets are used to store images which is done just by storing the set of edges thereby requiring less storage and are also used by the FBI to keep track of fingerprints by compressing them). Non-linear methods of denoising, based on thresholding the wavelet coefficients are optimal to carry out a large number of tasks involving removal of noise from the coefficients. This is done via Wavelet Shrinkage.

Despite the wide features of wavelets, little literature is available. A quick review could be found in Goyal and Mehra (2011). Fu *et al.* (2003), applied Meyer wavelets for regularization on a problem in nonlinear atmospheric dynamics, where the numerical implementation is done as shown in Kolaczyk (1994). The limitation with other regularization methods is that either noise is reduced significantly or good resolution (better approximation) is lost. Candau (2005), applied wavelet method alongside thresholding and compared the results with SVD. Malan *et al.* (2008) applied discrete wavelet transform followed by wavelet denoising in addition to a variable metric method to determine heat flux in the slab. Shannon wavelets in addition to wavelet dual least square method are applied on a particular form of an infinitely long cylinder which is axisymmetric to obtain surface temperature by Cheng and Fu (2009). They also worked on the stability and convergence of IHCP theoretically. Dou and Fu (2009), used Meyer wavelets to determine the unknown heat source in heat equation, which is spatially dependent by applying dual least square method. Bonesky *et al.* (2010), took IHCP occuring in steel furnace and used adaptive wavelet scheme in addition to soft thresholding. Assumed homogeneous conductivity and the initial temperature is known beforehand, the problem is to determine the shape of the inner wall of the furnace. Nazari *et al.* (2012), applied mollification method and wavelet prefiltering method, which are then compared for applied IHCP. The authors concluded that wavelet filters are better, whereas mollification filters can be applied with greater ease. The problem was to solve heat flux, which was solved using CGM and adjoint differential equation. Cheng *et al.* (2013), again applied Shannon wavelets, in dual least-square on IHCP this time involving convection term.

Wavelet thresholding and shrinking

Another name used in literature for wavelet shrinking is **denoising by thresholding**. Donoho along with others gave the concept of denoising. Shrinking is useful when we record certain data either experimentally or by forward analysis. The obtained values of data have a certain

amount of errors involved (e.g., measurement errors, random errors etc.) typically known as noise. Denoising endeavours to eliminate whatever noise is available and hold whatever signal is available, despite the frequency content of the signal. The problem under consideration is to recover the function (or signal) from the observed noisy function (or signal).

When discrete wavelet transform is applied to a spatially variable signal with Gaussian noise, then another signal having the same length is obtained. The obtained wavelet coefficients having a larger magnitude correspond to function (or signal) values while coefficients with smaller magnitude correspond to noise. The next task is to invert the obtained signal. Before inversion, a suitable threshold is applied, i.e., a suitable value is fixed such that coefficients with a higher value than the fixed 'threshold value' are retained and rest all are discarded. In this way, most of the noise is removed and denoising of the signal is achieved. Thus, by soft and hard choosing a suitable thresholding function, we obtain a nearly smooth reconstruction of the function (or the signal).

To denoise a particular noisy data $d_i = Kf_i + e_i$, i= 1,...,j, taken at $j = 2^{V+1}$ points, where e is the associated noise with a standard deviation 'σ', following steps are followed,

1. Apply wavelet transform to the data to obtain wavelet coefficients $\omega_{v,k}$, v=v_0, ..., V, k=0, ...,2^v-1 .

2. Apply thresholding function say $\eta_t(\omega)$ to the obtained coefficients $\omega_{v,k}$. This will give us a new set of coefficients $\hat{\omega}_{v,k}$.

3. Apply inverse wavelet transform on $\hat{\omega}_{v,k}$ to produce the estimate $\hat{Kf}$, which will give the denoised data.

Remarks:

1. **Hard Thresholding**: The hard thresholding operator for a function (or signal) is defined as

$$\eta(U,t) = \begin{cases} U & ;\ if\ |U| > t \\ 0 & ;\ otherwise \end{cases}.$$

2. **Soft Thresholding**: It is a function of the form,

$$\eta(U,t) = sgn(U)max(0,|U| - t).$$

The choice of 't' is very critical. A popular threshold is universal threshold,

$$t_u = \sqrt{2\log l}\sigma,$$

where l is the signal length and σ^2 is the noise variance. For a detailed discussion, one can refer Bouchouareb and Benatia (2014).

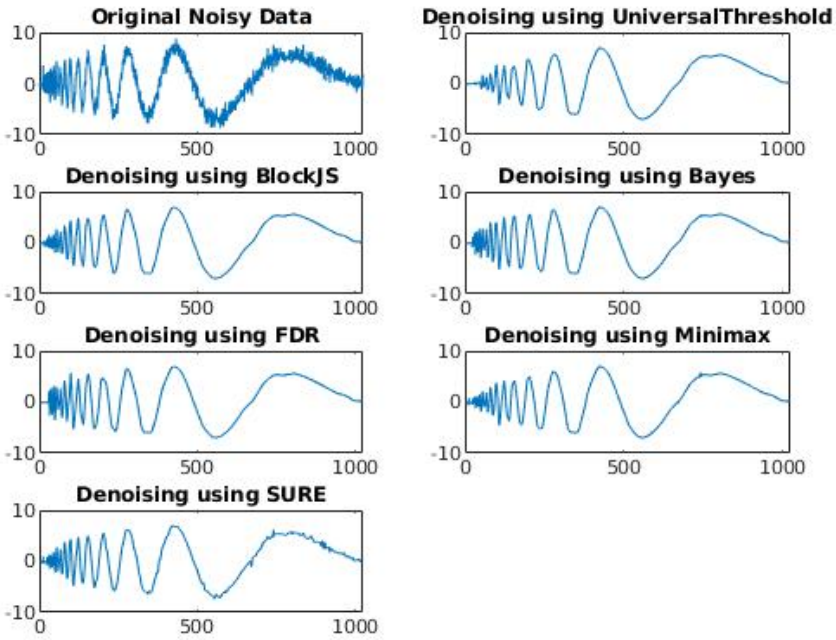

Fig. 2.10 Denoising using different denoising methods.

In Donoho and Johnstone (1994), RiskShrink with the minimax threshold, VisuShrink with the universal threshold was presented and information regarding both hard as well as soft thresholds in a general setting was presented that included perfect denoising in both the wavelet and Fourier space. In Donoho and Johnstone (1995), authors reported SureShrink with the SURE threshold, in addition to WaveJS with the James-Stein threshold, and LPJS also with the JamesStein threshold, this time in Fourier space. A visual comparison of 'SURE', 'UniversalThreshold', 'Minimax', 'FDR', 'Bayes', 'BlockJS' is shown in the following Fig.(2.10), where 5 level denoising is done using symlet 4. The wavelet and approximation coefficients for the same signal were also obtained, see Fig.(2.11) using Minimax method, utilizing MATLAB's Wavelet Analyzer.

Wavelet Vaguelette Decomposition (WVD) In the very start of 1992, David Donoho started working on inverse problems, for which he created a theoretical framework, using wavelets as a tool. This construction resembles, but proves to be better than SVD, Donoho (1995). In SVD, the matrix associated with operator 'K' was decomposed into singular vectors, whereas in WVD this decomposition takes place in the wavelet and vaguelette (wavelet-like) bases. For two problems taken from different areas, if the same operator is being used, SVD results in the same decomposition whereas in WVD 'Kf' is decomposed, taking into account the object to be recovered and hence is better. The theory of WVD is limited to a special class of homogeneous and linear operators defined over L^2 spaces.

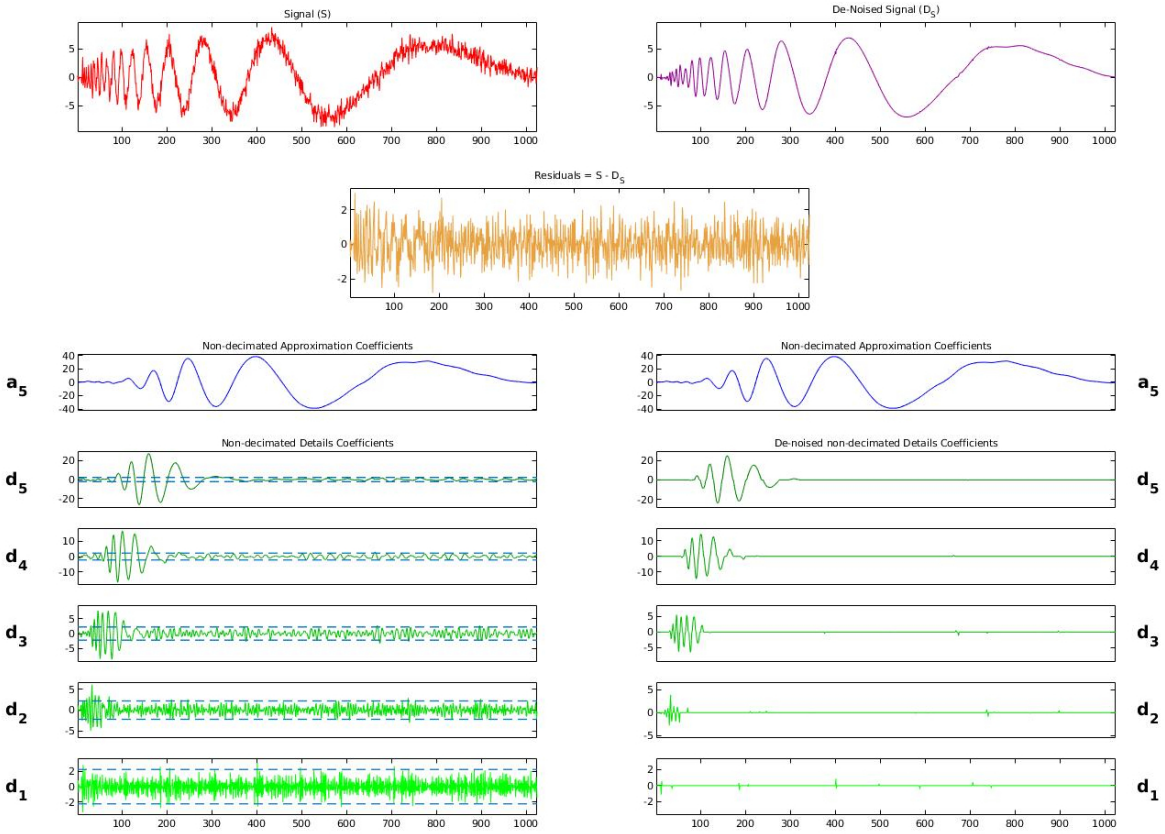

Fig. 2.11 Wavelet and scaling coefficients of noisy and denoised signal.

The process involves obtaining the coefficients which are used to represent functions in the wavelet basis from the existing and known values of Kf, by the construction of bounded linear functionals $c_\lambda : L^2(du) \longrightarrow \mathbb{R}$ such that

$$c_\lambda(Kf) =< f, \psi_\lambda >,$$

where $\psi_\lambda \in D(K) \cap R(K^*)$ and $\psi_\lambda =$ family of orthonormal wavelet basis.

Hence, decomposition of 'f' into the orthonormal wavelet basis ψ_λ becomes

$$f = \Sigma_\lambda < f, \psi_\lambda > \psi_\lambda \Longrightarrow \qquad f = \Sigma_\lambda c_\lambda(Kf)\psi_\lambda.$$

Thus, WVD provides a method to retrieve 'f' from the known values of Kf. Further, if the available Kf contain the Gaussian noise, then thresholding of the coefficients is done to denoise the reconstruction, i.e.,

$$\tilde{f} = \Sigma_\lambda \eta_{t_n}(c_\lambda(Kf))\psi_\lambda,$$

where η_{t_n} is the applied threshold. The process requires the use of efficient algorithms which needs to be constructed in order to obtain the coefficients associated with the operator K.

Few researchers till date implemented WVD on the inverse problem. In Keller (1999) made use of WVD in the local gravity field modelling. Ancey (2005) develops a technique based on WVD

to determine the shear rate using measurements taken from Couette rheometer such as torque and velocity. Ruiz-Medina *et al.* (2007), used WVD for the solution of pseudo-differential equations, describing the diffusion process for a class of spatiotemporal models. A technique based on WVD has been developed to interpret tomographic images taken by the camera, Yen *et al.* (2012). To the best of the authors knowledge, WVD has not been implemented on inverse problems taken from heat transfer, resulting in a future research direction.

(b) ***Truncated Singular Value Decomposition (TSVD)***

The most basic and easiest of all inversion methods is TSVD. The first step of this method involves writing K in the form of its SVD as follows: For the operator $\mathbf{K} : H_1 \longrightarrow H_2$ defined in equation (2.1) Let $\mathbf{K} \in \mathbb{R}^{m\times n}$ be a rectangular or square matrix associated with operator **K** and assume m is greater than or equal to n. Then the following is the SVD of K,

$$K = ADB^T = \sum_{i=1}^{n} a_i d_i b_i^T, \tag{2.37}$$

such that

$$a_i^T a_j = \delta_{ij}, \quad b_i^T b_j = \delta_{ij}, \tag{2.38}$$

and

$$Kb_i = d_i a_i, \quad K^T a_i = d_i b_i, \tag{2.39}$$

are satisfied. Here δ_{ij} denotes Kronecker delta, which takes value 1 when i=j and zero otherwise. Also $A = (a_1, \ldots, a_n) \in \mathbb{R}^{m\times n}$, $B = (b_1, \ldots, b_n) \in \mathbb{R}^{n\times n}$ and the non negative diagonal entries $d_1 \geq d_2 \geq \cdots \geq d_n \geq 0$ in non increasing order (decreasing order) forms the elements of matrix D = diag(d_1, …, d_n). The number 'd_i' represents the i^{th} singular value, of matrix K, whilst the i^{th} singular vectors are denoted by a_i and b_i, satisfying $A^T = A^{-1}$ and $B^T = B^{-1}$. The singular values 'd_i' become the eigen values, provided that the corresponding K is symmetric and positive definite. The greatest index corresponding to the non-zero singular value is denoted by 'a', $a = max\{j|1 \leq j \leq min(k,n), d_j > 0\}$, such that, $d_1 > 0, d_2 > 0, \ldots\ldots, d_a > 0, d_{a+1} = 0, \ldots\ldots, d_{min(k,n)} = 0$.

The following theorem, helps in inverting the matrix K when it is singular or ill-conditioned.

Theorem 2.2.1 *Mueller and Siltanen (2012), Let K be a $k \times n$ matrix denoted by $K = ADB^T$ (the SVD of K). The minimum norm solution of the equation $Kf = m$ is given by $K^\dagger m$, where*

$$K^\dagger m = BD^\dagger A^T m, \quad where \tag{2.40}$$

$$D^{\dagger} = \begin{pmatrix} \frac{1}{d_1} & 0 & \cdots & 0 & & \cdots & 0 \\ 0 & \frac{1}{d_2} & & & & & \vdots \\ \vdots & & \ddots & & & & \\ & & & \frac{1}{d_a} & & & \\ & & & & 0 & & \\ \vdots & & & & & \ddots & \vdots \\ 0 & \cdots & & & & \cdots & 0 \end{pmatrix}_{n \times k} \tag{2.41}$$

The matrix $K^{\dagger}$ is called the **pseudo inverse or the Moore-Penrose inverse** of K. Different methods for regularization, depending on the choice of regularization parameter are discussed ahead.

The small singular values d_a in the expression of the SVD of matrix 'K', create trouble in obtaining the pseudo inverse of D i.e., $D^{\dagger}$, as division by very small singular values makes the solution infeasible, leading towards numerical instability. Hence, to overcome this ill-posedness, a regularization parameter 'α' is fixed which could act as a filter. Most of the noise corresponds to these small singular values and solution to the large ones. Thus the selected filter will allow only large values to be retained, leaving small ones, which in turn eliminates error or irregularity, making the problem as well-posed.

For any $\alpha > 0$ define the truncated SVD (TSVD) by

$$K_{\alpha}^{\dagger} = B D_{\alpha}^{\dagger} A^{T}, \qquad where$$

$$D_{\alpha}^{\dagger} = \begin{pmatrix} \frac{1}{d_1} & 0 & \cdots & 0 & & \cdots & 0 \\ 0 & \frac{1}{d_2} & & & & & \vdots \\ \vdots & & \ddots & & & & \\ & & & \frac{1}{d_{a_\alpha}} & & & \\ & & & & 0 & & \\ \vdots & & & & & \ddots & \vdots \\ 0 & \cdots & & & & \cdots & 0 \end{pmatrix}_{n \times k} \tag{2.42}$$

and

$$a_{\alpha} = min\big\{max\{j | 1 \leq j \leq min(k,n), d_j > 0\}, max\{j | 1 \leq j \leq min(k,n), d_j > \alpha\}\big\}. \tag{2.43}$$

Martin and Dulikravich (1996) applied Boundary Element Method (BEM) to find a solution to steady IHCP, including the effects of heat generation. Unknown heat sources were predicted

using BEM, whose formulation involved an ill-conditioned matrix, solved both by SVD and Tikhonov regularization, out of which performance of SVD for matrix inversion was more.

Al-Najem *et al.* (1998) applied SVD on steady 2-D IHCP, with BEM for direct analysis. To determine the surface temperature in conducting material, least-square and integral transform method were used. IHCP was again solved in Shenefelt *et al.* (2002), using SVD. The approach involves decomposing matrix and then reducing it by deleting those rows and columns which have small singular values as these were responsible for the noise/error. Lagier *et al.* (2004) solved multidimensional unsteady IHCP, using SVD-BEM pair. Regularization, in this case, was achieved by truncating the small singular values, where the corresponding filter parameter was known a priori. Experimental results were also shown in support of the method. The authors suggested that the method could also be extended to 3-D space. Cabeza *et al.* (2005) provided an application of the sequential form of TSVD. Regularization, in this case, depends on two parameters, namely the rank of sensitivity matrix and the number of future temperatures. The current sequential SVD had been compared with sequential function specification method, given by Beck, both methods showed comparable results for several test cases. A generalization of the above work was reported in García *et al.* (2009). Inhomogeneous problems earlier required both fundamental and particular solutions. Wen *et al.* (2011) devised a method to solve the time-dependent IHCP, for which just the particular solutions were required. The method made use of radial basis functions with Laplace transform technique, with the implementation of SVD to overcome ill-posedness. Stable results were obtained for a case with large measurement errors. To recover the inner convective heat transfer coefficient, in the case, when flow occurs in a pipe, Cattani *et al.* (2015) used TSVD together with Quadrupole Method (QM). They have also compared their method with FEM, used in conjunction with Tikhonov regularization and Gaussian filtering methods, resulting in poorer performance of Gaussian filtering in comparison to others. Mousseau *et al.* (2001), presented an original apparatus to analyze heat transfer within a plate which is being cooled at a constant velocity. The apparatus is capable of determining temperatures and heat transfer coefficient between the contact fluid and the plate. Thomas *et al.* (2010) gave a new experimental design to estimate thermal conductivity and specific heat for orthotropic polymer composite. The authors used an experimental design for the implementation.

Apart from the above discussed methods, several numerical techniques have been developed. For the very first time, a solution to IHCP using numerical implementation of methods was provided by Bass (1980), where FEM and Beck's non-linear estimation procedure was implemented, to determine temperature and heat flux in the direct and inverse analysis respectively. A non-linear time dependent IHCP, involving radiative heat transfer at the boundary was studied by Mehta (1984), using finite differences and Newton-Raphson, Regula-Falsi numerical iterative methods. Weiland and Babary (1988), introduced a time marching numerical method for non-linear IHCP, whose main aim was to reduce the limit set for stabilizing parameters. Flach

and Özışık (1989), evaluated simultaneously thermal conductivity, which varied in space and heat capacity numerically. Reinhardt (1991) extended Beck's sequential method to solve IHCP in 2-D space. Ruperti *et al.* (1996), used an already available space marching technique, this time for the solution of IHTP including convection and radiation, and provided a generalized version of it. A non-iterative semi numerical approach to determine surface heat flux was presented by Taler (1996), where no initial temperature was required, with only requirement of previous and next data with respect to time. An initial valued IHCP was solved by Eldèn (1997) using the method of lines. The advantage involved in utilization of earlier proposed space marching schemes was the reduction of sensitivity using perturbation in the data. Also for regularization, an additional term was required to be added for a stable solution. Current approach approximates the equation instead of altering it, hence proved better. Authors further reported the use of Runge-Kutta numerical methods for the stability in various contexts. Osman *et al.* (1997) used sequential method for time variable alongwith the regularization technique. Shen (1999) used BEMs, namely collocation and weighted methods, where regularization has been done in Tikhonov's sense. Numerical study using collocation and TSVD was also discussed. Time independent heat transfer coefficient has been determined experimentally by Chantasiriwan (2000). Use of unstructured meshes, using control volume method has been used for irregular shaped bodies by Duda and Taler (2000), to find solution of non-linear IHCP. Throne and Olson (2001) compared newly developed generalized eigensystem with that of Tikhonov method, with earlier comparisons being made, having knowledge about true solution to fix regularization parameters. To overcome this difficulty of collecting a-priori information regarding the material, a sensor sensitivity method had been proposed. To retrieve heat source in IHTP, a numerical technique has been devised in Fatullayev (2002), using overspecified data, which estimates heat sources using linear polygon pieces, which were evaluated continuously from the minimization problem. Ling *et al.* (2003) investigated surface heat flux, where a non-recursive finite element method, in addition to least square minimization approach have been utilized, with a newly developed algorithm to tackle ill-posedness of the solution. Chen and Tuan (2005) used FEM together with Kalman filtering and iterative least square method, method being derived using residual innovation scheme in both 1-D and 2-D space. Further a comparison of newly constructed method with CGM has been done. A moving boundary problem was analysed to identify heat flux surface by Shidfar and Karamali (2005) where direct-inverse analysis has been carried out using method of fundamental solutions-least square residual minimization method. A discretization for three-dimensional singularly perturbed nonlinear elliptic partial differential equations was developed by Mohanty and Singh (2006) and variable mesh method for 1-D non-linear parabolic pde was given by Arora *et al.* (2006) and for non-linear singular pde by Mohanty (2007). Chen and Wu (2008) again utilized this hybrid approach to estimate heat transfer coefficient for the transient case in 2-D domain. An optimization method and a numerical predictor-corrector method have been implemented in isolation, to determine convective coefficient, Zhang and Delichatsios (2009). Mierzwiczak and Kołodziej (2011), calculated

thermal conductivity as a function of temperature in 2-D, steady IHCP. Lesnic and Mohsin (2012) applied a meshless method of fundamental solutions (MFS) to estimate inner boundary and surface heat transfer coefficients. Modified Helmholtz equation for a fin is a geometric inverse problem, which is stabilized by adding regularization terms in non-linear objective function. Authors Frąckowiak *et al.* (2015), took a Cauchy problem for Laplace equation and solved the corresponding Poisson equation, to determine source function. The problem was converted from the one in multiply to simply connected region. The properties of polymers mainly composites were studied by Dmitriev and Zhivenkova (2018), where thermal conductivity and heat transfer coefficient were determined. The numerical method introduced an iterative algorithm, which converts differential equation to the integro-functional equation. Fourth-order method based on half-step cubic spline approximations for the 1-D time-dependent quasilinear parabolic pdes Mohanty and Sharma (2020).

2.3 Discussion

In this chapter, a state-of-art review of available literature and methods have been done. Such a review cannot be complete in itself, as the scope of the subject is as wide as a complete book. The major advantages and disadvantages of several methods are listed ahead. IHTPs belong to a class of Ill-posed problems, thus it is difficult to solve such problems. To overcome ill-posedness, numerous regularization techniques were explored. Linear least square methods, Alifanov's CGM iterative method, Tikhonov regularization, Beck's sequential regularization, mollification method proved to be efficient regularization tools. TSVD is the simplest and most basic of all. Tikhonov regularization, being a popular tool for regularization, is currently in use. A limitation of SVD and Tikhonov's lies in the fact that these provide a reconstruction of a smooth function and generally miss out edges and sharp properties.

Apart from different regularization approaches, several inversion techniques have been explored. The analytical methods, which are available for a particular class, provide a strong foundation, for comparison of different numerical techniques. This motivates us to the first application (Objective 2), where the Adomian Decomposition Method (ADM) has been applied to find closed-form temperature solution. Another technique consisting of wavelets methods found sparse usage in literature for the solution of IHTP.

Sometimes in the determination of solution, a functional form of the unknown is predetermined. Such methods are called function specification method. Easier to implement, these methods are computationally more efficient when sequential estimation approach is applied. Thus, in the second application (Objective 2), a time-dependent functional form of heat flux is determined from a pin fin setup. A different class consisting of optimization methods was explored in literature. Deterministic optimization methods differ in the selection of descent direction. Gradient direction being a natural choice was utilized in the steepest descent method, CGM improved on the same. Researchers made use of CGM in a number of problems, making use of

its iterative regularization approach. Excessive usage of CGM showed its capability to handle IHTP with much ease. Whereas the Newton-Raphson method has faster convergence, Quasi-Newton's method reduces computational costs involved, with a simultaneous decrease in the rate of convergence, BFGS being used most. It has been concluded that gradient-based deterministic methods provide guaranteed convergence. However, a major limitation is that it utilizes a strong mathematical formulation, which is problem-dependent. Moreover, these result in local optima which no doubt capture the local information and features well but lack the global information, required for some problems. Another class of optimization methods which overcome the local convergence is of evolutionary algorithms. Algorithms like GA and DE differ in the order in which mutation and crossover operators are applied to them. In literature, the methods DE and GA were compared, with the former being better. Moreover, it has been observed that for more complex problems with non-linear terms, random processes play an effective role in the estimation of the solution. Neural networks are one such heuristic method. As most of the IHTPs are non-linear due to temperature-dependent properties, this motivates us to the second application (Objective 2), where evolutionary methods have been applied to find the solution to IHTP. To the best of author's knowledge, there is no unique optimization algorithm that solves every technical problem in general. Development of an efficient framework for inverse problem is the need, which lead us to our last objective.

Moving on, to understand and to analyse the process of heat transfer in the double-layered wall, next chapter reveals the application of heat transfer, where the steady-state temperature distribution and efficiency for composite walls using a semi-analytic technique is studied.

Chapter 3

Forward and Inverse Heat Transfer in Composite Walls

Minimization of the heat losses in certain systems and appliances is required for their efficient working. One remedy for the same is the use of composite walls. Composite walls are multi-layered blocks of similar or dissimilar materials which are placed together in a series or parallel combination. A quick review of one-dimensional composite walls could be found in the book, Hahn and Özışık (2012). Composites are made and put up in a way which enhances the mechanical properties. These composite walls found applications in many areas, for example, in the insulation of buildings under extreme weather conditions, Axaopoulos *et al.* (2014), Daouas (2011), Kaska and Yumrutas (2008), Ozel (2013a,b, 2014). These insulated multilayers can be used as walls of refrigerator, cold and hot water storage tanks, hotplates, etc. in which the heat exchange is to be minimized. Further applications of such energy systems include nuclear plants, chemical processes, in packaging, civil and automotive industry and space technology, Zhang *et al.* (2007), Ramadan (2009), Belghazi *et al.* (2010), Cortes and Diez (2010), Li and Lai (2013). The problem of heat transfer can be solved analogous to the series-parallel concept in electrical circuits by taking thermal resistance equivalent to electrical resistance, Cengel (2002).

Study of heat transfer in such composite systems becomes crucial when one needs to practically apply it. The problem involved in this study requires to calculate the temperature distribution at various points of the system given thermal properties of the materials involved. Many attempts, Bouzidi and Duhamel (1982), Maillet *et al.* (1994) were made in this direction. Sundén (1986) gave a numerical solution using forward difference method for the calculation of temperature. Heat flux at one side and convective-radiative boundary conditions at other side were considered. de Monte (2000, 2002) provided an analytical solution using separation of variables method (SVM) for the unsteady heat conduction problem where the thermal proper-

ties like conductivity, diffusivity and convective heat transfer coefficient were considered to be temperature-independent. He assumed the problem as one dimensional with no internal heat generation involved. Lu *et al.* (2006) studied the transient heat transfer of a multidimensional composite cylinder. Analytical solution using a combination of Laplace transform and SVM was used. An and Su (2011) worked on the transient problem of composite multi-layer walls by an improved lumped model where convective and radiative effects were also considered. Vasconcellos *et al.* (2012) presented a numerical solution using Green's Method. Li and Lai (2013) gave an analytical solution using the Laplace transform method for the two-layered hollow cylinder. Norouzi *et al.* (2013) performed a steady conductive heat transfer study in multilayer spherical composite laminates. Authors gave an analytical solution using a combination of SVM and recursive Thomas algorithm. Torabi and Zhang (2014c,a) came up with a medley of numerical and analytical methods to solve ODEs in case of the double-layer hollow composite cylinder. Convection coefficient and internal heat generation were considered to be independent of temperature. Torabi and Zhang (2014b) took temperature-dependent thermal conductivity and considered internal heat generation when heat loss occurred from composite walls both by convection and radiation. Jiang and Dai (2015) studied the three-dimensional steady-state and transient heat transfer in the double-layered plate (Coating/FGM) with temperature-independent thermal conductivity. They used the Poisson method along with Layer wise (LW) approach to deal with steady case while SVM along with LW approach was applied for the transient case to provide analytical solutions. Singh *et al.* (2016) considered temperature-dependent thermal properties but applied the same for a different problem involving convective and radiative fins. Again Torabi and Zhang (2016) gave an exact solution by SVM and Duhamel's Theorem for the transient asymmetric heat conduction in multilayered disk contemplating temperature-dependent heat generation and convective effects. Cavazzuti and Corticelli (2017) provided an algorithm which they implemented in python for one-dimensional steady-state heat conduction in planar walls. Bahadori *et al.* (2018) used mesh-free Monte Carlo simulations for heat conduction in three dimensional transient multilayered composite material. Also, Wang *et al.* (2018a) practised Ferrari's method to evaluate temperature distribution in functionally graded sandwich slabs for the steady-state, involving convective radiative boundary conditions.

In all the problems discussed above, many simplifications are made to obtain the final results. Such simplifications, no doubt, reduce the complexity of the associated problem but additionally moves away from a realistic situation. Thus, there is a need to consider a more general problem, taking into account radiation, convection, conduction, and thermal properties of the associated materials as temperature-dependent. The current chapter studies a steady-state analysis of composite walls. Moreover, all the input parameters are assumed to be temperature-dependent and all the thermal phenomenon are taken into account. The Adomian Decomposition Method (ADM) in association with the Newton Raphson method can deal with a complex non-linear situation and therefore is used for providing closed-form temperature expressions. An appli-

cation of composite walls to the industrial furnace is also discussed. Lastly, an invese analysis on composite walls is performed. The non-dimensional internal heat generation rates in both walls and thermal conductivity ratio are estimated, where the thermal properties are assumed temperature-independent.

3.1 Problem formulation

A double-layered composite wall composed of different materials is considered and the schematic for the same is shown in the Fig.(3.1). The thickness of inner 'i' and outer walls 'o' are x_b and $L - x_b$, respectively. With the variation of parameter x_b, the thickness of both materials can be changed. The thermal properties of the walls are temperature-dependent, i.e., thermal conductivity $k_i(T_i), k_o(T_o)$, thermal heat convection coefficients $h_i(T_i), h_o(T_o)$ and emissivity of surfaces $\varepsilon_i(T_i), \varepsilon_o(T_o)$ are taken as a linear function of temperature. Further, internal heat generation rates $q_i(T_i), q_o(T_o)$ inside the walls are assumed as cubic functions of temperature, as seen in Torabi and Zhang (2015), Goyal and Singhal (2018). For notations, one can see the nomenclature. Combined effects of conduction, convection and radiation are incorporated. The

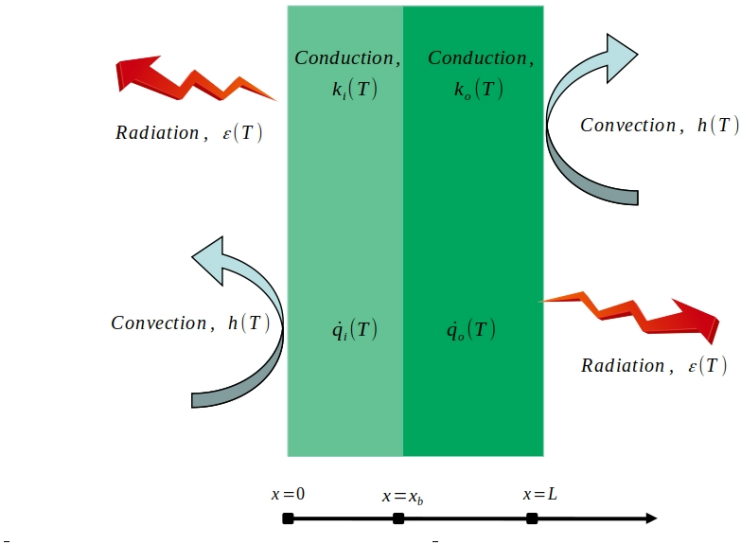

Fig. 3.1 Schematic of composite walls consisting of two layers of different materials, with tempearture-dependent conduction, convection, radiation and internal heat generation.

governing equations for the double-wall one dimensional problem in steady state were given as

follows, Torabi and Zhang (2015), Goyal and Singhal (2018)

$$\frac{d}{dx}\left[k_i(T_i)\frac{dT_i}{dx}\right] + \dot{q}_i(T_i) = 0, \qquad 0 < x < x_b, \tag{3.1a}$$

$$\frac{d}{dx}\left[k_o(T_o)\frac{dT_o}{dx}\right] + \dot{q}_o(T_o) = 0, \qquad x_b < x < L. \tag{3.1b}$$

The boundary conditions associated with the governing equations are as follows:

$$k_i(T_i)\frac{dT_i}{dx}\Big|_{x=0} = h_i(T_i)[T_i(x=0) - T_L] + \varepsilon_{r_i}(T_i)\sigma[T_i^4(x=0) - T_L^4], \tag{3.2a}$$

$$T_i|_{x=x_b} = T_o|_{x=x_b}, \tag{3.2b}$$

$$k_i(T_i)\frac{dT_i}{dx}\Big|_{x=x_b} = k_o(T_o)\frac{dT_o}{dx}\Big|_{x=x_b}, \tag{3.2c}$$

$$-k_o(T_o)\frac{dT_o}{dx}\Big|_{x=L} = h_o(T_o)[T_o(x=L) - T_C] + \varepsilon_{r_o}(T_o)\sigma[T_o^4(x=L) - T_R^4]. \tag{3.2d}$$

where,

$$\dot{q}_i(T_i) = \dot{q}_i(1 + a_iT_i + b_iT_i^2 + c_iT_i^3), \tag{3.3a}$$

$$\dot{q}_o(T_o) = \dot{q}_o(1 + a_oT_o + b_oT_o^2 + c_oT_o^3), \tag{3.3b}$$

$$k_i(T_i) = k_i[1 + g_i(T_i - T_L)], \tag{3.3c}$$

$$k_o(T_o) = k_o[1 + g_o(T_o - T_R)], \tag{3.3d}$$

$$\varepsilon_{r_i}(T_i) = \varepsilon_{r_i}[1 + \upsilon_i(T_i - T_L)], \tag{3.3e}$$

$$\varepsilon_{r_o}(T_o) = \varepsilon_{r_o}[1 + \upsilon_o(T_o - T_R)], \tag{3.3f}$$

and

$$h_i(T_i) = h_i\left\{\frac{T_i - T_C}{T_{ini} - T_C}\right\}^n, \tag{3.3g}$$

$$h_o(T_o) = h_o\left\{\frac{T_o - T_C}{T_{ini} - T_C}\right\}^n. \tag{3.3h}$$

Before attempting to solve the above equations, these equations are made non-dimensional. The benefits of non-dimensionalization include, the disappearance of very large numbers and appearance of very large quantities of physical interest such as Fourier number and Biot number. To make the problem dimensionless, we introduce the following quantities,

$$\theta_i = \frac{T_i}{T_L}, \quad \theta_o = \frac{T_o}{T_L}, \quad \theta_R = \frac{T_R}{T_L}, \quad \theta_{ini} = \frac{T_{ini}}{T_L}, \quad \theta_C = \frac{T_C}{T_L}, \quad X = \frac{x}{L}, \quad \zeta = \frac{x_b}{L},$$
$$\alpha_i = a_iT_L, \quad \alpha_o = a_oT_L, \quad \beta_i = b_iT_L^2, \quad \beta_o = b_oT_L^2, \quad \gamma_i = c_iT_L^3, \quad \gamma_o = c_oT_L^3,$$
$$\delta_i = g_iT_L, \quad \delta_o = g_oT_L, \quad \nu_i = \upsilon_iT_L, \quad \nu_o = \upsilon_oT_L, \quad Q_i = \frac{\dot{q}_iL^2}{k_iT_L}, \quad Q_o = \frac{\dot{q}_oL^2}{k_oT_L},$$
$$k_r = \frac{k_o}{k_i}, \quad Nc_i = \frac{h_iL}{k_i}, \quad Nc_o = \frac{h_oL}{k_o}, \quad Nr_i = \frac{\sigma\varepsilon_{r_i}LT_L^3}{k_i}, \quad Nr_o = \frac{\sigma\varepsilon_{r_o}LT_L^3}{k_o}. \tag{3.4}$$

After substitution of above quantities in equations (3.3a)-(3.3h), temperature-dependent thermal properties are as follows,

$$Q_i(\theta_i) = Q_i(1 + \alpha_i\theta_i + \beta_i\theta_i^2 + \gamma_i\theta_i^3), \tag{3.5a}$$
$$Q_o(\theta_o) = Q_o(1 + \alpha_o\theta_o + \beta_o\theta_o^2 + \gamma_o\theta_o^3), \tag{3.5b}$$
$$k_i(\theta_i) = k_i[1 + \delta_i(\theta_i - 1)], \tag{3.5c}$$
$$k_o(\theta_o) = k_o[1 + \delta_o(\theta_o - \theta_R)], \tag{3.5d}$$
$$\varepsilon_{r_i}(\theta_i) = \varepsilon_{r_i}[1 + \nu_i(\theta_i - 1)], \tag{3.5e}$$
$$\varepsilon_{r_o}(\theta_o) = \varepsilon_{r_o}[1 + \nu_o(\theta_o - \theta_R)], \tag{3.5f}$$
$$\text{and} \quad h_i(\theta_i) = h_i\left\{\frac{\theta_i - \theta_C}{\theta_{ini} - \theta_C}\right\}^n, \tag{3.5g}$$
$$h_o(\theta_o) = h_o\left\{\frac{\theta_o - \theta_C}{\theta_{ini} - \theta_C}\right\}^n. \tag{3.5h}$$

and correspondingly equations (3.1a)-(3.2d), in non dimensional form are written as follows,

$$\frac{d}{dX}\left[1 + \delta_i(\theta_i - 1)\frac{d\theta_i}{dX}\right] + Q_i[1 + \alpha_i\theta_i + \beta_i\theta_i^2 + \gamma_i\theta_i^3] = 0, \qquad 0 < X < \zeta, \tag{3.6a}$$
$$\frac{d}{dX}\left[1 + \delta_o(\theta_o - \theta_R)\frac{d\theta_o}{dX}\right] + Q_o[1 + \alpha_o\theta_o + \beta_o\theta_o^2 + \gamma_o\theta_o^3] = 0, \qquad \zeta < X < 1. \tag{3.6b}$$

and the corresponding boundary conditions as

$$[1 + \delta_i(\theta_i - 1)]\frac{d\theta_i}{dX}\Big|_{X=0} = Nc_i\left\{\frac{\theta_i - \theta_C}{\theta_{ini} - \theta_C}\right\}^n [\theta_i(X = 0) - 1] + Nr_i[1 + \nu_i(\theta_i - 1)](\theta_i^4(X = 0) - 1), \tag{3.7a}$$
$$\theta_i|_{X=\zeta} = \theta_o|_{X=\zeta}, \tag{3.7b}$$
$$(1 + \delta_i(\theta_i - 1))\frac{d\theta_i}{dX}\Big|_{X=\zeta} = k_r[1 + \delta_o(\theta_o - \theta_R)]\frac{d\theta_o}{dX}\Big|_{X=\zeta}, \tag{3.7c}$$
$$-[1 + \delta_o(\theta_o - \theta_R)]\frac{d\theta_o}{dX}\Big|_{X=1} = Nc_o\left\{\frac{\theta_o - \theta_C}{\theta_{ini} - \theta_C}\right\}^n [\theta_o(X = 1) - \theta_C] + Nr_o[1 + \nu_o(\theta_o - \theta_R)](\theta_o^4(X = 1) - \theta_R^4). \tag{3.7d}$$

The above dimensionless form in equations (3.6a)-(3.7d) depends on various parameters namely θ_i, θ_o, θ_R, θ_{ini}, θ_C, the non dimensional temperatures, ζ, the junction position, α_i, β_i, γ_i, α_o, β_o, γ_o, the internal heat generation parameters, k_r, δ_i, δ_o, the conductivity parameters, ν_i, ν_o, the emissivity parameters, Nc_i, Nc_o, Nr_i, Nr_o, the convection conduction and radiation conduction parameters. The system thus formed (3.6a)-(3.7d), being non-linear is solved by ADM as discussed in the next section. To determine the heat losses occurring in the walls, which is crucial to study for application purposes, the efficiency of the system is calculated.

The amount of heat at any time in Watts which enters the composite system,

$$Q_{In} = k_i(T_i)A_i \frac{dT_i}{dx}\Big|_{x=0}, \tag{3.8}$$

and heat loss from the composite system is given as

$$Q_{Out} = k_o(T_o)A_o \frac{dT_o}{dx}\Big|_{x=L}, \tag{3.9}$$

where A_i and A_o are surface areas of inner and outer wall respectively. The heat flux in Watts per metre square is

$$q''_{In} = \frac{T_L k_i[1 + d_i(T_i - T_L)]}{L} \frac{d\theta_i}{dX}\Big|_{X=0}, \tag{3.10}$$

$$q''_{Out} = \frac{T_L k_o[1 + d_o(T_o - T_R)]}{L} \frac{d\theta_o}{dX}\Big|_{X=1}. \tag{3.11}$$

Thus, the total heat flux became

$$q''_{Total} = q''_{In} + q''_{Out}. \tag{3.12}$$

Efficiency is then defined as

$$\eta_{eff} = \left[\frac{q''_{Total} - q''_{Out}}{q''_{Total}}\right] \times 100. \tag{3.13}$$

3.2 Methodology

3.2.1 Adomian Decomposition Method

ADM is an efficient method, which can overcome non-linearity with ease. It gives a closed form solution without linearizing the given problem, Adomian (2013), Wang (2004) and hence is better among other analytical methods like Variational Iteration Method (VIM), Variation of Parameters Method (VPM), Homotopy Perturbation Method (HPM), Bildik and Konuralp (2006), Inc and Akgül (2014). ADM calculates the solution by expanding the non-linear terms into an infinite series, which then truncates the series to a desired tolerance. Further, it is semi-analytical method which does not require discretization as in numerical techniques and intensive computer calculations, Jiao *et al.* (2002). Moreover, ADM is applicable to any linear or non-linear differential and integral equation, Wazwaz (2005). Adomian polynomials decompose a function $u(x,t)$ into sum of components

$$u(x,t) = \sum_{n=0}^{\infty} u_n(x,t),$$

for a nonlinear operator $\mathbf{F}$ as

$$\mathbf{F}(u(x,t)) = \sum_{n=0}^{\infty} A_n,$$

where A_i's are called Adomian polynomials, Adomian (1988). There is no well-defined technique for constructing a definite set of polynomials for arbitrary **F**, but different approaches are available for different situations. One possible set of polynomials are obtained as follows:

$$A_0 = \mathbf{F}(u_0) \tag{3.14}$$

$$A_1 = u_1\mathbf{F}'(u_0) \tag{3.15}$$

$$A_2 = u_2\mathbf{F}'(u_0) + \frac{1}{2!}u_1^2\mathbf{F}''(u_0) \tag{3.16}$$

$$A_3 = u_3\mathbf{F}'(u_0) + u_1u_2\mathbf{F}''(u_0 + \frac{1}{3!}u_1^3\mathbf{F}'''(u_0)) \tag{3.17}$$

and so on. In general,

$$A_n = \frac{1}{n!}\frac{d^n}{dz^n}\Big(\mathbf{F}(u(z))\Big)\Big|_{z=0}. \tag{3.18}$$

Now coming back to our equations (3.6a), (3.6b) and writing linear and non-linear terms separately gives us

$$\frac{d^2\theta_i}{dX^2} = -\delta_i\Big[\theta_i\Big(\frac{d^2\theta_i}{dX^2}\Big) + \Big(\frac{d\theta_i}{dX}\Big)^2\Big] + \delta_i\frac{d^2\theta_i}{dX^2} - Q_i(1+\alpha_i\theta_i) - Q_i\beta_i\theta_i^2 - Q_i\gamma_i\theta_i^3, \quad 0 < X < \zeta, \tag{3.19a}$$

$$\frac{d^2\theta_o}{dX^2} = -\delta_o\Big[\theta_o\Big(\frac{d^2\theta_o}{dX^2}\Big) + \Big(\frac{d\theta_o}{dX}\Big)^2\Big] + \delta_o\theta_R\frac{d^2\theta_o}{dX^2} - Q_o(1+\alpha_o\theta_o) - Q_o\beta_o\theta_o^2 - Q_o\gamma_o\theta_o^3, \quad \zeta < X < 1. \tag{3.19b}$$

Writing $\dfrac{d^2}{dX^2} = L_{XX}$ and $L_{XX}^{-1} = \int_0^X\int_0^X(...)\,dX\,dX$, we obtain

$$L_{XX}\theta_i = -\delta_i\Big[\theta_i\Big(\frac{d^2\theta_i}{dX^2}\Big) + \Big(\frac{d\theta_i}{dX}\Big)^2\Big] + \delta_i\frac{d^2\theta_i}{dX^2} - Q_i(1+\alpha_i\theta_i) - Q_i\beta_i\theta_i^2 - Q_i\gamma_i\theta_i^3, \quad 0 < X < \zeta \tag{3.20a}$$

$$L_{XX}\theta_o = -\delta_o\Big[\theta_o\Big(\frac{d^2\theta_o}{dX^2}\Big) + \Big(\frac{d\theta_o}{dX}\Big)^2\Big] + \delta_o\theta_R\frac{d^2\theta_o}{dX^2} - Q_o(1+\alpha_o\theta_o) - Q_o\beta_o\theta_o^2 - Q_o\gamma_o\theta_o^3. \quad \zeta < X < 1 \tag{3.20b}$$

Using the above explained Adomian decomposition, we write

$$\theta_i = \sum_{m=0}^{\infty}\theta_{im} = \theta_{i0} + \theta_{i1} + \theta_{i2} + \ldots\cdots + \theta_{i\infty}, \tag{3.21a}$$

$$\theta_o = \sum_{m=0}^{\infty}\theta_{om} = \theta_{o0} + \theta_{o1} + \theta_{o2} + \ldots\cdots + \theta_{o\infty}. \tag{3.21b}$$

Computation of θ_{im} and θ_{om} will be seen ahead. Adomian decomposition for nonlinear terms,

$$\theta_i\frac{d^2\theta_i}{dX^2} = \sum_{k=0}^{\infty}A_{ik}, \qquad \theta_o\frac{d^2\theta_o}{dX^2} = \sum_{k=0}^{\infty}A_{ok},$$

$$\Big(\frac{d\theta_i}{dX}\Big)^2 = \sum_{k=0}^{\infty} B_{ik}, \qquad \Big(\frac{d\theta_o}{dX}\Big)^2 = \sum_{k=0}^{\infty} B_{ok},$$
$$\theta_i^2 = \sum_{k=0}^{\infty} C_{ik}, \qquad \theta_o^2 = \sum_{k=0}^{\infty} C_{ok},$$
$$\theta_i^3 = \sum_{k=0}^{\infty} D_{ik}, \qquad \theta_o^3 = \sum_{k=0}^{\infty} D_{ok}, \tag{3.22}$$

where A_{ik}, B_{ik}, C_{ik}, D_{ik}, A_{ok}, B_{ok}, C_{ok} and D_{ok} are Adomian polynomials given as follows (Take k = 0, 1, 2)

$$A_{i0} = \theta_{i0}\frac{d^2\theta_{i0}}{dX^2}, \qquad C_{i0} = \theta_{i0}^2,$$
$$A_{i1} = \theta_{i1}\frac{d^2\theta_{i0}}{dX^2} + \theta_{i0}\frac{d^2\theta_{i1}}{dX^2}, \qquad C_{i1} = 2\theta_{i0}\theta_{i1},$$
$$A_{i2} = \theta_{i2}\frac{d^2\theta_{i0}}{dX^2} + \theta_{i1}\frac{d^2\theta_{i1}}{dX^2} + \theta_{i0}\frac{d^2\theta_{i2}}{dX^2}, \qquad C_{i2} = 2\theta_{i0}\theta_{i2} + \theta_{i1}^2,$$
$$\vdots \qquad\qquad \vdots$$
$$B_{i0} = \Big(\frac{d\theta_{i0}}{dX}\Big)^2, \qquad D_{i0} = \theta_{i0}^3,$$
$$B_{i1} = 2\Big(\frac{d\theta_{i0}}{dX}\Big)\Big(\frac{d\theta_{i1}}{dX}\Big), \qquad D_{i1} = 3\theta_{i0}^2\theta_{i1},$$
$$B_{i2} = \Big(\frac{d\theta_{i1}}{dX}\Big)^2 + 2\Big(\frac{d\theta_{i0}}{dX}\Big)\Big(\frac{d\theta_{i2}}{dX}\Big), \qquad D_{i2} = 3\theta_{i0}\theta_{i1}^2 + 3\theta_{i0}^2\theta_{i2}, \tag{3.23}$$
$$\vdots \qquad\qquad \vdots$$

The governing equations become,

$$L_{XX}\theta_i = -\delta_i\Big(\sum_{k=0}^{\infty} A_{ik}\Big) - \delta_i\Big(\sum_{k=0}^{\infty} B_{ik}\Big) + \delta_i\frac{d^2\theta_i}{dX^2} - Q_i(1+\alpha_i\theta_i) - Q_i\beta_i\Big(\sum_{k=0}^{\infty} C_{ik}\Big) - Q_i\gamma_i\Big(\sum_{k=0}^{\infty} D_{ik}\Big), \tag{3.24a}$$

$$L_{XX}\theta_o = -\delta_o\Big(\sum_{k=0}^{\infty} A_{ok}\Big) - \delta_o\Big(\sum_{k=0}^{\infty} B_{ok}\Big) + \delta_o\theta_R\frac{d^2\theta_o}{dX^2} - Q_o(1+\alpha_o\theta_o) - Q_o\beta_o\Big(\sum_{k=0}^{\infty} C_{ok}\Big) - Q_o\gamma_o\Big(\sum_{k=0}^{\infty} D_{ok}\Big). \tag{3.24b}$$

Operating L_{XX}^{-1} on both sides,

$$\theta_i = c_0 + Xc_1 - \delta_i L_{XX}^{-1}\Big(\sum_{k=0}^{\infty} A_{ik}\Big) - \delta_i L_{XX}^{-1}\Big(\sum_{k=0}^{\infty} B_{ik}\Big) + \delta_i L_{XX}^{-1}\frac{d^2\theta_i}{dX^2} - Q_i L_{XX}^{-1}(1+\alpha_i\theta_i) \\ -Q_i\beta_i L_{XX}^{-1}\Big(\sum_{k=0}^{\infty} C_{ik}\Big) - Q_i\gamma_i L_{XX}^{-1}\Big(\sum_{k=0}^{\infty} D_{ik}\Big), \tag{3.25a}$$

$$\theta_o = c_2 + Xc_3 - \delta_o L_{XX}^{-1}\Big(\sum_{k=0}^{\infty} A_{ok}\Big) - \delta_o L_{XX}^{-1}\Big(\sum_{k=0}^{\infty} B_{ok}\Big) + \delta_o\theta_R L_{XX}^{-1}\frac{d^2\theta_o}{dX^2} - Q_o L_{XX}^{-1}(1+\alpha_o\theta_o) \\ -Q_o\beta_o L_{XX}^{-1}\Big(\sum_{k=0}^{\infty} C_{ok}\Big) - Q_o\gamma_o L_{XX}^{-1}\Big(\sum_{k=0}^{\infty} D_{ok}\Big), \tag{3.25b}$$

where c_0, c_1, c_2, c_3 were constants, obtained as a result of integration and will be computed using non-linear boundary conditions. Using equations (3.21a), (3.21b), equations (3.25a), (3.25b) become,

$$\sum_{m=0}^{\infty}\theta_{im} = c_0 + Xc_1 - \delta_i L_{XX}^{-1}\Big(\sum_{k=0}^{\infty} A_{ik}\Big) - \delta_i L_{XX}^{-1}\Big(\sum_{k=0}^{\infty} B_{ik}\Big) + \delta_i L_{XX}^{-1}\sum_{m=0}^{\infty}\frac{d^2\theta_{im}}{dX^2} \\ - Q_i L_{XX}^{-1}\Big(1+\alpha_i\sum_{m=0}^{\infty}\theta_{im}\Big) - Q_i\beta_i L_{XX}^{-1}\Big(\sum_{k=0}^{\infty} C_{ik}\Big) - Q_i\gamma_i L_{XX}^{-1}\Big(\sum_{k=0}^{\infty} D_{ik}\Big), \tag{3.26a}$$

$$\sum_{m=0}^{\infty}\theta_{om} = c_2 + Xc_3 - \delta_o L_{XX}^{-1}\Big(\sum_{k=0}^{\infty} A_{ok}\Big) - \delta_o L_{XX}^{-1}\Big(\sum_{k=0}^{\infty} B_{ok}\Big) + \delta_o\theta_R L_{XX}^{-1}\Big(\sum_{m=0}^{\infty}\frac{d^2\theta_{om}}{dX^2}\Big) \\ - Q_o L_{XX}^{-1}\Big(1+\alpha_o\sum_{m=0}^{\infty}\theta_{om}\Big) - Q_o\beta_o L_{XX}^{-1}\Big(\sum_{k=0}^{\infty} C_{ok}\Big) - Q_o\gamma_o L_{XX}^{-1}\Big(\sum_{k=0}^{\infty} D_{ok}\Big). \tag{3.26b}$$

The components θ_{im} and θ_{om} are computed as

$$\theta_{i0} = c_0 + Xc_1 - Q_i L_{XX}^{-1}(1), \tag{3.27a}$$

$$\theta_{o0} = c_2 + Xc_3 - Q_o L_{XX}^{-1}(1), \tag{3.27b}$$

and the higher order terms $(m > 0)$ are obtained from the following recursive relations by

$$\theta_{i\,m} = \delta_i L_{XX}^{-1}\Big(\frac{d^2\theta_{i\,m-1}}{dX^2}\Big) - Q_i\alpha_i L_{XX}^{-1}\theta_{i\,m-1} - \delta_i L_{XX}^{-1}A_{i\,m-1} - \delta_i L_{XX}^{-1}B_{i\,m-1} \\ - Q_i\beta_i L_{XX}^{-1}C_{i\,m-1} - Q_i\gamma_i L_{XX}^{-1}D_{i\,m-1}, \tag{3.28a}$$

$$\theta_{o\,m} = \delta_o\theta_R L_{XX}^{-1}\Big(\frac{d^2\theta_{o\,m-1}}{dX^2}\Big) - Q_o\alpha_o L_{XX}^{-1}\theta_{o\,m-1} - \delta_o L_{XX}^{-1}A_{o\,m-1} - \delta_o L_{XX}^{-1}B_{o\,m-1} \\ - Q_o\beta_o L_{XX}^{-1}C_{o\,m-1} - Q_o\gamma_o L_{XX}^{-1}D_{o\,m-1}. \tag{3.28b}$$

Restricted to m terms, the approximations of θ_i and θ_o are as follows:

$$\theta_i \approx \sum_{j=0}^{m-1} \theta_{ij} = \theta_{i0} + \theta_{i1} + \ldots \cdots + \theta_{i\,m-1}, \tag{3.29a}$$

$$\theta_o \approx \sum_{j=0}^{m-1} \theta_{oj} = \theta_{o0} + \theta_{o1} + \ldots \cdots + \theta_{o\,m-1}, \tag{3.29b}$$

which converges to θ_i and θ_o as $m \to \infty$.

The functional form of temperature profile for inner wall material is obtained by summing

$$\theta_i \approx \sum_{j=0}^{m-1} \theta_{ij} = \theta_{i0} + \theta_{i1} + \ldots \cdots + \theta_{i\,m-1},$$

Few terms of the series with $m = 6$, (based on the analysis presented in Table (3.1)) thus obtained, are written as follows for the inner wall.

$$
\begin{aligned}
\boldsymbol{\theta_{i0}} =& c_0 + Xc_1 - \frac{Q_i X^2}{2},\\
\boldsymbol{\theta_{i1}} =& \frac{\gamma_i Q_i^4 X^8}{448} - \frac{\gamma_i Q_i^3 c_1 X^7}{56} + Q_i^3\Big(-\frac{\beta_i}{120} - \gamma_i\Big(\frac{1}{40} - \frac{c_1^2}{Q_i 20}\Big)\Big)X^6 + Q_i^2 c_1\Big(\frac{\beta_i}{20} - \gamma_i\Big(\frac{c_1^2}{Q_i 20} - \frac{3c_0}{20}\Big)\Big)X^5\\
&+ Q_i^2\Big(\Big(\frac{\alpha_i}{24} - \frac{\delta_i}{8}\Big) + \gamma_i\Big(\frac{c_0^2}{8} - \frac{c_0 c_1^2}{Q_i 4}\Big) + \beta_i\Big(\frac{c_0}{12} - \frac{c_1^2}{12}\Big)\Big)X^4 + Q_i c_1\Big(-\frac{\gamma_i c_0^2}{2} - \frac{\beta_i c_0}{3} + \frac{\delta_i}{2} - \frac{\alpha_i}{6}\Big)X^3\\
&+ \frac{Q_i}{2}\Big(\delta_i\Big(c_0 - 1 - \frac{c_1^2}{Q_i}\Big) - c_0\Big(\alpha_i - \beta_i c_0 - \gamma_i c_0^2\Big)\Big)X^2,\\
\boldsymbol{\theta_{i2}} =& -\frac{3\gamma_i^2 Q_i^7 X^{14}}{326144} + \frac{3\gamma_i^2 Q_i^6 c_1 X^{13}}{23296} + Q_i^6\gamma_i^2\Big(\frac{19c_0}{98560} - \frac{73c_1^2}{Q_i 98560} + \frac{19\beta_i}{\gamma_i 295680}\Big)X^{12} + \gamma_i^2 Q_i^5 c_1\Big(-\frac{57c_0}{24640}\\
&+ \frac{27c_1^2}{Q_i 12320} - \frac{19\beta_i}{\gamma_i 24640}\Big)X^{11} + \gamma_i^2 Q_i^5\Big(\beta_i\Big(\frac{181c_1^2}{\gamma_i Q_i 50400} - \frac{131c_0}{\gamma_i 100800}\Big) - \frac{\beta_i^2}{\gamma_i^2 10800} - \frac{131c_0^2}{67200}\\
&- \frac{c_1^4}{Q_i^2 300} + \frac{29\delta_i}{\gamma_i 13440} - \frac{\alpha_i}{\gamma_i 2688} + \frac{181c_0c_1^2}{Q_i 16800}\Big)X^{10} + Q_i^4\gamma_i^2\Big(\frac{\beta_i^2 c_1}{\gamma_i^2 1080} - \beta_i\Big(\frac{11\gamma_i c_1^3}{Q_i\gamma_i^2 1440} - \frac{131c_0c_1}{\gamma_i 10080}\Big)\\
&+ \frac{c_1^5}{Q_i^2 480} + \frac{5\alpha_i c_1}{\gamma_i 1344} - \frac{11c_0c_1^3}{Q_i 480} + \frac{131c_0^2c_1}{6720} - \frac{29\delta_i c_1}{\gamma_i 1344}\Big)X^9 + Q_i^4\gamma_i\Big(\alpha_i\Big(\frac{\beta_i}{\gamma_i 1120} - \frac{27c_1^2}{Q_i 2240} + \frac{3c_0}{320}\Big)\\
&- \delta_i\Big(\frac{43\beta_i}{\gamma_i 6720} - \frac{1}{112} - \frac{93c_1^2}{Q_i 1120} + \frac{9c_0}{320}\Big) + \beta_i^2\Big(\frac{c_0}{\gamma_i 560} - \frac{11c_1^2}{Q_i\gamma_i 3360}\Big) + \beta_i\Big(\frac{33c_0^2}{2240} - \frac{7c_0c_1^2}{Q_i 160}\\
&+ \frac{c_1^4}{Q_i^2 160}\Big) + \frac{33\gamma_i c_0^3}{2240} - \frac{21\gamma_i c_0^2c_1^2}{Q_i 320} + \frac{3\gamma_i c_0c_1^4}{Q_i^2 160}\Big)X^8 + Q_i^3 c_1\Big(\beta_i^2\Big(\frac{c_1^2}{Q_i 252} - \frac{c_0}{70}\Big) - \alpha_i\Big(\frac{\beta_i}{140}\\
&- \frac{11\gamma_i c_1^2}{Q_i 840} + \frac{2\gamma_i c_0}{35}\Big) - \delta_i\Big(\frac{41\gamma_i c_1^2}{Q_i 280} - \frac{43\beta_i}{840} + \frac{3\gamma_i}{56} - \frac{29\gamma_i c_0}{140}\Big) + \beta_i\Big(\frac{\gamma_i c_0c_1^2}{Q_i 20} - \frac{\gamma_i c_0^2}{10}\Big) + \frac{3\gamma_i^2 c_0^2c_1^2}{Q_i 40}\\
&- \frac{\gamma_i^2 c_0^3}{Q_i 10}\Big)X^7 + Q_i^3\Big(\delta_i\Big(\frac{\alpha_i}{40} - \beta_i\Big(\frac{1}{40} - \frac{3c_0}{40} + \frac{17c_1^2}{Q_i 120}\Big) + \frac{\gamma_i c_1^2}{Q_i 10} + \frac{3\gamma_i c_0^2}{20} - \frac{3\gamma_i c_0}{40} + \frac{\gamma_i c_1^4}{Q_i^2 10}\\
&- \frac{21\gamma_i c_0c_1^2}{Q_i 40}\Big) - \frac{\delta_i^2}{16} - \frac{\alpha_i^2}{720} - \beta_i^2\Big(\frac{c_0^2}{45} - \frac{c_0c_1^2}{Q_i 36}\Big) - \beta_i\Big(\frac{\gamma_i c_0^3}{12} - \frac{7\gamma_i c_0^2c_1^2}{Q_i 40}\Big) - \alpha_i\Big(\beta_i\Big(\frac{c_0}{45} - \frac{c_1^2}{Q_i 72}\Big)\\
&+ \frac{7\gamma_i c_0^2}{120} - \frac{11\gamma_i c_0c_1^2}{Q_i 120}\Big) - \frac{\gamma_i^2 c_0^4}{16} + \frac{7\gamma_i^2 c_0^3c_1^2}{Q_i 40}\Big)X^6 + Q_i^2 c_1\Big(\delta_i\Big(\beta_i\Big(\frac{1}{10} + \frac{2c_1^2}{15} - \frac{2c_0}{5}\Big) - \frac{\gamma_i c_1^2}{Q_i 20} - \frac{3\alpha_i}{20}\\
&+ \frac{3\gamma_i c_0}{10} + \frac{9\gamma_i c_0c_1^2}{Q_i 20} - \frac{3\gamma_i c_0^2}{4}\Big) + \alpha_i\Big(\frac{\gamma_i c_0^2}{5} + \frac{\beta_i c_0}{12}\Big) + \frac{3\delta_i^2}{8} + \frac{\alpha_i^2}{120} + \frac{\beta_i^2 c_0^2}{12} + \frac{9\gamma_i^2 c_0^4}{40} + \frac{3\beta_i\gamma_i c_0^3}{10}\Big)X^5\\
&+ \Big(\alpha_i\Big(\frac{\gamma_i Q_i^2 c_0^3}{6} + Q_i^2\frac{\beta_i c_0^2}{8}\Big) - \delta_i^2\Big(\frac{3c_1^2}{Q_i 4} - \frac{3c_0}{8} + \frac{3}{8}\Big) + \delta_i\Big(\alpha_i\Big(\frac{5c_1^2}{Q_i 24} - \frac{c_0}{3} + \frac{1}{12}\Big) + \beta_i\Big(-\frac{5c_0^2}{12}\\
&+ \frac{c_0}{6} + \frac{c_0c_1^2}{Q_i 2} - \frac{c_1^2}{Q_i 12}\Big) + \frac{\gamma_i c_0^2}{4} - \frac{\gamma_i c_0^3}{2} - \frac{\gamma_i c_0c_1^2}{Q_i 4} + \frac{7\gamma_i c_0^2c_1^2}{Q_i 8}\Big) + \frac{\alpha_i^2 c_0}{24} + \frac{\beta_i^2 c_0^3}{12} + \frac{\gamma_i^2 c_0^5}{8}\\
&+ \frac{(5\beta_i\gamma_i c_0^4}{24}\Big)X^4 + Q_i c_1\Big(\delta_i^2\frac{1 + c_1^2}{2} - c_0\Big) - \delta_i\Big(\beta_i\Big(\frac{c_0)}{3} - \frac{5c_0^2}{6}\Big) + \alpha_i\Big(\frac{1}{6} - \frac{2c_0}{3}\Big) + \frac{\gamma_i c_0^2}{2}\\
&- \gamma_i c_0^3\Big)\Big)X^3 + Q_i c_0\Big(\Big(-\frac{c_0}{2} + \frac{c_1^2}{Q_i 2} + \frac{1 - \frac{c_1^2}{Q_i c_0}}{2} - \frac{1}{c_0 2}\Big)\delta_i^2 + \Big(\frac{\gamma_i c_0^3}{2} - \beta_i\Big(\frac{c_0}{2} - \frac{c_0^2}{2}\Big) - \frac{\gamma_i c_0^2}{2}\\
&- \alpha_i\Big(\frac{1}{2} - \frac{c_0}{2}\Big)\Big)\delta_i\Big)X^2, \qquad (3.30)
\end{aligned}
$$

and so on.

The functional form of temperature profile for outer material is obtained by summing

$$\theta_o \approx \sum_{j=0}^{m-1} \theta_{oj} = \theta_{o0} + \theta_{o1} + \ldots\cdots + \theta_{o\,m-1},$$

where the values of θ_{oj} for the outer material, for $j = 1, 2, 3$, for $m = 6$ are given ahead.

$$
\begin{aligned}
\boldsymbol{\theta_{o0}} =& c_2 + Xc_3 - \frac{Q_o X^2}{2},\\
\boldsymbol{\theta_{o1}} =& \Big(\gamma_o \frac{Q_o^4}{448} X^8\Big) - \Big(\gamma_o \frac{Q_o^3 c_3}{56} X^7\Big) + Q_o^3\Big(-\frac{\beta_o}{120} - \gamma_o\Big(\frac{c_2}{40} - \frac{c_3^2}{Q_o 20}\Big)\Big) X^6 + Q_o^2 c_3\Big(\frac{\beta_o}{20} - \gamma_o\Big(\frac{c_3^2}{Q_o 20}\\
&- \frac{3c_2}{20}\Big)\Big) X^5 + Q_o^2\Big(\frac{\alpha_o}{24} - \Big(\frac{\delta_o}{8} + \gamma_o\Big(\frac{c_2^2}{8} - \frac{c_2 c_3^2}{Q_o 4}\Big) + \beta_o\Big(\frac{c_2}{12} - \frac{c_3^2}{Q_o 12}\Big)\Big)\Big) X^4 + Q_o c_3\Big(-\frac{\gamma_o c_2^2}{2}\\
&- \frac{\beta_o c_2}{3} + \frac{\delta_o}{2} - \frac{\alpha_o}{6}\Big) X^3 + Q_o\Big(\frac{\delta_o c_2}{2} - \frac{\delta_o c_3^2}{Q_o 2} - \frac{\delta_o \theta_{rad}}{2} - \frac{\alpha_o c_2}{2} - \frac{\beta_o c_2^2}{2} - \frac{\gamma_o c_2^3}{2}\Big) X^2,\\
\boldsymbol{\theta_{o2}} =& -\frac{3\gamma_o^2 Q_o^7 X^{14}}{326144} + \frac{3\gamma_o^2 Q_o^6 c_3 X^{13}}{23296} + Q_o^6\Big(\Big(\frac{19c_2\gamma_o^2}{98560} + \frac{19\beta_o\gamma_o}{295680}\Big) - \frac{73\gamma_o^2 c_3^2}{Q_o 98560}\Big) X^{12} + Q_o^5\gamma_o^2\Big(\frac{27c_3^3}{Q_o 12320}\\
&- \frac{57c_2c_3}{24640} + \frac{19\beta_o c_3}{\gamma_o 24640}\Big) X^{11} + Q_o^5\Big(\Big(\frac{181c_2\gamma_o^2c_3^2}{Q_o 16800} + \frac{181\beta_o\gamma_o c_3^2}{50400}\Big) - \Big(\frac{\beta_o^2}{10800} + \frac{131\gamma_o^2c_2^2}{67200} + \gamma_o\Big(\frac{\alpha_o}{2688}\\
&+ \frac{131\beta_o c_2}{100800}\Big) - \frac{29\delta_o\gamma_o}{13440}\Big) - \frac{\gamma_o^2 c_3^4}{Q_o^2 300}\Big) X^{10} + Q_o^4\Big(\Big(\frac{\beta_o^2 c_3}{1080} + \gamma_o\Big(\frac{5\alpha_o c_3}{1344} + \frac{131\beta_o c_2 c_3}{10080}\Big) + \frac{131\gamma_o^2 c_2^2 c_3}{6720}\\
&- \frac{29\delta_o\gamma_o c_3}{1344}\Big) - \frac{1}{Q_o}\Big(\frac{11c_2\gamma_o^2c_3^3}{480} + \frac{11\beta_o\gamma_o c_3^3}{1440}\Big) + \frac{\gamma_o^2 c_3^5}{Q_o^2 480}\Big) X^9 + \Big(Q_o^4\Big(\frac{\beta_o\alpha_o}{1120} - \delta_o\Big(\frac{43\beta_o}{6720}\\
&+ \gamma_o\Big(\frac{9c_2}{320} - \frac{\theta_{rad}}{112}\Big)\Big) + \frac{\beta_o^2 c_2}{560} + \gamma_o\Big(\frac{33\beta_o c_2^2}{2240} + \frac{3\alpha_o c_2}{320}\Big) + \frac{33\gamma_o^2 c_2^3}{2240}\Big) + \frac{c_3^2}{Q_o}\Big(\frac{93\delta_o\gamma_o}{1120} - \frac{11\beta_o^2}{3360}\\
&- \frac{21\gamma_o^2 c_2^2}{320} - \gamma_o\Big(\frac{27\alpha_o}{2240} + \frac{7\beta_o c_2}{160}\Big)\Big) + \frac{c_3^4}{Q_o^2}\Big(\frac{3c_2\gamma_o^2}{160} + \frac{\beta_o\gamma_o c_3^4}{160}\Big)\Big) X^8 + \Big(c_3^3\Big(\gamma_o\Big(\frac{11\alpha_o}{840} + \frac{\beta_o c_2}{20}\\
&- \frac{41\delta_o}{280}\Big) + \frac{\beta_o^2}{252} + \frac{3\gamma_o^2 c_2^2}{40}\Big) - Q_o^3 c_3\Big(\gamma_o c_2\Big(\frac{\beta_o c_2}{10} + \frac{2\alpha_o}{35}\Big) - \delta_o\Big(\frac{43\beta_o}{840} + \gamma_o\Big(\frac{29c_2}{140} - \frac{3\theta_{rad}}{56}\Big)\Big)\\
&+ \frac{\gamma_o^2 c_2^3}{10} + \frac{\beta_o\alpha_o}{140} + \frac{\beta_o^2 c_2}{70}\Big)\Big) X^7 + \Big(Q_o^2 c_3^2\Big(\gamma_o c_2\Big(\frac{7\beta_o c_2}{40} + \frac{11\alpha_o}{120}\Big) - \delta_o\Big(\gamma_o\Big(\frac{21c_2}{40} - \frac{\theta_{rad}}{10}\Big)\\
&+ \frac{17\beta_o}{120}\Big) + \frac{\beta_o^2 c_2}{36} + \frac{7\gamma_o^2 c_2^3}{40} + \frac{\beta_o\alpha_o}{72}\Big) - Q_o^3\Big(\frac{\delta_o^2}{16} - \delta_o\Big(\frac{\alpha_o}{40} + \frac{3\beta_o c_2}{40} - \frac{\beta_o\theta_{rad}}{40} - \gamma_o c_2\Big(\frac{3\theta_{rad}}{40}\\
&- \frac{3c_2}{20}\Big)\Big) + \frac{\alpha_o^2}{720} + \frac{\beta_o^2 c_2^2}{45} + \frac{\gamma_o^2 c_2^4}{16} + \gamma_o c_2^2\Big(\frac{\beta_o c_2}{12} + \frac{7\alpha_o}{120}\Big) + \frac{\beta_o\alpha_o c_2}{45}\Big) + \frac{\delta_o\gamma_o Q_o c_3^4}{10}\Big) X^6\\
&+ c_3\Big(\Big(\frac{3\delta_o^2}{8} + \frac{\alpha_o^2}{120} - \delta_o\Big(\gamma_o\Big(\frac{3c_2^2}{4} - \frac{3c_2\theta_{rad}}{10}\Big) + \Big(\frac{3\alpha_o}{20} - \frac{\beta_o\theta_{rad}}{10}\Big) + \frac{2\beta_o c_2}{5}\Big) + \gamma_o\Big(\frac{3\beta_o c_2^3}{10}\\
&+ \frac{\alpha_o c_2^2}{5}\Big) + \frac{\beta_o^2 c_2^2}{12} + \frac{9\gamma_o^2 c_2^4}{40} + \frac{\beta_o\alpha_o c_2}{12}\Big) Q_o^2 + \delta_o c_3^2\Big(\gamma_o\Big(\frac{9c_2}{20} - \frac{\theta_{rad}}{20}\Big) + \frac{2\beta_o}{15}\Big) Q_o\Big) X^5\\
&+ \Big(\Big(\delta_o\Big(\frac{\alpha_o\theta_{rad}}{12} - \frac{5\beta_o c_2^2}{12} + \gamma_o c_2^2\Big(\frac{\theta_{rad}}{4} - \frac{c_2}{2}\Big) - c_2\Big(\frac{\alpha_o}{3} - \frac{\beta_o\theta_{rad}}{6}\Big)\Big) + \frac{\alpha_o^2 c_2}{24} + \frac{\beta_o^2 c_2^3}{12} + \frac{\gamma_o^2 c_2^5}{8}\\
&+ \gamma_o c_2^3\Big(\frac{\beta_o c_2}{24} + \frac{\alpha_o}{6}\Big) + \frac{\delta_o^2}{8}\Big(3c_2 - 3\theta_{rad}\Big) + \frac{\beta_o\alpha_o c_2^2}{8}\Big) Q_o^2 + \Big(\delta_o c_3^2\Big(\Big(\frac{5\alpha_o}{24} - \frac{\beta_o\theta_{rad}}{12}\Big)\\
&+ \gamma_o\Big(\frac{7c_2^2}{8} - \frac{c_2\theta_{rad}}{4}\Big) + \frac{\beta_o c_2}{2}\Big) - \frac{3\delta_o^2}{4}\Big) Q_o\Big) X^4 + Q_o c_3\Big(\Big(\delta_o\Big(\gamma_o c_2^2\Big(c_2 - \frac{\theta_{rad}}{2}\Big) + \frac{c_2}{3}\Big(2\alpha_o\\
&- \beta_o\theta_{rad}\Big) - \frac{\alpha_o\theta_{rad}}{6} + \frac{5\beta_o c_2^2}{6}\Big) - \delta_o^2\Big(c_2 - \theta_{rad}\Big)\Big) + \frac{\delta_o^2 c_3^2}{2}\Big) X^3 + \Big(Q_o\Big(\delta_o\Big(c_2^2\Big(\frac{\alpha_o}{2} - \frac{\beta_o\theta_{rad}}{2}\Big)\\
&+ \frac{\beta_o c_2^3}{2} - \gamma_o\Big(\frac{c_2^3\theta_{rad}}{2} - \frac{c_2^4}{2}\Big) - \frac{\alpha_o c_2\theta_{rad}}{2}\Big) - \delta_o^2\Big(\frac{c_2^2}{2} - c_2\theta_{rad} + \frac{\theta_{rad}^2}{2}\Big)\Big) + \frac{\delta_o^2 c_3^2}{2}\Big(c_2 - \theta_{rad}\Big)\Big) X^2,
\end{aligned}
\tag{3.31}
$$

and so on.

3.2.2 Newton-Raphson Method

In the computation of temperature, all the parameters except the constants of integration c_0, c_1, c_2, c_3 are known. Newton Raphson's method is implemented to calculate these constants. After substitution of expressions θ_i and θ_o in the four boundary conditions namely equations (3.7a)-

(3.7d), rearranged in equations (3.32a)-(3.32d), unknown constants are calculated.

$$f_1 = [1+\delta_i(\theta_i-1)]\frac{d\theta_i}{dX}\Big|_{X=0} - Nc_i\left\{\frac{\theta_i-\theta_C}{\theta_{ini}-\theta_C}\right\}^n [\theta_i(X=0)-1] - Nr_i[1+\nu_i(\theta_i-1)](\theta_i^4(X=0)-1), \tag{3.32a}$$

$$f_2 = \theta_i|_{X=\zeta} - \theta_o|_{X=\zeta}, \tag{3.32b}$$

$$f_3 = (1+\delta_i(\theta_i-1))\frac{d\theta_i}{dX}\Big|_{X=\zeta} - k_r[1+\delta_o(\theta_o-\theta_R)]\frac{d\theta_o}{dX}\Big|_{X=\zeta}, \tag{3.32c}$$

$$f_4 = -[1+\delta_o(\theta_o-\theta_R)]\frac{d\theta_o}{dX}\Big|_{X=1} - Nc_o\left\{\frac{\theta_o-\theta_C}{\theta_{ini}-\theta_C}\right\}^n [\theta_o(X=1)-\theta_C] - Nr_o[1+\nu_o(\theta_o-\theta_R)](\theta_o^4(X=1)-\theta_R^4). \tag{3.32d}$$

The Newton Raphson method for multiple variables is represented as

$$\begin{pmatrix} c_0^{(N+1)} \\ c_1^{(N+1)} \\ c_2^{(N+1)} \\ c_3^{(N+1)} \end{pmatrix} = \begin{pmatrix} c_0^{(N)} \\ c_1^{(N)} \\ c_2^{(N)} \\ c_3^{(N)} \end{pmatrix} - \begin{pmatrix} \frac{\partial f_1}{\partial c_0^{(N)}} & \frac{\partial f_1}{\partial c_1^{(N)}} & \frac{\partial f_1}{\partial c_2^{(N)}} & \frac{\partial f_1}{\partial c_3^{(N)}} \\ \frac{\partial f_2}{\partial c_0^{(N)}} & \frac{\partial f_2}{\partial c_1^{(N)}} & \frac{\partial f_2}{\partial c_2^{(N)}} & \frac{\partial f_2}{\partial c_3^{(N)}} \\ \frac{\partial f_3}{\partial c_0^{(N)}} & \frac{\partial f_3}{\partial c_1^{(N)}} & \frac{\partial f_3}{\partial c_2^{(N)}} & \frac{\partial f_3}{\partial c_3^{(N)}} \\ \frac{\partial f_4}{\partial c_0^{(N)}} & \frac{\partial f_4}{\partial c_1^{(N)}} & \frac{\partial f_4}{\partial c_2^{(N)}} & \frac{\partial f_4}{\partial c_3^{(N)}} \end{pmatrix}^{-1} \begin{pmatrix} f_1^{(N)} \\ f_2^{(N)} \\ f_3^{(N)} \\ f_4^{(N)} \end{pmatrix} \tag{3.33}$$

where 'N' is the iteration number. With an initial guess (1.14, 0.58, 1, 0.8), chosen carefully, as the method is highly sensitive to the initial guess, the iterations start, at $N = 0$ and are stopped when the error between successive terms is less than 10^{-12}. These integral constants converge to a particular value after 27 iterations as illustrated in Fig.(3.2a). For the same parameters and same constants, functions $f_1,\ f_2,\ f_3,\ f_4$ tend to zero as can be seen in Fig.(3.2b).

This proves the convergence of Newton Raphson's method and we shall be using it for further calculations. In the following sections, we provide the comparison of the method, followed by the results and discussion of the present work.

3.3 Results and Discussion

3.3.1 Comparison

When ADM is applied on double layered wall, the obtained results are compared and validated with Torabi and Zhang (2015), who used Differential Transform Method (DTM) for the same set of parameters, as shown in Figures (3.3a) and (3.3b). In Fig. (3.3a), the variation of temperature profile with variation in Q_i and in Fig.(3.3b), with k_r are plotted against wall thickness. It is clear from the plots that the present results are in good agreement with results obtained by DTM, Torabi and Zhang (2015). Comparison of ADM with results in the literature asserts its

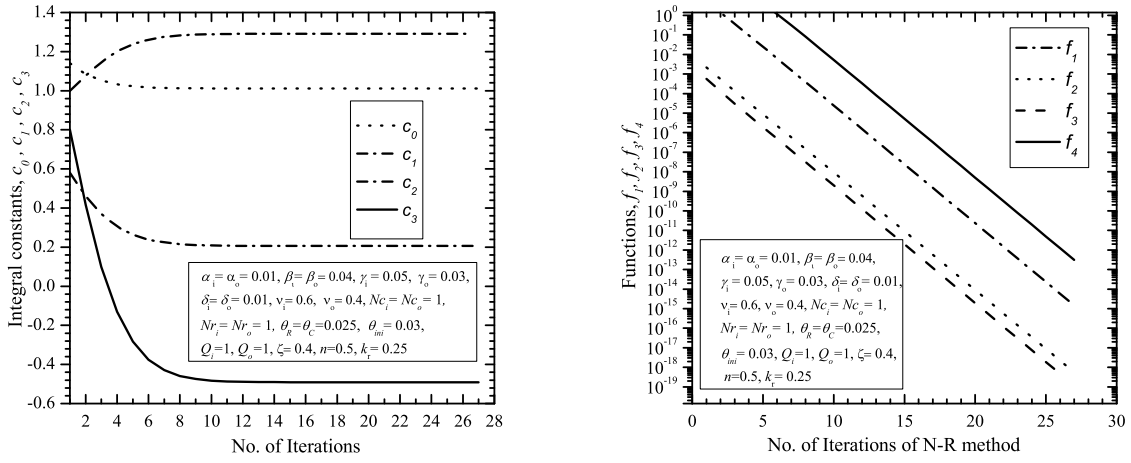

(a) **(b)**

Fig. 3.2 The variation of (a) Integral constants and (b) functions $f_1,\ f_2,\ f_3,\ f_4$ representing the boundary conditions with the no. of iterations in Newton-Raphson method.

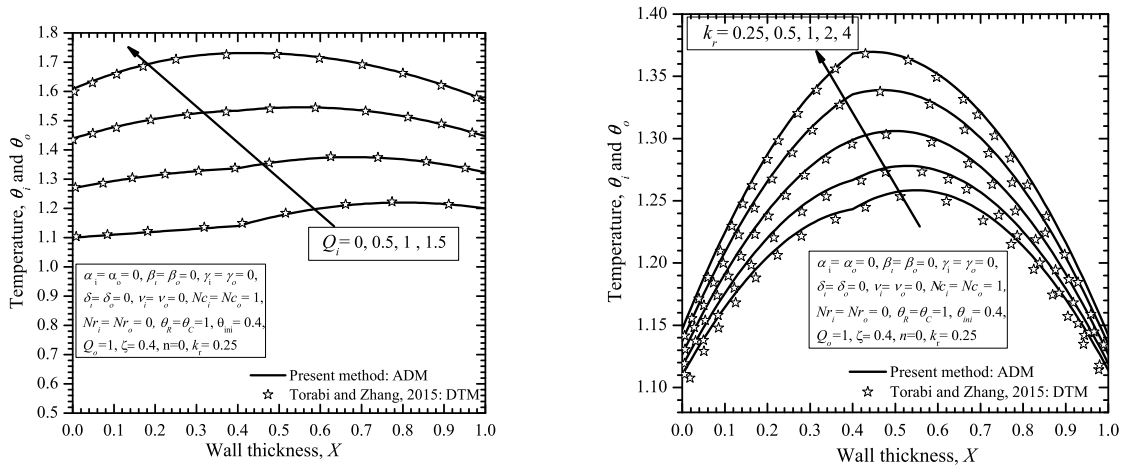

(a) **(b)**

Fig. 3.3 Comparison of ADM with DTM, Torabi and Zhang (2015), for variation in (a) Q_i and (b) k_r respectively, where temperature (θ_i and θ_o) were plotted with respect to wall thickness X.

applicability and hence we used it to obtain the functional form of temperature profiles of the double-layered wall.

To obtain an approximate closed-form solution to θ_i and θ_o, we need to restrict (3.21a) and (3.21b) to (3.29a) and (3.29b) respectively, by selecting the minimum number of terms (m), which provided more accurate solution along with least computational efforts. A study has been made for the same with a set of parameters as mentioned in Table (3.1), where for a different number of terms taken in the sum, represented by 'm', the temperature profile is compared. The comparison is made on the basis of computational time as well as the deviation of temperature profiles using the concept of absolute error.

A remarkable change in CPU time (567s - 871s) is observed on increasing the value of m from $m = 6$ to $m = 7$ in Table (3.1) as compared to the CPU time (525s - 567s) for $m = 5$ to $m = 6$. Moreover, a sudden jump in accuracy is obtained on moving from $m = 5$ to $m = 6$, as the order of corresponding errors are decreased from $O(10^{-8})$ to $O(10^{-10})$ as compared to the orders $O(10^{-10})$ to $O(10^{-11})$, for $m = 6$ to $m = 7$ respectively. Therefore $m = 6$ is selected for further computations keeping in mind the trade-off between accuracy and computational time. Here Intel(R) Core(TM) i7-4790 CPU with 3.60GHz clock speed and 8.00GB RAM is used for the calculations.

Having carefully selected the value of m, the effects of dimensionless parameters on temperature profile and efficiency of the system have been studied. For a better understanding, further discussions are divided into five subsections. In the first subsection, the effect of convection and radiation sink temperatures are observed when these are different, which often occurs in realistic situations. In the second subsection, the variation of temperature profile with respect to dimensionless parameters Nc_i, Nc_o, Nr_i, Nr_o, Q_i, Q_o, ζ for inner and outer layers has been studied. Moreover, the suitable values of these parameters for maximum efficiency are proposed. The third subsection illustrates variations of temperature and efficiency concerning the coefficients involved in temperature-dependent thermal properties. In the fourth subsection, an application of composite walls to furnace is seen. An inverse analysis is carried out in the fifth subsection.

3.3.2 Effect of sink temperatures on temperature and efficiency

There are several situations possible, apart from $\theta_C = \theta_R$, where sink temperatures for convection θ_C and radiation θ_R can variate or are different. It has been observed in Fig.(3.4) that when radiation temperature is changed from 0.025 to 0.015, keeping all other thermal parameters constant, the temperature distribution is increased by an order of 10^{-8}, which is insignificant. Furthermore, the increase in efficiency is of the order 10^{-4} which again is unremarkable. It is, therefore, advisable to remodel the problem with $\theta_C = \theta_R$, equal to 0.025, for the present study, even if they are not equal in general.

Table 3.1 Selection of the number of terms required in ADM for computation based on observation of associated absolute error in temperature distribution and the corresponding CPU time.

No. of Terms(m)	CPU time (s)	Parameters ($\zeta = 0.5$; $Nc_i = 4$; $Nc_o = 1$; $Nr_i = Nr_o = 1$; $\alpha_i = \alpha_o = 0.01$; $\beta_i = \beta_o = 0.04$; $\gamma_i = 0.05$; $\gamma_o = 0.03$; $\delta_i = \delta_o = 0.01$; $k_r = 0.01$; $Q_i = Q_o = 1$; $\theta_C = \theta_R = 0.025$; $\theta_{ini} = 0.03$; $n = 0.5$;										
		Wall Thickness, X										
		0	0.1	0.2	0.3	0.4	0.5	0.6	0.7	0.8	0.9	1.0
		Temperature θ_i and θ_o										
2	420	1.0299	1.0796	1.1180	1.1451	1.1608	1.1651	1.0130	0.8499	0.6760	0.4914	0.2964
3	426	1.0299	1.0794	1.1178	1.1448	1.1604	1.1647	1.0126	0.8495	0.6756	0.4912	0.2963
Absolute Error with m= 2 and 3		5.05×10^{-5}	1.4×10^{-4}	2.4×10^{-4}	3.2×10^{-4}	3.7×10^{-4}	4.0×10^{-4}	4.3×10^{-4}	4.0×10^{-4}	3.3×10^{-4}	2.3×10^{-4}	1.1×10^{-4}
4	476	1.0299	1.0794	1.1178	1.1448	1.1604	1.1647	1.0126	0.8495	0.6757	0.4912	0.2963
Absolute Error with m= 3 and 4		1.3×10^{-6}	3.7×10^{-6}	6.0×10^{-6}	8.2×10^{-6}	9.9×10^{-6}	1.1×10^{-5}	2.5×10^{-5}	3.4×10^{-5}	3.6×10^{-5}	3.0×10^{-5}	1.6×10^{-5}
5	525	1.0299	1.0794	1.1178	1.1448	1.1604	1.1647	1.0126	0.8495	0.6757	0.4912	0.2963
Absolute Error with m= 4 and 5		$\mathbf{2.8\times 10^{-8}}$	$\mathbf{8.0\times 10^{-8}}$	$\mathbf{1.3\times 10^{-7}}$	$\mathbf{1.8\times 10^{-7}}$	$\mathbf{2.3\times 10^{-7}}$	$\mathbf{2.5\times 10^{-7}}$	$\mathbf{1.2\times 10^{-6}}$	$\mathbf{1.8\times 10^{-6}}$	$\mathbf{2.0\times 10^{-6}}$	$\mathbf{1.8\times 10^{-6}}$	$\mathbf{1.0\times 10^{-6}}$
6	**567**	1.0299	1.0794	1.1178	1.1448	1.1604	1.1647	1.0126	0.8495	0.6757	0.4912	0.2963
Absolute Error with m= 5 and 6		$\mathbf{8.9\times 10^{-10}}$	$\mathbf{2.6\times 10^{-9}}$	$\mathbf{4.2\times 10^{-9}}$	$\mathbf{5.9\times 10^{-9}}$	$\mathbf{7.4\times 10^{-9}}$	$\mathbf{8.5\times 10^{-9}}$	$\mathbf{7.4\times 10^{-8}}$	$\mathbf{1.2\times 10^{-7}}$	$\mathbf{1.5\times 10^{-7}}$	$\mathbf{1.3\times 10^{-7}}$	$\mathbf{7.9\times 10^{-8}}$
7	**871**	1.0299	1.0794	1.1178	1.1448	1.1604	1.1647	1.0126	0.8495	0.6757	0.4912	0.2963
Absolute Error with m= 6 and 7		3.5×10^{-11}	1.0×10^{-10}	1.6×10^{-10}	2.3×10^{-10}	2.9×10^{-10}	3.5×10^{-10}	4.5×10^{-9}	7.8×10^{-9}	9.6×10^{-9}	9.2×10^{-9}	5.4×10^{-9}

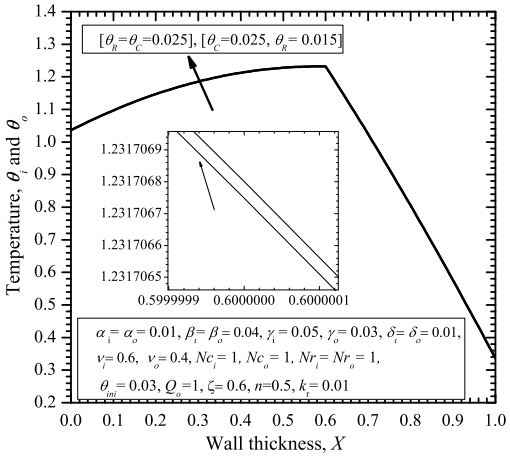

Fig. 3.4 Variation of temperature (θ_i, θ_o) with $\theta_R \neq \theta_C$ and $\theta_R = \theta_C$

3.3.3 Effects of thermal input parameters for inner and outer materials on temperature and efficiency

The conduction-convection parameters, Nc_i or Nc_o for inner and outer material, respectively are related with the convective heat transfer from the surface of the wall. In the present study, it is found that an increase in Nc_i, causes a decrease in temperature as shown in Fig.(3.5a). This trend may be attributed to an increase in heat transfer from the inner wall to the surroundings. The figure shows that θ_i is higher than 1, which means, the wall temperature at $X = 0$ is higher than the surrounding temperature T_i at the i-side of the wall, i.e. $X = 0$. Hence, more heat is leaving the wall on the i-side when Nc_i increases, that explains why the temperature of the wall decreases.

To achieve a suitable value of Nc_i we must establish a balance between temperature and efficiency. The efficiency for various parameters is calculated using expression (3.13), for $T_L = 1273.15\,K$, $L = 0.1\,m$, $k_i = 25\,Wm^{-1}K^{-1}$, $k_o = k_r \times k_i$ and is shown in Table (3.2). As it is clearly seen in Table (3.2) that there is an increase in efficiency although this increase is not significant. Thus, a higher value of convection-conduction coefficient in inner material would result in an appropriate value. Likewise, when conduction-convection parameter for outer material, Nc_o is increased, temperature profile remains the same for the inner material but significant downward variation as shown in Fig.(3.5b) is observed. It is found from the Table (3.2) that the efficiency decreases remarkably as Nc_o is increased. This is due to the fact that when convection is increased for the outer material, more amount of heat is lost to the surroundings and thus lowering the temperature for the outer material. Hence, a suitable value for Nc_o should be as small as possible.

The conduction-radiation parameters, Nr_i and Nr_o for inner and outer materials, respectively

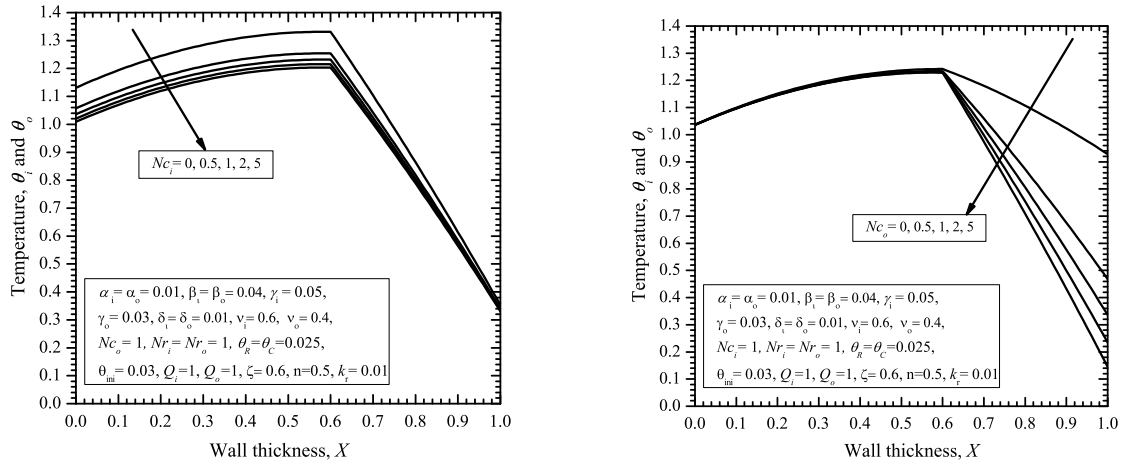

(a) **(b)**

Fig. 3.5 Effect of conduction-convection parameters for (a) inner wall (Nc_i) and (b) outer wall (Nc_o) on the temperature distribution (θ_i, θ_o) respectively.

Table 3.2 Effect of variation of non-dimensional thermal parameters (Nc_i, Nc_o, Nr_i, Nr_o, Q_i, Q_o, ζ) on Efficiency, η_{eff}

For $k_r = 0.01$, $\alpha_i = \alpha_o = 0.01$, $\beta_i = \beta_o = 0.04$, $\gamma_i = 0.05$, $\gamma_o = 0.03$, $\delta_i = \delta_o = 0.01$, $\theta_C = \theta_R = 0.025$, $Nc_i = 1$, $Nc_o = 1$, $Nr_i = 1$, $Nr_o = 1$, $Q_i = 1$, $Q_o = 1$ $\theta_{ini} = 0.03$, $\nu_i = 0.6$, $\nu_o = 0.4$, $n = 0.5$, $\zeta = 0.6$,					
Nc_i	0	0.5	1	2	5
η_{eff}	96.24%	96.39%	96.44%	96.47%	96.50%
Nc_o	0	0.5	1	2	5
η_{eff}	98.54%	96.91%	96.44%	96.08%	95.76%
Nr_i	0	0.5	1	2	5
η_{eff}	96.42%	96.43%	96.48%	96.44%	96.46 %
Nr_o	0	0.5	1	2	5
η_{eff}	96.44%	96.44%	96.44%	96.44 %	96.43%
Q_i	0	0.5	1	1.5	2
η_{eff}	0%	93.52 %	96.44%	97.42%	97.92%
Q_o	0	0.5	1	1.5	2
η_{eff}	96.67%	96.56%	96.44%	96.32%	96.21%
ζ	0.1	0.2	0.5	0.7	0.9
η_{eff}	88.85%	93.86%	96.48%	96.06%	92.60%

are related with the radiative heat transfer from the surface of the wall. As shown in Fig.(3.6a), an increase in parameter Nr_i, results in a decrease of temperature and at the same time, it results in a minor increase in efficiency as shown in Table (3.2). Hence an appropriate value of Nr_i would be greater in magnitude such that greater efficiency and temperature values are obtained for the case. A similar analysis is done for the parameter Nr_o. From Fig.(3.6b), it can be seen that there is a marginal change of $O(10^{-4})$ in the temperature profile with respect to variation in Nr_o. Furthermore, it is presented in Table (3.2) that the efficiency decreases, with an increase in Nr_o. Therefore, it is concluded that for better results Nr_o should be kept as small as possible.

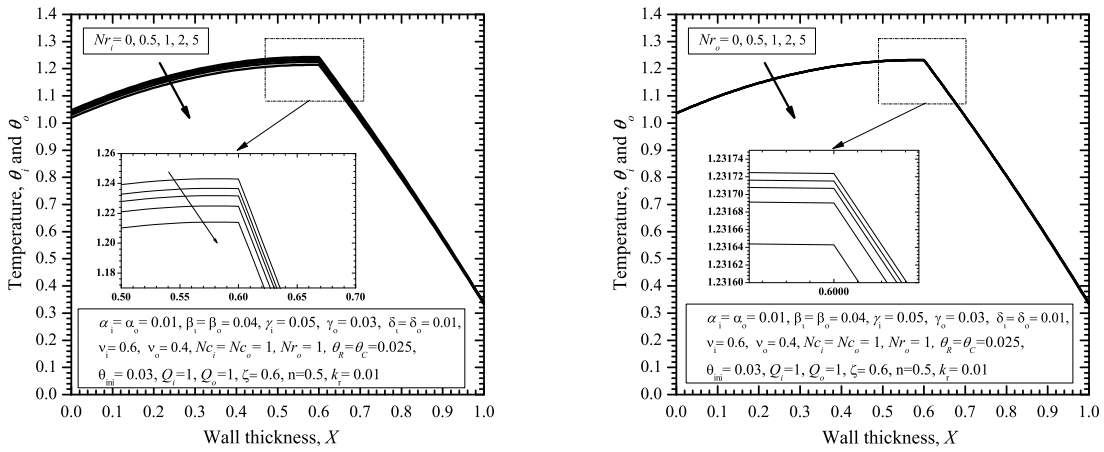

(a) **(b)**

Fig. 3.6 Effect of conduction-radiation parameter for (a) inner wall (Nr_i) and (b) outer wall (Nr_o) on the temperature distribution (θ_i, θ_o) respectively.

Next, we consider the effect of internal heat generation parameters, Q_i and Q_o on temperature and efficiency. These parameters are responsible to generate heat within the walls. It is shown in Fig.(3.7a) that on increasing Q_i, the temperature profile increases as expected. Corresponding to $Q_i = 0$, the value of θ_i at $X = 0$ is less than one, which leads to reverse heat transfer from outer to the inner wall and hence zero value of the efficiency is seen in Table (3.2) as per equation (3.13), for $Q_i = 0$. Further, we investigate the effect of an increase in Q_i on the efficiency. It is found that more heat generation leads to an increase in performance.

From Fig.(3.7b), it is observed that an increase in temperature distribution is insignificant, when internal heat generation in outer material, Q_o is increased. Further, it can be seen in Table (3.2) that efficiency decreases, and again the decrease is negligible. Hence it could be concluded that for best performance, Q_o should be set to zero, as no significant changes are observed by the variation of Q_o.

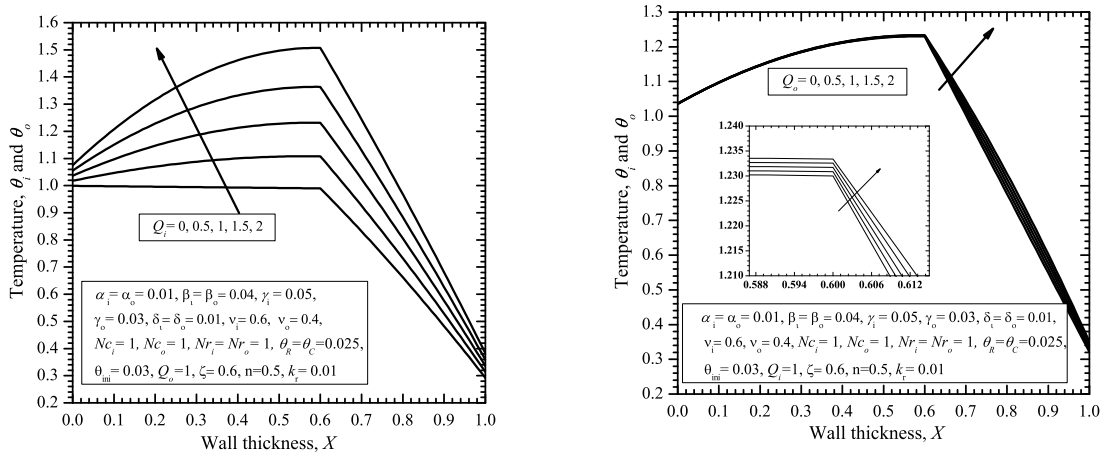

(a) **(b)**

Fig. 3.7 Effect of internal heat generation rate for (a) inner wall (Q_i) and (b) outer wall (Q_o) on the temperature distribution ($\theta_i,\ \theta_o$) respectively.

Fig.(3.8) illustrates the response of junction's position ζ on temperature and efficiency as ζ varies from 0.1 to 0.9, i.e., when the thickness of the inner wall is increased, which simultaneously decreases the thickness of the outer wall. On increasing the junction's length, a rise in temperature is observed as shown in Fig.(3.8). For observing the variation in efficiency with the change in the position of the junction, Table (3.2) can be referred. It could be seen that efficiency first increases until ζ achieves a value of 0.5 and then starts decreasing. This can be attributed to the fact that till $\zeta = 0.5$, the heat losses are marginal but after $\zeta = 0.5$, heat losses significantly increase due to a very thin outer wall.

3.3.4 Effect of the functional form of temperature-dependent properties on temperature and efficiency

It is very important to analyse the effect of the coefficients of temperature-dependent properties on the performance of the composite walled system. This analysis is done on four types of coefficients corresponding to internal heat generation, thermal conductivity, conductive heat transfer and emissivity. At first we consider the coefficients of internal heat generation $\alpha_i, \alpha_o, \beta_i, \beta_o, \gamma_i, \gamma_o$ for investigation. As the coefficients of internal heat generation appearing in equations (3.5a) and (3.5b) are decreased, the temperature is also decreased, as shown in Fig.(3.9a). This is due to the fact that when these coefficients decrease, the total amount of heat generated both in inner as well as outer materials decreases and hence a decreasing trend is observed in Fig.(3.9a).

Likewise, the efficiency also decreases with decreasing coefficients of internal heat generation as seen in Table (3.3). From the Table (3.3), it is recommended that for a maximum performance

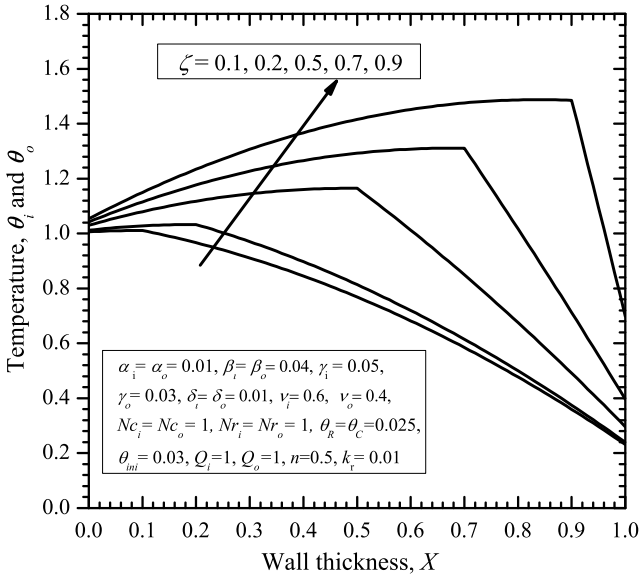

Fig. 3.8 Effect of variation in the junction length (ζ) between composite walls on the temperature distribution ($\theta_i,\ \theta_o$).

Table 3.3 Effect of temperature-dependent thermal parameters on Efficiency, η_{eff}, when all other parameters were kept constant.

Parameters ($k_r = 0.01,\ Nc_i = Nc_o = 1,\ Nr_i = Nr_o = 1,\ Q_i = Q_o = 1,\ \zeta = 0.6$ $\theta_C = \theta_R = 0.025,\ \theta_{ini} = 0.03$)		η_{eff}
Coefficients of heat generation rate $\delta_i = \delta_o = 0.01,\ \nu_i = 0.6,\ \nu_o = 0.4,\ n = 0.5$	$\alpha_i = \alpha_o = 0.01,\ \beta_i = \beta_o = 0.04$ $\gamma_i = 0.05,\ \gamma_o = 0.03$	96.44%
	$\alpha_i = \alpha_o = 0,\ \beta_i = \beta_o = 0$ $\gamma_i = 0,\ \gamma_o = 0$	96.04%
	$\alpha_i = \alpha_o = -0.01,\ \beta_i = \beta_o = -0.04$ $\gamma_i = -0.05,\ \gamma_o = -0.03$	95.56%
Coefficients of thermal conductivity $\alpha_i = \alpha_o = 0.01,\ \beta_i = \beta_o = 0.04,\ \gamma_i = 0.05,\ \gamma_o = 0.03$ $\nu_i = 0.6,\ \nu_o = 0.4,\ n = 0.5$	$\delta_i = \delta_o = 0.01$	96.44 %
	$\delta_i = \delta_o = 0$	96.46%
	$\delta_i = \delta_o = -0.01$	96.48%
Exponent of convection coefficient $\alpha_i = \alpha_o = 0.01,\ \beta_i = \beta_o = 0.04,\ \gamma_i = 0.05,\ \gamma_o = 0.03$ $\delta_i = \delta_o = 0.01,\ \nu_i = 0.6,\ \nu_o = 0.4$	$n = 0.5$	96.44%
	$n = 0$	97.96%
	$n = -0.5$	98.32%
Coefficients for the emissivity $\alpha_i = \alpha_o = 0.01,\ \beta_i = \beta_o = 0.04,\ \gamma_i = 0.05,\ \gamma_o = 0.03$ $\delta_i = \delta_o = 0.01,\ n = 0.5$	$\nu_i = 0.6,\ \nu_o = 0.4$	96.44%
	$\nu_i = 0,\ \nu_o = 0$	96.44%
	$\nu_i = -0.6,\ \nu_o = -0.4$	96.44%

of 96.44 %, the following values of coefficients could be chosen $\alpha_i = \alpha_o = 0.01$, $\beta_i = \beta_o = 0.04$, $\gamma_i = 0.05$, $\gamma_o = 0.03$. Fig.(3.9b) shows that when the slopes of the dimensionless thermal conductivity in equations (3.5c) and (3.5d) are varied, there is a marginal change of order 10^{-4} in temperature, and the same can be observed for efficiency from Table (3.3). Therefore the performance of the walls is insensitive to these parameters, giving the flexibility to be chosen arbitrarily with the specified domain. On decreasing the exponent of temperature-dependent convective heat transfer coefficient in equations (3.5g) and (3.5h), temperature for both inner as well as outer walls starts increasing as depicted in the Fig.(3.9c). As the convective heat transfer decreases by decreasing the exponent, the heat loss occurring in the walls is less and hence higher is the temperature distribution in the walls. Further, there is an increase in efficiency which agrees with the above statement and the increase is found to be approximately 2% as the exponent varies from 0.5 to -0.5. In Fig.(3.9d), the effects of temperature-dependent parameters, i.e., ν_i, ν_o, for the emissivity in the equations (3.5e) and (3.5f), have been observed for the temperature distribution and performance. It is found from the observation that the temperature distribution increases with the increase in ν_i, ν_o. But the increment is found to be very less and is of the order of 10^{-4}. Moreover, the investigation suggested that there is no effect of ν_i, ν_o on the performance of the walls as seen in Table (3.3). After analyzing the efficiency and the temperature profile, the effects of convective and radiative parameters, the temperature-dependent properties and thermo-physical parameters on the temperature profile are observed. A very useful application of composite walls as an industrial furnace is discussed in the next section.

3.3.5 Application of composite walls to furnace

We know, various types of furnaces are used in industries, Trinks *et al.* (2003), with the main aim to heat up or melt specific materials like steel, copper etc., so that these could be cast into the desired form of interest. The performance of a particular furnace depends upon its ability to hold back a large amount of heat in addition to generating heat. Hence, a furnace of such kind is modeled in which composite walls are taken into account. There are two layers of different material in the furnace. A closer look at the furnace consisting of the composite walls is revealed in Fig.(3.10).

What thickness does either of these walls should have and what material should be used in their construction is what that affects the performance of the furnace. So, the study of heat transfer in composite walls becomes crucial for this analysis. The mathematical equations representing the phenomenon of heat transfer becomes non-linear and hence a semi-analytical method called Adomian decomposition is used to tackle this difficulty as shown previously. This type of mathematical analysis is important to get an insight into heat transfer because construction of different furnaces and then doing experiments becomes infeasible sometimes leading to exploitation of resources. Hence a mathematical model of the problem, which predicts the results is important for such kind of analysis. Further, the role of temperature-dependent internal heat

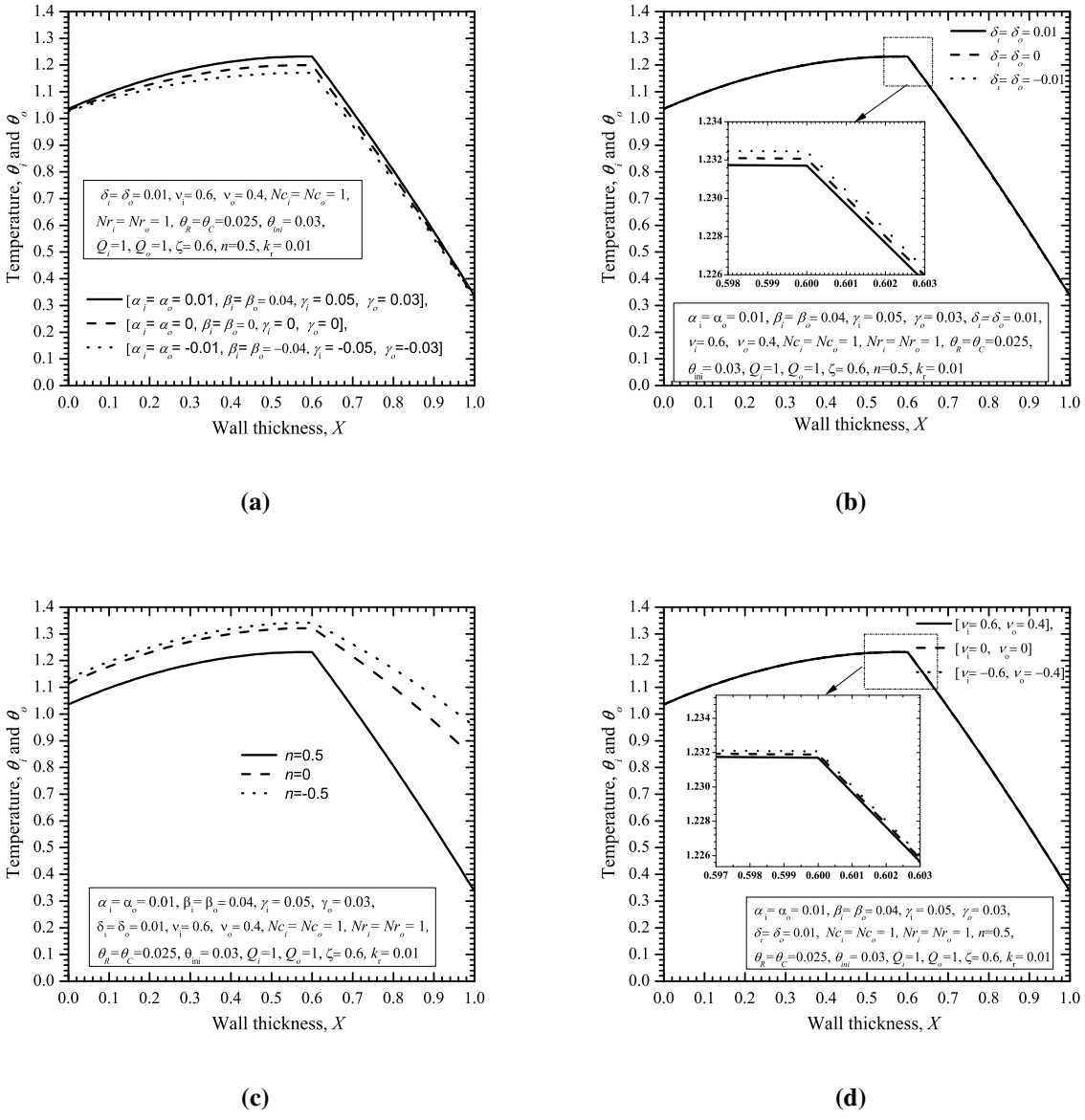

Fig. 3.9 Effect of (a) heat generation (α_i, α_o, β_i, β_o, γ_i, γ_o) (b) thermal conductivity (δ_i, δ_o) (c) heat transfer coefficient (n) (d) emissivity coefficients (ν_i, ν_o) on temperature distribution (θ_i, θ_o) respectively.

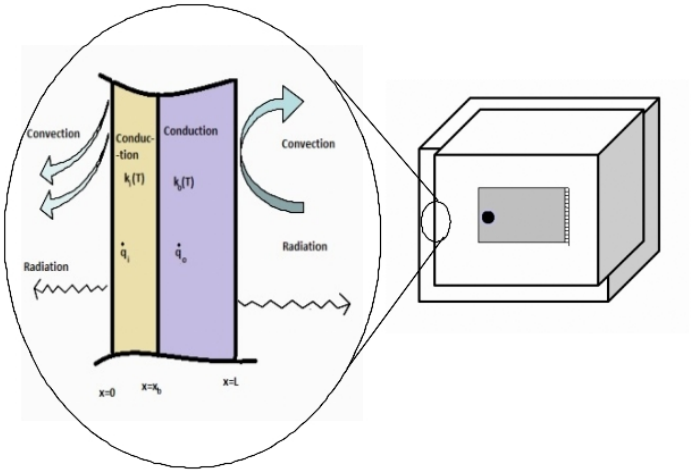

Fig. 3.10 Furnace with Composite walls

generation rate on the temperature profile is seen. It has been observed that as the heat generation in the inner wall of the furnace, Q_i, increases, more heat is generated and transferred, increasing the temperature inside of the furnace. If $Q_i = 0$, no heat is being produced in the inner wall to the material to be melt. Instead inner wall starts gaining heat from the material, resulting in a non-practical approach. Moreover, for the increasing values of Q_i, efficiency increases, as, more is the heat generation, greater is the performance of the furnace. Whereas, when Q_o is increased, the temperature does not increase significantly. Also, the efficiency decreases on increasing Q_o for furnace, as more energy is provided to the overall system, and there is no significant increase in the performance. Thus, it is concluded that for the furnace to work effectively, an insulating outer material is required, such that no heat is generated for the outer material. To confirm this, an inverse analysis to retrieve internal heat generation is discussed in the next section.

3.3.6 Inverse analysis in composite walls

This section aims to build a procedure for inverse analysis, where the heat generation inside the double-layered walls is predicted, based on the temperature measurements of the walls. The steady-state temperature distribution has already been obtained through the forward analysis using ADM. From the context of previous sections, it was observed that the semi-analytical solution obtained through ADM is mathematically significant, providing the closed-form temperature distribution. However, its computational time is large (11.93s) as compared to the bvp5c solver (0.29s) for the parameters mentioned ahead in the text. Therefore, for the present study, MATLAB based numerical solver bvp5c has been used to determine the temperature profile of the walls. The heat is transferred by all the thermal modes, i.e., conduction, convection and radiation with the thermal properties of the associated materials considered as temperature-independent. The inverse problem is formulated as an optimization problem. The objective

function is formulated in the sense of least squares as, $J = ||T(Q_i, Q_o, k_r) - \tilde{T}||_2^2$, where J is to be minimized. Here $\tilde{T}$ is the temperature matrix obtained from the direct method, also called exact temperature profile. The thermal parameters used to obtain the temperature profile are $k_r = 0.01$, $\alpha_i = \alpha_o = 0$, $\beta_i = \beta_o = 0$, $\gamma_i = \gamma_o = 0$, $\delta_i = \delta_o = 0$, $\theta_C = \theta_R = 0.025$, $Nc_i = Nc_o = 1$, $Nr_i = Nr_o = 1$, $Q_i = Q_o = 1$, $\theta_{ini} = 0.03$, $\nu_i = \nu_o = 0$, $n = 0$, $\zeta = 0.6$. Also, $T(Q_i, Q_o, k_r)$ is the guessed value of temperature corresponding to the estimated parameters with $||.||_2$ representing the l_2 norm. For minimization, the Whale Optimization Algorithm (WOA) is used, whose details are provided in chapter-5, section-methodology. Here, the WOA parameters tuned for the inversion involve, number of search agents as 10 and maximum number of iterations as 500.

There are various applications where the composite walls generate heat internally which may be due to the presence of electrical coils inside the furnace. The practical measurement of this internal heat generation is a tedious task. Therefore, the retrieval of internal heat generation rate parameters, Q_i and Q_o is required with the aid of inverse analysis. In addition to the retrieval of Q_i and Q_o, the thermal conductivity ratio, k_r, is also retrieved simultaneously. For manufacturing a certain furnace that can maintain a specific temperature, information about the material to be used is required. This information is provided by the parameter k_r, which gives a ratio of thermal conductivity of the outer material to the inner material of the walls. The selection of the correct material would enhance the working efficiency of the furnace. For the present study, in the forward method, the heat generation in inner and outer walls is considered as $Q_i = Q_o = 1$. Further, a typical case of melting furnace is considered in the forward analysis, where inner material is highly conductive as compared to the outer material, i.e., $k_o << k_i$ and $k_r = 0.01$. The retrieved internal heat generation rate in both inner and outer walls, Q_i and Q_o respectively, along with the thermal conductivity ratio, k_r is seen in Fig.(3.11a-3.11c). The convergence plot of WOA is available in Fig.(3.11d). The convergence is obtained in around 30 iterations, with the order of convergence O(10^{-7}). The results for three different runs are presented in Table (3.4).

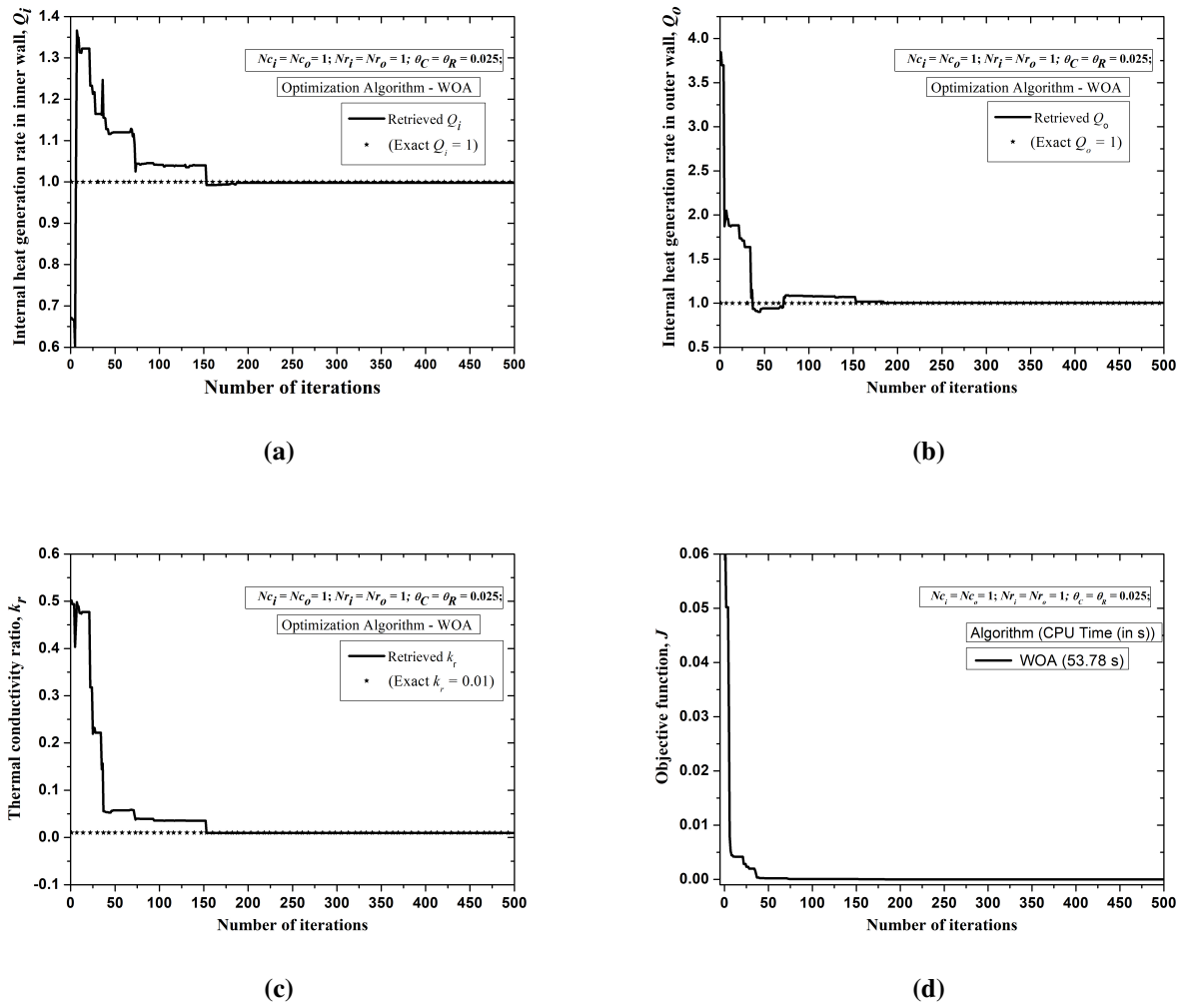

Fig. 3.11 (a) Retrieved internal heat generation rate, Q_i, (b) retrieved internal heat generation rate, Q_o, (c) retrieved thermal conductivity ratio, k_r, and (d) convergence plot of WOA, when no error is present.

Next, to study the sensitivity of the inversion process with respect to the perturbation in measured temperature, an error analysis is carried out. For this purpose, the noisy forward data has been simulated by adding random errors to the exact data. The temperature profile with 1%, 3%, 5% and 10% measurement errors has been intentionally included. Fig.(3.12) illustrates the comparison of the exact temperature profile with that of noisy data, when a uniformly generated error (e), of 1%, 3%, 5% and 10% has been added to the exact data. This noisy profile mimics the measured temperature data obtained during experiments. This noisy temperature profile is utilized to simultaneously retrieve Q_i, Q_o and k_r respectively. The retrieved non-dimensional parameters are seen in Fig.(3.13a-3.13c). The retrieval data is also presented in Table (3.4). The estimated Q_i and Q_o for both walls matches well with the exact values up to 3% error in measurement temperatures. Moreover, the estimated values of Q_i are in agreement even with 10%

of measurement error. However, the retrieved $k_r = 0$ signifies the case where there is perfect insulation in the outer wall. This is indeed the ideal case. The convergence curve representing the value of the objective function J, with the number of iterations for 1%, 3%, 5% and 10% measurement errors is seen in Fig.(3.13d). It can be observed that the convergence is obtained in approximately 10 iterations.

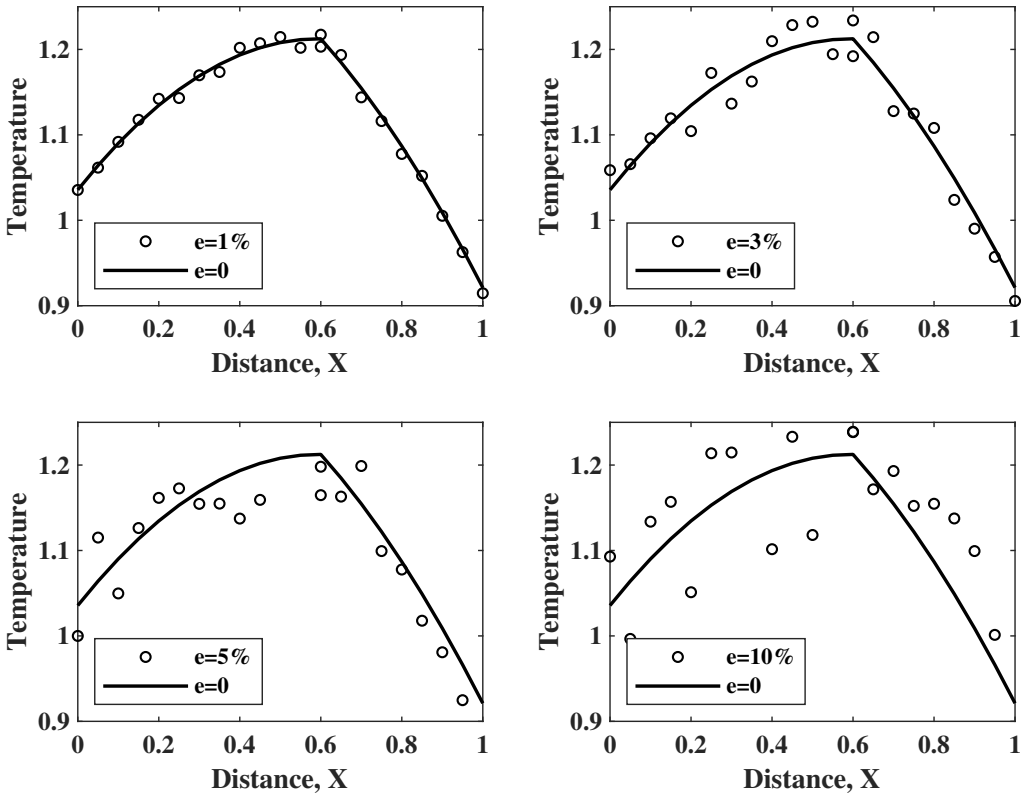

Fig. 3.12 Noisy temperature profile (e = 0, 1%, 3%, 5% and 10%) of the composite walls.

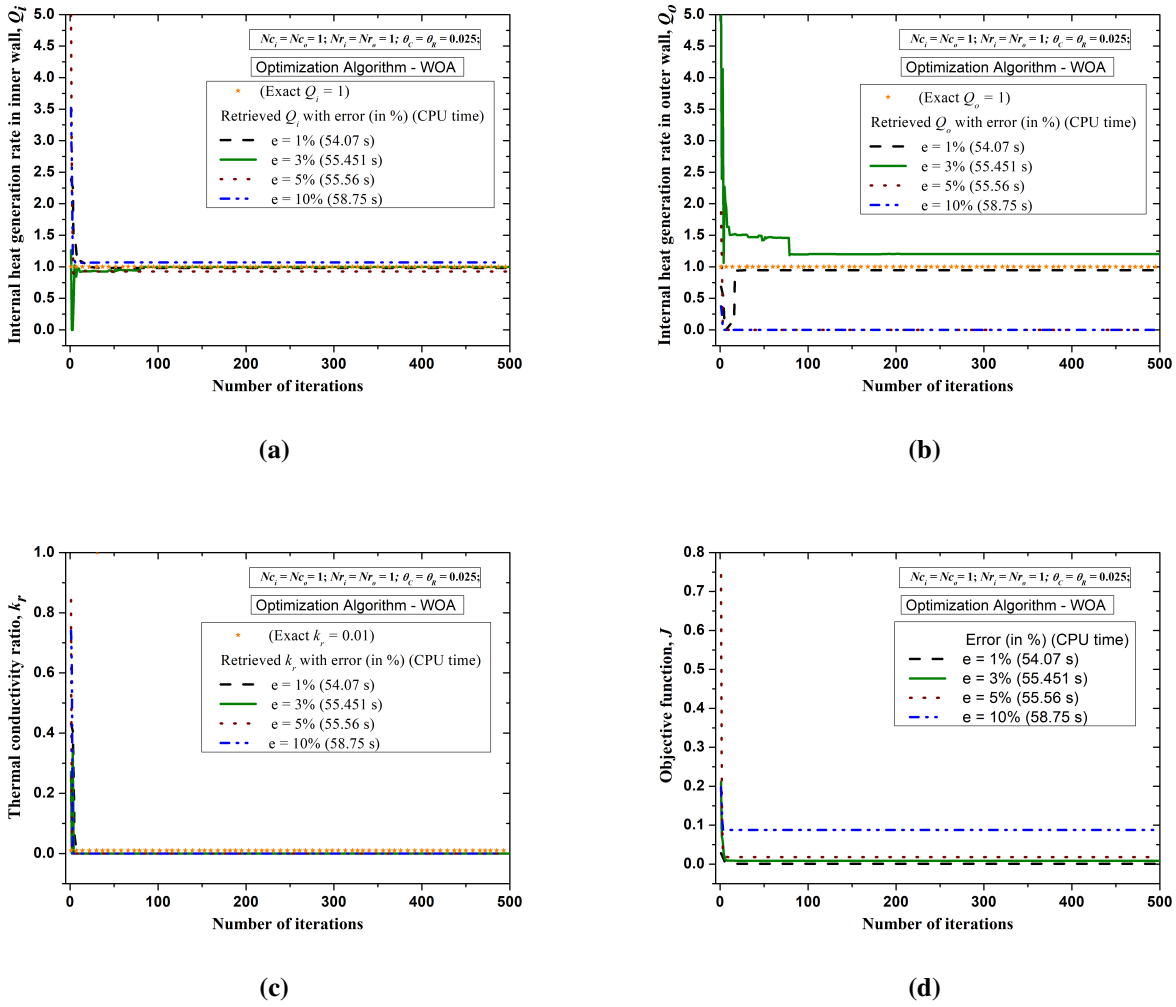

Fig. 3.13 (a) Retrieved internal heat generation rate, Q_i, (b) retrieved internal heat generation rate, Q_o, (c) retrieved thermal conductivity ratio, k_r, and (d) convergence plot of WOA, when error, e = 1%, 3%, 5% and 10% is present.

Table 3.4 Comparison of retrieved internal heat generation rates for both inner and outer wall and thermal conductivity ratio, for different runs of WOA with $e = 0, 1\%, 3\%, 5\%, 10\%$, range of [$Q_i$, Q_o, k_r] = [0-10, 0-10, 0-1].

Run no.	WOA (No. of search agents: 10, No, of iterations: 500)				
error,	Relative error in retrieved parameters			Min. Fitness	CPU time
$e(\%)$	Q_i	Q_o	k_r	function, J	(in s)
	Exact values				
	1	1	0.01		
Without measurement errors,					
$e_r = 0\%$					
1	0.998	1.004	0.009	1.3×10^{-7}	53.78
2	1.027	0.971	0.019	1.3×10^{-5}	53.96
3	0.981	0.979	0	5.4×10^{-6}	57.48
With measurement errors, $e \neq 0$					
$e_r = 1\%$					
1	0.981	0.946	0	7.4×10^{-4}	54.07
2	0.977	0.966	0	7.5×10^{-4}	57.49
3	0.98	0.953	0	7.4×10^{-4}	54.28
$e_r = 3\%$					
1	0.998	1.204	0	8.4×10^{-3}	55.41
2	1.043	1.345	0.039	8.4×10^{-3}	54.05
3	1.048	1.245	0.028	8.3×10^{-3}	53.95
$e_r = 5\%$					
1	0.926	0	0	1.8×10^{-2}	55.56
2	0.926	0	0	1.8×10^{-2}	58.05
3	0.825	0.717	0	1.5×10^{-2}	54.63
$e_r = 10\%$					
1	1.068	0	0	8.7×10^{-2}	58.74
2	1.069	0	0	8.7×10^{-2}	57.23
3	1.069	0	0	8.7×10^{-2}	55.93

To check the correctness of the retrieved parameters, the temperature distribution has been reconstructed. For this reconstruction, the retrieved parameters given in Table (3.4) for run 1, along with the parameters $\theta_C = \theta_R = 0.025$, $Nc_i = Nc_o = 1$, $Nr_i = Nr_o = 1$, $\theta_{ini} = 0.03$, $\zeta = 0.6$ are used. The comparison of exact and reconstructed temperature profile when the error, $e = 0\%$, 1%, 3%, 5%, 10% is present in the forward data, plotted with the wall distance, X, is illustrated in Fig.(3.14). An excellent matching of reconstructed temperature field and the exact field, even when the forward data contain noise, proves that the obtained set of parameters is correct. However, the temperature profile seems to vary for outer layer with 5% and 10%

measurement error.

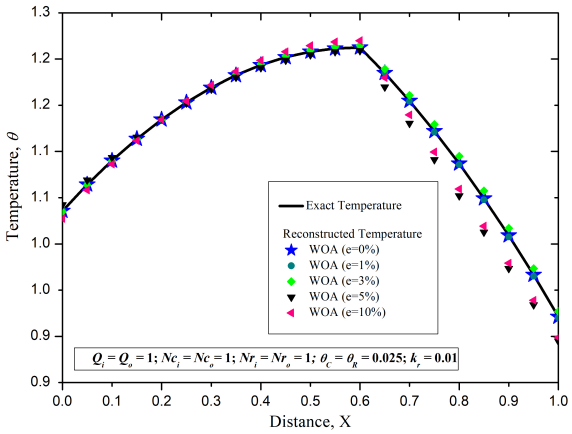

Fig. 3.14 Comparison of exact and reconstructed temperature profile when the error $e = 0\%,\ 1\%,\ 3\%, 5\%,\ 10\%$ is present in the forward data for WOA, plotted with the wall distance, X.

3.4 Observations

From the analysis, it is observed that for better performance Nc_i and Nr_i should be chosen as large as possible whereas Nc_o and Nr_o should be chosen with smaller magnitudes. It is concluded that for the outer material, the temperature-dependent internal heat generation rate Q_o must be as small as possible. Moreover, it is observed that the coefficient involved in the functional form of thermal conductivity δ_i and δ_o and emissivity ν_i and ν_o do not have any significant impact on the performance. For the coefficients involved in internal heat generation, the maximum efficiency obtained is 96.44% which corresponds to positive values of coefficients $\alpha_i = \alpha_o = 0.01$, $\beta_i = \beta_o = 0.04$, $\gamma_i = 0.05$, $\gamma_o = 0.03$, suggesting internal heat generation as an increasing function of temperature. Similarly, for the coefficients involved in convective heat transfer, the maximum value of efficiency is 98.32% which corresponds to a lower negative value of the exponent, suggesting the heat transfer coefficient to be a negative exponent. The application of composite walls in the furnace is seen and it is concluded that for the furnace to work effectively, an insulating outer material is required, for which Q_o must be zero. Lastly, an inverse analysis to predict simultaneously Q_i, Q_o and k_r is performed. An error analysis concludes a good retrieval up to 3% measurement errors in temperature. The results were confirmed by reconstructing the temperature profile.

After the implementation of ADM-NR for the forward analysis and calculating the inversion results with bvp5c-WOA, we shall implement a forward and inverse analysis for a pin fin in the next chapter. For that, an experimental setup of pin fin is selected, where time-dependent heat flux would be retrieved as discussed ahead.

Chapter 4

Forward, Experimental and Inverse Heat Transfer in Pin Fin

In the race of efficient transfer of heat, economical and reliable methods are required. Fins serve the purpose of the transfer of thermal energy between the systems. Fins are extended secondary surfaces which increase the rate of heat transfer by increasing the primary surface area of the object, to which they are attached, Kern and Kraus (1972). Fins find various applications in the air-cooled internal combustion engines, Yoshida *et al.* (2006), Sagar *et al.* (2017a,b), refrigeration condenser tubes, Shojaeefard *et al.* (2017), Lewpiriyawong *et al.* (2019), Li *et al.* (2015), automobile radiator, Habibian *et al.* (2018), Dittus and Boelter (1985), Zhang *et al.* (2017), electric transformers, Raeisian *et al.* (2019), semiconductors, Park *et al.* (2019), Hikavyy *et al.* (2016), Thoti and Lakshmi (2017), reciprocating air compressors, Heidari *et al.* (2017), heat sinks of laptops/servers and many more. The shape of the fin plays a crucial role in its performance and different shapes have been considered for thermal analysis, Wan *et al.* (2017), Singla and Das (2014), Cormier *et al.* (2014), Wang and Yang (2010), Lin *et al.* (2011), Singla *et al.* (2016). A pin fin having the advantages such as ease of manufacturing, being inexpensive, Abbas *et al.* (2009) is widely used and thus selected for the current analysis. Other than shape, heat transfer in fins is governed by several temperature-dependent properties of the material involved. Properties such as thermal conductivity, input heat flux, thermal absorption or emittance of heat via radiation or the media properties like convective heat transfer coefficient or emissivity affect the thermal profile of the fin. These factors are hard to measure directly and thus estimated with the aid of inverse analysis. The two modes for obtaining the input data for inverse analysis are mathematical methods, Abbas and Youssef (2012) and experimental study, Choudhary *et al.* (2019), Wang *et al.* (2018b). The first mode has glitches such as simplification of models, infeasible solutions, whereas, the other one is costly and time-consuming. Therefore, in the present work, experiments are performed along with the mathematical study.

As discussed in chapter 1, analyzing the thermal profile of an object via a priori information is called forward problem. Computational tools like ANSYS, Reddy *et al.* (2015) and MATLAB, Singh *et al.* (2008), Sevilgen (2017), Singhal *et al.* (2020) have been utilized previously for the solution of the direct problem. Being well-posed in nature, such a problem is solved easily. Pdepe tool is most suitable for parabolic PDEs in one-dimension and hence is used currently in the direct analysis.

It is evident from the literature that many assumptions are made for simplification during the inverse analysis of a problem. Chen *et al.* (2014) retrieved heat flux in two-dimension using conjugate gradient method (CGM) without convection and radiation and Huang *et al.* (2015) in three-dimension using Levenberg-Marquardt Method (LMM) without radiation. Reddy and Dulikravich (2017) designed cooling arrays of micro-pin fins using genetic algorithm assuming constant thermal properties and ignoring radiation. Pakrouh *et al.* (2015) used Taguchi method for optimization of the heat sink, assuming constant thermal properties with conduction only. The inverse analysis is done using CGM, for moving heat source in the machining process, Luchesi and Coelho (2012), ignoring convection and radiation. The assumptions made in literature, no doubt simplifies the system by removing non-linearity but does so at the cost of accuracy and performance.

An important thermal parameter namely heat flux is required to be determined in many applications such as industrial boilers, Chinsuwan *et al.* (2014), reheating furnace, Weisz-Patrault *et al.* (2014), solar building applications, Herrando *et al.* (2019), heat exchangers, Dhiman and Prasad (2017), disc brake system, Yang and Chen (2011), bone drilling, Wang *et al.* (2016) etc. The direct measurement of the same is almost impossible, Singh *et al.* (2017). A detailed description of heat flux measurement techniques for the boiler waterwalls is available in Sankar *et al.* (2016). The heat flux for the surface of barrel has been retrieved for the first time by KF and recursive least-squares estimation in Ji *et al.* (1997). A similar methodology is used to predict heat flux form a graded-index medium, Wen *et al.* (2019). The CFD simulation is carried out on the control rod reactor process, Cebula and Taler (2014) to predict heat flux. Multiple parameters are estimated along with heat flux using LMM, Cui *et al.* (2016b). The two-dimensional heat conduction problem, Cebula *et al.* (2018) is considered for predicting local heat flux. Furthermore, for fins, determination of heat flux is done in Lin *et al.* (2011), Yang *et al.* (2013), Lee *et al.* (2012), Chen *et al.* (2017b). In all published literature, the time-dependent heat flux is not determined for fins, except Lee and Yang (2003), Lee *et al.* (2004) who did so by utilizing computationally generated temperature profile, lacking experimentation. It thus becomes a necessity to retrieve time and temperature-dependent heat flux, taking into account the mathematical or experimental temperature data from pin fin. The importance of estimation of heat flux is to evaluate the accurate performance of finned heat sink devices, which are directly connected to the surfaces in nuclear reactors, micro-controllers, pipes etc. Similarly, the retrieval of time-dependent heat flux from the surface of hot and cold junctions is useful in evaluating

the accurate performance of thermoelectric power generators.

In this chapter, a time-dependent functional form of heat flux has been retrieved for a pin fin with mathematical and experimental temperature data using the Golden section search method (GSSM). The geometry and details about experimental setup are given in the next sections.

4.1 Experimental Setup

To analyze the effect of one-dimensional conduction, natural convection and radiation, the heat transfer on the extended surface is studied through experiments. The test rig is shown in Fig.(4.1). The apparatus consists of the extended surface, electric heater, thermocouples, data logger and a monitor. The details of each component is discussed as follows.

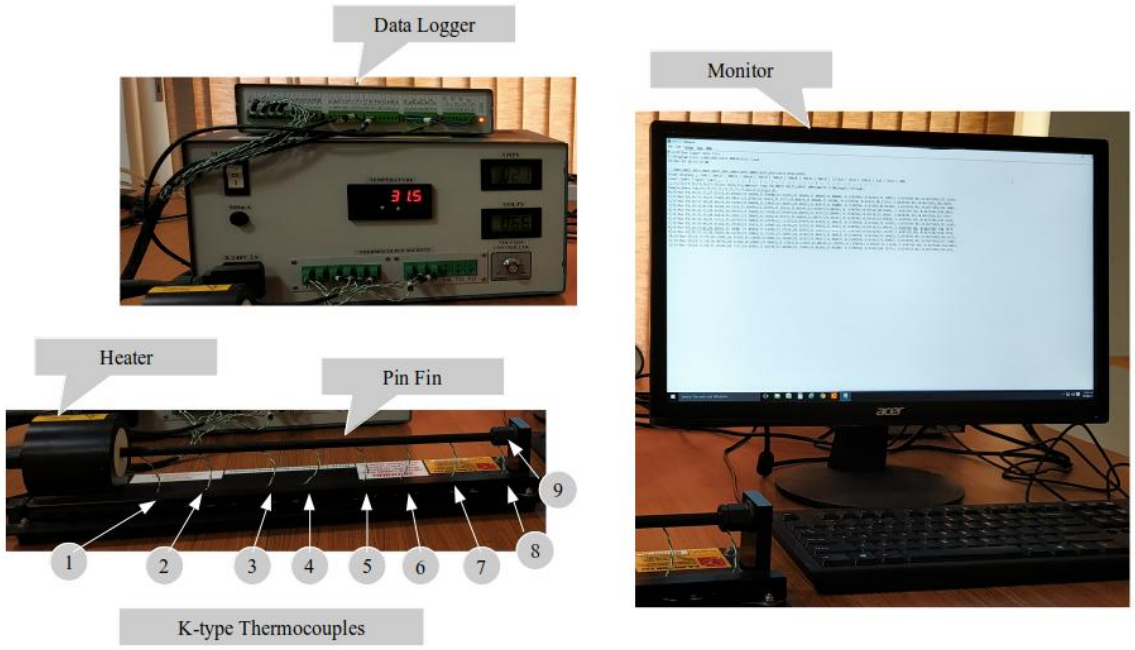

Fig. 4.1 Experimental setup of the extended surface.

A 10 mm diameter brass rod of approximately 350 mm effective length is mounted horizontally with a support at the heated end and a mounting steady is placed at the opposite end. The surface of the fin is painted with resistant matt black paint to maintain an thermal emissivity close to unity.

Inside an insulated housing is a 240 V electric heater in direct contact with the brass rod. The heater has a nominal power rating of approximately 30 Watts at 240V AC. The power supplied to the heated cylinder is provided by the heat transfer service unit through the power lead. The heat transfer service unit also allows the variation of the power input to the heater by control of the voltage supply to the heater element. For safety purposes, a thermostate is also utilized,

which limits the maximum temperature of the heater to approximately 150° C.

Eight k-type thermocouples are located at 50 mm intervals along the rod. K-type thermal sensors are Nickel-Chromium base metal thermocouples, which are inexpensive, reliable and have a wide temperature range of -270 to 1260°C. In addition, these have accuracy of ± 2.2°C. These thermal sensors record the surface temperature of the fin by connecting to the heat transfer service unit through the miniature plugs. The thermocouples are attached to the rod in such a way to minimize the errors from conduction effects. An additional thermocouple is mounted on the extreme end of the extended surface, to record the ambient air temperature. To protect the thermocouples from damage, all the terminations are mounted firmly. The obtained thermal data involved uncertainty due to measurements. The relative uncertainty in the input temperature is 0.016, with relative uncertainties in voltage and current being 0.031 and 0.065 respectively, calculated using $\max_n \left[\max_t \left(\frac{T_n(t) - \text{mean}}{\text{mean}} \right) \right]$. To minimize the uncertainty involved, three measurements under the same conditions are recorded, whose average is utilized in the study.

DAQ is the process of digitizing the temperature data using a thermocouple, so that it can be analyzed and stored in a computer. A windows based data acquisition software, LabVIEW, is used with the heat transfer service unit and a data logger. The heat transfer service unit has a power inlet and outlet of 240V and 8A. The power outlet on the rear panel is used for supplying power to the extended surface with current loads upto a maximum of 8A. This outlet is used to vary heated power on the attached extended surface unit. The voltage is controlled manually using the control knob of the voltage controller.

Once the setup is ready, experiments are performed by heating the one end of extended surface, where the remaining exposed length of the fin is allowed to cool by natural convection and radiation. This results in a decreasing temperature distribution along the bar that is measured by regularly spaced thermocouples as described above. The temperature profile of the fin is noted through data logger, for $V = 80$V, $I = 0.027$A; $V = 60$V, $I = 0.018$A; and $V = 70$V, $I = 0.022$A, until the system attained steady-state.

For different values of heat flux, three different cases are studied. Firstly, the temperature profile of the rod has been noted, when a constant heat flux of 0.98 is supplied. Then a triangular heat flux is given by switching the electric heater off after a specified duration. Lastly, a realistic heat flux is input to the left end of fin, and temperature measurements are recorded. In this case, the electric heater is kept on, until the system attained its steady-state.

Moreover, during experimentation, the value of convective heat transfer coefficient 'h' is unknown to us. A known, constant heat flux 'Φ = 0.98' and h = 5 Wm^{-2}K^{-1} is used to get the synthetic temperature data using forward analysis and utilizing that temperature profile, convective heat transfer coefficient 'h' is determined using inverse analysis. This study has

been performed in Singh *et al.* (2019), Singh (2019). The obtained 'h' for no error, 1%, 3%, 5% and 10% measurement errors, is 4.89 $Wm^{-2}K^{-1}$, 5.18 $Wm^{-2}K^{-1}$, 4.08 $Wm^{-2}K^{-1}$, 5.17 $Wm^{-2}K^{-1}$, and 4.82 $Wm^{-2}K^{-1}$, respectively. Thus, taking the average convective heat transfer coefficient, when no error and 1% measurement error is present in the temperature data, h = 5.035 $Wm^{-2}K^{-1}$ is retrieved through inverse analysis. This obtained value of 'h' has been used in retrieval of time-dependent heat flux, which is the problem discussed ahead.

All the parameters associated with the setup are given in Table (4.1). Next, the mathematical modeling of the above setup is discussed.

Table 4.1 Experimental parameters used in computations.

$\rho = 8520$ kg/m^3	h_b = 5.035 W/m^{2}K, ($3 \leq h_b \leq 25$)	Time step, d$\tau = 0.4167$	Final time, $\tau = 5$
$c_p = 375$ J/kgK	$\varepsilon_o = 0.95$, ($0 \leq \varepsilon_o \leq 1$)	Grid size, d$\xi = 0.1429$	Material of the fin: Brass
$k = 121$ W/mK	$N_c = 2$, ($1.3 \leq N_c \leq 10$)	$N_r = 0.1$, ($0 \leq N_r \leq 0.5$)	$N_{br} = 0.002$, ($0 \leq N_{br} \leq 0.004$)
$T_b = 298$ K	$T_a = 295$ K	$L = 0.35$ m	$Bi = 0.07$, ($0.0086 \leq Bi \leq 0.07$)
$d = 0.01$ m	$A = 7.854 \times 10^{-5}$ m^2	$P = 0.03014$ m	$\Phi = 0.98$; Using ($q = V \times I \times t/A$)

4.2 Problem formulation

The schematic of the setup is shown in Fig.(4.2). The mathematical model is inspired by the experimental setup. Assumptions made during the analysis are:

- No heat is generated within the fin.
- Cross-sectional area of the fin is considered uniform.
- Heat conduction occurs in one-dimension only.
- Contact thermal resistance is considered negligible.

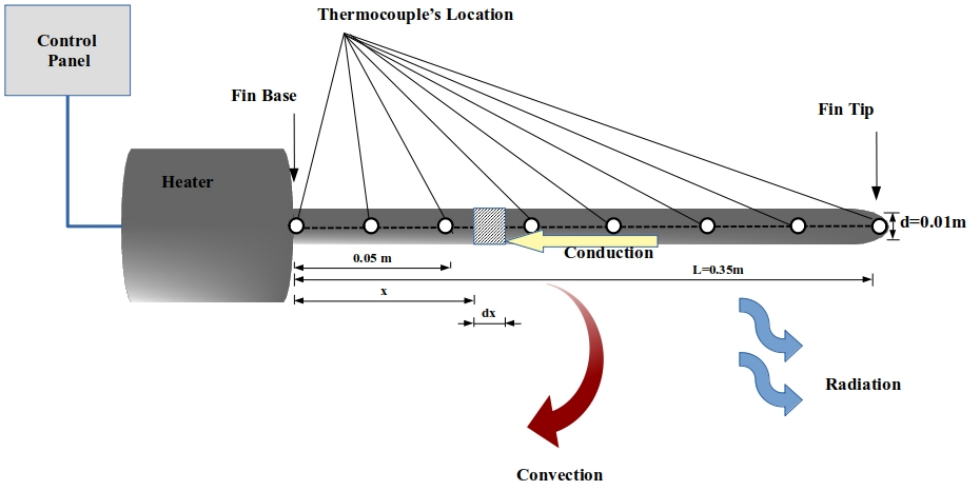

Fig. 4.2 A schematic diagram of the extended surface.

The governing equations, initial condition and the boundary conditions for the cylindrical pin fin are given respectively as follows,

$$\frac{\partial}{\partial x}\left[k(T)A_{cs}\frac{\partial T}{\partial x}\right] - h(T)P(T-T_a) - \varepsilon(T)\sigma P(T^4-T_a^4) = \rho c_p A\frac{\partial T}{\partial t}, \quad t>0,\ 0<x<L, \tag{4.1}$$

$$T(t=0) = T_a = 22^{\circ}C, \quad 0<x<L, \tag{4.2}$$

$$-k(T)\frac{\partial T}{\partial x}\Big|_{x=0} = q|_{x=0}, \tag{4.3}$$

$$-k(T)A_{cs}\frac{\partial T}{\partial x}\Big|_{x=L} = h(T)A_{cs}[T(x=L)-T_a] + \varepsilon(T)\sigma A_{cs}[T^4(x=L)-T_a^4]. \tag{4.4}$$

with temperature-dependent properties as:

$$k(T) = k_a[1+g(T-T_a)], \tag{4.5}$$

$$h(T) = h_b\left\{\frac{T-T_a}{T_b-T_a}\right\}^n, \tag{4.6}$$

$$\varepsilon(T) = \varepsilon_o[1-\upsilon(T-T_a)]. \tag{4.7}$$

For non-dimensionlization, following quantities are used.

$$\theta=\frac{T}{T_b}, \theta_a=\frac{T_a}{T_b}, \Phi=\frac{qL}{k_aT_b}, Bi=\frac{h_bL}{k_a}, \xi=\frac{x}{L}, \beta=gT_b,$$
$$\gamma=\upsilon T_b, N_c=\frac{h_bPL^2}{k_aA_{cs}}, N_r=\frac{\sigma\varepsilon_oPL^2T_b^3}{k_aA_{cs}}, N_{br}=\frac{\sigma\varepsilon_oLT_b^3}{k_a}, \tau=\frac{k_at}{L^2\rho c_p}.$$

The governing equation, initial condition and boundary conditions become,

$$\frac{\partial}{\partial\xi}\Big[\frac{\partial\theta}{\partial\xi}+\beta\theta\frac{\partial\theta}{\partial\xi}-\beta\theta_a\frac{\partial\theta}{\partial\xi}\Big]-N_c\left\{\frac{\theta-\theta_a}{1-\theta_a}\right\}^n[\theta-\theta_a]-N_r[1+\gamma(\theta-\theta_a)](\theta^4-\theta_a^4)=\frac{\partial\theta}{\partial\tau}, \quad (4.8)$$

$$\theta_a=0.88, \quad \tau=0, \quad (4.9)$$

$$(1+\beta(\theta-\theta_a))\frac{\partial\theta}{\partial\xi}\Big|_{\xi=0}=\Phi \quad (4.10)$$

$$(1+\beta(\theta-\theta_a))\frac{\partial\theta}{\partial\xi}=Bi\left\{\frac{\theta-\theta_a}{1-\theta_a}\right\}^n[\theta-\theta_a]+N_{br}[1-\gamma(\theta-\theta_a)](\theta^4-\theta_a^4), \quad \xi=1. \quad (4.11)$$

The main focus of this case is to retrieve time-varying heat flux with the aid of inverse analysis. The apriori heat flux takes the following three functional forms,

$$\begin{aligned}
&\Phi=0.98\\
&\Phi=\begin{cases}\Phi_c\tau, & :\text{if } 0\le\tau\le\tau_1,\\ \Phi_c\tau_1\big(\frac{\tau-\tau_2}{\tau_1-\tau_2}\big), & :\text{if } \tau_1\le\tau\le\tau_2,\\ 0, & :\text{otherwise.}\end{cases}\\
&\Phi=\begin{cases}\Phi_c\sqrt{1.5\tau}, & :\text{if } 0\le\tau\le\tau_1,\\ \Phi_c\sqrt{1.5\tau_1}, & :\text{if } \tau_1<\tau.\end{cases}
\end{aligned} \quad (4.12)$$

The system (4.8)-(4.11) is non-linear and the temperature response is obtained through forward analysis and then the inverse is being performed to retrieve the input heat flux as discussed in the next section.

4.3 Methodology

4.3.1 Forward Analysis

To obtain the solution of the forward problem, the governing partial differential equation is converted into a number of ordinary differential equations which are subsequently solved using the Runge-Kutta method. The task is accomplished using the MATLAB 'pdepe' solver (solver for initial-boundary value problems for a system of parabolic-elliptic partial differential equations), Skeel and Berzins (1990), Singh and Singla (2019). The following MATLAB commands are used

1. $[c, f, s]$ = *pdefun*(x, t, u, DuDx),
   (To generate the functions involved in the governing equation.)

2. u = *icfun* (x),
   (To generate the functions involved in the initial condition.)

3. $[pl, ql, pr, qr]$ = *bcfun* (xl, ul, xr, ur, t),
   (To generate the functions involved in the boundary conditions.)

4. *Sol* = *pdepe*(m, $pdefun$, $icfun$, $bcfun$, $xmesh$, $tspan$), generates the solution.

4.3.2 Inverse Analysis

The function $\Phi(\tau)$ is regarded as the unknown, while everything else is known. The objective is to predict the unknown time-dependent function, merely from the apriori known temperature data $\tilde{\theta}$, obtained either from solver or experimental setup. To estimate the same, an optimization technique is required. In this optimization process, the following objective function is minimized using the Golden Section Search Method (GSSM). GSSM was proposed by Kiefer (1953) and is a variant of the Fibonacci search method. GSSM does not require gradient calculations, hence reduces the computational cost significantly. The method converges fast as it optimizes using direct search approach. The limitation of this method is that it can retrieve a single parameter but work perfectly for the present retrieval. The details of the algorithm are discussed ahead.

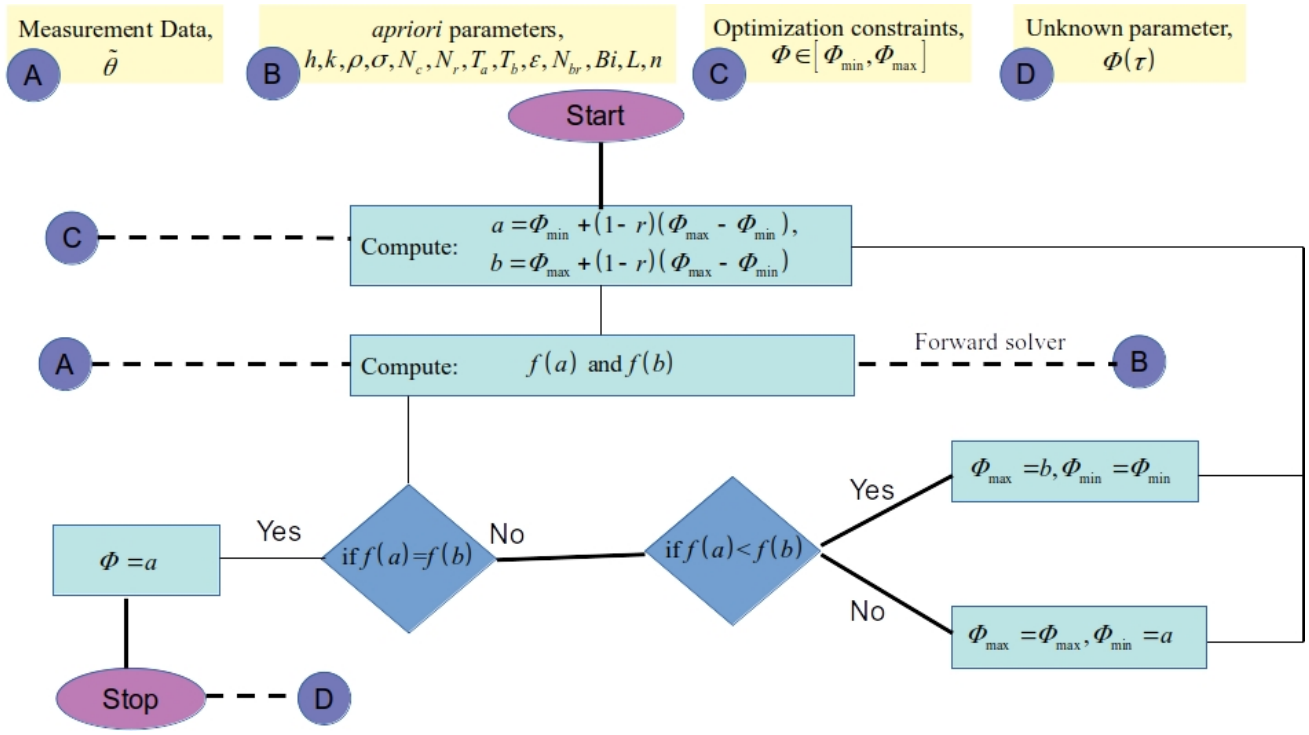

Fig. 4.3 Flow chart of Golden section search method (GSSM).

Golden Section Search Method (GSSM)

Let 'Φ' denotes heat flux to be retrieved. It is assumed that temperature measurements say 'θ' are available at certain points through experiments or by forward analysis. The updated measurements '$\tilde{\theta}$' are calculated from the inverse analysis. The block A is input for 'θ'. Block B act as input, where various thermal parameters, h, k, ρ, σ, N_c, N_r, T_a, T_b, ε, N_{br}, Bi, L, n are assigned the values described in Table (4.1). Initial guess interval $[\Phi_{min}, \Phi_{max}]$ is passed initially, which form a constraint for optimization. Now comes the role of inverse technique which can be seen diagrammatically in Fig.(4.3). The method starts by describing an ini-

tial guess provided by block C in Fig.(4.3). The algorithm then refines the guesses as, $a = \Phi_{min}+(1-r)(\Phi_{max}-\Phi_{min})$ and $b = \Phi_{max}-(1-r)(\Phi_{max}-\Phi_{min})$, where $r = \dfrac{\sqrt{5}-1}{2} = 0.618$, satisfying the property $r = \dfrac{1}{1+r}$. Here 'r' is called inverse golden number, which is responsible for deriving the name of the method. These new points a and b, are at a distance of 'r' from the original points Φ_{min} and Φ_{max}. The objective function for the i^{th} time step, given by the following equation is then calculated for a, b.

$$f(\bar{\Phi}) = ||\theta_i(\Phi) - \tilde{\theta}_i||. \tag{4.13}$$

If $f(a) < f(b)$, then discard the interval to right of b, i.e., keep $\Phi_{min} = \Phi_{min}$ and $\Phi_{max} = b$, otherwise $\Phi_{max} = \Phi_{max}$ and $\Phi_{min} = a$, in the next iteration. The interval then reduces to $[\Phi_{min}, b]$ or $[a, \Phi_{max}]$ respectively. The whole point of doing this lies in the fact that while reducing the interval to achieve a minimum objective, the ratio, often called reduction ratio, $\dfrac{\Phi_{max}-\Phi_{min}}{b-\Phi_{min}}$ and $\dfrac{\Phi_{max}-\Phi_{min}}{\Phi_{max}-a}$ remains 1.618, which is the golden number. The iterations above are continued until a fixed number of iterations are crossed or the objective function achieves a sufficiently small value.

4.4 Results and Discussion

In this section, we have presented the results obtained from forward and inverse analysis, their comparison and discussed the estimated unknown parameter namely heat flux. It can be noted that for the calculations of the temperature profiles in forward analysis, parameters of experimental setup given in Table (4.1) are used. Feasible range of each parameter is also calculated and is mentioned in Table (4.1). While performing the experiments, it is observed that a steady-state has been achieved after two hours of continuous run i.e., $\tau = 2.226$, but to be sure about the steady-state, $\tau = 5$ has been used for the analysis. Further, the computed and experimental trend of retrieved heat flux has been observed. Lastly, the effect of errors is seen through error analysis. The maximum tolerance limits for heat flux is observed.

4.4.1 Comparison

To demonstrate the comparison part of the present forward method, the temperature profile of pin fin, obtained using 'pdepe' solver is compared with results of Das and Kundu (2018). In the cited literature, authors have considered a rectangular fin with internal heat generation along with insulated and constant temperature boundaries. The results are compared in Fig.(4.4) for the parameters chosen as $\beta = 0.2$, $\theta_a = Q = 0$, $N_c = 1$, $N_r = 0.2$ and found to be in good agreement. Further, to emphasize the comparison part, the temperature profile obtained is scrutinised for the expected results.

4.4.2 Forward pdepe results

After comparison, the temperature distribution corresponding to different heat flux of equation (4.12) is presented in Fig.(4.5), at different time steps. Then the effect of natural convection parameter, N_c and natural radiation parameter, N_r on the temperature distribution, is illustrated

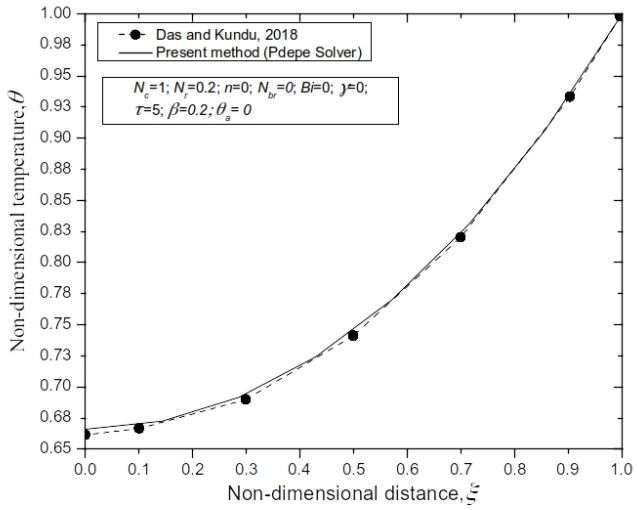

Fig. 4.4 Comparison of Matlab's pdepe solver with Das and Kundu (RK-4 method), with parameters $\beta = 0.2,\ \theta_a = Q = 0,\ N_c = 1,\ N_r = 0.2$.

in Fig.(4.6). It is observed that the temperature decreases with an increase in N_c and N_r. These trends are theoretically expected too, as with an increase in N_c and N_r more heat transfer takes place.

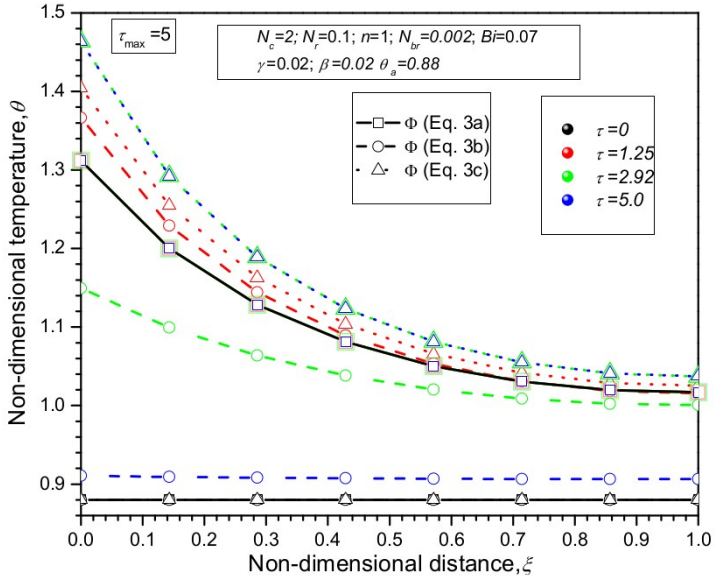

Fig. 4.5 Temperature profile at different time steps, when constant, triangular and realistic heat flux is utilized.

Having obtained the computational temperature profile through the forward strategy, the retrieval of the heat flux is discussed ahead. Retrieval is done under dynamic conditions utilizing

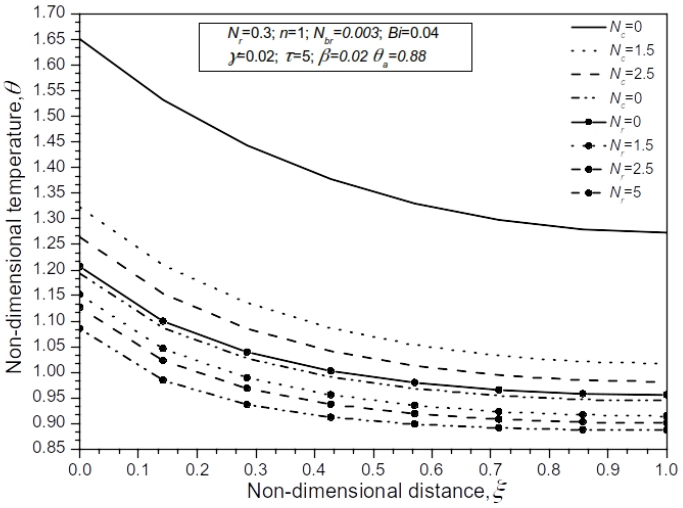

Fig. 4.6 Expected temperature profile with different values of N_c and N_r.

the objective function, Equation (4.13). Further, subcases are made to discuss constant, linear triangular and non-linear realistic heat fluxes respectively, when the computed temperature profile has no error and when an error of 1%, 2%, 4%, 5% is present. Thereafter, the retrieval of heat flux is obtained using the experimental temperature profile.

4.4.3 Retrieval under dynamic conditions, without error in temperature

For retrival of single parameter, GSSM has proved to be an excellent method. Given the thermal distribution in the form of temperature profile with respect to distance for different time steps, Fig.(4.5). The efficiency of GSSM is obtained by observing the convergence rates. The heat flux, Φ converges gradually to the optimal value of 0.98, with the corresponding objective function's value O(10^{-10}) after 17^{th} iteration, Fig.(4.7).

The objective function evaluated at various time steps, given in equation (4.12), results in retrieval of heat flux, which is more close to reality as compared to the objective function evaluated as a whole. Unlike the static case, Singhal *et al.* (2019), in the dynamic retrieval case, the forward analysis utilizes an exact flux of 0.98, but the inverse is carried out, with objective function calculated at each time step. The plots of recovered heat flux and exact heat flux are shown in Fig.(4.8a). The comparison of the retrieved heat flux with the exact flux is nearly the same.

In the next subcase, the exact heat flux, equation (4.12, case b) is utilized for the forward part. This flux is assumed to vary linearly, where initially, power in the form of flux is provided, which behave as a linear function of time, until a maximum required heat is generated within the system. This heat then starts decreasing again linearly with respect to time. This trend corresponds to the on-off situation which is required in the auto cut of any heating system,

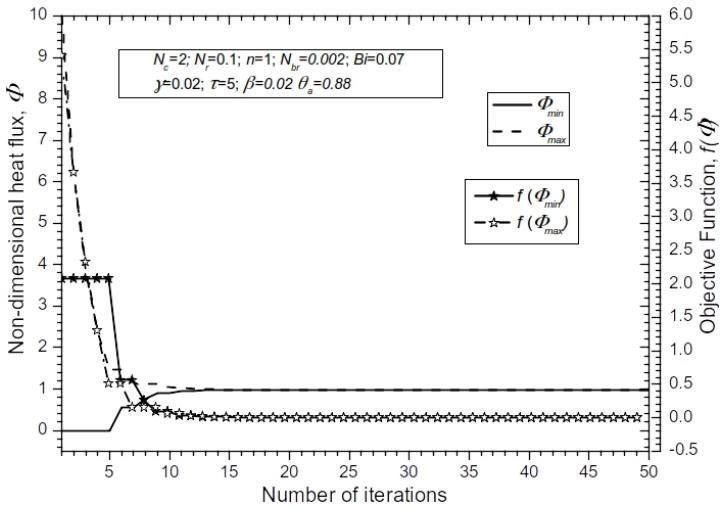

Fig. 4.7 Variation of retrieved heat flux and objective function using GSSM, with the number of iterations.

Parthasarathy and Balaji (2008). The temperature profile obtained using this flux is then utilized to retrieve flux. Fig.(4.8b) proved the performance of the inverse technique when estimated heat flux with no error in input temperatures is plotted against exact heat flux, equation (4.12, case b). Here, at the time of retrieval, the functional form of heat flux is not known apriori.

The above considered two forms of Φ have rare appearances in reality. In real-life applications, power in the form of increasing non-linear heat flux is provided resulting in an initial rise followed by a steady-state temperature, Agrawal (2016). The mathematical form of such a heat flux Φ is given in Equation (4.12, case c), which is used for further analysis. This non-linear heat flux, is fed into the forward system. The temperature profile is noted and the inverse analysis is carried out, in which no information about the functional form of heat flux is available. Inverse calculations utilize the heat flux retrieved at previous time steps. As no information regarding the nature of heat flux is available, the heat flux is approximated, treating it as a straight line. Thus, the curve of heat flux is retrieved using the segments of straight lines between various time steps. Such a retrieval approach is most prominent to recover heat flux which mimics the actual situation quite effortlessly. Fig.(4.8c) showcases the exact heat flux and the estimated heat flux when no errors are involved in temperatures. On a closer look, small deviations at the second time step are justified as the retrieval approach uses a straight line as a functional form of heat flux between the successive time steps.

4.4.4 Retrieval under dynamic conditions, with error in temperature

After retrieving the heat flux for different cases in the previous subsection, in this subsection, the effect of various measurement errors in temperature is observed on the reconstruction. The

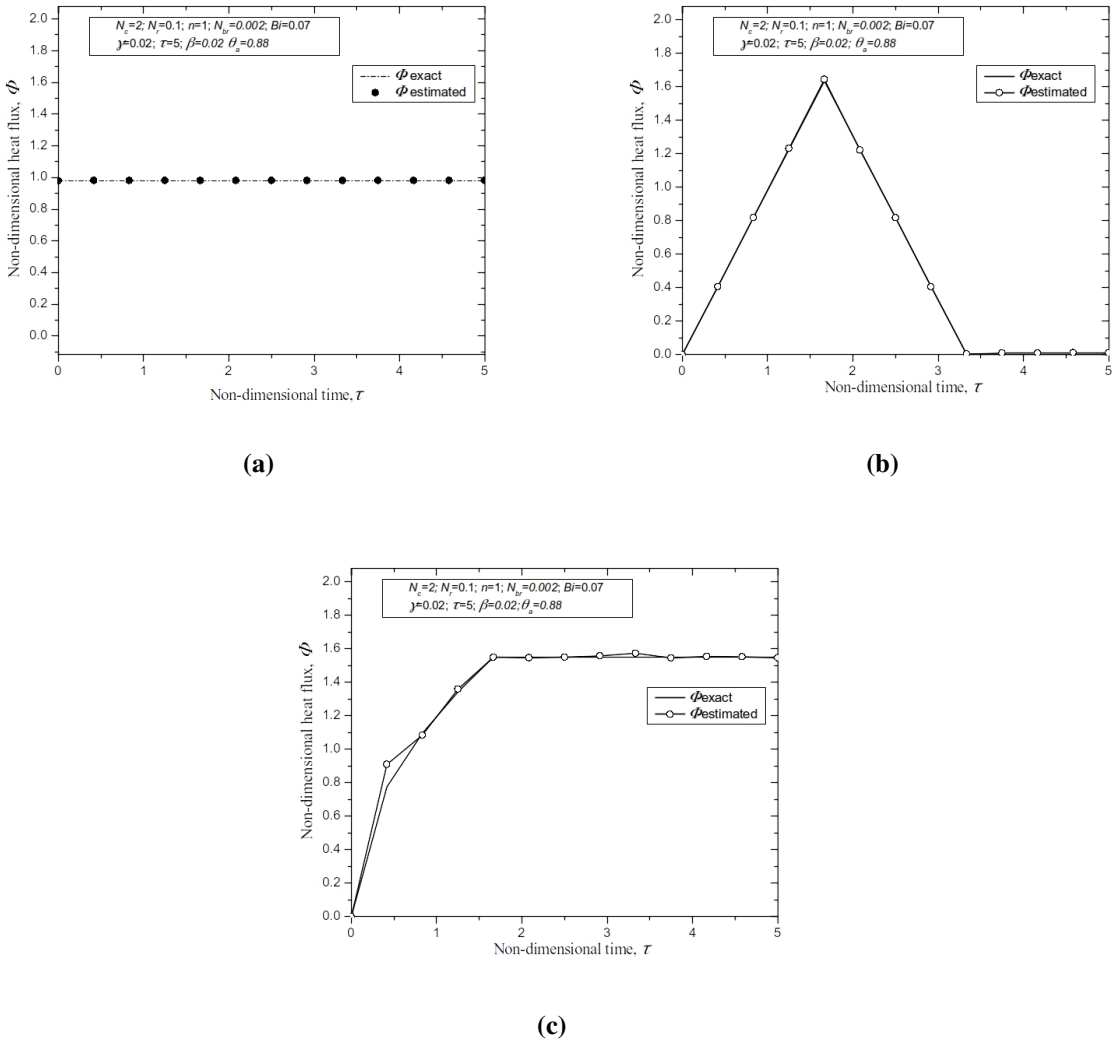

Fig. 4.8 Retrieved heat flux (a) constant, (b) triangular profile, (c) realistic profile, without error e_r under dynamic conditions.

performance of the model is determined by studying the impact of reconstruction error. The first task is to obtain apriori temperature profile from forward methodology using Φ given in Equation (4.12). The obtained temperature profiles with added e_r, 1%, 2%, 4%, 5% are shown in Fig.(4.9) and these profiles are used to retrieve the heat flux with inverse methodology. The GSSM is used to minimize the objective function with initial guess of $[\Phi_{min}, \Phi_{max}] = [0, 10]$, as discussed previously.

For $\Phi = 0.98$ used in the forward analysis, Fig.(4.10a) shows the plots of recovered heat flux, with random errors of 1%, 2%, 4%, 5% in temperatures. The maximum and minimum absolute errors, using the mean and standard deviation of recovered heat flux are shown in Table (4.2). It is observed that the error in estimated heat flux increases with an increase in the error of input

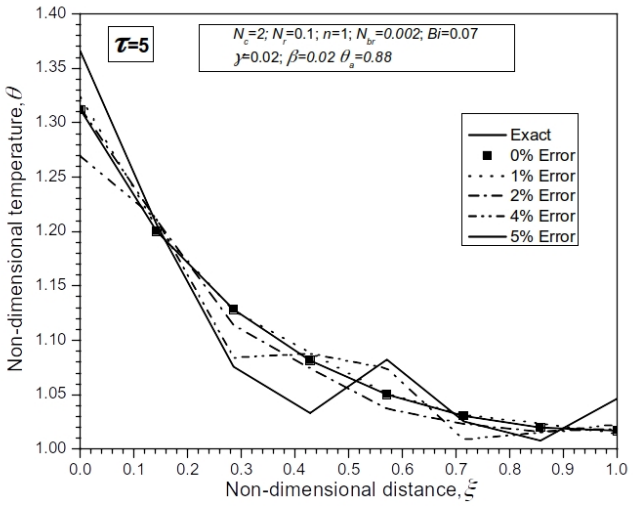

Fig. 4.9 Temperature profile, with $\Phi = 0.98$, obtained using forward analysis with 1%, 2%, 4% and 5% error.

temperature, as expected. Further, to maintain the device's temperature within an interval of 3% error, tolerance bound of 6.8% has been estimated for retrieved heat flux. This bound justifies itself with the statistics of Table (4.2), because to maintain the temperature within an interval of 4% error, tolerance bound of 11% is required, which is not acceptable.

Next, the apriori temperature data is obtained using Φ given in Equation (4.12, case b) which imitates flux increasing up to a certain point and then decreasing as discussed previously. Fig.(4.10b) shows the retrieved heat flux with 1%, 2%, 4%, 5% error in input temperatures when the linear triangular Φ given in Equation (4.12, case b) is used in forward analysis. Such estimation is good when the error introduced in input temperatures are below 3%. Deviations are seen in the cases when 4% and 5% errors are embedded. Exponential growth in output error is observed, after 2% of the input error. Hence, a cut-off is marked at 2% which leads to an error of 9.6% in the retrieved heat flux.

Fig.(4.10c) showcases the exact and estimated heat flux when 1%, 2%, 4%, 5% errors are involved in temperature profile obtained using nonlinear Φ given in Equation (4.12, case c). Small deviations at the second time step can be seen which are justified as the retrieval approach assumes the linear functional form of heat flux between the successive time steps. Fig.(4.10c) along with Table (4.2), reveals that despite many deviations in reconstruction, the technique works quite satisfactorily providing realistic results.

4.4.5 Experimental results analysis

Here, we discuss about the retrieved heat flux when the temperature profile is obtained using experimental setup with parameters given in Table (4.1). It can be noted that, to minimize

Table 4.2 Relative error in recovered heat flux, with different measurement error in temperature, under dynamic conditions.

		Profile of heat flux (HF) at surface of fin								
		Case a: constant; Eq. (4.12)			Case b: triangular; Eq. (4.12)			Case c: realistic; Eq. (4.12)		
S.No.	$e_r(\%)$	Error (%)		Obj. Function	Error (%)		Obj. Function	Error (%)		Obj. Function
		Max.	Min.		Max.	Min.		Max.	Min.	
1	0%	O(10^{-8})	O(10^{-8})	5.26×10^{-21}	1.17	0.033	3.22×10^{-8}	13.39	0.013	1.89×10^{-8}
1		**3.41**	0.34	$\mathbf{2.77 \times 10^{-4}}$	2.50	0.23	2.50×10^{-4}	12.80	0.17	3.18×10^{-4}
2	1%	3.28	0.20	4.25×10^{-4}	4.50	**0.30**	$\mathbf{3.05 \times 10^{-4}}$	**13.58**	**0.81**	$\mathbf{3.75 \times 10^{-4}}$
3		2.68	**0.57**	$\mathbf{1.77 \times 10^{-4}}$	**4.93**	0.16	$\mathbf{1.62 \times 10^{-4}}$	10.11	0.65	5.29×10^{-4}
1		6.89	**0.43**	$\mathbf{1.18 \times 10^{-3}}$	**9.63**	**0.30**	$\mathbf{6.73 \times 10^{-4}}$	9.85	**0.85**	$\mathbf{1.72 \times 10^{-3}}$
2	2%	**8.50**	0.0033	$\mathbf{1.50 \times 10^{-3}}$	8.71	0.30	6.98×10^{-4}	6.83	0.24	8.49×10^{-4}
3		4.05	0.034	1.32×10^{-3}	5.33	0.30	3.32×10^{-4}	**14.72**	0.75	$\mathbf{5.28 \times 10^{-4}}$
1		**6.80**	0.17	$\mathbf{2.81 \times 10^{-3}}$	14.03	0.27	2.55×10^{-3}	16.81	**1.88**	$\mathbf{3.04 \times 10^{-3}}$
2	3%	3.92	0.99	2.44×10^{-3}	**15.80**	**0.30**	$\mathbf{2.60 \times 10^{-3}}$	**19.12**	0.19	$\mathbf{2.25 \times 10^{-3}}$
3		2.09	**1.05**	$\mathbf{3.17 \times 10^{-3}}$	5.32	0.30	2.03×10^{-3}	15.13	0.46	2.08×10^{-3}
1		**11.94**	**0.53**	$\mathbf{3.70 \times 10^{-3}}$	9.61	0.30	3.29×10^{-3}	23.94	0.81	4.52×10^{-3}
2	4%	8.62	0.022	4.02×10^{-3}	**21.91**	**0.30**	$\mathbf{6.05 \times 10^{-3}}$	22.48	0.79	4.91×10^{-3}
3		11.71	0.32	3.94×10^{-3}	21.32	0.30	3.16×10^{-3}	**26.55**	**2.22**	$\mathbf{7.19 \times 10^{-3}}$
1		**15.36**	0.13	$\mathbf{2.52 \times 10^{-3}}$	20.70	0.033	4.15×10^{-3}	25.50	0.39	4.04×10^{-3}
2	5%	14.08	**2.71**	$\mathbf{1.08 \times 10^{-2}}$	**22.48**	0.018	$\mathbf{3.63 \times 10^{-3}}$	**36.76**	**0.99**	$\mathbf{9.01 \times 10^{-3}}$
3		12.30	0.86	7.13×10^{-3}	21.54	**0.30**	$\mathbf{3.15 \times 10^{-3}}$	26.38	0.065	3.22×10^{-3}

the uncertainty involved, three measurements under the same conditions are recorded, whose average is utilized. To start with, the system is given input heat flux for a specific period of time which emulates the Φ in Equation (4.12, case a) indicating a situation when the system under consideration is switched off after some time. Fig.(4.11a) shows the retrieved heat flux for three different experimental data. On comparing Fig.(4.11a) and Fig.(4.8b), one can see similar trends, hence it is concluded that the computed results are matching to the experimental results. It can be noted that heat flux obtained from experimental and computational studies are of different magnitudes due to the fact that few parameters like h, β, γ are not exactly available for experiments and can only be approximated which leads to discrepancy. The maximum uncertainties in reconstructed heat flux are 9.5%, 8% and 9% for $V = 80$V $I = 0.027$A, $V = 60$V $I = 0.018$A, $V = 70$V $I = 0.022$A respectively, which are shown as error bars. Trend lines for the reconstruction are plotted along with the mean for different voltages and currents. Details of retrieved data is given in Table (4.3). Next, the system is given the input heat flux for a longer duration which emulates the Φ in Equation (4.12, case c). Fig.(4.11b) shows the retrieved heat flux and it is observed that the trends are similar to that of Fig.(4.8c). The maximum uncertainties in reconstructed heat flux are 5%, 6% and 2% for $V = 80$V $I = 0.027$A, $V = 60$V $I = 0.018$A, $V = 70$V $I = 0.022$A respectively. Details of retrieved heat flux is given in Table (4.3).

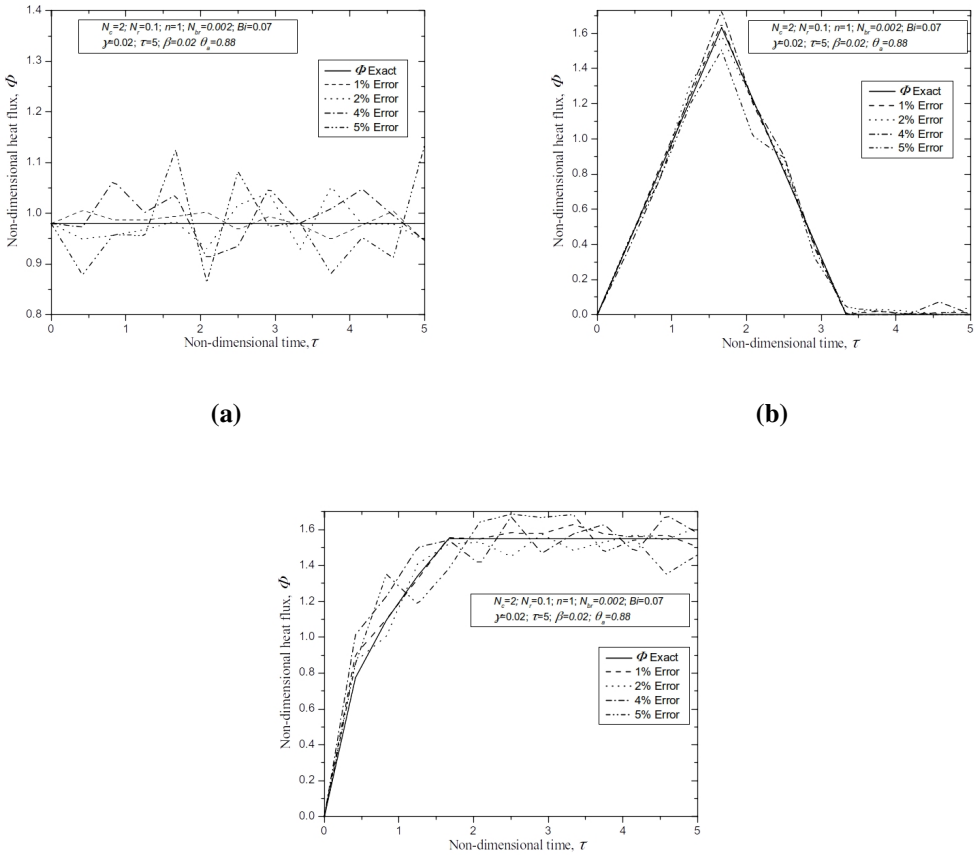

Fig. 4.10 Retrieved heat flux (a) constant, (b) triangular profile, (c) realistic profile, with error $e_r = 1\%,\ 2\%,\ 4\%,\ 5\%$ under dynamic conditions.

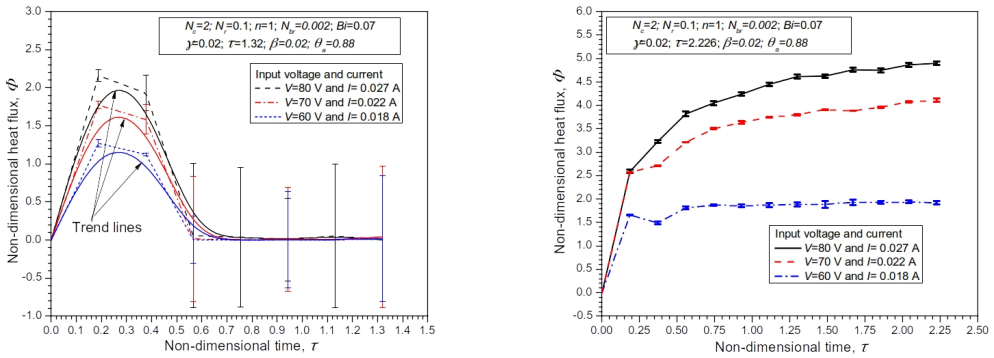

Fig. 4.11 Retrieval of heat flux (a) triangular and (b) realistic profile from experimental temperature distribution.

Table 4.3 Estimated heat flux using the temperatures obtained by experiments, for $V = 80$V, $I = 0.027$A; $V = 60$V, $I = 0.018$A; $V = 70$V, $I = 0.022$A.

τ	$V = 80$V $I = 0.027$A		$V = 60$V $I = 0.018$A		$V = 70$V $I = 0.022$A	
	Case 1: retrieved triangular heat flux by experimental temperature data					
	Run 1	Run 2	Run 1	Run 2	Run 1	Run 2
0.000	0.000	0.000	0.000	0.000	0.000	0.000
0.1885	2.3303	1.9892	1.2048	1.3356	1.8613	1.6838
0.3771	2.3769	1.4820	1.0993	1.1482	1.8856	1.2805
0.5657	0.1150	0.003	0.0056	0.003	0.0305	0.003
0.7542	0.0679	0.003	0.003	0.003	0.003	0.003
0.9428	0.0101	0.003	0.003	0.0132	0.0160	0.003
1.1314	0.1016	0.003	0.003	0.003	0.003	0.003
1.32	0.003	0.003	0.003	0.0316	0.0827	0.003
	Case 2: retrieved realistic heat flux by experimental temperature data					
	Run 1	Run 2	Run 1	Run 2	Run 1	Run 2
0.000	0.000	0.000	0.000	0.000	0.000	0.000
0.1855	2.6824	2.4900	1.6509	1.6676	2.5740	2.5708
0.3710	3.3129	3.1419	1.4419	1.5365	2.7323	2.6913
0.5565	4.0061	3.6213	1.7608	1.8612	3.2123	3.2004
0.7420	4.2238	3.8744	1.8394	1.9003	3.5492	3.4485
0.9275	4.3917	4.0826	1.8115	1.8975	3.7321	3.5419
1.113	4.6039	4.2917	1.7989	1.9421	3.7688	3.7128
1.2985	4.8001	4.4219	1.7939	1.9706	3.8525	3.7453
1.484	4.7672	4.4748	1.7571	2.0140	3.9356	3.8832
1.6695	4.9514	4.5630	1.8224	2.0357	3.8849	3.8735
1.855	4.9330	4.5590	1.8685	1.9815	3.9158	4.0049
2.0405	5.0535	4.6740	1.8847	1.9920	4.0064	4.1461
2.226	5.0702	4.7221	1.8510	1.9836	3.9738	4.2395

4.5 Observations

The inverse retrieval of the functional heat flux for a pin fin with nonlinearity is performed and the input parameters are defined based on experimental setup. The retrieval is exercised for theoretical as well as experimental analysis and the retrieved heat fluxes from both studies under transient conditions follow the same trends. The effect of measurement errors in the temperature measured by sensors on the retrieved heat flux has been examined. The following observations are made in this chapter about the maximum accepted tolerance.

1. The acceptable measurement errors are 3%, 2%, and 2% with a maximum error of 6.8%, 9.6%, and 14% under the dynamic condition for the constant, triangular and realistic profile of heat flux respectively.

2. Further, the uncertainties in reconstructed heat flux have been quantified from experimental setup for $V = 80\text{V}, 60\text{V}, 70\text{V}$ and $I = 0.027\text{A}, 0.018\text{A}, 0.022\text{A}$ and found to be 9.5%, 8% and 9%, for triangular and 5%, 6% and 2% for realistic heat profiles, respectively.

Chapter 5

Regularized Comparative Inversion Approach for IHTP

As discussed in chapter 2, a large number of inversion techniques have been developed by the eminent scientists, engineers and mathematicians but what if the techniques available were not utilized to an extent that they should? Although developing and improving the existing algorithms for parameter estimation in every inversion field, particularly IHTP is a promising direction for any researcher, however, is there any technique that works globally for every inverse problem? During the study, no such algorithm was reported for non-linear problems. The next obvious question is to ask whether there be any general procedure by which researchers working on inverse problems may select an algorithm by comparison which is suitable particularly to them, such that the overall efficiency of estimation magnifies to a significant amount. Thus, the need of the hour is to work on the effectiveness of the inverse methods.

Motivated by this need, in this chapter, we have developed a novel comparison procedure to compare and select the best algorithm for IHTP, which could be implemented easily to any other area of inverse problems. The proposed procedure is useful because there is no particular algorithm, which is suitable to solve an inverse problem from every domain, as stated in no free lunch theorem, [Wolpert and Macready (1997)]. This theorem states that no optimization algorithm works for every set of problem. Thus, the proposed comparative procedure could be applied to any domain involving estimation of parameters using inverse analysis. Based on the literature survey which reveals the presence of a large number of inversion algorithms, the new inverse formulation involves a combination of the suitable forward, regularization and corresponding optimization techniques.

In this study, the forward analysis utilizes Matlab based pdepe for the computation of surface temperature. The regularization is proposed by the modification in the objective function. The

objective functions lasso, Tikhonov and elastic net were proposed for the purpose instead of the traditional least-squares. Whereas for minimization, several optimization algorithms were picked from different categories, namely, evolution-based Differential Evolution (DE), swarm-based (Particle Swarm Optimization (PSO), Whale Optimization Algorithm (WOA)), nature-based (Water Cycle Algorithm (WCA), Butterfly Optimization Algorithm (BOA)), physics-based (Atom Search Algorithm (ASO)) and a hybrid (Grey Wolf Optimization and Cuckoo Search (GWOCS)). These methods are efficient and thus can be tailored according to the needs of the problem. The decision for the efficient algorithm was made using TOPSIS, where the top three algorithms were reported for IHTP.

Building onto the application of the extended surface, particularly pin fin, studied in chapter 4, the comparative procedure is implemented to obtain the best inversion technique. The results obtained using this procedure were easily tested with the experimental data. The temperature profile of the fin is obtained using thermocouples at various locations. The material properties of the fin surface are generally not available. Such properties have adequate information regarding the material being used and thus are used to make appropriate decisions while designing. These properties cannot be determined directly, because the associated problem becomes ill-posed and hence is difficult to solve. Thus, a regularized inverse method is required to estimate these material properties. In addition to the effects of thermal radiation, convection, conduction, temperature-dependent thermal properties, critical parameters were estimated. To determine which parameters were important and sensitive towards error, a sensitivity analysis had been carried out. These critical parameters were estimated using the inverse algorithm.

For the inverse analysis, optimization algorithms, like Genetic Algorithm (GA), Simulated Annealing (SA), Simplex Search Method (SSM), Differential Evolution (DE) have been implemented by Das (2012), Panda and Das (2015), Das (2014, 2011), Kiwan and Al-Nimr (2000), Das and Ooi (2013), Panda *et al.* (2014), Das *et al.* (2017). Several one-dimensional transient heat transfer problems have been solved to determine the time-dependent heat flux, Mzad (2015), Mohammadiun and Rahimi (2011), Mohammadiun *et al.* (2011), Sriram *et al.* (2016), Kryzhanivskyy *et al.* (2017). To determine which inverse method work better for a nonlinear problem of inverse heat transfer, comparison of nature-based algorithms taken from different pools was done. Earlier works, including such a comparison, were given by Yildiz (2013), Rana *et al.* (2013) and Saleh *et al.* (2018), where they compared (DE, Taguchi method), (GA, DE, PSO, Ant Bee Colony optimization (ABC)) and (WOA, Moth-Flame optimization, Dragonfly Algorithm) for the structural design optimization problem, structure stability analysis of Ni_n clusters and for minimization of network power losses in radial distribution systems respectively. In the domain of heat transfer, the comparison was made by Daun *et al.* (2006) and Weres *et al.* (2009). They compared (Tikhonov method, Truncated Singular Value decomposition, Conjugate Gradient method, SA) and (tabu search, GA, SA, variable-metric algorithm, trust-region algorithm) for inverse design of radiant enclosures and for inverse finite element

analysis in biological materials, respectively. Literature limited to inverse heat conduction problems includes a comparison of numerical methods with sequential time marching method by Raynaud and Beck (1988), function specification method, iterative regularization, Tikhonov's regularization by Beck *et al.* (1996b) and ABC with Ant Colony optimization by Hetmaniok *et al.* (2012). The experimental setup and the mathematical formulation is discussed ahead.

5.1 Problem formulation

The experimental setup used for the results of this chapter was shown in Fig.(4.1). The geometry of the cylindrical extended surface was shown in Fig.(4.2), whose mathematical model is inspired by the experimental setup as discussed previously in chapter 4. The parameters used in the forward analysis are mentioned in Table (5.1). The mathematical formulation corresponding

Table 5.1 Dimensional and non-dimensional parameters values used in forward analysis, taken from experimental setup.

Fin parameters	
Dimensional	Non-dimensional
L = 0.35 m	h_b = 5
d = 0.01 m	ε_0 = 0.95
Material is Brass	Nc = 2
A = 7.85 $\times$ 10^{-5} m^2	Nr = 0.5826
P = 0.03014 m	Bi = 0.0146
ρ = 8520 kg/m^3	N_{br} = 0.0042
c_p = 375 J/kg-K	dτ = 0.4167
k = 121 W/mK	dx = 0.1429
T_a = 295 K	τ = 5
T_b = 298 K	

to the present study is as follows. At any arbitrary location, x, the governing energy equation can be expressed as below,

$$\frac{\partial}{\partial x}\left[k(T)A_{cs}\frac{\partial T}{\partial x}\right] - h(T)P(T-T_a) - \varepsilon(T)\sigma P(T^4 - T_a^4) = \rho c_p A\frac{\partial T}{\partial t},\ 0 < x < L, \quad (5.1)$$

with initial condition as,

$$T(t=0) = T_a = 295.15\,\text{K}, \quad 0 < x < L, \quad (5.2)$$

and boundary conditions as,

$$-k(T)\frac{\partial T}{\partial x}\Big|_{x=0} = q\Big|_{x=0}, \quad (5.3)$$

$$-k(T)A_{cs}\frac{\partial T}{\partial x}\Big|_{x=L} = h(T)A_{cs}[T(x=L) - T_a] + \varepsilon(T)\sigma A_{cs}[T^4(x=L) - T_a^4]. \quad (5.4)$$

where the temperature-dependent properties are Huang *et al.* (1995), Mosayebidorcheh *et al.* (2014),

$$k(T) = k_0 + k_1 e^{\frac{T}{k_2}} + k_3(T - T_a), \tag{5.5a}$$

$$\varepsilon(T) = \varepsilon_0[1 - \delta_1(T - T_a) - \delta_2(T - T_a)^2], \tag{5.5b}$$

$$h(T) = h_b\Big\{\frac{T - T_a}{T_b - T_a}\Big\}^n. \tag{5.5c}$$

Following quantities are introduced for non-dimensionalization,

$$\begin{gathered}\theta = \frac{T}{T_b}, \quad \theta_a = \frac{T_a}{T_b}, \quad X = \frac{x}{L}, \quad \alpha_1 = \frac{k_1}{k_0}, \quad \beta = \frac{T_b}{k_2}, \quad \eta = \frac{T_b k_3}{k_0}, \quad \gamma_1 = \delta_1 T_b, \\ \gamma_2 = \delta_2 T_b^2, \quad Nc = \frac{h_b P L^2}{A_{cs} k_0}, \quad Nr = \frac{\sigma \varepsilon_0 P L^2 T_b^3}{A_{cs} k_0}, \quad Bi = \frac{h_b L}{k_0}, \quad N_{br} = \frac{\sigma \varepsilon_0 L T_b^3}{k_0}, \\ \Phi = \frac{qL}{T_b k_0}, \quad \tau = \frac{t k_0}{c_p \rho L^2}.\end{gathered} \tag{5.6}$$

After substitution of the above quantities in equations (5.5), temperature-dependent thermal properties become,

$$k(T) = k_0[1 + \alpha_1 e^{\theta\beta} + \eta(\theta - \theta_a)], \tag{5.7a}$$

$$\varepsilon(T) = \varepsilon_0[1 - \gamma_1(\theta - \theta_a) - \gamma_2(\theta - \theta_a)^2], \tag{5.7b}$$

$$h(T) = h_b\Big\{\frac{\theta - \theta_a}{1 - \theta_a}\Big\}^n. \tag{5.7c}$$

The equations (5.1)-(5.4), in non-dimensional form become,

$$\begin{aligned}\frac{\partial}{\partial X}\Big[\Big(1 + \alpha_1 e^{\theta\beta} \;+\; \eta(\theta - \theta_a)\Big)\frac{\partial \theta}{\partial X}\Big] - Nr[1 - \gamma_1(\theta - \theta_a) - \gamma_2(\theta - \theta_a)^2](\theta^4 - \theta_a^4) \\ - \; Nc\Big(\frac{\theta - \theta_a}{1 - \theta_a}\Big)^n(\theta - \theta_a) = \frac{\partial \theta}{\partial \tau}, \; 0 < X < 1,\end{aligned} \tag{5.8}$$

with initial condition as,

$$\theta_a(\tau = 0) = \frac{T_a}{T_b} = \frac{295.15\,\mathrm{K}}{298.15\,\mathrm{K}} = 0.9899, \quad 0 < X < 1, \tag{5.9}$$

and boundary conditions as,

$$-(1 + \alpha_1 e^{\theta\beta} + \eta(\theta - \theta_a))\frac{\partial \theta}{\partial X}\Big|_{X=0} = \Phi\Big|_{X=0}, \quad \tau > 0, \tag{5.10}$$

$$\begin{aligned}-(1 + \alpha_1 e^{\theta\beta} + \eta(\theta - \theta_a))\frac{\partial \theta}{\partial X}\Big|_{X=1} &= N_{br}(1 - \gamma_1(\theta - \theta_a) - \gamma_2(\theta - \theta_a)^2)[\theta^4 - \theta_a^4]\Big|_{X=1} \\ &\quad + Bi\Big(\frac{\theta - \theta_a}{1 - \theta_a}\Big)^n[\theta - \theta_a]\Big|_{X=1}, \quad \tau > 0, .\end{aligned} \tag{5.11}$$

The above dimensionless form in equations (5.8)-(5.11) depends on several parameters namely θ, θ_a, the non-dimensional temperatures, X, the junction position, τ, represents the non-dimensional time, α_1, β, η, the conductivity parameters, γ_1, γ_2, the emissivity parameters,

$Bi,\ Nc,\ Nr,\ N_{br}$, the Biot number, the convection conduction and radiation conduction parameters respectively, Φ represents the heat flux. The system thus formed (5.8)-(5.11), being non-linear is solved during forward analysis and then the inverse is being performed to retrieve the parameters of interest as discussed in the next section.

5.2 Methodology

5.2.1 Sensitivity Analysis

To determine which input parameters are critical towards error, a sensitivity analysis is done. The sensitivity analysis is carried out on $\Phi,\ \beta,\ \alpha_1,\ \gamma_1,\ \gamma_2,\ Nc,\ Nr,\ Bi,\ N_{br}$, with exact values defined as $[0.98,\ 0.5,\ 4.5,\ 0.02,\ 0.0001,\ 2,\ 0.5826,\ 0.0146,\ 0.0042]$, to study their relative influence on each other. The sensitivity index for a parameter, S is defined as the modulus of the percentage change in the dependent variable temperature, produced by an elementary change (1%) in the parameter when other parameters are held fixed. Symbolically, if $S = [S_\Phi,\ S_\beta,\ S_{\alpha_1},\ S_{\gamma_1},\ S_{\gamma_2},\ S_{Nc},\ S_{Nr},\ S_{Bi},\ S_{N_{br}}]$ denote the sensitivity coefficients, then these are evaluated using the following formulae,

$$S_\Phi = \frac{\partial\theta}{\partial\Phi},\ S_\beta = \frac{\partial\theta}{\partial\beta},\ S_{\alpha_1} = \frac{\partial\theta}{\partial\alpha_1},\ S_{\gamma_1} = \frac{\partial\theta}{\partial\gamma_1},\ S_{\gamma_2} = \frac{\partial\theta}{\partial\gamma_2},\ S_{Nc} = \frac{\partial\theta}{\partial Nc},\ S_{Nr} = \frac{\partial\theta}{\partial Nr},$$

$$S_{Bi} = \frac{\partial\theta}{\partial Bi},\ S_{N_{br}} = \frac{\partial\theta}{\partial N_{br}}.$$

5.2.2 Regularization

When data values are measured experimentally, a certain amount of error or noise is incorporated in the measurements, making the inverse problem, an ill-posed problem. To make an ill-posed problem as well-posed and to stabilize it, regularization needs to be done. Regularization was originally introduced by Tikhonov and Arsenin (1977a). Based on modification in the least-squares objective function,

$$J = ||\theta(f) - \tilde{\theta}||_2^2, \tag{5.12}$$

several regularization strategies, namely, Tikhonov regularization, lasso estimates and elastic net regularization are implemented, Aloraini (2017). The modification in the objective function is such that there is a minimal deviation of approximated solution $\theta(f)$ from the exact one $\tilde{\theta}$. The objective function to be minimized includes **Tikhonov regularization**, also termed as Ridge regression, defined as,

$$J = ||\theta(f) - \tilde{\theta}||_2^2 + \alpha||f||_2, \tag{5.13}$$

where $f = [\Phi,\ \beta,\ Nc,\ Nr,\ N_{br},\ Bi]$, represents the vector of unknown parameters and 'α' represents the regularization parameter. **Lasso (least absolute shrinkage and selection operator) estimator** used is given as follows:

$$J = ||\theta(f) - \tilde{\theta}||_2^2 + \alpha||f||_1. \tag{5.14}$$

The objective function of **elastic net regularization** is given as

$$J = ||\theta(f) - \tilde{\theta}||_2^2 + \alpha[(1-\lambda)||f||_2 + \lambda||f||_1], \tag{5.15}$$

with 'λ' as the mixing parameter of both Tikhonov and Lasso regularization. According to Özısık (1993), if a large number of parameters are to be estimated, oscillatory behaviour in the solution is obtained with α tending to 0, thus making the problem unstable. Moreover, with larger α values, the solution is damped, deviating largely from the exact solution. Thus, a proper selection of α, in the range $[10^{-2} - 10^{-4}]$ is required, Özısık (1993).

5.2.3 Optimization algorithms

Treating the obtained temperature data $\tilde{\theta}$ as input parameter, Φ, β, Nc, Nr, Bi, N_{br} are assumed unknowns which are to be retrieved with the inverse analysis. An initial guess for these unknown parameters is made. This guessed parameter value f is then used to obtain temperature profile $\theta(f)$, whose deviation from the exact temperature $\tilde{\theta}$ is minimized using equation, (5.12) - (5.15). For minimization, optimization algorithms, DE, PSO, WOA, WCA, GWOCS, BOA and ASO are used. The flowchart of DE and PSO was discussed in chapter 2, (2.2.2)). The parameters used for computation are presented in Table (5.2).The remaining optimization algorithms used for comparison in the present study are discussed ahead.

(a) *Whale Optimization Algorithm (WOA)*

Mirjalili and Lewis (2016) proposed whale optimization algorithm based on the social behaviour of humpback whales. A proper balance between exploration and exploitation help avoid local minima in this case. To locate global minima, operators corresponding to search for prey are applied first. This is done via updating the position of vector randomly, similar to that of whales. Thereafter, the operator associated with encircling the prey is applied and then the operator corresponding to bubble-net foraging behaviour of humpback whales is applied. The algorithm started by initializing the whale population Y_i $(i = 1, \ldots\ldots, n)$. Corresponding to each vector Y_i, objective function, equation (5.15) is calculated, which is labelled as fitness. Vector corresponding to minimum fitness is labelled best Y^*. For every iteration and for every search agent, a, A, C, l and p are updated utilizing the following expressions,

$$\vec{A} = 2\vec{a}.\vec{r} - \vec{a}, \quad \vec{C} = 2.\vec{r},$$

where r, p are random numbers in $[0, 1]$ and l in $[-1, 1]$ respectively, with $\vec{a}$ decreased from 2 to 0 linearly. Humpback whales follow their prey either in shrinking circular movements or along a spiral-shaped path randomly, with equal probabilities. Depending on the value of p, WOA chooses spiral or circular movement. Thus, for $p \geq 0.5$, the position of the current search vector is updated using,

$$\vec{Y}(t+1) = \vec{D'}.e^{bl}.cos(2\pi l) + \vec{Y}^*(t), \tag{5.16}$$

where $\vec{D'} = |\vec{Y}^*(t) - \vec{Y}(t)|$, with b as the constant defining the shape of the logarithmic spiral. If $p < 0.5$, then WOA decides whether exploration or exploitation is to be done, which in turn

is decided by $|\vec{A}|$. If $|\vec{A}| \geq 1$, exploration is done, by randomly selecting a search agent $\vec{Y}_{rand}$. The position is updated using,

$$\vec{Y}(t+1) = \vec{Y}_{rand} - \vec{A}.\vec{D}, \quad \text{where,} \quad \vec{D} = |\vec{C}.\vec{Y}_{rand} - \vec{Y}|. \tag{5.17}$$

If $|\vec{A}| < 1$, exploitation was done using,

$$\vec{Y}(t+1) = \vec{Y}^*(t) - \vec{A}.\vec{D}, \quad \text{where,} \quad \vec{D} = |\vec{C}.\vec{Y}^*(t) - \vec{Y}(t)|. \tag{5.18}$$

The operator $|\ |$ denote the absolute value and . denote element-wise multiplication. Once the position is updated for each particle, the new particle's fitness is calculated. In addition, it is ensured that the particle lies in the search space. Y^* is updated based on the best fitness and the process repeats until the maximum number of iterations is reached. The flow chart for WOA is given in the Fig.(5.1) below.

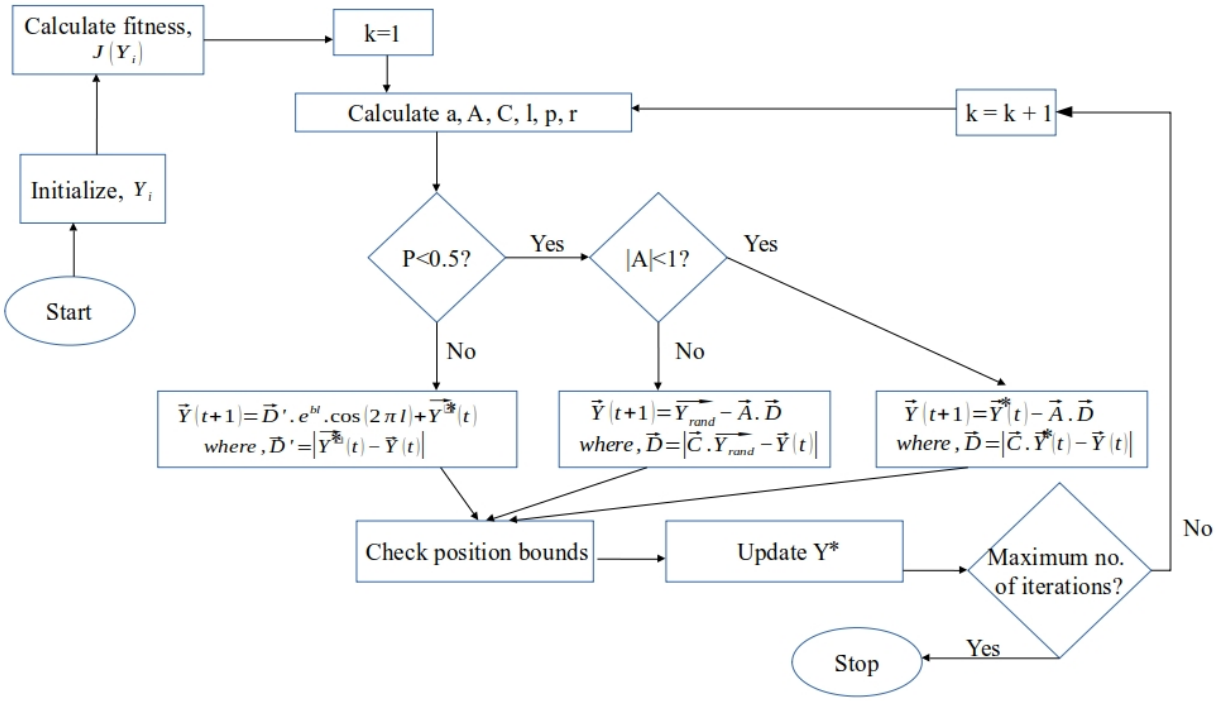

Fig. 5.1 Flow chart of the Whale Optimization Algorithm.

(b) *Water Cycle Algorithm (WCA)*

Eskandar *et al.* (2012), proposed nature-inspired optimization algorithm, based on the water cycle process. This algorithm works by assuming that the rivers are formed in the mountains by the melting of snow or glaciers. These streams merge into rivers, which ultimately join the sea. From the sea, evaporation takes place, resulting in cloud formation leading to rain or precipitation due to condensation. This cycle repeats itself after a definite number of steps.

WCA starts by specifying initial parameters, Number of rivers and sea (N_{sr}), d_{max}, Number of

raindrops (N_{pop}), Maximum number of iteration (max_iteration). An initial population consisting of streams, rivers and sea is created randomly by the following equations.

$$\text{Population of raindrops} = \begin{bmatrix} \text{Raindrop}_1 \\ \vdots \\ \text{Raindrop}_{N_{pop}} \end{bmatrix} = \begin{bmatrix} y_1^1 & y_2^1 & \cdots & y_{N_{var}^1} \\ \vdots & \vdots & \ddots & \vdots \\ y_1^{N_{pop}} & y_2^{N_{pop}} & \cdots & y_{N_{var}^{N_{pop}}} \end{bmatrix} \tag{5.19}$$

$$N_{sr} = \text{Number of rivers} + \underbrace{1}_{sea}, \tag{5.20}$$

$$N_{Raindrops} = N_{pop} - N_{sr}, \tag{5.21}$$

where N_{var} is the maximum dimension of the solution. Then the cost of each raindrop is calculated using equation (5.15). The intensity of the flow of rivers flowing to the specific sea is calculated using,

$$NS_n = \text{round}\left\{ \left| \frac{J_n}{\sum_{i=1}^{N_{sr}} J_i} \right| \times N_{Raindrops} \right\}, \quad n = 1, \ldots, N_{sr}. \tag{5.22}$$

The stream flow to the rivers and the river flow to the sea by the following,

$$Y_{Stream}^{i+1} = Y_{Stream}^{i} + \text{rand} \times c \times (Y_{River}^{i} - Y_{Stream}^{i}), \tag{5.23}$$

$$Y_{River}^{i+1} = Y_{River}^{i} + \text{rand} \times c \times (Y_{Sea}^{i} - Y_{River}^{i}), \tag{5.24}$$

where rand $\in [0, 1]$ is uniformly distributed random number and $c \in [1, 2]$. The stream with the minimum cost then replaces the associated river and the river with the minimum cost replaces the corresponding sea. If $|X_{Sea}^{i} - X_{River}^{i}| < d_{max}$, $i = 1, \ldots, N + sr - 1$, then evaporation and raining occurs. Here d_{max} is a number with small magnitude. The evaporation and raining process occur by the following relations,

$$X_{Stream}^{new} = \text{LB} + \text{rand} \times (\text{UB} - \text{LB}), \tag{5.25}$$

$$X_{Stream}^{new} = X_{Sea} + \sqrt{\mu} \times \text{randn}(1, N_{var}), \tag{5.26}$$

where LB, UB denote lower and upper bounds, $\sqrt{\mu}$ represent standard deviation and randn is the normally distributed random number. The value of d_{max} is reduced using the expression,

$$d_{max}^{i+1} = d_{max}^{i} - \frac{d_{max}^{i}}{\text{max\_iteration}}. \tag{5.27}$$

With the updated values, if the convergence criterion is met, the algorithm is stopped, otherwise, the iterative process continued. A flow chart for the same is given in Fig.(5.2).

(c) *Grey Wolf Optimization and Cuckoo Search (GWOCS)*

Grey wolf optimization works on the hunting hierarchy of the grey wolves on the basis of leadership. Given by Mirjalili *et al.* (2014), the algorithm starts by initializing the wolf population Y_i randomly and obtaining the corresponding fitness function $J(Y_i)$ using equation (5.15). Wolves hunt in groups with an average size of 11-20 wolves. The leader is called 'α' wolf followed by

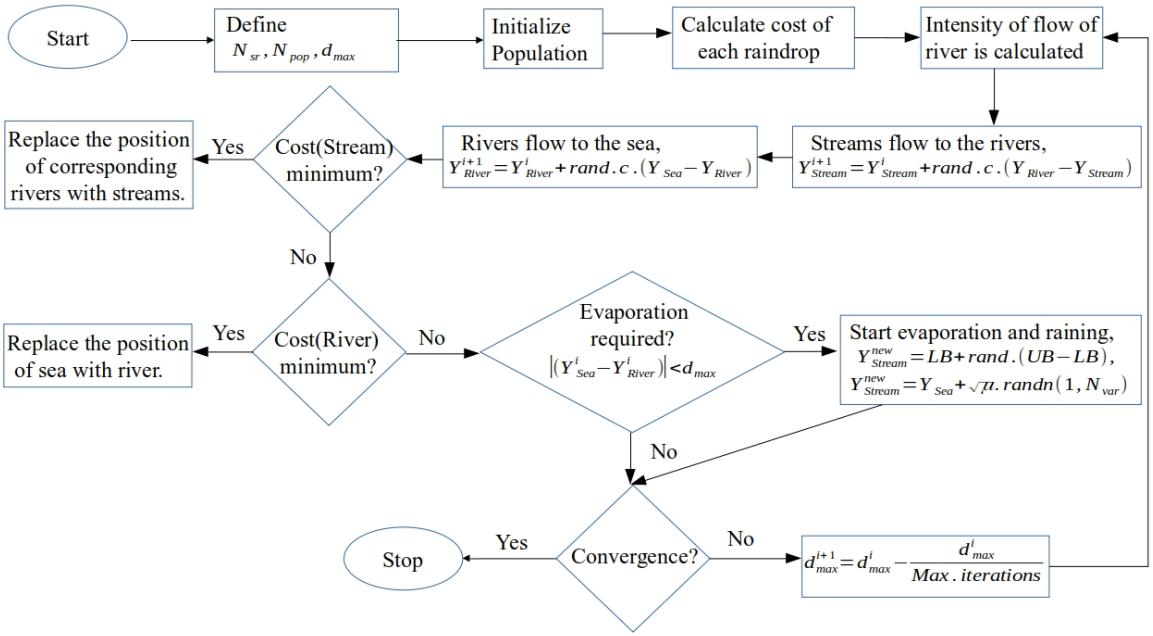

Fig. 5.2 Flow chart of the Water Cycle Algorithm.

'β' and 'γ' wolves. The leader is the one with the best fitness, i.e., the distance of the wolf and the prey should be minimum. The position of the search agent is then updated by taking the mean,

$$\begin{aligned} \vec{Y}(t+1) &= \frac{\vec{Y_1} + \vec{Y_2} + \vec{Y_3}}{3}, \\ \text{where, } \vec{Y_i} = \vec{Y_j} - \vec{A_i}.\vec{D_j}, \text{ with } \vec{D_j} &= |\vec{C_i}.\vec{Y_j} - \vec{Y}|, \\ i &= 1, 2, 3,\ j = \alpha,\ \beta,\ \gamma \end{aligned} \tag{5.28}$$

Note that the $\vec{A}$, $\vec{C}$ are obtained as $\vec{A} = 2\vec{a}.\vec{r_1} - \vec{a}$ and $\vec{C} = 2.\vec{r_2}$ respectively, where r_1, r_2 are random vectors and a linearly decreases from 2 to 0. The problem encountered while using GWO is in the selection of step size, which allows the distance between the prey and the wolf to decrease randomly, leading towards local minima. Thus, the control is shifted to Cuckoo Search (CS), where the step size is modified on the basis of the best position. Cuckoo search depends not only on time but also on habitat search. CS is based on brood parasitism of some cuckoo bird species which lay their eggs in other species nest, leading the other species to get rid of alien eggs or to abandon the nest to build a new one. CS is developed by Yang and Deb (2009). A hybrid GWOCS algorithm utilizes the capability of both GWO and CS. The step size is updated using the following relation

$$\text{step}^{\text{new}} = w.\text{step}^{\text{old}}(s - \text{best}),$$

where $w = 0.001$ is the weight, step^{new}, step^{old} is the current and previous step size, with s as the position of α, β and γ wolf respectively. Once, the positions are updated in the above way,

the control is again sent back to GWO and the process continues until the convergence criterion is met. The flow chart for GWOCS is given in the Fig.(5.3) below.

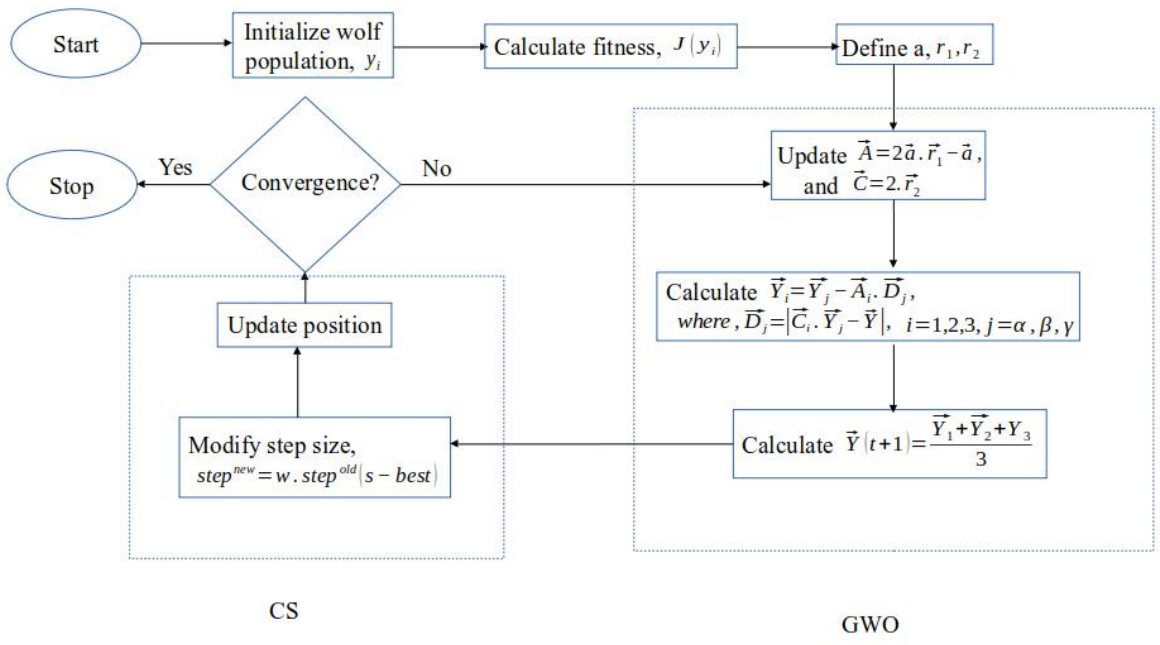

Fig. 5.3 Flow chart of the hybrid Grey Wolf Optimization and Cuckoo Search algorithm.

(d) ***Butterfly Optimization Algorithm (BOA)***

Arora and Singh (2019), proposed a global optimization algorithm based on the natural behaviour of butterflies. BOA copies the food search and mating behaviour of butterflies, based on their sense of smell. Butterflies have known to distinguish between various fragrances accurately. Their search for food majorly nectar is based on identifying smell even from long distances. For the purpose of optimization, it is assumed that all butterflies emit fragrance, by virtue of which, other butterflies attract them. Possible attraction occurs in the predefined landscape of solutions. A butterfly with the best fragrance will attract other butterflies towards it randomly.

The algorithm starts by generating an initial population of butterflies, y_i. The dimension of the solution set and their fitness is calculated by equation (5.15). The stimulus intensity, I is determined by the fitness value, $J(y_i)$. It represents the intensity by which other butterflies are drawn to the best fragrance emitting butterfly. Thereafter, sensor modality c, power exponent, a and switch probability, p are defined. The parameters a, $c \in [0, 1]$, where parameter a is the power exponent, which controls the variation of absorption of smell. When other butterflies sense, emitted fragrance completely, a is set to 1, and when a is set to 0, other butterflies cannot sense the fragrance at all. The parameter c, determined the speed of convergence of BOA. The parameter p represented the switch probability, responsible for switching the algorithm's global

and local search, which is affected by factors like wind, rain, etc. For each solution vector, represented by butterfly, the fragrance is calculated using the following relation.

$$f = cI^a \tag{5.29}$$

The best fragrance among all butterflies is marked. A random movement of butterflies is ensured by generating a random number r in the interval $[0, 1]$. If $r < p$, then all butterflies move towards the best butterfly, resulting in local search, otherwise, these move randomly. The position of each butterfly is updated for global search and local search by using the following equations respectively.

$$y_i^{t+1} = y_i^t + (r^2 g^* - y_i^t) f_i, \tag{5.30}$$

$$y_i^{t+1} = y_i^t + (r^2 y_j^t - y_k^t) f_i, \tag{5.31}$$

where y_j^t, y_k^t are j$^{\text{th}}$ and k$^{\text{th}}$ butterflies respectively, for t$^{\text{th}}$ iteration, g^* is the current best butterfly found on the basis of fragrance. The value of a is updated, and the iterations are repeated until convergence criterion is met. The flow chart for BOA is given in the Fig.(5.4) below.

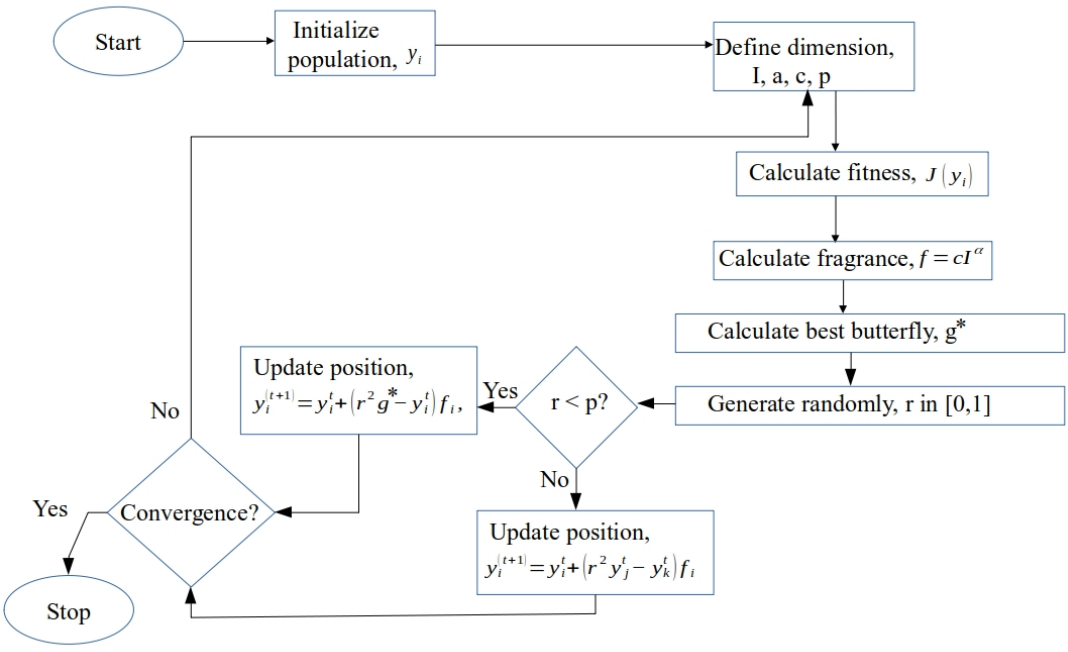

Fig. 5.4 Flow chart of the Butterfly Optimization Algorithm.

(e) *Atom Search Optimization (ASO)*

Inspired by the molecular dynamics, a physics-based optimization algorithm is developed by Zhao *et al.* (2019). The population of the solution consists of atoms, whose position is measured by its mass. Each atom within the population interacts (attracts or repels) its nearest neighbours. The information between different atoms including the best one flows from constraint force.

Algorithm balances local and global search by identifying the fitness of each atom. The atoms with a larger mass, show better fitness, whereas those with lighter mass have the least fitness. Atoms with a larger mass, lead to smaller acceleration, thereby increasing the local search, whereas the atoms with smaller mass, lead to larger acceleration, thereby increasing the global search. The algorithm firstly initializes a random set of solutions (say Y atoms). Thereafter, the fitness value for each atom is calculated using an objective function, equation (5.15). Initially, the best fitness value is assumed to be infinite. This is done because the associated problem is of minimization. The fitness of each atom is then compared with the best fitness value. Best atom is updated if a better fitness is achieved, otherwise, the mass of each atom is calculated using the following relations,

$$m_i(t) = \frac{M_i(t)}{\sum_{j=1}^{N} M_j(t)}, \quad \text{where,} \quad M_i(t) = e^{\frac{J_{best}(t) - J_i(t)}{J_{worst}(t) - J_{best}(t)}}, \tag{5.32}$$

where N represents the total number of atoms, for the i^{th} atom and t^{th} iteration. J_{best} and J_{worst} represent the best and worst fitness values, respectively which are calculated as $J_{best}(t) = \min_{i\in\{1,\ldots,N\}} J_i(t)$ and $J_{worst}(t) = \max_{i\in\{1,\ldots,N\}} J_i(t)$. For each atom, its K neighbours are determined using the following expression, $K(t) = N - (N-2)\sqrt{\frac{t}{T}}$, where T is the total number of iterations. The acceleration of the atoms is calculated next by evaluating the interaction force F_i and the constraint force G_i, using the following relations,

$$F_i^d(t) = \sum_{j\in Kbest} \text{rand}_j F_{ij}^d(t), \quad \text{where, } F_{ij}(t) = \frac{24\epsilon(t)}{\sigma(t)}\left[2\left(\frac{\sigma(t)}{r_{ij}(t)}\right)^{13} - \left(\frac{\sigma(t)}{r_{ij}(t)}\right)^{7}\right]\frac{r_{ij}(t)}{r_{ij}^d(t)}. \tag{5.33}$$

In the above equation, ϵ is the depth of the potential well, representing the strength of the interaction, σ is the length scale of the collision diameter, $r_{ij} = y_j - y_i$, is the position of the i^{th} atom, d is the d^{th} dimension, $Kbest$ is the subset of an atom population consisting of first K atoms with the best fitness function value.

The interaction force, equation (5.33) comes into play due to L-J potential, which is the vector sum of the attraction and the repulsion exerted from other atoms. The constraint force $G_i = \lambda(t)(y_{best}^d(t) - y_i^d(t))$, where $\lambda(t) = \beta e^{\frac{-20t}{T}}$ is the Lagrange multiplier with weight β, is caused by the bond length potential, which is the weighted difference between each atom and the best atom.

Thereafter, acceleration, velocity and position is updated by the following expressions,

$$a_i^d(t) = \frac{F_i^d}{m_i^d(t)} + \frac{G_i^d}{m_i^d(t)}, \tag{5.34}$$

$$v_i^d(t+1) = \text{rand}_i^d v_i^d(t) + a_i^d(t), \tag{5.35}$$

$$y_i^d(t+1) = y_i^d(t) + v_i^d(t+1). \tag{5.36}$$

This iterative procedure continues until the maximum number of iterations are reached or an

error bound is satisfied. The best solution is stored in Y_{best}. A flow chart for the same is given in Fig.(5.5).

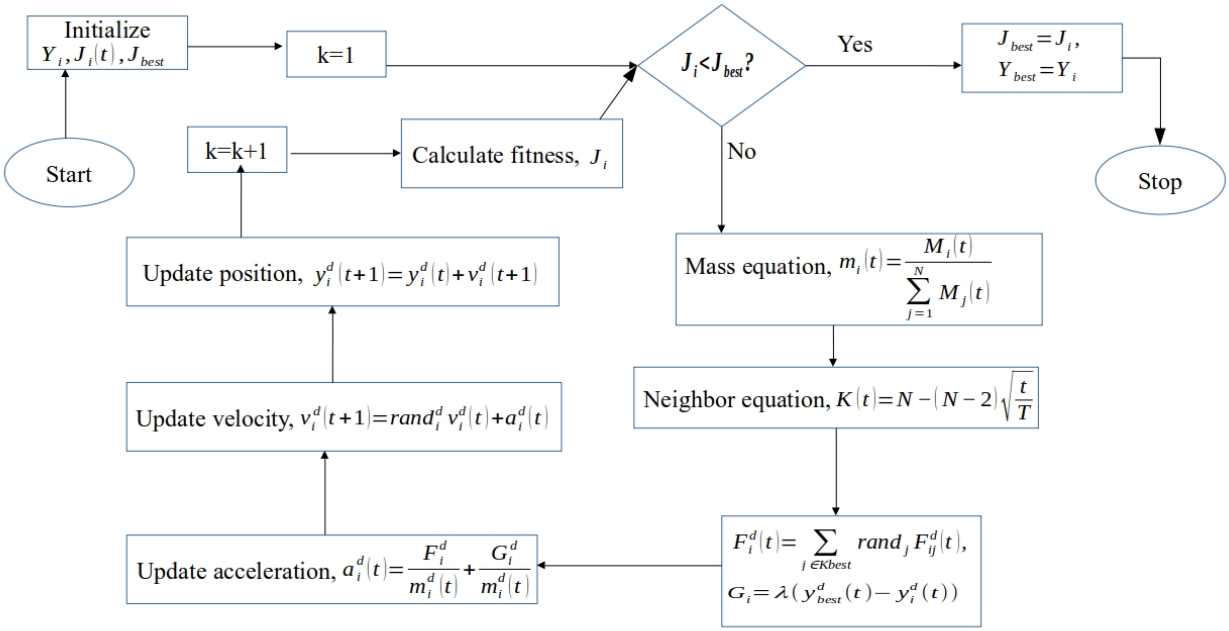

Fig. 5.5 Flow chart of the Atom Search Optimization.

5.2.4 TOPSIS

To compare these optimization algorithms with multiple attributes, the Technique for Order Preference by Similarity to Ideal Solution (TOPSIS) is used. The attributes Beiranvand *et al.* (2017) include CPU time in seconds, minimum objective function value, error in retrieved temperature, error in retrieved unknown parameters, namely, Φ, β, NC, Nr, Bi, N_{br}. The method is summarized as follows.

1. Construct a normalized decision matrix,

$$r_{ij} = \frac{m_{ij}}{\sqrt{\sum_{j=1}^{9} m_{ij}^2}}, \quad i = 1, \ldots, 7,\ j = 1, \ldots, 9.$$

   Here m_{ij} represent the entries of the decision matrix.

2. Construct the weighted, normalized decision matrix, $v_{ij} = w_{ij} r_{ij}$, where w_j is the weight for the jth criterion.

3. Determine the ideal best and ideal worst solution,

$$V_j^+ = \min_j\{v_{1j}, \ldots, v_{7j}\}, \quad V_j^- = \max_j\{v_{1j}, \ldots, v_{7j}\},\ j = 1, \ldots, 9.$$

4. Calculate the separation measures for each alternative,
   (a) Separation from ideal best is $S_i^+ = [\sum_{j=1}^{9} v_{ij} - V_j^+]^{\frac{1}{2}}$,
   (b) Separation from ideal worst is $S_i^- = [\sum_{j=1}^{9} v_{ij} - V_j^-]^{\frac{1}{2}}$.

5. Calculate the relative closeness to ideal solution P_i, $P_i = \dfrac{S_i^-}{S_i^+ + S_i^-}$. Rank the preference order, with P_i close to 1.

5.3 Results and Discussion

As stated previously, in this work, to estimate the unknown extended surface parameters, an inverse analysis has been carried out. An experimental test rig is set up to observe the temperature profile of the fin, using thermocouples. For the inverse analysis, several optimization algorithms are used and the best among these is to be determined.

5.3.1 Comparison

To check the correctness of the forward method (Matlab's pdepe solver), the temperature profile of the fin has been compared, after modifications, with that of Differential Transform Method (DTM) Ganji *et al.* (2011), as shown in Fig.(5.6). The parameters used are $Nc = 1$, $Nr = 0.675$, $Bi = 0$, $N_{br} = 0$, $n = 0$, $\alpha_1 = 0$, $\gamma_1 = \gamma_2 = 0$, $\beta = 0$, $\eta = 0.03$, $\theta_a = 0$.

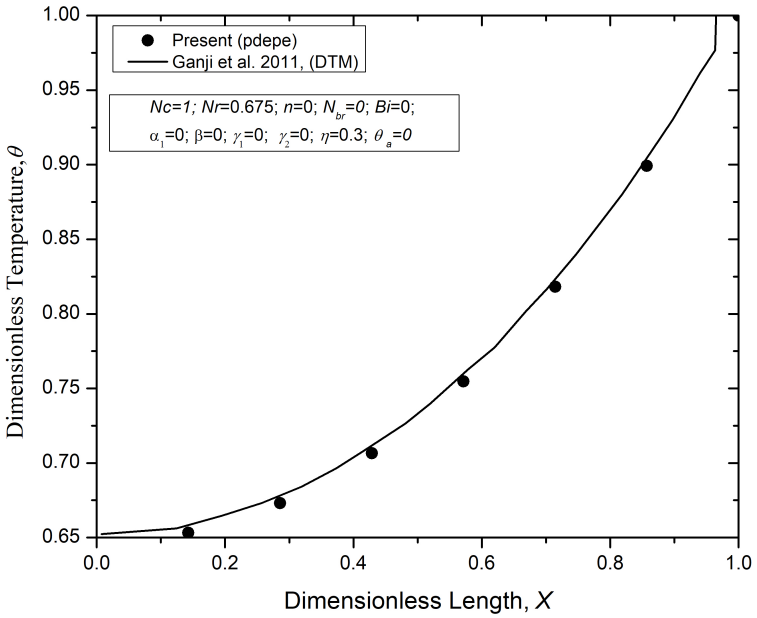

Fig. 5.6 Comparison of pdepe with DTM Ganji *et al.* (2011), where dimensionless temperature θ is plotted with respect to dimensionless length, X.

In order to scrutinize the comparison, pdepe has further been compared with Finite Difference Method (FDM) Aziz and Torabi (2012), as shown in Fig.(5.7). The parameters used are $Nc =$

1, $Nr = 1$, $Bi = 0$, $N_{br} = 0$, $n = 2$, $\alpha_1 = 0$, $\gamma_1 = -0.2$, $\gamma_2 = 0$, $\beta = 0$, $\theta_a = 0.4$. The temperatures are obtained by varying parameter $\eta = -0.6,\ -0.2,\ 0,\ 0.2,\ 0.6$, corresponding to thermal conductivity. The obtained profile is in good agreement with that of Aziz and Torabi, (2012).

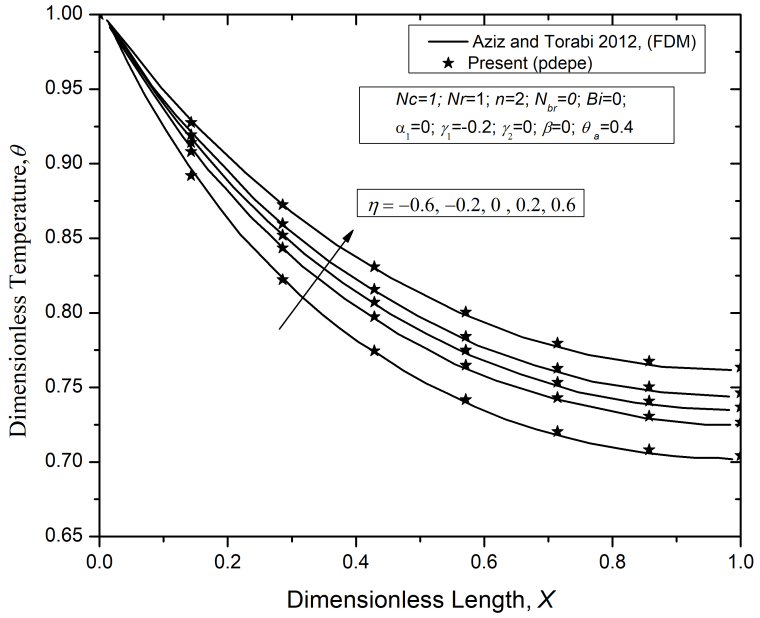

Fig. 5.7 Comparison of pdepe with FDM Aziz and Torabi (2012), for variation in thermal conductivity coefficient η, where dimensionless temperature θ was plotted with respect to dimensionless length, X.

5.3.2 Sensitivity Analysis

Once the forward method has been validated, in order to determine the cause of ill-posedness, a sensitivity analysis is done. With small perturbation (1%) in the input (unknown parameters), a large change in the output (temperature) is seen. Fig.(5.8), illustrates the sensitivity coefficients for different non-dimensional parameters. It is clearly seen that when 1% perturbation to $\Phi = 0.98$, $\beta = 0.5$, $\alpha_1 = 4.5$, $\gamma_1 = 0.02$, $\gamma_2 = 0.0001$, $Nc = 2$, $Nr = 0.3297$, $Bi = 0.0146$, $N_{br} = 2.455 \times 10^{-6}$, a large change in average value of temperature is seen with respect to Φ followed by Nr, Nc, β, α_1, Bi, γ_1, γ_2, N_{br}. The average sensitivity coefficients are $S_\Phi = 3.5 \times 10^{-2}$, $S_{Nr} = 1.68 \times 10^{-2}$, $S_{Nc} = 1.46 \times 10^{-2}$, $S_\beta = 9.81 \times 10^{-3}$, $S_{\alpha_1} = 2.06 \times 10^{-3}$, $S_{Bi} = 1.65 \times 10^{-3}$, $S_{\gamma_1} = 3.22 \times 10^{-4}$, $S_{\gamma_2} = 1.97 \times 10^{-5}$, $S_{N_{br}} = 0$. The unknown parameters to be retrieved are chosen as Φ, β, Nc, Nr, Bi, N_{br}, based on their requirement for estimation along with the sensitivity coefficients. The input heat flux Φ plays an important role in initiating the heat transfer process. The mode of heat transfer on the extended surface is effected with the radiation-conduction parameter Nr and the convection-conduction

parameter Nc. The parameter β represents the thermal conductivity of the material of the fin surface. In addition, the parameters Bi and N_{br} effect the exchange of heat at the fin tip. Therefore, these parameters are considered critical, as these affect the temperature largely and are thus needed to be estimated via inverse analysis as mentioned ahead.

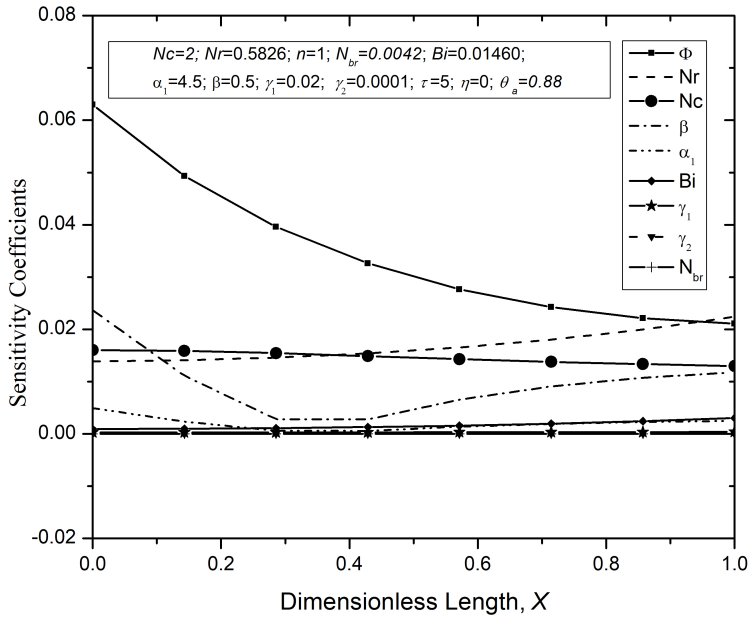

Fig. 5.8 Sensitivity coefficients S, with 1% perturbation in $\Phi = 0.98$, $\beta = 0.5$, $\alpha_1 = 4.5$, $\gamma_1 = 0.02$, $\gamma_2 = 0.0001$, $Nc = 2$, $Nr = 0.3297$, $Bi = 0.0146$, $N_{br} = 2.455 \times 10^{-6}$.

Based on the sensitivity analysis, the critical parameters to be determined are selected. A forward analysis is done using the parameters of the fin, which are obtained using experimental setup as listed in Table (5.1). Thereafter, an inverse analysis is carried out, which has been divided into three subsections ahead. In the first subsection 5.3.3, to overcome ill-posedness, different regularization techniques are implemented. A regularization technique is then selected, in addition to selection of a suitable regularization parameter, on the basis of minimum error. Once the regularization technique has been decided, selection of best optimization technique is done in subsections 5.3.4 and 5.3.5. Thus, to choose the best inversion technique, for retrieving the chosen parameters of extended surface, a comparison based on TOPSIS, utilizing simulated and experimentally obtained forward data has been done next.

5.3.3 Comparison of regularization techniques

In the current analysis the comparison of regularization techniques, which makes the associated problem most well posed, is done. Firstly, the regularization parameter 'α' is selected, taking Tikhonov regularization as the said technique (ref equation (5.13)), as seen from Fig.(5.9). Different runs using Particle swarm optimization algorithm are taken by varying α in the range

$\{10^{-11} - 10^{8}\}$. The results in Fig.(5.9) suggest that $\alpha = 10^{-4}$ provide significant reduction in total relative error, $T_e = e_\Phi + e_\beta + e_{Nc} + e_{Nr} + e_{Bi} + e_{N_{br}}$ of the retrieved unknowns 'f', followed by $\alpha = 10^{-8}$ and $\alpha = 10^{-10}$. Here e_Φ, e_β, e_{Nc}, e_{Nr}, e_{Bi}, $e_{N_{br}}$ represents the relative error in Φ, β, Nc, Nr, Bi, N_{br} respectively. Parameters used during this estimation are $L = 0.35\,\text{m}$, $A = 7.854 \times 10^{-5}\,\text{m}^2$, $P = 0.0314\,\text{m}$, $\eta = 0$, $\tau = 5$, $T_b = 298.15\,\text{K}$, $T_a = 295.15\,\text{K}$, $n = 1$, $\varepsilon_0 = 0.95$, $\alpha_1 = 4.5$, $\alpha_2 = 0$, $\gamma_1 = 0.02$, $\gamma_2 = 0.0001$. A similar analysis is done using Lasso and elastic net objective functions.

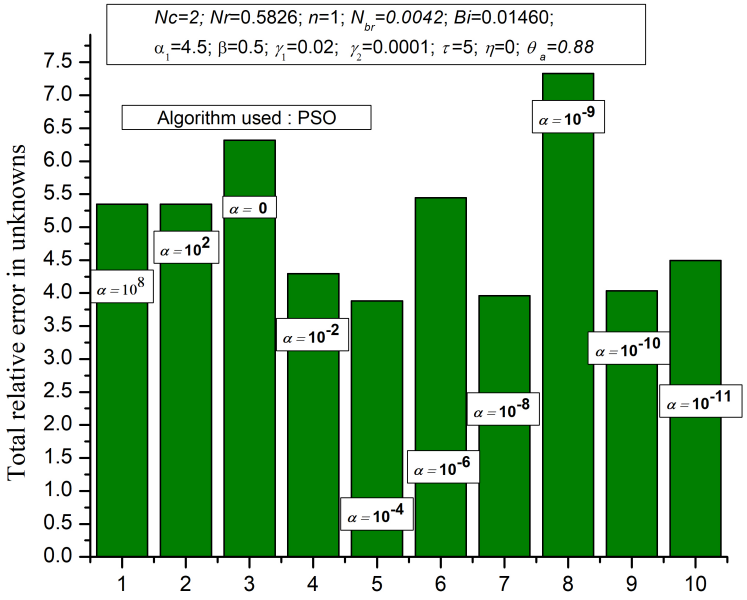

Fig. 5.9 Selection of regularization parameter α, based on minimum total relative error using PSO.

Furthermore, a comparison between the Ridge regression (2-norm), Lasso estimator (1-norm) and the elastic net regularization (a combination of 1-norm and 2-norm) is done. The above procedures regularize the problem by modifying the associated objective function. Regularization parameter $\alpha = 10^{-4}$ is used. Absolute error in retrieved parameter is plotted for each parameter (Φ, β, Nc, Nr, Bi, N_{br}). Moreover, the mixing parameter 'λ' is also varied to study its effect on the error. From Fig.(5.10), it is concluded that elastic net regularization with $\lambda = 0.9$, suggesting a combination of 90% Lasso estimator and 10% Ridge regression, give least absolute error. On the basis of CPU time, minimum time (33s) is taken when Ridge regression is utilized, followed by elastic net (90% lasso and 10% Ridge) (34s) and elastic net (50% lasso and 50% Ridge) (35s). Considering both the CPU time and absolute error in retrieved parameters, it is thus suggested to choose elastic net (90% lasso and 10% Ridge), with $\alpha = 10^{-4}$ for further computation.

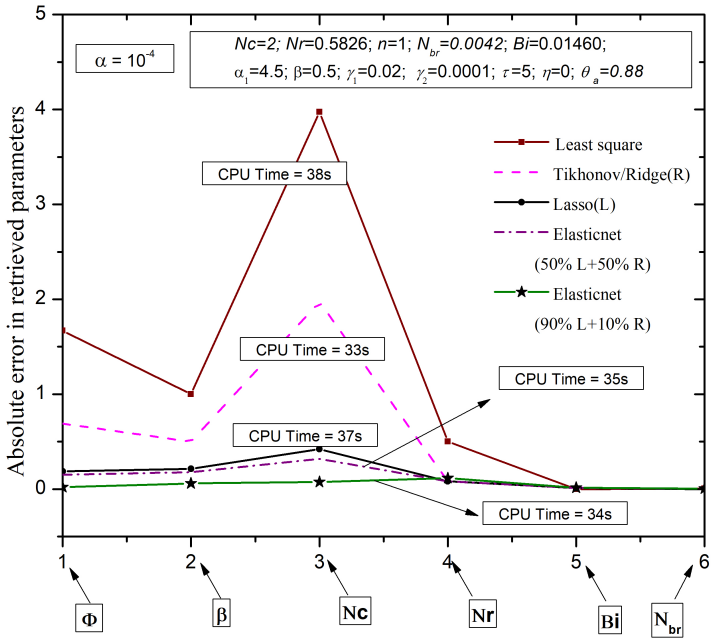

Fig. 5.10 Selection of objective function, (with $\alpha = 10^{-4}$, using PSO algorithm), which is best suited for regularization.

5.3.4 Comparison of optimization algorithms, with simulated forward data

Usually for the retrieval of the unknown parameters, temperature profiles at the surface is assumed to be known. However, in situations, with extreme conditions (environmental, cost, etc.), where it becomes impossible to conduct experiments the temperature profile is obtained through forward analysis. Using the parameters listed in Table (5.1), forward analysis to obtain a simulated temperature profile is done. Using the then obtained temperatures, the unknown parameters are obtained. The obtained parameters differ in every run of the algorithm, due to the stochastic nature of these algorithms. Therefore, to limit the biasedness offered by these algorithms, we perform the analysis three times and utilize their average value. To validate the correctness of this average retrieved value, the retrieved temperature profile is compared with that of exact (forward), as shown in Fig.(5.11). The retrieval matches efficiently with that of exact surface temperature for all algorithms except for ASO, showing its inefficiency for inverse heat transfer problems.

With the selected objective function as elastic net (90% lasso and 10% Ridge), with $\alpha = 10^{-4}$, the next task is to choose among the pool of different optimization algorithms. For the purpose, optimization algorithms are picked from different categories, namely, evolution based (DE), swarm-based (PSO, WOA), nature-based (WCA, BOA), physics-based (ASO) and a hybrid (GWOCS). The parameters utilized in every algorithm is seen in Table (5.2). The conver-

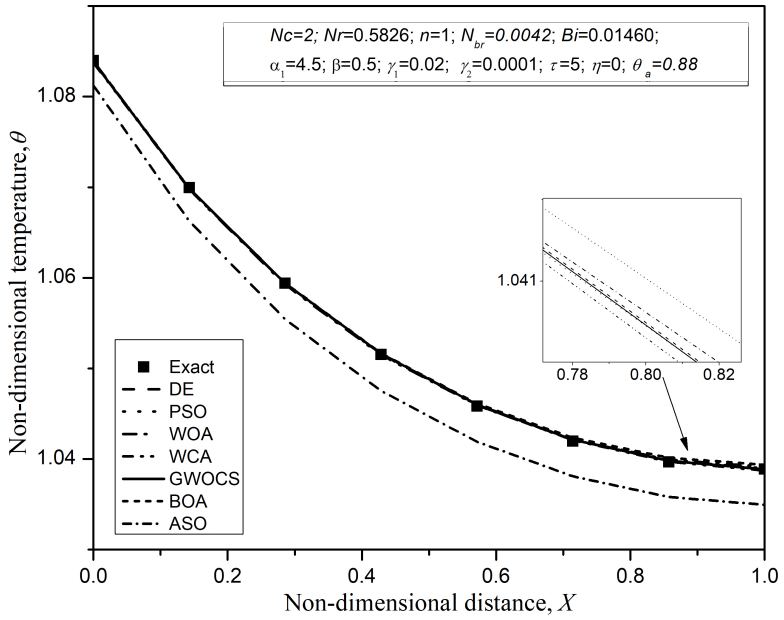

Fig. 5.11 Retrieved temperature profile θ with different optimization algorithms, plotted with respect to dimensionless length, X.

gence trends for each algorithm is displayed in Fig.(5.12). In this case, BOA converges rapidly followed by GWOCS, WCA and WOA. With a maximum of 20 iterations, every algorithm acquires a stable minimum objective function value and thus converges. Moreover, on the basis of time WCA is the best. The reason for this is because least CPU time 25s, is required by WCA for the complete computation.

Next, the retrieved parameters Φ, β, Nc, Nr, Bi, N_{br} are plotted with the number of iterations, along with their exact values used in forward analysis. A glimpse is shown in Fig.(5.13). The solid black line shows the exact parameter value ($\Phi = 0.98$, $\beta = 0.5$, $Nc = 2$, $Nr = 0.5826$, $Bi = 0.0146$, $N_{br} = 0.0042$). The best retrieval is obtained by PSO for Φ, Nc followed by WCA for Nr, N_{br}, WOA for β and BOA for Bi, respectively. The corresponding relative error in retrieved unknowns is shown in Fig.(5.14), with the number of iterations. The least relative error is seen to be given by WCA in most of the cases (Φ, Nr, Bi, N_{br}).

To get a complete picture of the comparison as a whole, Table (5.3) can be referred. Decision criteria is chosen based on Beiranvand *et al.* (2017). Using the above-discussed TOPSIS criterion for decision making, when multiple decision parameters are involved, BOA turns out to be best among all optimization algorithms, with performance parameter 0.77. WOA and WCA follows BOA in performance with performance parameter 0.75 and 0.74 respectively. The detailed illustration of every algorithm with multiple decision factors is seen in Table (5.3).

Table 5.2 Parameters used in each optimization algorithm.

Algorithm	Parameter	Value
DE	Population Size	30
	Mutation rate, F	0.75
	Crossover rate, CR	0.9
	Number of generations	50
PSO	No. of variables	6
	Number of Particles	4
	Maximum number of iterations	500
	Maximum inertia weight	0.9
	Minimum inertia weigtht, $w_{max},\ w_{min}$	0.2
	Confidence cognitive and social vectors, $c_{w1},\ c_{w2}$	2
WOA	No. of search agents	30
	Maximum number of iterations	100
WCA	Maximum number of iterations	50
	Evaporation condition constant, d_{max}	1×10^{-6}
	Number of rivers and sea, N_{sr}	4
	Population Size, N_{pop}	30
	Number of decision variables, N_{var}	6
GWOCS	Number of search agents	30
	Maximum number of iterations	500
BOA	Number of search agents	30
	Maximum number of iterations	50
	Probability switch, p	0.8
	power exponent, a	0.1
	sensory modality, c	0.01
ASO	Number of Atoms	5
	Maximum number of iterations	10
	Depth weight, α	50
	Multiplier weight, β	0.2

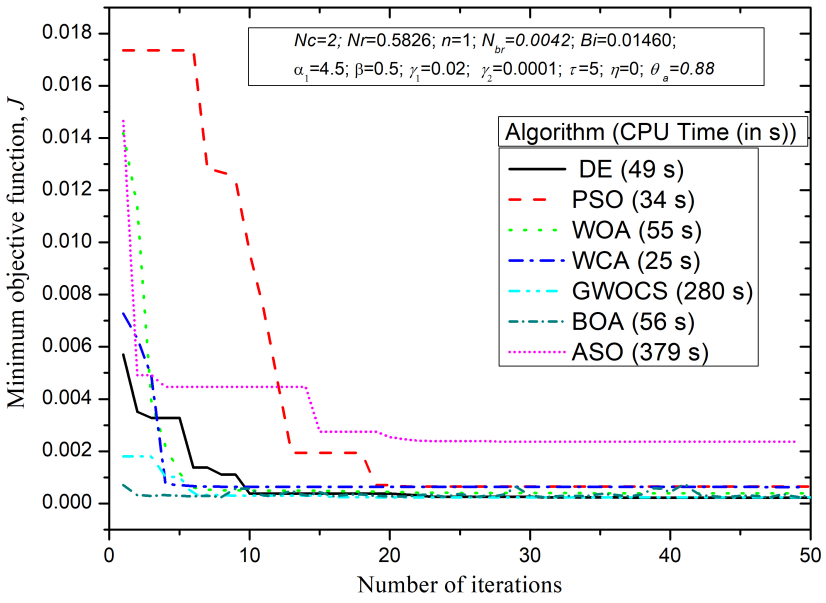

Fig. 5.12 Convergence plots for optimization algorithms, plotted with the number of iterations, with the corresponding CPU time required for computation.

5.3.5 Comparison of optimization algorithms, with experimental forward data

To obtain the temperature profile of the surface of the fin, an experiment is set up (Input voltage: 70V, Input current: 0.022A). Using the then obtained temperature, Φ, β, Nc, Nr, Bi, N_{br}, are retrieved such that the objective function, equation (5.15) is minimized. Different optimization algorithms are summoned to carry out inverse analysis where the error between the experimental temperature and the computed temperature (with the guessed value of unknowns) is minimized. Parameters used in the inverse computations are the same as given in Table (5.1). The variation in the objective function for different algorithms is seen in Fig.(5.15). The trends give a clear indication that WCA converges in the first iteration, whereas PSO converges rapidly in the first 5-6 iterations, followed by WOA. Other aspects for comparison of different algorithms can be seen in Table (5.4) using TOPSIS. Factors for comparison involve computational time, objective function's value, error in retrieved parameters and error in retrieved temperature. It must be noted that the minimum value of all decision parameters is required here for the reasons explained ahead. Individually, an algorithm which takes the least computational time turns out to be the best. Also, the one with the minimum objective function value should be chosen. Moreover, less error either in temperature or in retrieved parameters is desired for the overall procedure to be effective. Thus, to judge an algorithm based on all such criteria, TOPSIS analysis is carried out. It has been concluded that WOA (with performance parameter 0.78)

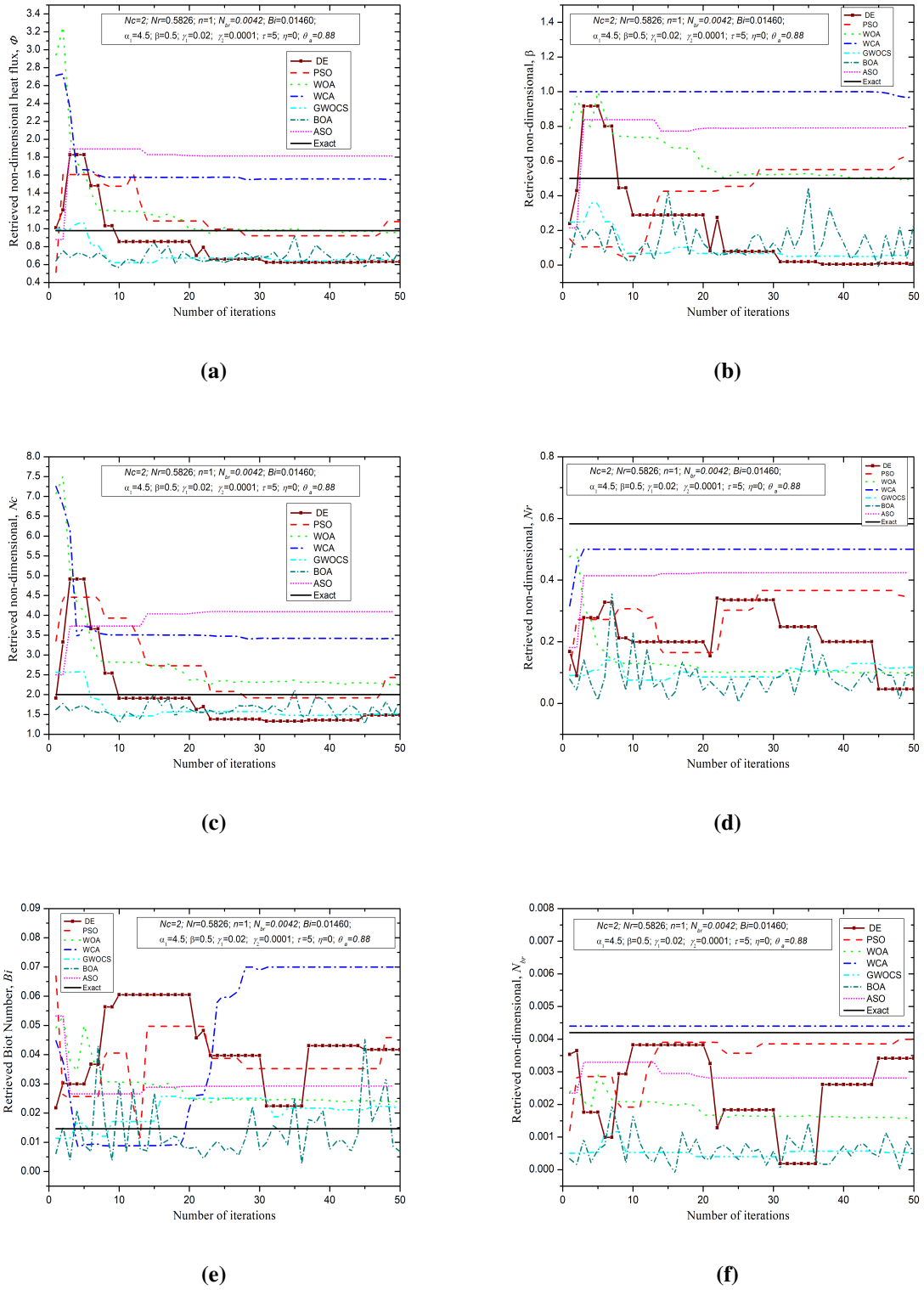

Fig. 5.13 Comparison of retrieved parameters, (a) Φ, (b) β, (c) Nc, (d) Nr, (e) Bi and (f) N_{br} of different algorithms, with their exact values $\Phi = 0.98,\ \beta = 0.5,\ Nc = 2,\ Nr = 0.5826,\ Bi = 0.0146,\ N_{br} = 0.0042.$

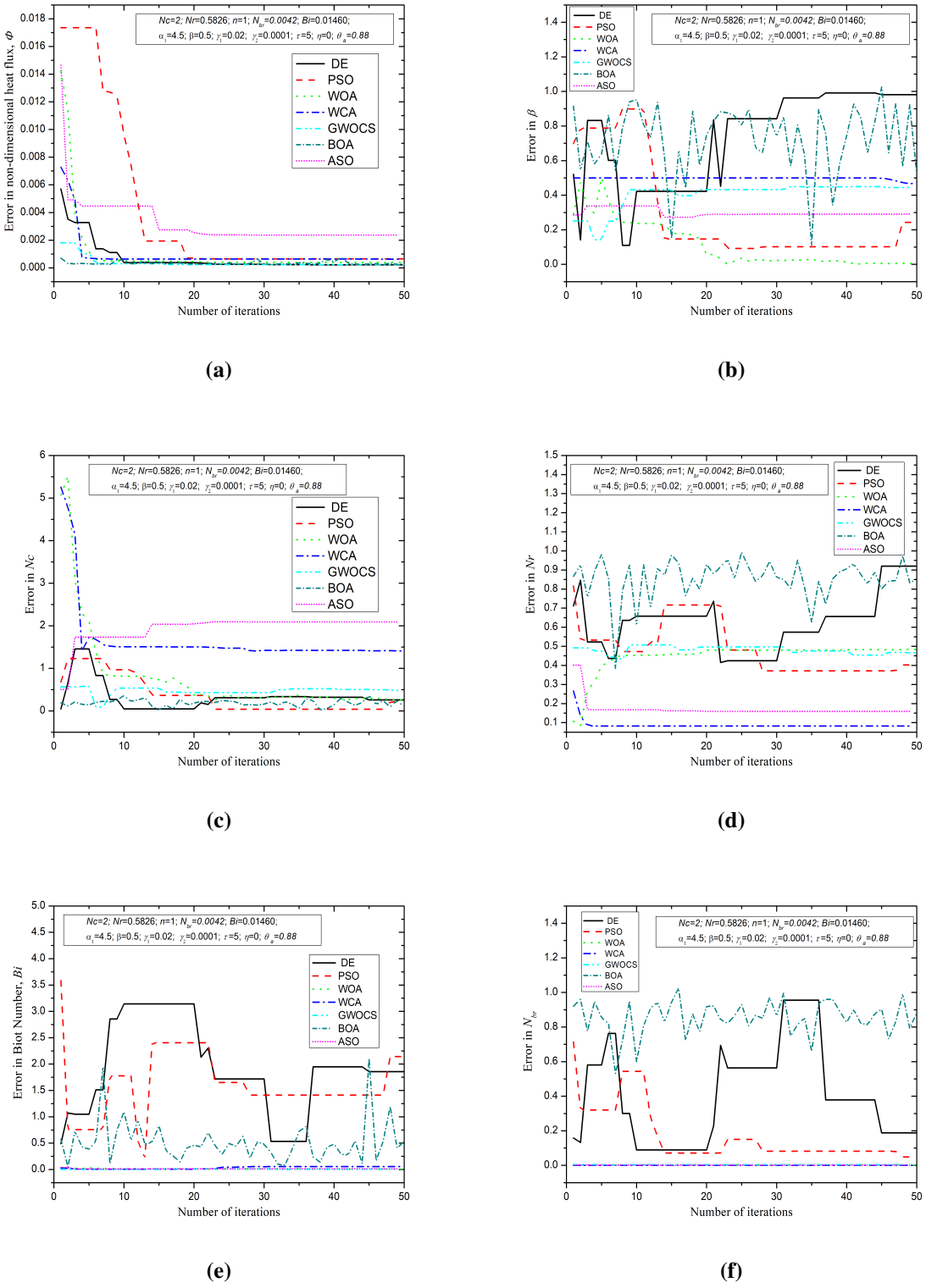

Fig. 5.14 Relative error in (a) Φ, (b) β, (c) Nc, (d) Nr, (e) Bi and (f) N_{br}, with the number of iterations.

Table 5.3 Decision matrix used in TOPSIS, showing multiple attributes corresponding to each optimization algorithm.

Algorithm	CPU Time (in s)	Min. J	Φ	β	Nc	Nr	Bi	N_{br}	Max. error in θ	P_i	Rank
			Exact Parameter values								
			0.98	0.5	2	0.5826	0.0146	0.0042	-		
			Relative error in unknowns								
			Retrieved parameters								
DE	49.29	2.2×10^{-4}	0.36	0.98	0.29	0.80	1.91	0.61	3.4×10^{-4}	0.72	4
			0.6222	0.0094	1.4173	0.1139	0.0426	0.0016	-		
PSO	33.99	4.4×10^{-4}	0.42	0.82	0.59	0.84	1.93	0.54	2.3×10^{-4}	0.71	5
			1.1454	0.5756	2.7106	0.094	0.0387	0.0021	-		
WOA	54.94	2.4×10^{-4}	0.31	0.85	0.19	0.95	0.23	0.91	2.5×10^{-4}	0.75	2
			0.6758	0.077	1.6235	0.0308	0.0113	0.0004	-		
WCA	24.79	2.4×10^{-4}	0.32	0.84	0.24	0.83	2.51	0.09	2.1×10^{-4}	0.74	3
			0.6651	0.0794	1.5277	0.101	0.0513	0.0041	-		
GWOCS	280.24	2.2×10^{-4}	0.36	0.97	0.29	0.79	2.01	0.84	1.7×10^{-4}	0.62	6
			0.626	0.0165	1.4206	0.1232	0.044	0.0007	-		
BOA	**55.82**	**2.7** $\times 10^{-4}$	**0.28**	**0.71**	**0.20**	**0.69**	**0.34**	**0.87**	**4.6** $\times 10^{-4}$	**0.77**	**1**
			0.7077	**0.1466**	**1.5979**	**0.1759**	**0.0096**	**0.0006**	-		
ASO	379.42	1.58×10^{-3}	0.34	0.32	0.86	0.89	2.26	0.60	6.7×10^{-3}	0.39	7
			1.0796	0.4659	3.2627	0.0621	0.0477	0.0017	-		

works best when experimental temperature data is utilized in the inverse analysis, followed by BOA (performance parameter 0.60) and WCA (performance parameter 0.50) respectively.

For the best inversion technique for parameter estimation in the extended surface, it is suggested to select elastic net (90% lasso and 10% Ridge) objective function for minimization, with $\alpha = 10^{-4}$. Moreover, for the optimization part, the top three algorithms are BOA ($P_i = 0.77$), WOA ($P_i = 0.75$) and WCA ($P_i = 0.74$), when simulated forward data is utilized. Whereas WOA ($P_i = 0.78$), BOA ($P_i = 0.60$) and WCA ($P_i = 0.50$) respectively are observed as good algorithms when experimental forward data is used, as resulted by TOPSIS.

5.4 Observations

The major observations from this chapter are summarized below.

1. Parameters Φ, β, Nc, Nr, Bi, N_{br} are observed to be critical using sensitivity analysis.

2. For regularization, elastic net (90% lasso and 10% Ridge) objective function is best, with

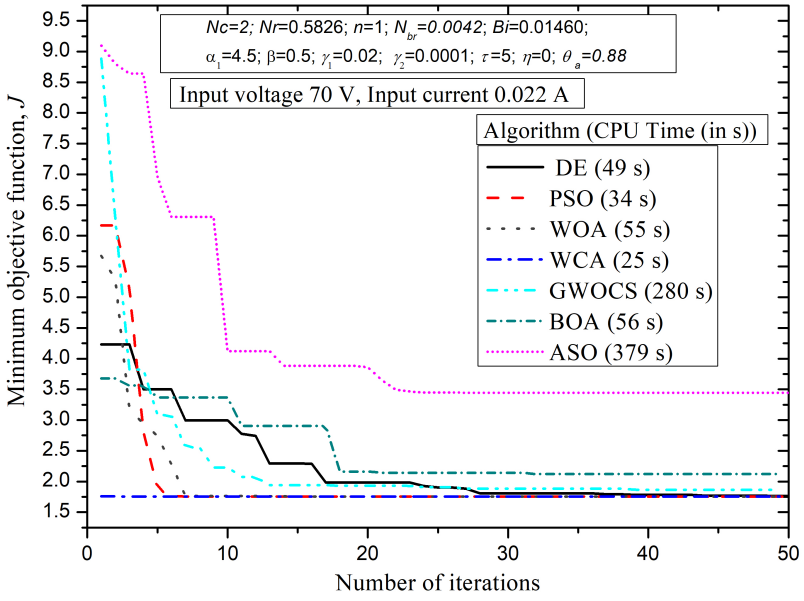

Fig. 5.15 Convergence plots for optimization algorithms, with the number of iterations, when experimental temperature profile is used.

regularization parameter $\alpha = 10^{-4}$ among ordinary least squares, Ridge and Lasso estimator.

3. BOA (performance parameter 0.77) is the best among other optimization algorithms, followed by WOA (performance parameter 0.75) and WCA (performance parameter 0.74) respectively when the temperature profile has been simulated using pdepe.

4. WOA (performance parameter 0.78) works best when experimental temperature data is utilized followed by BOA (performance parameter 0.60) and WCA (performance parameter 0.50) respectively.

This methodology thus provides a robust procedure for comparing and selecting the best inversion technique in IHTP and the procedure can be easily implemented to any domain of interest. In the next chapter, an application of this comparative procedure is seen for a problem taken from the medical domain.

Table 5.4 Decision matrix used in TOPSIS, showing multiple attributes corresponding to each optimization algorithm, with an experimental temperature profile.

Algorithm	CPU Time (in s)	Min. J	Φ	β	Nc	Nr	Bi	N_{br}	Max. error in θ	P_i	Rank
			Exact Parameter values								
			0.98	0.5	2	0.5826	0.0146	0.0042	-		
			Relative error in unknowns								
			Retrieved parameters								
DE	61.43	1.76	9.19	0.99	0.56	0.97	2.07	0.36	0.18	0.44	6
			9.9918	0.0012	1.3011	0.0159	0.055	0.0032	-		
PSO	32.72	1.75	9.20	1	0.35	1	2.66	0.68	0.18	0.42	7
			10	0	1.3	0	0.0495	0.0015	-		
WOA	**65.13**	**1.75**	**3.06**	**0.33**	**0.18**	**0.32**	**0.69**	**0.12**	**0.18**	**0.78**	**1**
			10	**0**	**1.3**	**0**	**0.07**	**0.0015**	-		
WCA	29.72	1.75	9.20	1	0.35	1	3.79	0.04	0.18	0.50	3
			10	0	1.3	0	0.07	0.0044	-		
GWOCS	32	1.85	9.20	0.93	0.35	0.76	1.46	0.64	0.18	0.49	4
			10	0.0338	1.3	0.1382	0.0359	0.0015	-		
BOA	64.68	2.34	6.13	0.66	0.30	0.65	1.95	0.13	0.20	0.60	2
			6.4726	0.0232	0.6639	0.0654	0.0202	0.0031	-		
ASO	30.38	4.88	6.92	0.16	0.42	0.71	1.28	0.69	0.30	0.45	5
			7.7713	0.5205	2.0564	0.168	0.0334	0.0013	-		

Chapter 6

Application of Regularized Comparative Inversion Approach in Bioheat Transfer

Bioheat transfer is an emerging area of research, with a particular interest in studies involving humans. The human body continuously releases and absorb heat from the surroundings, depending on the environmental conditions and temperature. A great deal of efforts in the direction is seen by Salloum *et al.* (2007), Nagham *et al.* (2014), Mohamad *et al.* (2014), Mariam *et al.* (2020), where they modeled the heat exchange of human body with the surroundings, taking into account the role of clothing. The advances in modeling of bioheat transfer lead to the construction of fractional-order models, Singh *et al.* (2011) and dual-phase-lag bioheat models, Kumar *et al.* (2017), Askarizadeh and Ahmadikia (2015). Although quite advanced bioheat models are developed, Pennes bioheat model has widely been used among researchers today for its simplicity and analyzing the heat transfer mechanism in human tissue, Bhowmik *et al.* (2013a) and hence it is used in the current analysis.

Almost all thermal and physiological parameters in Pennes model are treated as constants, however, blood perfusion rate may deviate with temperature, Melo *et al.* (2017). Thus, the retrieval of blood perfusion rate by inverse analysis provides a way to dive deeper into such formulations. Another active field of research is towards the treatment of malignancy by hyperthermia and thermal ablation, Singh and Melnik (2020), Kumari *et al.* (2020). Studies on estimation of thermophysical properties and tumor characteristics for breast tissue are given in Figueiredo *et al.* (2020), Das and Mishra (2013b, 2014, 2015). Panda and Das (2018) applied the golden section search method for abnormalities in the skin surface. A study of the human brain on thermal stress analysis is authored by Aijaz and Dar (2017).

Agnelli *et al.* (2011a,b) have worked on shape optimization using non-invasive diagnostics from images. They had applied the adjoint method which is a gradient-based method. Being faster in

computation, the limitation of gradient-based methods is that gradient calculations are required in each iteration, which increases the cost of computation, Colaço *et al.* (2006). Besides, the formulation changes from problem to problem. Another disadvantage of using gradient-based methods is that such algorithms cannot avoid local optimum and may sometimes provide results, which are not up to the mark.

Unlike deterministic methods, nature-inspired optimization methods do not calculate the gradient of the objective function in each iteration. These in fact treat the optimization problem as a black box. The meta-heuristic optimization algorithms simulate the natural processes like the behaviour of birds or ants, the hunting mechanism of wolves or whales, which ultimately converge towards the global optimum. Aziz *et al.* (2017) studied multilevel thresholding image segmentation using Whale Optimization Algorithm and Moth-Flame Optimization. Chen *et al.* (2019), used a balanced whale optimization algorithm composed of Lévy flight and chaotic local search for the constraint design problem. Dheeba and Selvi (2010) used the particle swarm optimization algorithm based clustering technique for tumor detection in the digital mammogram.

Exploration and exploitation are two important aspects of any optimization algorithm. Taking advantage of faster convergence (exploitation) and robustness of looking for the global optimum in the entire feasible region (exploration), hybrid algorithms strengthen themselves in comparison to other heuristic algorithms. The main focus of such algorithms is to utilize the distinct and good characteristics of a different algorithm, to quickly identify the region of global optimum, Colaço *et al.* (2006). These hybrid algorithms are efficient and thus can be tailored according to the problem requirement. Gheisarnejad (2018), gave a hybrid harmony search and cuckoo optimization algorithm for load frequency control. Ant Colony Optimization algorithm and harmony search were developed by Amini and Ghaderi (2013) for locating the structural dampers. An evolutionary algorithm was implemented Nowak *et al.* (2008) on bioheat problem to identify non-linear heat generation rate in living tissue.

Whenever thermal data is captured through instruments like thermocouples or imaging camera, a certain amount of error is also captured, FLIR (2018). This embedded noise add uncertainty and the corresponding inversion process become ill-posed. To convert the ill-posed character into the well-posed character, regularization should be performed, Singhal *et al.* (2020). Thus, the current work aims to observe the effect of errors on the retrieval, along with the necessary regularization strategy.

In this chapter, we will see the application of the proposed comparative framework, where the best algorithm WOA has been compared with a hybrid GWOCS regularized inversion algorithms on the bioheat transfer problem for tumor detection. Firstly, the thermal exchange via temperature distribution between tissue and tumor would be studied. Then the presence of tumor in the brain tissue will be estimated by retrieving the blood perfusion rate. The effect of

regularization parameters, the number of search agents are also analysed. Lastly, the sensitivity of unknown perfusion rate towards measurement errors in temperature would be observed with the appropriate error analysis. The retrieval of the perfusion rate would be scrutinized by reconstruction of the thermal profile. To proceed further, let us discuss the problem statement in the next section.

6.1 Bioheat Transfer Model

Consideration is given to brain tissue with tumor. For the one-dimensional analysis, a slice of the malignant human brain, as shown in Fig.(6.1), is considered. Different layers correspond to brain tissue, tumor, skull and scalp. The left end of this slice is the central core of the brain, hence adiabatic thermal conditions have been assumed, which are justified by symmetry. The right end corresponds to the surface of the brain which is exposed to the natural environment.

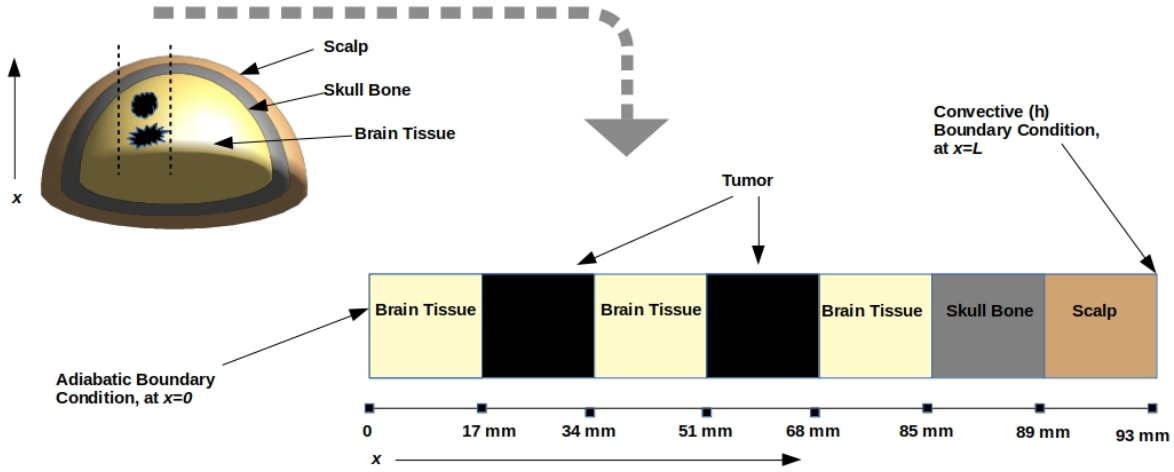

Fig. 6.1 Geometry of one-dimensional brain tissue with several layers.

For the present study, the continuum Pennes Bioheat Model, Pennes (1948), known for its simplicity, has been used for modeling the heat transfer in brain tissue. The underlying assumptions, Nowakowska and Buliński (2017), Jiji (2009) of the model are as follows.

- Uniform thermal conductivity and metabolic heat generation.
- Pre-arteriole and pre-venule heat transfer are not considered.
- Direction of blood flow is not considered.
- Heat exchange effect of local vessels within the vicinity of capillaries is neglected.

The governing energy equation within each tissue layer is given as follows.

$$\rho_i\, c_{pi}\, \frac{\partial T_i}{\partial t} = k_i \frac{\partial^2 T_i}{\partial x^2} + \underbrace{\omega_{bi}\rho_b\, c_{pb}(T_a - T_i) + Q_{mi}}_{\text{source term}}, \qquad i = 1, \ldots, 7 \tag{6.1}$$

Here layer i =1,3,5, correspond to brain tissue, layer i =2,4, correspond to tumor, layer $i = 6$ corresponds to skull bone, layer $i = 7$ corresponds to scalp. The properties associated with i^{th} layer, which are given by c_{pi}, k_i, ρ_i, ω_{bi}, Q_{mi}, represents specific heat, thermal conductivity, density, perfusion rate, metabolic heat generation respectively for i^{th} layer. The initial temperature of the tissue is given by the following seven initial conditions.

$$T_i = 36^{\circ}\text{C} \qquad \text{at } t = 0, \;\; 0 < x < L \tag{6.2}$$

Having assumed the left boundary to be located at the center of hemispherical brain at $x_0 = 0$ and the right boundary at $x_7 = L = 93$mm, with intermediate boundaries at the interfaces $x_1 = 17$mm, $x_2 = 34$mm, $x_3 = 51$mm, $x_4 = 68$mm, $x_5 = 85$mm, $x_6 = 89$mm, the boundary conditions are given by the following 14 equations,

$$\left.\frac{\partial T_1}{\partial x}\right|_{x=0} = 0 \text{ at } x = x_0 = 0, \; t > 0 \tag{6.3}$$

$$T_{i-1} = T_i, \qquad i = 2, \ldots, 7, \quad \text{at} \quad x = x_{i-1}, \; t > 0, \tag{6.4}$$

$$k_{i-1}\frac{\partial T_{i-1}}{\partial x} = k_i \frac{\partial T_i}{\partial x}, \qquad i = 2, \ldots, 7, \quad \text{at} \quad x = x_{i-1}, \; t > 0, \tag{6.5}$$

$$T_7|_{x=L} = h(T_\infty - T_7) \text{ at } x = x_7 = L, \; t > 0. \tag{6.6}$$

To analyse the temperature profile within different layers and see what methodology has been developed, let us move to the next section.

6.2 Methodology

The methodology to estimate the presence of tumor in the human brain is based on the inverse analysis. The process starts when the temperature profile of the tissue is obtained experimentally. For simulation, we have assumed that there is exactly two tumor within the brain. To mimic the experimental temperature profile, we have specified the geometry as in Fig.(6.1). To generate the thermal data corresponding to the brain tissue using the Pennes bioheat model, forward analysis is carried out. Such kind of forward analysis would not be required if the real data of the patient is available.

6.2.1 Forward Analysis

To obtain the thermal profile using equation (6.1), we have used a MATLAB based solver Pdepe (parabolic and elliptic partial differential equation). It is based on Runga-Kutta method which

converts the partial differential equations to a set of ordinary differential equations. For Pdepe the governing equation (6.1) must be in written in the standard form as

$$c\Big(x,t,T,\frac{\partial T}{\partial x}\Big)\frac{\partial T}{\partial t} = x^{-m}\frac{\partial}{\partial x}\Big(x^m f\Big(x,t,T,\frac{\partial T}{\partial x}\Big)\Big) + s\Big(x,t,T,\frac{\partial T}{\partial x}\Big). \tag{6.7}$$

As we have seven different layers $i = 1,\ldots,7$, $m = 0$,

$$c_i = \rho_i\, c_{pi},$$

$$f_i = k_i\frac{\partial T}{\partial x},$$

$$s_i = \omega_{bi}\rho_b\, c_{pb}(T_a - T_i) + Q_{mi}.$$

The initial condition is specified in the form $T(x,t=0) = To$, where our $To = 36°$C. The boundary conditions have standard equations

$$p(x,t,T) + q(x,t)f\Big(x,t,T,\frac{\partial T}{\partial x}\Big).$$

For the present case, we only need to specify the leftmost boundary at $x = 0$ and rightmost boundary at $x = L$, defined using the following terms, $p_l = 0$, $q_l = 1/k_i$, $p_r = h(T_\infty - T_r)$, $q_r = 0$. Here the subscript l corresponds to the left boundary and the subscript r corresponds to the right boundary. The remaining 12 boundaries are treated continuous by pdepe. Then the following commands generate three function files defining the problem governing equation, initial conditions and boundary conditions.

- $\big[\,c_i, f_i, s_i\,\big]$ = `GoverningEq`$(x,t,T,DTDx)$,
- T_o = `IC`(x),
- $\big[\,p_l, q_l, p_r, q_r\,\big]$ = `BC`(x_l, T_l, x_r, T_r, t).

The temperature profile is then generated using the following MATLAB command.

```
Temperature = pdepe(m, GoverningEq, IC, BC, xmesh, tspan)
```

The parameters due to tissue and tumor are listed in Table (6.1), which has been input in the direct analysis. It is important to note that the perfusion rate might not be available at the time of detection through real temperature. Thus, it is estimated through inverse analysis discussed ahead. For the present purpose of simulation we have consulted literature Das and Mishra (2013a), Zhu and Diao (2001).

Table 6.1 Properties of brain tissue and tumor, Das and Mishra (2013a), Zhu and Diao (2001).

Parameters	Blood	Scalp	Bone	Brain Tissue	Tumor
Specific heat, c_p, (J (kg. K)$^{-1}$)	3.8×10^3	4.0×10^3	2.3×10^3	3.7×10^3	3.7×10^3
Density, ρ, (kg.m^{-3})	1.05×10^3	1.0×10^3	1.05×10^3	1.05×10^3	1.05×10^3
Thermal conductivity, k, (W(m. K)$^{-1}$)	-	3.4×10^{-1}	1.16×10^0	5.0×10^{-1}	5.0×10^{-1}
Perfusion rate, ω, (s^{-1})	-	3.3×10^{-4}	3.0×10^{-4}	8.33×10^{-3}	5.0×10^{-4}
Metabolic heat generation rate, Q_m, (W m^{-3})	-	3.6×10^2	3.7×10^2	2.5×10^4	2.5×10^4
Thickness, (m)	-	4.0×10^{-3}	4.0×10^{-3}	8.5×10^{-2}	1.7×10^{-2}

6.2.2 Inverse Analysis

Having obtained the temperature profile via forward analysis, the next step is to determine the coefficient representing the blood perfusion rate. The inverse problem is formulated as an optimization problem. The objective function is formulated in the sense of least squares by the following equation.

$$J = ||T(\omega_i) - \tilde{T}\,||_2^2, \tag{6.8}$$

Here the objective J is to be minimized subject to constraints $0.0001 < \omega_i < 0.01$. Here $\tilde{T}$ is the temperature matrix obtained from the direct method, also called exact temperature profile, $T(\omega)$ is the guessed value of temperature corresponding to the estimated perfusion rates and $||.||_2$ represents l_2 norm. Moreover, as the inverse problem is ill-posed in nature, thus regularization is to be done. For regularization, the objective function, given in equation (6.8), is modified in such a way that the error between the exact and approximate solution is minimized. The objective function of Tikhonov, also termed as Ridge is formulated by the following equation, Singhal *et al.* (2020).

$$J = ||T(\omega_i) - \tilde{T}\,||_2^2 + \alpha||\omega_i||_2, \tag{6.9}$$

where 'α' represents the regularization parameter. Next, the Lasso estimator is given by the following expression, where $||.||_1$ represents l_1 norm.

$$J = ||T(\omega_i) - \tilde{T}||_2^2 + \alpha||\omega_i||_1. \tag{6.10}$$

The objective function of elastic net regularization is given as

$$J = ||T(\omega_i) - \tilde{T}||_2^2 + \alpha[(1-\lambda)||\omega_i||_2 + \lambda||\omega_i||_1], \tag{6.11}$$

with 'λ' as the mixing parameter of both Tikhonov and Lasso regularization, Singhal *et al.* (2020). In order to choose the parametric values of α in the range (10^2-10^{-11}) and λ in the interval (0,1), a study has been carried out in the next section. In order to analyze the sensitivity of estimated perfusion rate towards measurement errors (e) in temperature ($\tilde{T}$), an uniform

distribution in (-1,1) has been applied. Thus, the objective functions given in equation (6.11) has been modified as follows, where $\tilde{T} + e$ is the measured temperature field with errors.

$$J = ||T(\omega_i) - (\tilde{T} + e)||_2^2 + \alpha[(1-\lambda)||\omega_i||_2 + \lambda||\omega_i||_1], \tag{6.12}$$

To solve this minimization problem, we shall use bio-inspired stochastic algorithms namely Whale Optimization Algorithm (WOA), selected based on previous chapter and Hybrid Grey Wolf and Cuckoo Search Optimization Algorithm (GWOCS) which were discussed in the previous chapter. The inversion process is shown in Fig.(6.2).

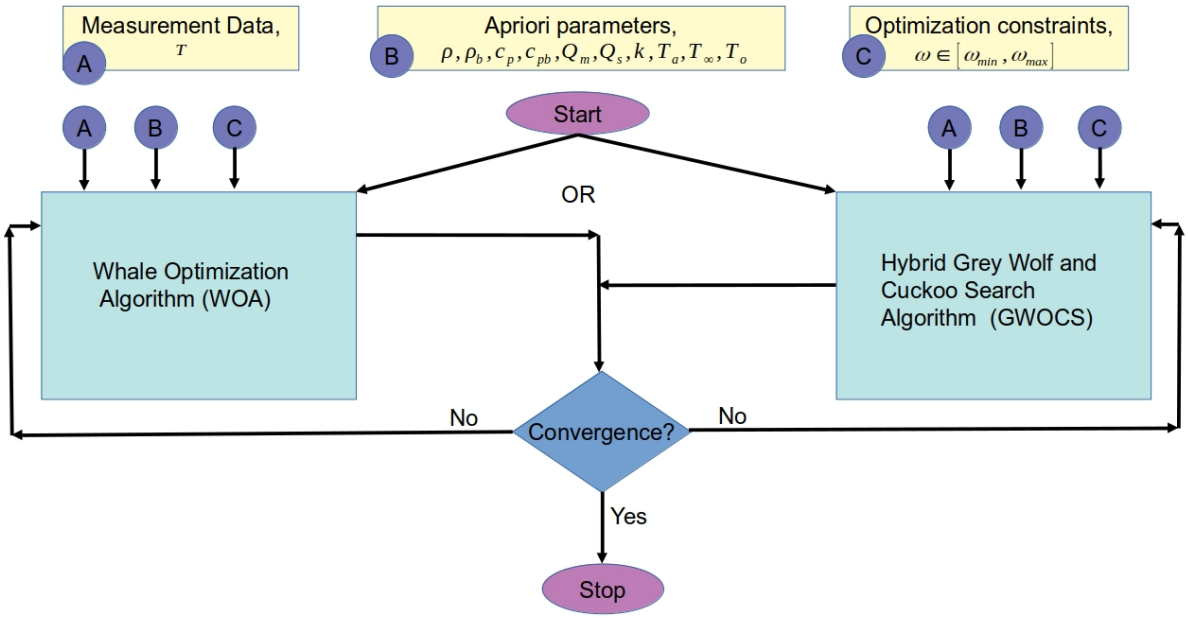

Fig. 6.2 Flow chart for inverse process, including data from forward analysis, apriori parameters and constraints.

We have discussed the forward and inverse solution methodology. The inverse problem, which is ill-posed, after regularization becomes well-posed, where the unknown perfusion rate has been calculated by minimizing objective function, equations (6.8)-(6.11). Two swarm-based algorithms have been implemented to perform this minimization. The suitability of the above listed objective functions for the current problem is also studied in detail in the next section.

6.3 Results and Discussions

6.3.1 Comparison

The direct method based on MATLAB's pdepe, results in providing the temperature profile of the brain tissue. The parameters used are as listed in Table (6.1). The code is validated both for single layer and multiple layers with discontinuity. Fig.(6.3a) shows the comparison results with Das and Mishra (2013a) when no tumor is present within the brain tissue. The

parameters used are $T_a = 37°C$, $Q_s = 0$, $c_{pb} = 3800$ J(kgK)$^{-1}$, $\rho_b = 1052$ kgm^{-3}, $L = 0.04$ m, $Q_m = 25000$ Wm^{-3}, $c_p = 3650$ J(kgK)$^{-1}$, $\rho = 1040$ kgm^{-3}, $\omega_b = 0.008$ s^{-1}. The temperature profile obtained agrees well with Das and Mishra (2013a). Fig.(6.3b) illustrate the comparison result when multiple tumor are present inside the brain. In this case, pdepe code is validated considering different layers. The parameters used are $T_a = 37°C$, $Q_s = 0$, $c_{pb} = 3800$ J(kgK)$^{-1}$, $\rho_b = 1052$ kgm^{-3}, $L = 0.04$ m, $T_o = 38.4°C$. The tumor is located at 0.005m -0.015 m.

6.3.2 Forward pdepe results

After comparison of the direct code, the thermal profile within the brain tissue has been generated both with and without the presence of tumor. The parameters used to generate a thermal profile for different tumor and tissue characteristics are listed in Table (6.1). Fig.(6.4a) and Fig.(6.4b) are the surface plots where the temperature distribution for normal brain tissue and malignant brain tissue is seen for all points in space $0 \leq x \leq L$ and time-domain $0 \leq t \leq 200s$. At positions where tumor cells are present, temperature shows smooth bumps. Moreover, line plot in Fig.(6.4c) shows the temperature profile at $t = 200$s, where two tumors are present at positions 0.017m-0.034m and 0.051m-0.068m respectively. Thus, two bumps are seen in the temperature profile. A large decrease in temperature at the right boundary, which corresponds to the brain's outer surface is due to heat loss to the surrounding via thermal convection. The heat transfer coefficient, $h = 10$ Wm^{-2}K^{-1} and the ambient temperature $T_\infty = 23°C$ has been used.

The variation in the temperature distribution with time is seen in Fig.(6.5). For tissue without tumors, the temperature remains the same in the interior of brain, i.e., when $x \in (0, 0.051\text{m})$, refer Fig.(6.5a). However, a decrease in temperature is seen near the right boundary, which suggests that heat is being lost due to thermal convection. In case of tissue with multiple tumors Fig.(6.5b), this is not the case. We know every cell in the body produces new cells by cell division. Whenever during this division, if some portion of the cell get damage or mutation occurs, then a cancer cell is produced in its vicinity, Katheder *et al.* (2017). As a result, a large number of damaged cells starts developing in a particular organ resulting in the tumor formation. Thus, tumor cells require extra energy from its surrounding cells and tissues for the growth, resulting in a higher temperature over time. This fact is observed in Fig.(6.5b) reporting the correctness of the model. As time increases, an increase in temperature is analysed. This increase in temperature is due to faster proliferation and increased metabolic activity. Generally, solid tumors are poorly vascularized and the blood vessels together with lymphatic vessels inside tumor are defective. This leads to slower movement of blood inside these vessels causing ineffective means of dumping the heat produced as a result of metabolic activities. Thus, over time, higher temperature in tumorous cells is observed.

6.3.3 Regularization for ill-posedness

In order to calculate the unknown blood perfusion rate, the inversion technique should be converted from ill-posed to well-posed. This is done by applying regularization by modifying

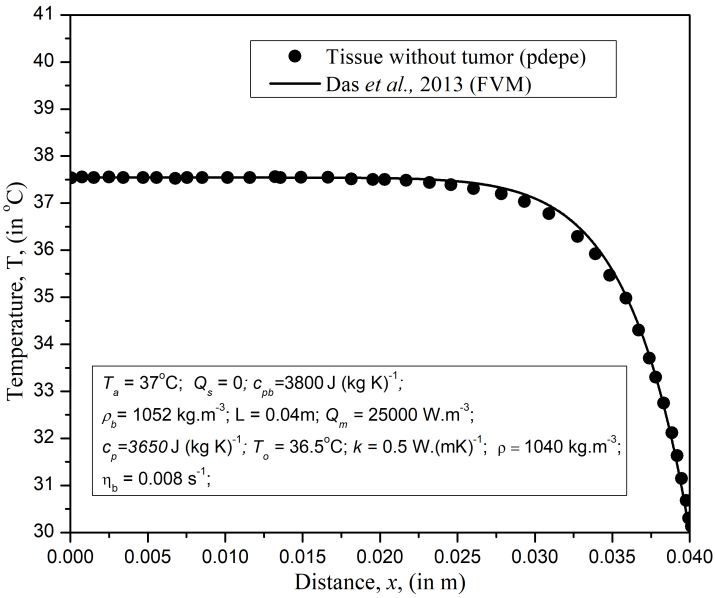

(a)

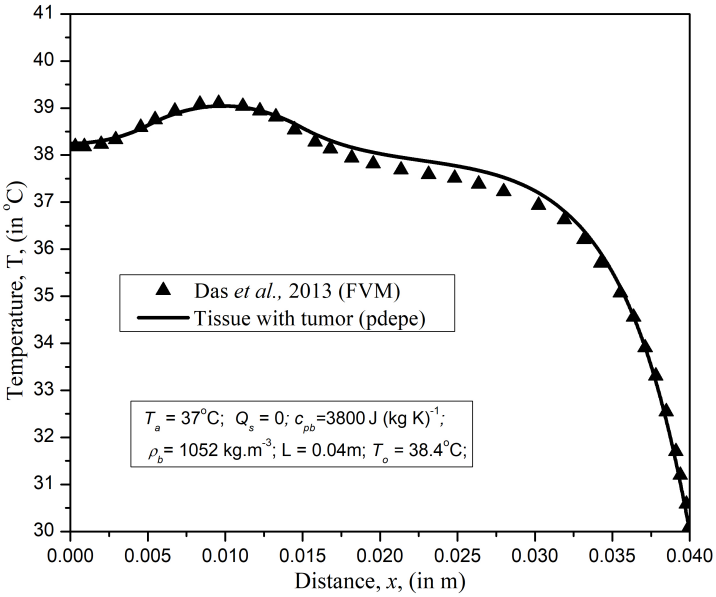

(b)

Fig. 6.3 Comparison of Matlab's Pdepe with Das and Mishra (2013a) for (a) tissue without tumor, (b) tissue with tumor.

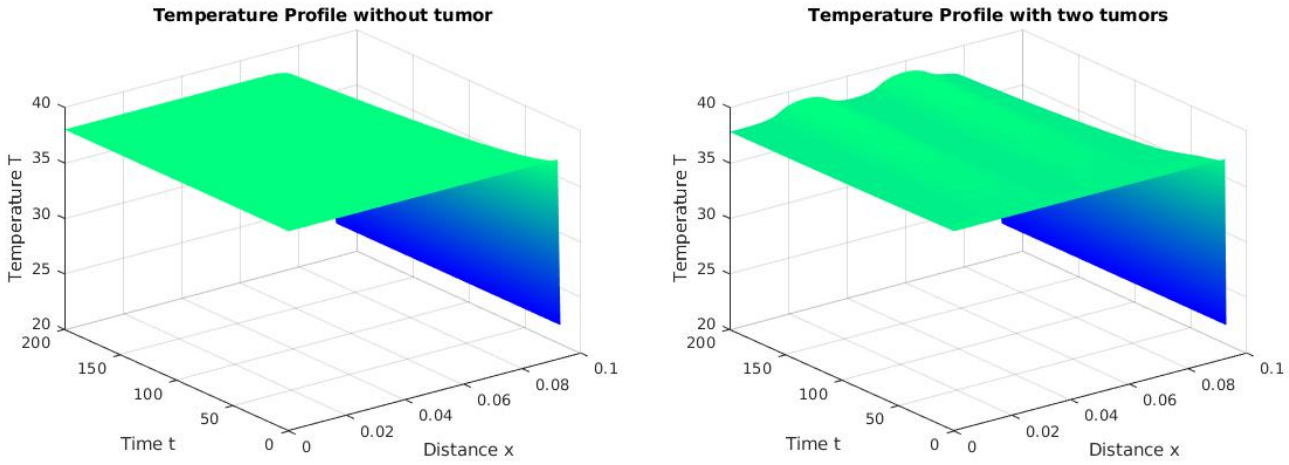

(a) **(b)**

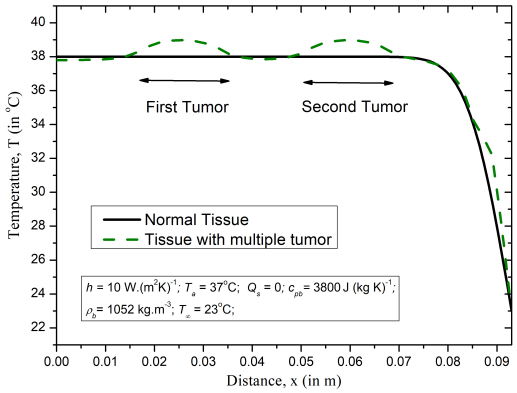

(c)

Fig. 6.4 Temperature profile of normal brain tissue (a) without tumor, (b) with two tumors for $0 \leq t \leq 200s$ and $0 \leq x \leq L$, (c) with and without tumors for $t = 200s$ and $0 \leq x \leq L$, with forward parameters, $h = 10$ W.(m^{2}K)$^{-1}$, $T_a = 37°$C, $Q_s = 0$, $c_{pb} = 3800$ J(kgK)$^{-1}$, $\rho_b = 1052$ kgm^{-3}, $T_\infty = 23°$C

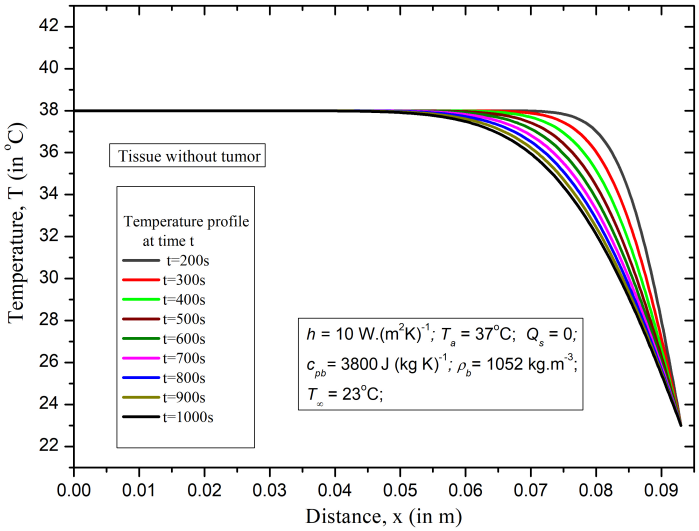

(a)

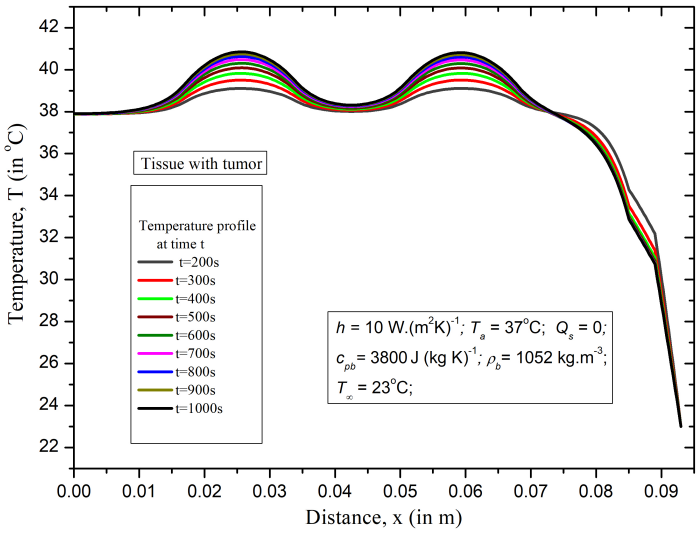

(b)

Fig. 6.5 Temperature profile of brain tissue (a) without tumor, (b) with tumor, at different time coordinate, t and $0 \leq x \leq L$.

the objective function as discussed earlier. Here the regularization parameter α has to be selected from the range (10^2-10^{-11}), Singhal *et al.* (2020). The Total Relative Error (TRE), TRE=$\sum_i (\text{RE})_i$ and Total Absolute Error (TAE), TAE=$\sum_i (\text{AE})_i$ in the unknown blood perfusion rate (for each layer) has been calculated. The regularization parameter, α has been analyzed for the values 10^2, 10^{-2}, 10^{-4}, 10^{-6}, 10^{-8}, 10^{-9}, 10^{-10}, 10^{-11}. The results are given in Fig.(6.6a) and Fig.(6.6b) when the corresponding algorithm is WOA. Fig.(6.6a) suggests that the least TRE in perfusion rate is 1.48, corresponding to $\alpha = 10^{-2}$, whereas Fig.(6.6b) suggests that the least TAE in perfusion rate is 0.0009, corresponding to $\alpha = 10^{-8}$. Hence, for selecting an appropriate objective function, $\alpha = 10^{-2}$ and $\alpha = 10^{-8}$ is selected based on this analysis for WOA. A similar analysis has been carried out for GWOCS, where $\alpha = 10^{-4}$ is selected.

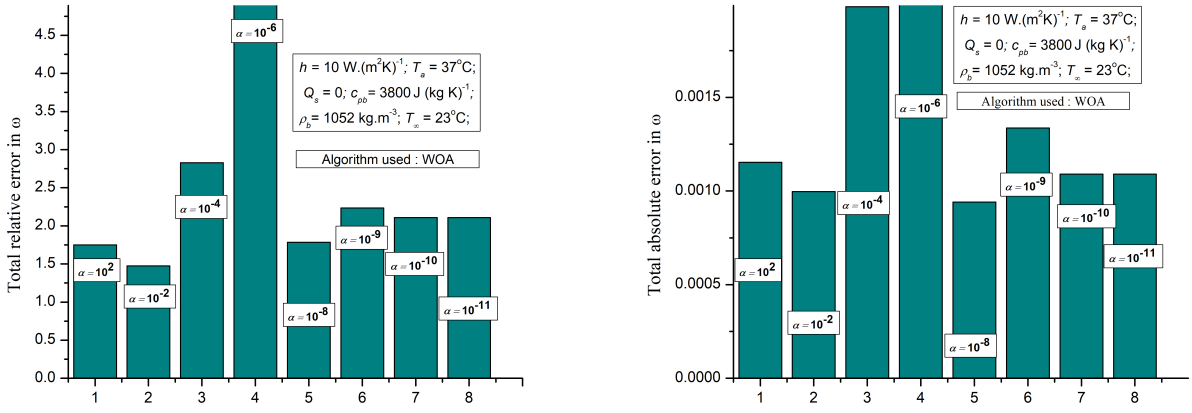

(a) **(b)**

Fig. 6.6 Based on minimum (a) total relative error (b) total absolute error in perfusion rate using WOA, selection of regularization parameter α.

The maximum RE in the perfusion rate has been illustrated in Fig.(6.7), where the objective function is to be selected. Here RE is studied for the objective functions given in equations (6.8)-(6.11) for $\alpha = 0$ (no regularization), $\alpha = 10^{-2}$ and $\alpha = 10^{-8}$ respectively, based on the previous study. Clearly, for $\alpha = 10^{-2}$, elastic net regularization followed by Tikhonov give the least error. The results are also presented in Table (6.2). Now as elastic net regularization has been selected with $\alpha = 10^{-2}$ for WOA, we shall select the mixing parameter λ. Fig.(6.8) shows the maximum RE in perfusion rate for different values of the mixing parameter ($\lambda = 0.1 - 0.9$). For $\lambda = 0$ and $\lambda = 1$, the elastic net regularization is nothing but Tikhonov and Lasso respectively. The results in Fig.(6.8) suggest elastic net regularization, with $\lambda = 0.1$, $\alpha = 10^{-2}$ shows the least RE for WOA, as required. Similar analysis has been carried out for GWOCS, where elastic net with $\lambda = 0.9$, $\alpha = 10^{-4}$ shows the least RE. Thus, the regularized inversion strategy based on the above study has been implemented in further work for both the algorithms.

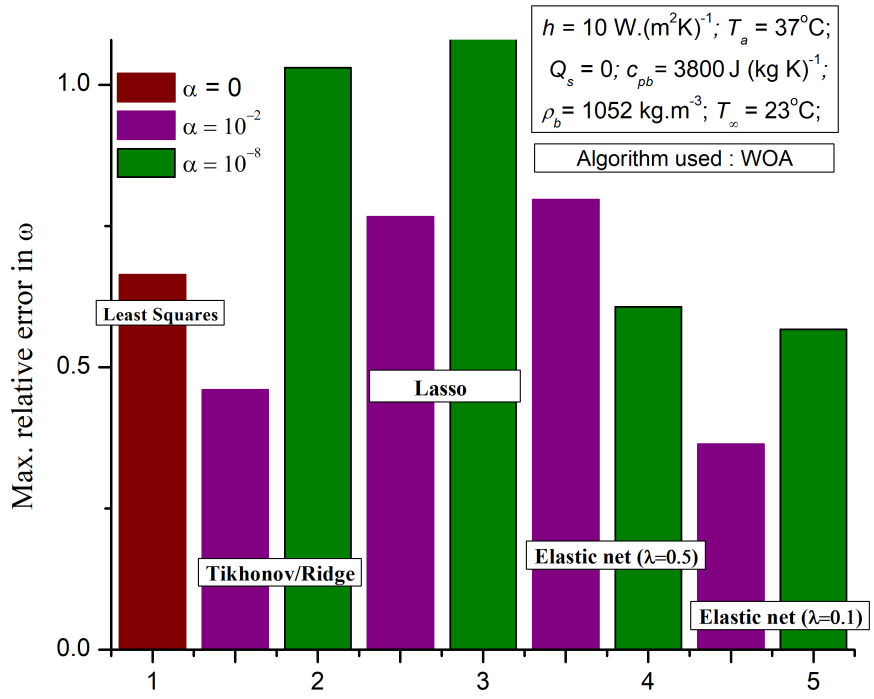

Fig. 6.7 Based on minimum total relative error in perfusion rate using WOA, selection of the objective function for no regularization, regularization with $\alpha = 10^{-2}$ and $\alpha = 10^{-8}$.

Table 6.2 Results of different objective functions when no regularization $\alpha = 0$, regularization with $\alpha = 10^{-2}$ and $\alpha = 10^{-8}$ is performed.

	Max. RE	Min. fitness value	CPU time			
Least Square ($\alpha = 0$)	0.66	1.59	129.1			
	$\alpha = 10^{-2}$			$\alpha = 10^{-8}$		
	Max. RE	Min. fitness value	CPU time (in s)	Max. RE	Min. fitness value	CPU time (in s)
Tikhonov/Ridge	0.46	0.72	132.1	1.03	0.39	131.7
Lasso	0.77	1.36	131.7	1.08	3.36	130.4
elastic net ($\lambda = 0.5$)	0.79	1.30	128.8	0.61	0.92	129.4
elastic net ($\lambda = 0.1$)	0.36	0.27	131.5	0.56	0.76	130.2

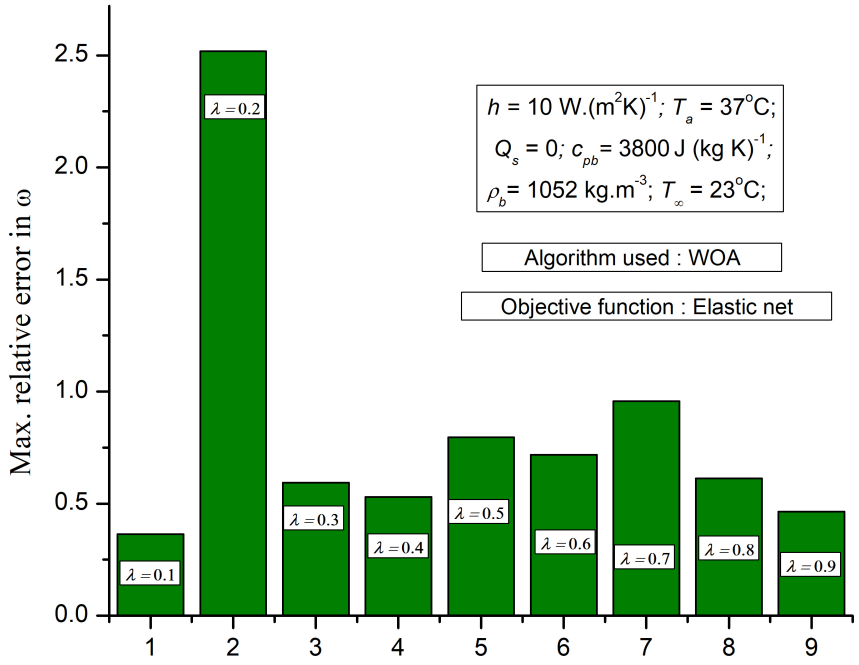

Fig. 6.8 Based on minimum total relative error in perfusion rate using WOA, selection of the mixing parameter λ, with $\alpha = 10^{-2}$.

6.3.4 Inverse optimization Results

When the temperature profile is known, as we have obtained by forward analysis, the unknowns are estimated by minimizing equation (6.11), where $\alpha = 10^{-2}$ with $\lambda = 0.1$ for WOA and $\alpha = 10^{-4}$ with $\lambda = 0.9$ for GWOCS. The parameters of algorithms have been set with the number of search agents as 30 with a maximum of 100 iterations. The temperatures of the tissue (refer Fig.(6.4c)) along with the apriori information (refer Table (6.1)) is then fed to both WOA and GWOCS to estimate the blood perfusion rate (ω_i). The obtained blood perfusion rate ω_i, $(i = 1, \ldots, 7)$ for $e = 0\%$, is shown in Fig.(6.11a) and Fig.(6.11b) for WOA and GWOCS respectively. In the following subsections, the effect of the number of search agents used in WOA and GWOCS is seen. Thereafter, the effect of measurement errors in the temperature profile on the retrieval of the perfusion rate is discussed. The obtained perfusion rate with noisy temperature data is scrutinized by reconstructing the temperature field as discussed in the subsequent subsections.

Effect of number of search agents in WOA and GWOCS

A study showing the effect of the number of search agents both in WOA and GWOCS is presented in Table (6.3). The obtained minimum objective function value is given with 300 as the maximum number of iterations. Moreover, the amount of CPU time in seconds is observed

for both algorithms, with the current system configuration, Intel(R) Core(TM) i5-8250U CPU @1.60GHz along with 16GB RAM. The CPU time for both algorithms is approximately the same. The minimum objective function value predicted by GWOCS, $O(10^{-4})$, is better than the corresponding WOA, $O(10^{-2})$. The transition when the number of search agents is from 20 to 30, reduces the objective function value from $O(10^{-1})$ to $O(10^{-2})$ for WOA and $O(10^{-2})$ to $O(10^{-4})$ for GWOCS respectively. Thus, the optimal number of search agents is observed to be 30 in both cases. Fig.(6.9) shows the convergence plot of WOA and GWOCS for the different number of search agents. The convergence of WOA and GWOCS is obtained well before 50 iterations, in each case. The rate of convergence for every given number of search agents is rapid with a smooth convergence curve.

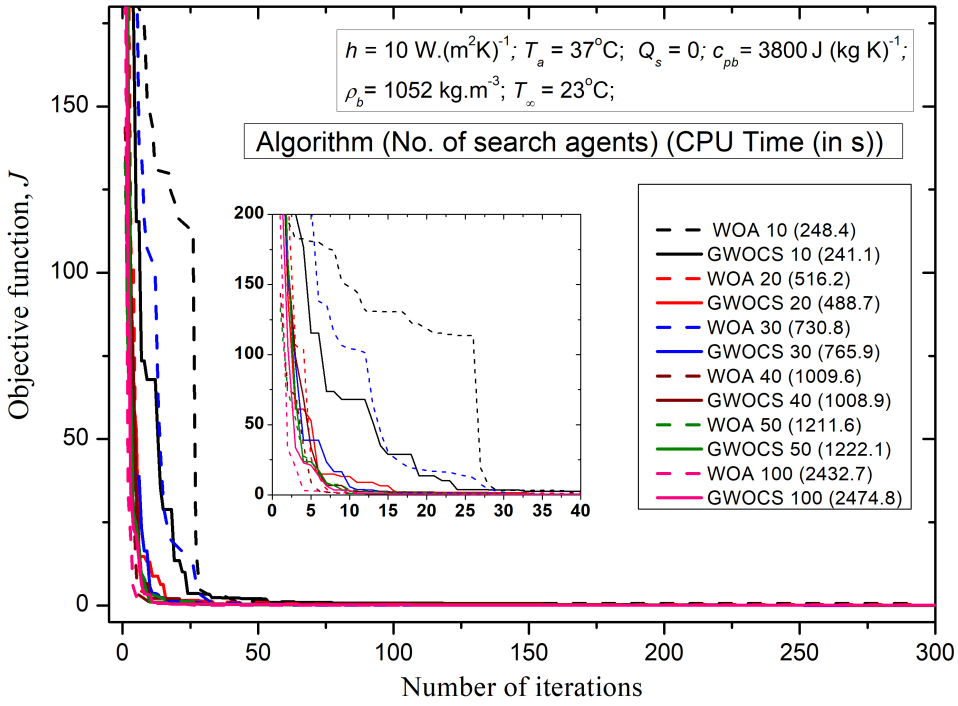

Fig. 6.9 Convergence plots for optimization algorithms WOA and GWOCS, plotted with the number of iterations, with the corresponding CPU time required for computation, when number of search agents are 10, 30, 50, 100.

Error analysis and the retrieval of perfusion rate

To test the current methodology, the noisy forward data has been simulated by adding random errors to the exact data. The need for such an analysis lies in the fact that most of the instruments capturing the thermal profile are not accurate and hence may result in providing an erroneous temperature profile, FLIR (2018). Thus, for the current analysis, the temperature profile with 1%, 2%, 3%, 4%, 7%, 10% measurement errors has been intentionally included. Fig.(6.10)

Table 6.3 Effect of search agents on the convergence and CPU time by WOA and GWOCS, with 300 iterations.

	WOA		GWOCS	
No. of search agents	Min. objective value	CPU time (in s)	Min. objective value	CPU time (in s)
10	0.56	248.4	0.01	241.1
20	0.27	516.2	0.03	488.7
30	0.04	730.8	5.4×10^{-4}	765.9
40	0.18	1009.6	3.06×10^{-3}	1008.9
50	0.08	1211.6	9.1×10^{-4}	1222.1
100	0.02	2432.7	0.01×10^{-4}	2474.8

illustrates the comparison of the exact temperature profile with that of noisy data, when a uniformly generated error (e), of 1%, 2%, 3%, 4% has been added to the exact data. This noisy profile mimics the measured temperature data obtained during experiments. The tissue parameters used are as listed in Table(6.1), with $t = 200s$ and $0 \leq x \leq L$. The perfusion rate, within the range $[0.0001 - 0.01]$ has been estimated by minimizing equation (6.12), where $\alpha = 10^{-2}$ with $\lambda = 0.1$ for WOA and $\alpha = 10^{-4}$ with $\lambda = 0.9$ for GWOCS using the generated noisy temperature profile.

The retrieved blood perfusion rate along with the exact perfusion rate, are plotted in Fig.(6.11a) using WOA and using GWOCS in Fig.(6.11b). These plots show the retrieved perfusion rate when an uniform random measurement error, e of 0%, 1%, 2%, 3%, 4%, 7%, 10% is present in the temperature distribution. Corresponding to the exact perfusion rates, ω_1, ω_2, ω_3, ω_4, ω_5, ω_6, ω_7, which are 0.00833, 0.0005, 0.00833, 0.0005, 0.00833, 0.0003, 0.00033, the retrieved value (for e=0%) matches perfectly. When the forward data contain an error of 1%, 2%, 3%, 4%, 7%, a little deviation of the same order is seen compared with the exact values for both WOA and GWOCS. For 10% measurement error in the temperature profile, it becomes difficult to distinguish between the normal tissue and tumor, resulting in misleading observations. Thus, the current methodology provides a good estimation of the presence of tumor, with an error bound of 7%. These plots have been shown for run 1, where the corresponding relative errors are given in Table (6.4) for WOA, with elastic net regularization ($\alpha = 10^{-2}$, $\lambda = 0.1$) and in Table (6.5) for GWOCS, with elastic net regularization ($\alpha = 10^{-4}$, $\lambda = 0.9$) respectively. WOA and GWOCS being stochastic, give different results every time we run. Hence, for the current analysis, each algorithm is run three times and the results are presented in Table (6.4, 6.5). For every run with WOA (number of search agents used are 30 and the maximum number of iterations are 100), the corresponding CPU time lies in the range of 239-265s. The CPU time

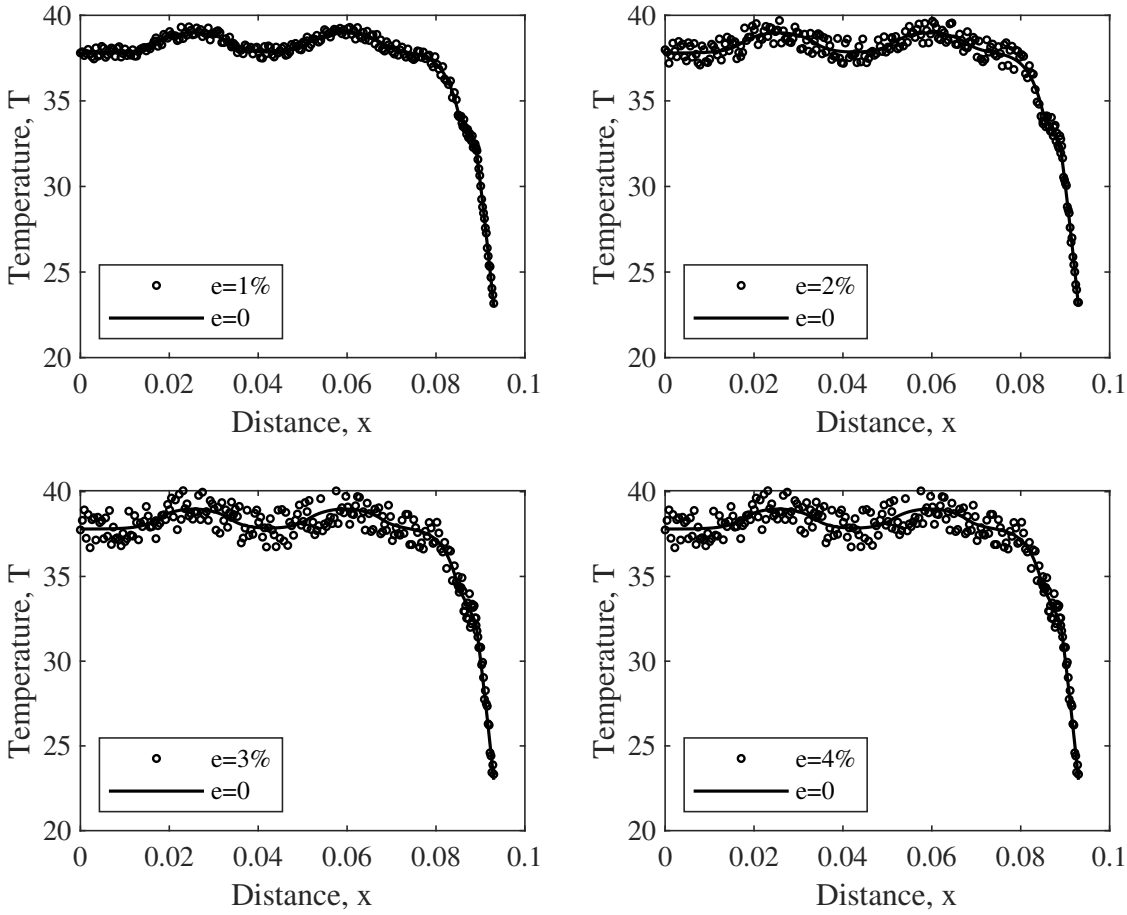

Fig. 6.10 Noisy temperature profile (e = 0, 1%, 2%, 3%, 4%) of the brain tissue with tumors for $t = 200s$ and $0 \leq x \leq L$.

for GWOCS lies in the range of 248-277s. The convergence of the method is conveyed through the residual J, given in the equation (6.12). As the error in the input temperature data go on increasing, the respective residual increases, as expected for both algorithms. The relative error corresponding to each layer is also presented in Table (6.4, 6.5). It can be seen in Fig.(6.11) that even if the input data contain random errors, the presence of tumor is detected quite effectively, with a clear distinction of two tumors from the brain tissue. Moreover, the effect of errors in the input temperature distribution show a little deviation with $e = 2\%$ by WOA, Fig.(6.11a) and deviation for $e = 2\%, 4\%$ by GWOCS, Fig.(6.11b) respectively.

Reconstruction of temperature via retrieved perfusion rate

To check the correctness of the retrieved perfusion rate for all layers, the temperature distribution has been reconstructed. For this reconstruction, the retrieved perfusion rates given in Table (6.4, 6.5) for run 1, along with the parameters of Table (6.1) are used. The comparison of exact and reconstructed temperature profile when the error $e = 0\%, 1\%, 2\%, 3\%, 4\%, 7\%, 10\%$ is present in the forward data for both WOA and GWOCS, plotted with the distance, x

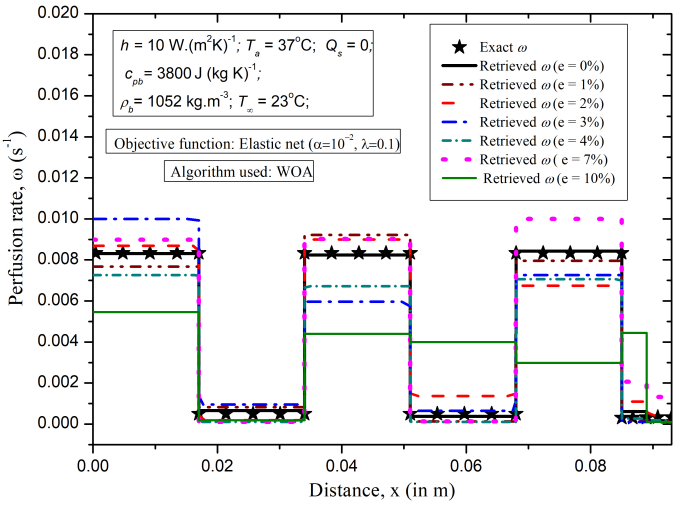

(a)

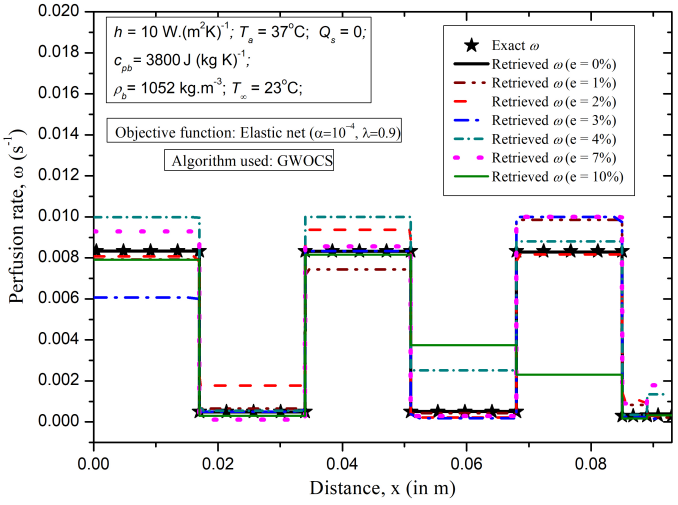

(b)

Fig. 6.11 Exact and retrieved blood perfusion rate ω, using (a) WOA, with elastic net regularization ($\alpha = 10^{-2},\ \lambda = 0.1$) (b) GWOCS, with elastic net regularization ($\alpha = 10^{-4},\ \lambda = 0.9$).

Table 6.4 Comparison of retrieved blood perfusion rate of each layer, for different runs of WOA with $e = 0, 1\%, 2\%, 3\%, 4\%, 7\%, 10\%$, range of [$\omega_i$] = [0.0001-0.01].

Run no.	WOA (No. of search agents: 30, No, of iterations: 100)								
error,	Relative error in perfusion rate							Min. Fitness	CPU time
$e(\%)$	ω_1	ω_2	ω_3	ω_4	ω_5	ω_6	ω_7	function, J	(in s)
	Exact values perfusion rate (s^{-1})								
	0.00833	0.0005	0.00833	0.0005	0.00833	0.0003	0.00033		
Without measurement errors,									
$e = 0$	0.0028	0.33	0.011	0.25	0.01	1.04	0.50	0.34	244.5
With measurement errors, $e \neq 0$									
$e_r = 1\%$									
1	0.08	0.64	0.11	0.75	0.04	0.57	0.43	8.36	253.6
2	0.03	0.15	0.10	0.28	0.10	4.16	0.65	8.17	249.4
3	0.11	0.76	0.08	0.74	0.01	1.26	0.66	9.66	262.2
$e_r = 2\%$									
1	0.04	0.62	0.08	1.74	0.19	2.63	0.29	33.3	246.6
2	0.11	0.72	0.12	2.40	0.13	0.12	0.61	33.8	252.9
3	0.08	0.73	0.04	0.77	0.19	1.36	0.63	34.2	261.6
$e_r = 3\%$									
1	0.20	0.90	0.28	0.29	0.13	0.67	0.70	75.0	241.0
2	0.27	0.14	0.24	0.92	0.13	2.24	0.70	74.0	258.7
3	0.18	2.98	0.18	0.73	0.05	8.62	0.59	71.3	265.0
$e_r = 4\%$									
1	0.13	0.8	0.19	0.8	0.15	0.09	0.43	127.4	239.4
2	0.19	0.49	0.16	0.76	0.19	6.87	3.43	132.4	263.9
3	0.04	3.93	0.14	0.8	0.13	9.39	0.70	128.7	261.0
$e_r = 7\%$									
1	0.08	0.8	0.08	0.73	0.20	5.89	3.00	1018.1	1797.3
2	0.09	0.10	0.02	0.25	0.20	1.60	3.74	1018.6	1792.9
3	0.05	0.80	0.11	0.60	0.20	0.42	4.74	1018.1	1790.4
$e_r = 10\%$									
1	0.34	0.61	0.47	7.00	0.64	13.8	0.69	2041.3	1831.64
2	0.22	0.80	0.54	5.61	0.72	11.39	0.70	2041.1	1839.9
3	0.20	0.70	0.01	7.92	0.64	0.89	0.55	2039.9	1865.8

Table 6.5 Comparison of retrieved blood perfusion rate of each layer, for different runs of GWOCS with $e = 0, 1\%, 2\%, 3\%, 4\%$, 7%, 10%, range of [ω_i] = [0.0001-0.01].

Run no.	GWOCS (No. of search agents: 10, No, of iterations: 300)								
error,	Relative error in perfusion rate							Min. Fitness	CPU time
$e(\%)$	ω_1	ω_2	ω_3	ω_4	ω_5	ω_6	ω_7	function, J	(in s)
	Exact values perfusion rate (s^{-1})								
	0.00833	0.0005	0.00833	0.0005	0.00833	0.0003	0.00033		
Without measurement errors,									
$e = 0$	0.0002	0.015	0.0004	0.022	0.004	0.17	0.09	4.5×10^{-3}	248.8
With measurement errors, $e \neq 0$									
$e_r = 1\%$									
1	0.05	0.32	0.11	0.13	0.18	1.76	0.35	7.77	277.9
2	0.04	0.88	0.02	0.56	0.12	0.62	0.55	8.42	250.4
3	0.02	0.01	0.06	0.02	0.09	0.94	0.14	7.75	254.4
$e_r = 2\%$									
1	0.03	2.54	0.12	0.55	0.02	2.52	0.08	33.2	250.3
2	0.19	0.35	0.17	0.47	0.12	7.91	0.70	33.1	253.4
3	0.20	0.12	0.05	1.17	0.19	0.47	0.57	35.9	252.5
$e_r = 3\%$									
1	0.27	0.01	3.7×10^{-4}	0.63	0.20	0.16	0.52	73.9	251.5
2	0.08	2.18	0.26	0.31	0.04	5.40	5.17	81.4	252.9
3	0.25	0.78	0.15	0.79	0.02	2.36	0.24	75.4	267.3
$e_r = 4\%$									
1	0.20	0.09	0.20	4.03	0.06	0.16	3.08	129.1	263.2
2	0.08	0.80	0.31	0.37	0.07	23.7	0.69	130.8	253.5
3	0.34	1.20	0.07	0.80	0.05	27.3	0.58	126.0	256.2
$e_r = 7\%$									
1	0.12	0.78	0.03	0.41	0.20	1.99	4.40	1017.9	1829.8
2	0.11	0.76	0.04	0.62	0.20	1.49	4.48	1017.9	1848.6
3	0.12	0.72	0.04	0.67	0.20	3.62	3.88	1017.9	1855.9
$e_r = 10\%$									
1	0.05	0.40	0.02	6.49	0.72	0.42	0.02	2039.8	1901.6
2	0.15	0.14	0.12	7.40	0.73	0.29	0.62	2039.8	1913.3
3	0.05	0.68	0.01	5.94	0.72	0.08	0.60	2039.9	1931.7

is illustrated in Fig.(6.12). An excellent matching of reconstructed temperature field and the exact field, even when the forward data contain noise, proves that the obtained set of perfusion rate is appropriate. However, the temperature profile seems to vary for 10% measurement error. Moreover, the maximum deviation in the reconstructed temperature profile when an error, e of 0%, 1%, 2%, 3%, 4%, 7%, 10% is present in the forward data for both WOA and GWOCS is presented in Table (6.6). The deviation is studied by the corresponding maximum and average relative error in the reconstructed temperature profile. The maximum deviation is of the order O(10^{-2}), except for the case of 10% error where it is O(10^{-1}), calculated by both PDEPE-WOA and PDEPE-GWOCS. Thus, the proposed regularized inversion technique PDEPE-WOA and PDEPE-GWOCS is suitable for the purpose when multiple tumors are to be detected by the retrieval of blood perfusion rate.

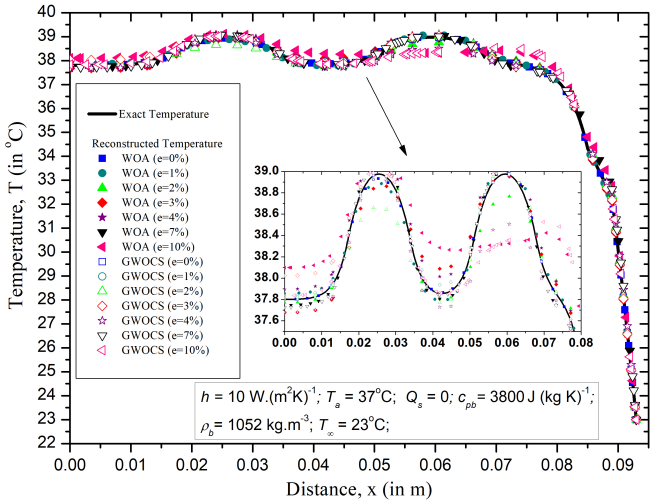

Fig. 6.12 Comparison of exact and reconstructed temperature profile when the error $e = 0\%$, 1%, 2%, 3%, 4%, 7%, 10% is present in the forward data for both WOA and GWOCS, plotted with the distance, x.

6.4 Observations

In the present chapter, PDEPE-WOA and PDEPE GWOCS regularized inversion techniques are compared to detect the presence of tumor in brain tissue. Pennes model is used for the formulation of the bioheat transfer within the human brain. Different segments are classified into different layers. The temperature profile is obtained by pdepe. For retrieval of unknown blood perfusion rate ω_i, bio-inspired optimization algorithms WOA and GWOCS are compared based on the developed comparative framework. Besides, for regularization, Tikhonov, lasso and elastic net regularizations are implemented. As the real temperature data contains error, thus an error analysis on the current problem is also done. The following observations are made.

Table 6.6 Maximum deviation in the reconstructed temperature profile when an error, e of 0%, 1%, 2%, 3%, 4%, 7%, 10% is present in the forward data for both WOA and GWOCS.

Error, $e(\%)$	Max. Relative error		Average Relative error	
(Forward data)	WOA	GWOCS	WOA	GWOCS
$e = 0$	1.24×10^{-3}	2.21×10^{-4}	4.46×10^{-4}	4.51×10^{-5}
$e_r = 1\%$	1.22×10^{-2}	1.17×10^{-2}	5.44×10^{-3}	5.31×10^{-3}
$e_r = 2\%$	2.42×10^{-2}	2.62×10^{-2}	1.03×10^{-2}	1.01×10^{-2}
$e_r = 3\%$	3.63×10^{-2}	3.14×10^{-2}	1.49×10^{-2}	1.46×10^{-2}
$e_r = 4\%$	4.59×10^{-2}	4.54×10^{-2}	2.09×10^{-2}	2.06×10^{-2}
$e_r = 7\%$	8.71×10^{-2}	8.41×10^{-2}	3.78×10^{-2}	3.78×10^{-2}
$e_r = 10\%$	1.21×10^{-1}	1.24×10^{-1}	5.21×10^{-2}	5.21×10^{-2}

1. At positions where tumor cells are present, temperature rises in the form of smooth bumps.

2. With the increase in time, the temperature of the cancer cells increases, whereas no change is seen in the tissue without tumor.

3. Elastic net regularization, with $\lambda = 0.1$, for $\alpha = 10^{-2}$ for WOA and with $\lambda = 0.9$, for $\alpha = 10^{-4}$ for GWOCS shows the least relative error.

4. The optimal number of search agents is observed to be 30, with the objective function of order O(10^{-2}) for WOA and O(10^{-4}) for GWOCS. Also, the convergence of WOA and GWOCS is obtained before 50 iterations.

5. The CPU time for retrieval by WOA is 239-265s, whereas for GWOCS is 248-277s.

6. The presence of tumor is detected quite effectively, with a clear distinction of two tumors from the brain tissue. A little deviation in retrieved perfusion rate with $e = 2\%$ by WOA and with $e = 2\%, 4\%$ by GWOCS is seen.

7. An excellent matching of reconstructed temperature field and the exact field, even when the forward data contain noise $e = 0\%$, 1%, 2%, 3%, 4%, 7% concludes that the obtained set of perfusion rate is appropriate for tumor detection.

8. An error bound of 7% is marked for a meaningful detection of tumor.

Thus, the proposed comparative procedure was found suitable for the bio-heat transfer problem. The regularized inversion techniques PDEPE-WOA and PDEPE-GWOCS are suitable for the purpose when multiple tumors are to be detected by the retrieval of blood perfusion rate. In the next chapter, the overall conclusions of the thesis are discussed. In addition, the future scope of

the current research has also been given.

Chapter 7

Conclusion and Future Directions

The major outcomes of the thesis revolve around finding the solution of inverse problems in the heat transfer setting. The retrieval of boundary condition (heat flux), thermophysical properties (thermal conductivity, heat transfer coefficient, conduction-convection, conduction-radiation) and biological tissue properties (blood perfusion rate) has been satisfactorily performed. The efficiency of the composite walls and the maximum loss of heat in the extended surface has been studied. Moreover, the detection of tumor by observing the temperature profile and by estimating the value of blood perfusion rate indicates the regions of malignancy. The usability of various algorithms in IHTP, starting from golden section search method, for retrieval of a single parameter, to the regularized versions of inversion technique, for retrieval of multiple parameters with uncertainty, strengthen the computational domain of IHTP. The procedure for comparing and selecting the best inversion algorithm has been developed, which can be used in any field of interest.

7.1 Conclusion

The thesis starts with the motivation of selection of the inversion technique best fit for a given problem. To compare the existing methods and to see whether these could be compared to a more general problem, an exhaustive literature survey was done. All of the available methods were studied. A classification based on the similar characteristics of both regularization and inversion techniques was made. The literature revealed that TSVD was the simplest technique for inversion, while the linear least-squares method, Alifanov's CGM iterative method, Tikhonov's regularization, Beck's sequential regularization and mollification methods were most efficient. On the other hand, the inverse solution techniques were classified into analytical and semi-analytical methods, methods without minimization and methods involving minimization. In the first class of analytical methods, methods like Laplace transform, separation of variables, boundary element method together with Green's function and convolution integrals were seen. Further, ADM in conjunction with Fourier transformation was used in IHCP. For any study,

in particular for the current thesis, having a handful of analytical methods, where closed-form expressions are obtained become necessary, as these expressions behave as standard for any numerical technique. Thus, the literature survey on analytical methods, motivated us to obtain closed-form expression for a non-linear problem of interest from heat transfer.

For the second objective, i.e., implementation of the selected technique on realistic problems taken from heat transfer systems, the first problem selected consists of composite walls, which are multi-layered walls, stacked together side by side. The selected system has many applications. In particular, its application in the industrial furnace was seen. The maximum performance of the furnace was suggested when the internal heat generation rate in the outer wall becomes zero. The corresponding efficiency was 96.67%, if the outer selected material act as insulation, preventing any kind of heat loss, which is an important requirement for any furnace. Constructing the furnace and performing experiments is an arduous task, leading to exploitation of time as well as resources. Thus, a mathematical model of the composite-walled system was created, where the mathematical equations, governing the heat transfer are highly non-linear. To overcome this non-linearity, ADM in conjunction with Newton-Raphson method was applied. The closed-form expression for temperature profile of the walls was obtained. Based on the absolute error, O(10^{-7}) in the temperature profile and the corresponding CPU time (567s), a major contribution was supplied by the first six terms of the infinite temperature series. Thus, for the computation, in the expression for temperature, only six terms were kept, neglecting others. A study on the effects of parameters on the efficiency of the system was also conducted. A maximum efficiency of 98.32% and 96.44% was obtained for the exponent of convective heat transfer, $n = -0.5$ and the coefficients of internal heat generation, $\alpha_i = \alpha_o = 0.01$, $\beta_i = \beta_o = 0.04$, $\gamma_i = 0.05$, $\gamma_o = 0.03$, respectively. Thus, if these parameters were selected in the application consisting of composite walled system, the performance efficiency would be maximum.

Having implemented semi-analytic, ADM method to study the forward heat transfer in composite walls, the classification on inversion techniques was visited again. Inversion methods without minimization involved TSVD, which performed natural regularization but at the same time over smooth the solution. Another class of methods include optimization methods, where minimization was performed. These methods were further categorized into deterministic and evolutionary methods. With the faster convergence rate, deterministic methods provide guaranteed convergence to the local minima. However, a major limitation is that these gradient-based deterministic methods utilize a formulation, which changes as soon as the problem is modified. For the IHTPs, complexity increases due to the presence of several temperature-dependent properties, thus evolutionary algorithms were identified suitable for the solution of IHTPs.

Motivated by this need, the implementation of evolutionary algorithms on the second application of fins under the second objective was done. Fins have wide applications such as in

industrial boilers and heat exchangers. Apart from the application part, the contributions of the second application, unlike the steady-state analysis of composite walls, was to involve the transient state retrieval of heat flux through inverse analysis. For the current study, an experimental setup with thermocouples as temperature sensors was selected, and experiments were performed to obtain the temperature profile of the fin. A mathematical model with temperature-dependent thermal parameters was created. The created model was highly non-linear and was solved using Matlab's pdepe. The obtained temperature profile was utilized to retrieve the functional form of time-dependent heat flux. As only a single parameter was to be retrieved, thus GSSM was implemented, which was found suitable in literature for the retrieval of a single parameter. Under dynamic conditions, heat flux was retrieved using both the computed and experimental temperature profiles. The observed retrieval trends were similar. To contribute towards the performance of the fin, the effect of measurement errors on the retrieval was depicted. The acceptable measurement errors in temperature are 3%, 2%, and 2% with a maximum error of 6.8%, 9.6%, and 14% respectively for the constant, triangular and realistic profile of heat flux under dynamic conditions. This analysis was done when the temperature profile was obtained through forward analysis. However, in various applications, the temperature measurements are recorded through "not so accurate" instruments. Such instruments contain uncertainty. Corresponding to the temperature profile at $V = 80$V, 60V, 70V and $I = 0.027\text{A}, 0.018\text{A}, 0.022\text{A}$, the quantified uncertainties in the reconstructed heat flux for the triangular case were reported as 9.5%, 8% and 9%. Also, for the retrieval of realistic heat flux, these uncertainties were 5%, 6% and 2%, respectively. Thus, an error bound for the retrieval of heat flux was determined for the case when measurement temperature data contains errors. The proposed procedure is useful to determine the auto-cut for various devices for their efficient working.

After retrieving the heat flux in fin, the next study involved retrieval of several parameters through inverse analysis. Based on the sensitivity of these parameters with 1% perturbation, six parameters, namely, Φ, β, Nc, Nr, Bi, N_{br} were considered critical. These parameters affect the temperature largely, as these represent important heat transfer parameters, with Φ responsible for initializing the heat transfer process, Nc, Nr responsible for the mode of heat transfer, β responsible for material thermal conductivity and Bi, N_{br} for heat transfer at the fin tip. The temperature profile was obtained both through experiments and Matlab's pdepe. To retrieve these identified parameters, a suitable inversion algorithm was explored in the literature. In the literature, no such unique algorithm was reported, which was capable to solve every kind of non-linear parameter estimation. The main research question, "Is there a technique that works globally for every inverse problem?", which was asked in view of the first objective, was answered partially. To get a complete picture, another question, "What if the available techniques were not utilized to an extent that they should?" was posed. The literature survey reported that no such method was available, which work for the non-linear inverse problem from every field. This was explained using No Free Lunch (NFL) theorem. Therefore, to fulfil the third

objective, a general comparative procedure was developed, such that the researchers may select an algorithm by comparison, which is particularly suitable to them. The significance of this formulation is to enhance the overall efficiency of parameter estimation through inverse analysis. This formulation was developed on highly non-linear, ill-posed inverse problem of extended surfaces. To mitigate the associated ill-posedness, regularization by modification in the objective function was proposed. A suitable objective function out of least squares, Tikhonov/Ridge regularization, lasso estimators and elastic net techniques was selected by comparing the total relative error and the CPU time. Elastic net regularization ($\lambda = 0.9$) was selected with an error of 0.39 and CPU time of 34s. The regularization parameter $\alpha = 10^{-4}$ was selected based on the minimum total relative error (3.87). Thereafter, optimization was performed to retrieve the identified critical parameters, with algorithms taken from different categories. TOPSIS analysis was implemented to compare among evolution-based (DE), swarm-based (PSO, WOA), nature-based (WCA, BOA), physics-based (ASO) and hybrid (GWOCS) algorithms. Using the pdepe-based temperature profile, the best algorithm, along with their performance parameter was obtained in the order BOA (0.77), WOA (0.75) and WCA (0.74), respectively. However, WOA (0.78) worked best when experimental temperature profile was utilized, suggesting the robustness of WOA, with elastic regularization ($\lambda = 0.9$, $\alpha = 10^{-4}$) for extended surfaces. A framework for comparing several algorithms was proposed where a ranking was provided by TOPSIS. This developed framework could easily be implemented for any other inverse problem for parameter estimation.

To test the applicability of the proposed framework, a third application under the second objective was implemented. The best inversion algorithm obtained previously, WOA and a hybrid GWOCS were utilized and their suitability, together with the bio-medical problem to detect tumor in the human brain was studied. Pennes model was used for the formulation of the bioheat transfer within the human brain, which was solved using Matlab's pdepe. Different segments were classified into different layers. Using inverse analysis, the unknown blood perfusion rate ω_i was retrieved in the regularized environment. As the real temperature data contains error, thus an error analysis on the current problem was also done. It was observed that at positions where tumor cells were present, the temperature rises. Moreover, with an increase in time, the temperature of the cancer cells increased, whereas no change in the tissue without tumor is seen. This observation in the forward analysis is a slight hint of the presence of tumor. For the inversion process, after the forward analysis with pdepe, regularization was performed. It was observed that elastic net regularization with parameters, $\lambda = 0.1$, $\alpha = 10^{-2}$ for WOA and $\lambda = 0.9$, $\alpha = 10^{-4}$ for GWOCS shows the least RE. After regularization, the perfusion rate was retrieved, where the presence of tumor is detected quite effectively, with a clear distinction of two tumors from the brain tissue. A little deviation in retrieved perfusion rate with $e = 2\%$ by WOA and with $e = 2\%, 4\%$ by GWOCS is seen. The obtained perfusion rate was used to reconstruct temperature profile, to check the quality of retrieval. An excellent matching of

reconstructed temperature field and the exact field, even when the forward data contain noise $e = 0\%, 1\%, 2\%, 3\%, 4\%, 7\%$, concludes that the obtained set of perfusion rate is appropriate for tumor detection. Thus, the proposed comparative procedure was found suitable for the bio-heat transfer problem.

7.2 Future Directions

There is a never-ending future scope for the current thesis. Few directions are listed below.

Experimental studies involving the exchange of heat in heat exchanger could be one possible direction for research. In this thesis, a comparative framework has been constructed, with application to extended surfaces. Thus, the methodology can be generalized to study both the heat and mass transfer processes involved in heat exchangers.

The error analysis performed in this thesis could be utilized in the production of appliances, where a tolerance limit has to predefine for the device to work effectively.

For the tumor detection, the forward model presented by Pennes can be improved. It could be done by considering the effect of temperature on the thermal properties or by implementing the dual-phase and fractional bioheat models. Moreover, time-dependent retrieval through the given inversion strategy could also be performed. In addition, real-time experimental temperature data could be utilized for the detction of tumor through thermal images.

In addition to parameter estimation, current techniques could also be implemented for function estimation. Moreover, inverse techniques involving optimization algorithms with multiple objectives could be one possible direction.

Extending the results of the present work to higher dimensions with irregular geometries is one possible direction.

Another direction for the development of new inversion technique involves that by wavelets. Despite the huge advantages of wavelets, wavelet methods found sparse usage in literature for the solution of IHTP. Only the Meyer wavelets and Shannon wavelets were used in the combination of the least-square method, whereas a large number of other wavelets, for example, Morlet wavelets, Daubechies wavelets, diffusion wavelets, spectral graph wavelet etc. can be used. Being an emerging area in IHTPs, new methods and techniques could be developed using wavelets. One such method for IHTP includes vaguelette.

In addition to wavelet techniques, one can apply the technique of wavelet shrinking for regularization. This technique can efficiently clean the data. Moreover, there is a never-ending scope to generate and test hybrid techniques, using wavelets, deterministic methods, any analytical or semi-analytical method and heuristic method. Developing such techniques and exploring the developed techniques by providing solutions to the challenging problems of interest, for

example, heat transfer in aviation could be seen as a future direction of work in IHTPs.

Apart from constructing newer and better techniques, the applicability of methods to solve everyday inverse problems would be significant and an enlightening process.

Bibliography

Abbas, I.A. and Youssef, H.M. (2012). A nonlinear generalized thermoelasticity model of temperature-dependent materials using finite element method. *Int. J. Thermophys.*, **33**, 1302–1313.

Abbas, I.A., El-Amin, M. and Salama, A. (2009). Effect of thermal dispersion on free convection in a fluid saturated porous medium. *Int J Heat Fluid Flow*, **30**, 229–236.

Adomian, G. (1988). A review of the decomposition method in applied mathematics. *J. Math. Anal. & Appl.*, **135**, 501–544.

Adomian, G. (2013). *Solving frontier problems of physics: the decomposition method*. Springer Science & Business Media.

Agazzi, A., Sobotka, V., LeGoff, R. and Jarny, Y. (2014). Inverse method for the cooling system design in injection moulding–application to a 't-shaped'piece. *Inverse Probl Sci En.*, **22**, 707–726.

Agnelli, J.P., Barrea, A.A. and Turner, C.V. (2011a). Tumor location and parameter estimation by thermography. *Math Comput Model*, **53**, 1527–1534.

Agnelli, J.P., Padra, C. and Turner, C.V. (2011b). Shape optimization for tumor location. *Comput. Math. with Appl.*, **62**, 4068–4081.

Agrawal, K. (2016). An analytical approach for inverse heat conduction problem. *SSRG Int. J. Mech. Eng.*, **3**, 362–365.

Aijaz, M. and Dar, J.G. (2017). Mathematical analysis of bioheat equation for the study of thermal stress on human brain. *Appl. Math. Inf. Sci.*, **5**, 33–39.

Al-Najem, N., Osman, A., El-Refaee, M. and Khanafer, K. (1998). Two dimensional steady-state inverse heat conduction problems. *Int Commun Heat Mass*, **25**, 541 – 550.

Alifanov, O. and Nenarokomov, A. (1999). Three-dimensional boundary inverse heat conduction problem for regular coordinate systems. *Inverse Probl. in engineering*, **7**, 335–362.

Alifanov, O. and Nenarokomov, A. (2001). Boundary inverse heat conduction problem: algorithm and error analysis. *Inverse Probl. in Engineering*, **9**, 619–644.

Alifanov, O., Nenarokomov, A. and Gonzalez, V. (2008). Radiative-conductive inverse problem for lumped parameter systems. In *Journal of Physics: Conference Series*, vol. 135, 012005.

Alifanov, O., Nenarokomov, A. and Gonzalez, V. (2009). Study of multilayer thermal insulation by inverse probl. method. *Acta Astronaut.*, **65**, 1284–1291.

Alifanov, O., Budnik, S., Nenarokomov, A. and Netelev, A. (2012). Estimation of thermal properties of materials with application for inflatable spacecraft structure testing. *Inverse Probl Sci En.*, **20**, 677–690.

Alifanov, O.M. (1994). *Inverse Heat Transfer Problems*. Springer-Verlag, New York.

Alifanov, O.M. and Artyukhin, E.A. (1975). Regularized numerical solution of nonlinear inverse heat-conduction problem. *J. Engg. Physics Thermophysics*, **29**, 934–938.

Alifanov, O.M., Artyukhin, E. and Rumyantsev, A. (1995). *Extreme Methods for Solving Ill-Posed Problems with Applications to Inverse Heat Transfer Problems*. Begell House, New York.

Alifanov, O.M., Nenarokomov, A., Budnik, S., Michailov, V. and Ydin, V. (2004). Identification of thermal properties of materials with applications for spacecraft structures. *Inverse Probl Sci En.*, **12**, 579–594.

Aloraini, A. (2017). On the prediction accuracies of three most known regularizers: ridge regression, the lasso estimate, and elastic net regularization methods. *IJAIA*, **8**, 29–36.

Amini, F. and Ghaderi, P. (2013). Hybridization of harmony search and ant colony optimization for optimal locating of structural dampers. *Appl. Soft Comput.*, **13**, 2272–2280.

An, C. and Su, J. (2011). Improved lumped models for transient combined convective and radiative cooling of multi-layer composite slabs. *Appl. Therm. Engg.*, **31**, 2508–2517.

Ancey, C. (2005). Solving the couette inverse problem using a wavelet-vaguelette decomposition. *J Rheol*, **49**, 441–460.

Arora, S. and Singh, S. (2019). Butterfly optimization algorithm: a novel approach for global optimization. *Soft Comput.*, **23**, 715–734.

Arora, U., Karaa, S. and Mohanty, R. (2006). A new stable variable mesh method for 1-d non-

linear parabolic partial differential equations. *Appl. Math. Comput.*, **181**, 1423–1430.

Artyukhin, E. and Nenarokomov, A. (1984). Deriving the thermal contact resistance from the solution of the inverse heat-conduction problem. *J. Eng. Phys.*, **46**, 495–499.

Askarizadeh, H. and Ahmadikia, H. (2015). Analytical study on the transient heating of a two-dimensional skin tissue using parabolic and hyperbolic bioheat transfer equations. *Appl. Math. Model.*, **39**, 3704–3720.

Aviles-Ramos, C., Haji-Sheikh, A. and Beck, J. (1998). Exact solution of heat conduction in composite materials and application to inverse probl. *J Heat Transfer*, **120**, 592–599.

Axaopoulos, I., Axaopoulos, P. and Gelegenis, J. (2014). Optimum insulation thickness for external walls on different orientations considering the speed and direction of the wind. *Appl. Energy*, **117**, 167–175.

Aziz, A. and Torabi, M. (2012). Convective-radiative fins with simultaneous variation of thermal conductivity, heat transfer coefficient, and surface emissivity with temperature. *Heat Transfer Asian Res.*, **41**, 99–113.

Aziz, M.A.E., Ewees, A.A. and Hassanien, A.E. (2017). Whale optimization algorithm and moth-flame optimization for multilevel thresholding image segmentation. *Expert Syst. Appl.*, **83**, 242–256.

Backus, G. and Gilbert, J. (1967). Numerical applications of a formalism for geophysical inverse probl. *Geophys. J. Roy. Astr. Soc.*, **13**, 247–276.

Backus, G. and Gilbert, J. (1968). The resolving power of gross earth data. *Geophys. J. Roy. Astr. Soc.*, **16**, 169–205.

Badeva, V. and Morozov, V. (1991). *Problèmes incorrectement posés: théorie et applications en identification, filtrage optimal, contrôle optimal, analyse et synthèse de systèmes, reconnaissance d'images*. Masson, Paris.

Badrinarayanan, S. and Zabaras, N. (1996). A sensitivity analysis for the optimal design of metal-forming processes. *Comput Methods Appl Mech Eng*, **129**, 319–348.

Bahadori, R., Gutierrez, H., Manikonda, S. and Meinke, R. (2018). A mesh-free monte-carlo method for simulation of three-dimensional transient heat conduction in a composite layered material with temperature dependent thermal properties. *Int. J. Heat Mass Transfer*, **119**, 533–541.

Bailleul, J.L., Sobotka, V., Delaunay, D. and Jarny, Y. (2003). Inverse algorithm for optimal processing of composite materials. *Compos. Part A Appl. Sci. Manuf.*, **34**, 695–708.

Bangian-Tabrizi, A. and Jaluria, Y. (2018). An optimization strategy for the inverse solution of a convection heat transfer problem. *Int. J. Heat Mass Transf.*, **124**, 1147 – 1155.

Bard, Y.B. (1974). *Nonlinear Parameter Estimation*. Acad. Press, New York.

Bass, B. (1980). Application of the finite element method to the nonlinear inverse heat conduction problem using beck's second method. *J. Ind. Eng. Int.*, **102**, 168–176.

Beale, E.M.L. (1972). A derivation of conjugate gradients. *Numerical Methods for Nonlinear Optimization*, 39–43.

Beck, J., Blackwell, B. and Haji-Sheikh, A. (1996a). Comparison of some inverse heat conduction methods using experimental data. *Int. J. Heat Mass Transf.*, **39**, 3649 – 3657.

Beck, J., Blackwell, B. and Haji-Sheikh, A. (1996b). Comparison of some inverse heat conduction methods using experimental data. *Int. J. Heat Mass Transf.*, **39**, 3649–3657.

Beck, J.V. (1970). Nonlinear estimation applied to the nonlinear inverse heat conduction problem. *Int. J. Heat Mass Transf.*, **13**, 703 – 716.

Beck, J.V. (1979). Criteria for comparison of methods of solution of the inverse heat conduction problem. *Nucl. Eng. Des.*, **53**, 11 – 22.

Beck, J.V. and Arnold, K.J. (1977). *Parameter Estimation in Engineering and Science*. Wiley Interscience, New York.

Beck, J.V. and Murio, D.A. (1986). Combined function specification-regularization procedure for solution of inverse heat conduction problem. *AIAA J.*, **24**, 180–185.

Beck, J.V., Blackwell, B. and Clair Jr, C.R.S. (1985). *Inverse heat conduction: Ill-posed problems*. A Wiley-lnterscience Publication.

Beiranvand, V., Hare, W. and Lucet, Y. (2017). Best practices for comparing optimization algorithms. *Optim. Eng.*, **18**, 815–848.

Belegundu, A.D. and Chandrupatla, T.R. (1999). *Optimization Concepts And Applications In Engineering*. Prentice Hall.

Belghazi, H., Ganaoui, M.E. and Labbe, J.C. (2010). Analytical solution of unsteady heat conduction in a two layered material in imperfect contact subjected to a moving heat source. *Int. J. Therm. Sci*, **49**, 311–318.

Berdnik, V.V. and Mukhamedyarov, R. (2003). Application of the method of neural networks to solution of the inverse problem of heat transfer. *High Temp.*, **41**, 839–843.

Bertelli, F., Silva-Santos, C.H., Bezerra, D.J., Cheung, N. and Garcia, A. (2015). An effective inverse heat transfer procedure based on evolutionary algorithms to determine cooling conditions of a steel continuous casting machine. *Mater. Manuf. Process*, **30**, 414–424.

Bhowmik, A., Singh, R., Repaka, R. and Mishra, S.C. (2013a). Conventional and newly developed bioheat transport models in vascularized tissues: A review. *J. Therm. Biol.*, **38**, 107–125.

Bhowmik, A., Singla, R.K., Roy, P.K., Prasad, D.K., Das, R. and Repaka, R. (2013b). Predicting geometry of rectangular and hyperbolic fin profiles with temperature-dependent thermal properties using decomposition and evolutionary methods. *Energy Convers. Manag.*, **74**, 535–547.

Bildik, N. and Konuralp, A. (2006). Two-dimensional differential transform method, adomian's decomposition method, and variational iteration method for partial differential equations. *Int J Comput Math*, **83**, 973–987.

Bonesky, T., Dahlke, S., Maass, P. and Raasch, T. (2010). Adaptive wavelet methods and sparsity reconstruction for inverse heat conduction problems. *Adv Comput Math*, **33**, 385–411.

Bouchouareb, R. and Benatia, D. (2014). Comparative study between wavelet thresholding techniques (hard, soft and invariant-translation) in ultrasound images. *J. BioSci. Biotechnol.*, **6**, 29–38.

Bouzidi, M. and Duhamel, P. (1982). Study of the transient heat conduction regime in the composite wall of an anode firing furnace. In *International Heat Transfer Conference Digital Library*, Begel House Inc.

Broyden, C.G. (1965). A class of methods for solving nonlinear simultaneous equations. *Math. Comp.*, **19**, 577–593.

Broyden, C.G. (1967). Quasi-newton methods and their applications to function minimization. *Math. Comp.*, **21**, 368–380.

Burggraf, O. (1964). An exact solution of the inverse problem in heat conduction theory and applications. *J. Heat Transfer.*.

Cabeza, J.M.G., García, J.A.M. and Rodríguez, A.C. (2005). A sequential algorithm of inverse heat conduction problems using singular value decomposition. *Int. J. Therm. Sci.*, **44**, 235 – 244.

Candau, Y. (2005). Solving inverse heat conduction problem with discrete wavelet transform. *Inverse Probl Sci En.*, **13**, 329–339.

Cattani, L., Maillet, D., Bozzoli, F. and Rainieri, S. (2015). Estimation of the local convective

heat transfer coefficient in pipe flow using a 2d thermal quadrupole model and truncated singular value decomposition. *Int. J. Heat Mass Transf.*, **91**, 1034 – 1045.

Cavazzuti, M. and Corticelli, M.A. (2017). An algorithm for solving steady-state heat conduction in arbitrarily complex composite planar walls with temperature-dependent thermal conductivities. *Appl. Therm. Engg.*, **115**, 825–831.

Cebula, A. and Taler, J. (2014). Determination of transient temperature and heat flux on the surface of a reactor control rod based on temperature measurements at the interior points. *Appl. Therm. Eng.*, **63**, 158–169.

Cebula, A., Taler, J. and Ocłoń, P. (2018). Heat flux and temperature determination in a cylindrical element with the use of finite volume finite element method. *Int. J. Therm. Sci.*, **127**, 142–157.

Cengel, Y.A. (2002). *Heat transfer: a practical approach*. McGraw-Hill.

Chan, T.F. and Shen, J. (2005). *Image processing and analysis: Variational, PDE, Wavelet and Stochastic Methods*. SIAM, Philadelphia, PA.

Chang, C.W., Liu, C.H. and Wang, C.C. (2018). Review of computational schemes in inverse heat conduction problems. *Smart Sci.*, **6**, 94–103.

Chantasiriwan, S. (2000). Inverse determination of steady-state heat transfer coefficient. *Int Commun Heat Mass*, **27**, 1155 – 1164.

Chen, H., Xu, Y., Wang, M. and Zhao, X. (2019). A balanced whale optimization algorithm for constrained engineering design problems. *Appl. Math. Model.*, **71**, 45–59.

Chen, H.T. and Wu, X.Y. (2007). Estimation of surface conditions for nonlinear inverse heat conduction problems using the hybrid inverse scheme. *Numer. Heat Transf. , Part B: Fundamentals*, **51**, 159–178.

Chen, H.T. and Wu, X.Y. (2008). Investigation of heat transfer coefficient in two-dimensional transient inverse heat conduction problems using the hybrid inverse scheme. *Int J Numer Methods Eng*, **73**, 107–122.

Chen, T.C. and Tuan, P.C. (2005). Input estimation method including finite-element scheme for solving inverse heat conduction problems. *Numer. Heat Transf. , Part B: Fundamentals*, **47**, 277–290.

Chen, W.L., Chou, H.M., Lee, H.L. and Yang, Y.C. (2014). An inverse hyperbolic heat conduction problem in estimating base heat flux of two-dimensional cylindrical pin fins. *Int Commun Heat Mass*, **52**, 90 – 96.

Chen, W.L., Chou, H.M. and Yang, Y.C. (2017a). Inverse estimation of the unknown base heat flux in irregular fins made of functionally graded materials. *Int. Comm. Heat Mass Transfer*, **87**, 157–163.

Chen, W.L., Chou, H.M. and Yang, Y.C. (2017b). Inverse estimation of the unknown base heat flux in irregular fins made of functionally graded materials. *Int Commun Heat Mass*, **87**, 157–163.

Cheng, C., Lin, H.H. and Aung, W. (2003). Optimal shape design for packaging containing heating elements by inverse heat transfer method. *Heat Mass Transf*, **39**, 687–692.

Cheng, C.H. and Chang, M.H. (2003). Shape identification by inverse heat transfer method. *J Heat Transfer*, **125**, 224–231.

Cheng, W. and Fu, C.L. (2009). Solving the axisymmetric inverse heat conduction problem by a wavelet dual least squares method. *Bound. Value Probl.*, **2009**, 260941.

Cheng, W. and Ma, Y.J. (2016). A modified regularization method for an inverse heat conduction problem with only boundary value. *Bound. Value Probl.*, **2016**, 100.

Cheng, W., Zhang, Y.Q. and Fu, C.L. (2013). for an inverse heat conduction problem with convection term. *Electron. J. Differ. Equ.*.

Chinsuwan, A., Dutta, A. and Janlasad, N. (2014). Prediction of the heat flux profile on the furnace wall of circulating fluidized bed boilers. *J Energy Inst*, **87**, 314–320.

Choudhary, V., Kumar, M. and Patil, A.K. (2019). Experimental investigation of enhanced performance of pin fin heat sink with wings. *Appl. Therm. Eng.*, **155**, 546–562.

Cohen, A., Hoffmann, M. and Reiss, M. (2004). Adaptive wavelet galerkin methods for linear inverse probl. *SIAM J Numer Anal*, **42**, 1479–1501.

Colaco, M.J. and Orlande, H.R.B. (1999). Comparison of different versions of the conjugate gradient method of function estimation. *Numer. Heat Transf. , Part A: Applications*, **36**, 229–249.

Colaco, M.J., Orlande, H.R.B. and Dulikravich, G.S. (2006). Inverse and optimization problems in heat transfer. *J. of the Braz. Soc. of Mech. Sci. & Eng*, **28**, 1–24.

Colaço, M.J., Orlande, H.R.B. and Dulikravich, G.S. (2006). Inverse and optimization problems in heat transfer. *J. Braz. Soc. Mech. Sci. & Eng.*, **28**, 1–24.

Cormier, Y., Dupuis, P., Farjam, A., Corbeil, A. and Jodoin, B. (2014). Additive manufacturing of pyramidal pin fins: Height and fin density effects under forced convection. *Int. J. Heat*

Mass Transf., **75**, 235–244.

Cortes, C. and Diez, L. (2010). New analytical solution of heat transfer in insulated wires. *Int. J. Therm. Sci.*, **49**, 2391–2399.

Cortés, O., Urquiza, G., Hernandez, J. and Cruz, M.A. (2007). Artificial neural networks for inverse heat transfer problems. In *Electronics, Robotics and Automotive Mechanics Conference (CERMA 2007)*, 198–201.

Cui, M., Zhu, Q. and Gao, X. (2014). A modified conjugate gradient method for transient nonlinear inverse heat conduction problems: A case study for identifying temperature-dependent thermal conductivities. *J Heat Transfer*, **136**.

Cui, M., Yang, K., liang Xu, X., dong Wang, S. and wei Gao, X. (2016a). A modified levenberg-marquardt algorithm for simultaneous estimation of multi-parameters of boundary heat flux by solving transient nonlinear inverse heat conduction problems. *Int. J. Heat Mass Transf.*, **97**, 908 – 916.

Cui, M., Yang, K., Xu, X.l., Wang, S.d. and Gao, X.w. (2016b). A modified levenberg–marquardt algorithm for simultaneous estimation of multi-parameters of boundary heat flux by solving transient nonlinear inverse heat conduction problems. *Int. J. Heat Mass Transf.*, **97**, 908–916.

Cui, M., Zhao, Y., Xu, B. and wei Gao, X. (2017). A new approach for determining damping factors in levenberg-marquardt algorithm for solving an inverse heat conduction problem. *Int. J. Heat Mass Transf.*, **107**, 747 – 754.

Czèl, B. and Gróf, G. (2012). Inverse identification of temperature-dependent thermal conductivity via genetic algorithm with cost function-based rearrangement of genes. *Int. J. Heat Mass Transf.*, **55**, 4254 – 4263.

Czél, B., Woodbury, K.A. and Gróf, G. (2014). Simultaneous estimation of temperature-dependent volumetric heat capacity and thermal conductivity functions via neural networks. *Int. J. Heat Mass Transf.*, **68**, 1–13.

Daouas, N. (2011). A study on optimum insulation thickness in walls and energy savings in tunisian buildings based on analytical calculation of cooling and heating transmission loads. *Energy Convers Manage*, **88**, 156–164.

Das, K. and Mishra, S.C. (2013a). Estimation of tumor characteristics in a breast tissue with known skin surface temperature. *J. Therm. Biol.*, **38**, 311–317.

Das, K. and Mishra, S.C. (2013b). Estimation of tumor characteristics in a breast tissue with known skin surface temperature. *J. Therm. Biol.*, **38**, 311–317.

Das, K. and Mishra, S.C. (2014). Non-invasive estimation of size and location of a tumor in a human breast using a curve fitting technique. *Int Commun Heat Mass*, **56**, 63–70.

Das, K. and Mishra, S.C. (2015). Simultaneous estimation of size, radial and angular locations of a malignant tumor in a 3-d human breast–a numerical study. *J. Therm. Biol.*, **52**, 147–156.

Das, R. (2011). A simplex search method for a conductive–convective fin with variable conductivity. *Int. J. Heat Mass Transf.*, **54**, 5001–5009.

Das, R. (2012). Application of genetic algorithm for unknown parameter estimations in cylindrical fin. *Appl. Soft Comput.*, **12**, 3369–3378.

Das, R. (2014). Forward and inverse solutions of a conductive, convective and radiative cylindrical porous fin. *Energ Convers Manage*, **87**, 96–106.

Das, R. and Kundu, B. (2018). Estimation of internal heat generation in a fin involving all modes of heat transfer using golden section search method. *Heat Transf. Eng.*, **39**, 58–71.

Das, R. and Ooi, K. (2013). Application of simulated annealing in a rectangular fin with variable heat transfer coefficient. *Inverse Probl Sci En*, **21**, 1352–1367.

Das, R. and Prasad, D.K. (2015). Prediction of porosity and thermal diffusivity in a porous fin using differential evolution algorithm. *Swarm Evol. Comput.*, **23**, 27 – 39.

Das, R. and Singla, R.K. (2014). Inverse heat transfer study of a nonlinear straight porous fin using hybrid optimization. In *Gas Turbine India Conference*, vol. 49644, V001T04A001, American Society of Mechanical Engineers.

Das, R., Singh, K. and Gogoi, T.K. (2017). Estimation of critical dimensions for a trapezoidal-shaped steel fin using hybrid differential evolution algorithm. *Neural Comput Appl*, **28**, 1683–1693.

Daun, K., França, F., Larsen, M., Leduc, G. and Howell, J.R. (2006). Comparison of methods for inverse design of radiant enclosures. *J Heat Transfer*, **128**, 269–282.

Davies, J. (1966). Input power determined from temperatures in simulated skin protected against thermal radiation. *J Heat Transfer*, **88**, 154–159.

De Jong, K.A. (1975). *An Analysis of the Behavior of a Class of Genetic Adaptive Systems.*. Ph.D. thesis, University of Michigan.

de Monte, F. (2000). Transient heat conduction in one-dimensional composite slab. a natural analytic approach. *Int. J. Heat Mass Transfer*, **43**, 3607–3619.

de Monte, F. (2002). An analytic approach to the unsteady heat conduction processes in one-

dimensional composite media. *Int. J. Heat Mass Transfer*, **45**, 1333–1343.

Deb, A., Roy, J.S. and Gupta, B. (2014). Performance comparison of differential evolution, particle swarm optimization and genetic algorithm in the design of circularly polarized microstrip antennas. *IEEE Trans. Antennas Propag.*, **62**, 3920–3928.

Deng, S. and Hwang, Y. (2006). Applying neural networks to the solution of forward and inverse heat conduction problems. *Int. J. Heat Mass Transf.*, **49**, 4732–4750.

Deng, Z.C., Yu, J.N. and Yang, L. (2008). Optimization method for an evolutional type inverse heat conduction problem. *J. Phys. A Math. Theor.*, **41**, 035201.

Dennis, J. and Schnabel, R. (1983). *Numerical Methods for Unconstrained Optimization and Nonlinear Equations*. Prentice Hall.

Deolmi, G. and Marcuzzi, F. (2013). A parabolic inverse convection-diffusion-reaction problem solved using space-time localization and adaptivity. *Appl. Math. Comput.*, **219**, 8435 – 8454.

Dheeba, J. and Selvi, T. (2010). Bio inspired swarm algorithm for tumor detection in digital mammogram. In *International Conference on Swarm, Evolutionary, and Memetic Computing*, 404–415.

Dhiman, S. and Prasad, J. (2017). Inverse estimation of heat flux from a hollow cylinder in cross-flow of air. *Appl. Therm. Eng.*, **113**, 952–961.

Diligenskaya, A.N. and Rapoport, É.Y. (2016). Method of minimax optimization in the coefficient inverse heat-conduction problem. *J. Eng. Phys. Thermophys.*, **89**, 1008–1013.

Ding, P. (2012). Solution of inverse convection heat transfer problem using an enhanced particle swarm optimization algorithm. *J Heat Transfer*.

Ding, P. and Sun, D.L. (2015). Resolution of unknown heat source inverse heat conduction problems using particle swarm optimization. *Numer. Heat Transf. , Part B: Fundamentals*, **68**, 158–168.

Dittus, F. and Boelter, L. (1985). Heat transfer in automobile radiators of the tubular type. *Int. Commun. Heat Mass*, **12**, 3–22.

Dmitriev, O.S. and Zhivenkova, A.A. (2018). Numerical-analytical solution of the nonlinear coefficient inverse heat conduction problem. *J. Eng. Phys. Thermophys.*.

Donoho, D.L. (1995). Nonlinear solution of linear inverse probl. by wavelet-vaguelette decomposition. *Appl. Comp. Har. Anal.*, **2**, 101 – 126.

Donoho, D.L. and Johnstone, I.M. (1994). Ideal spatial adaption via wavelet shrinkage.

Biometrika, **81**, 425–455.

Donoho, D.L. and Johnstone, I.M. (1995). Adapting to unknown smoothness via wavelet shrinkage. *J. Amer. Stat. Asso.*, **90**, 1200–1224.

Dou, F.F. and Fu, C.L. (2009). Determining an unknown source in the heat equation by a wavelet dual least squares method. *Appl. Math. Lett.*, **22**, 661 – 667.

Dowding, K.J. and Beck, J.V. (1999). A sequential gradient method for the inverse heat conduction problem (ihcp). *J Heat Transfer*, **121**.

Dubot, F., Favennec, Y., Rousseau, B., Jarny, Y. and Rousse, D.R. (2016). Quasi-optimal tikhonov penalization and parameterization coarseness in space-dependent function estimation. *Inverse Probl Sci En.*, **24**, 465–481.

Duda, P. and Taler, J. (2000). Numerical method for the solution of non-linear two-dimensional inverse heat conduction problem using unstructured meshes. *Int J Numer Methods Eng*, **48**, 881–899.

Dulikravich, G.S. and Martin, T.J. (1996). *Inverse Shape and Boundary Condition Problems and Optimization in Heat Conduction (Chapter-10)*. Taylor and Francis.

El Bagdouri, M. and Jarny, Y. (1987). Optimal boundary control of a thermal system: inverse conduction problem. *IFAC Proceedings Volumes*, **20**, 389–393.

Eldèn, L. (1997). Solving an inverse heat conduction problem by a "method of lines". *J Heat Transfer*, **119**.

Emery, A. (2008). Inverse probl. with errors in the independent variables errors-in-variables, total least squares, and bayesian inference. In *ASME International Mechanical Engineering Congress and Exposition*, vol. 48715, 881–892.

Engl, H.W., Hanke, M. and Neubaue, A. (1996). *Regularization of Inverse Probl.*. Kluwer Academic Publishers, The Netherlands.

Eskandar, H., Sadollah, A., Bahreininejad, A. and Hamdi, M. (2012). Water cycle algorithm-a novel metaheuristic optimization method for solving constrained engineering optimization problems. *Comput Struct*, **110**, 151–166.

Farahani, S., Kowsary, F. and Jamali, J. (2014). Direct estimation of local convective boiling heat transfer coefficient in mini-channel by using conjugated gradient method with adjoint equation. *Int Commun Heat Mass*, **55**, 1 – 7.

Farzad, M. and Mathieu, S. (2016). Estimation of thermal conductivity, heat transfer coefficient,

and heat flux using a three dimensional inverse analysis. *Int. J. Therm. Sci.*, **99**, 258 – 270.

Fatullayev, A.G. (2002). Numerical solution of the inverse problem of determining an unknown source term in a heat equation. *Math Comput Simul*, **58**, 247 – 253.

Favennec, Y., Girault S, M. and Petit, D. (2006). The adjoint method coupled with the modal identification method for nonlinear model reduction. *Inverse Probl Sci En.*, **14**, 153–170.

Fazeli, H. and Mirzaei, M. (2012). Shape identification problems on detecting of defects in a solid body using inverse heat conduction approach. *J. Mech. Sci. Technol*, **26**, 3681–3690.

Ferlauto, M. (2014). An inverse method of designing the cooling passages of turbine blades based on the heat adjoint equation. *P I Mech Eng A-J Pow*, **228**, 328–339.

Figueiredo, A.A.A., Fernandes, H.C., Malheiros, F.C. and Guimaraes, G. (2020). Influence analysis of thermophysical properties on temperature profiles on the breast skin surface. *Int Commun Heat Mass*, **111**, 104453.

Flach, G.P. and Özışık, M.N. (1989). Inverse heat conduction problem of simultaneously estimating spatially varying thermal conductivity and heat capacity per unit volume. *Numer. Heat Transf. , Part A: Applications*, **16**, 249–266.

Fletcher, R. (2000). *Practical Methods of Optimization*. John Wiley & Sons.

Fletcher, R. and Powell, M.J.D. (1963). A rapidly convergent descent method for minimization. *Computer J.*, **6**, 163–168.

Fletcher, R. and Reeves, C.M. (1964). Function minimization by conjugate gradients. *Comput. Journal*, **7**, 149–154.

FLIR (2018). Infrared camera accuracy and uncertainty in plain language. https://www.flir.in/discover/rd-science/infrared-camera-accuracy-and-uncertainty-in-plain-language/, accessed: 2020-12-07.

Frąckowiak, A., Botkin, N.D., Ciałkowski, M. and Hoffmann, K.H. (2015). Iterative algorithm for solving the inverse heat conduction problems with the unknown source function. *Inverse Probl Sci En.*, **23**, 1056–1071.

Frank, I. (1963). An application of least squares method to the solution of the inverse problem of heat conduction. *J. Heat Transfer.*.

Fu, C.L., Zhu, Y.B. and Qiu, C.Y. (2003). Wavelet regularization for an inverse heat conduction problem. *J. Math. Anal. Appl.*, **288**, 212 – 222.

Ganji, D., Rahimi, M., Rahgoshay, M. and Jafari, M. (2011). Analytical and numerical investigation of fin efficiency and temperature distribution of conductive, convective, and radiative straight fins. *Heat Transfer Asian Res.*, **40**, 233–245.

García, J.A.M., Cabeza, J.M.G. and Rodríguez, A.C. (2009). Two-dimensional non-linear inverse heat conduction problem based on the singular value decomposition. *Int. J. Therm. Sci.*, **48**, 1081–1093.

Geng, F. and Lin, Y. (2009). Application of the variational iteration method to inverse heat source problems. *Comput. Math. with Appl.*, **58**, 2098 – 2102.

Gheisarnejad, M. (2018). An effective hybrid harmony search and cuckoo optimization algorithm based fuzzy pid controller for load frequency control. *Appl. Soft Comput.*, **65**, 121–138.

Giedt, W.H. (1955). The determination of transient temperatures and heat transfer at a gas-metal interface applied to a 40-mm gun barrel. *Jet Propulsion*, **25**, 158–162.

Goldberg, D.E. (1989). *Genetic Algorithms in Search, Optimization, and Machine Learning*. Addison-Wesley Pub Co.

Goldstein, R., Eckert, E., Ibele, W., Patankar, S., Simon, T., Kuehn, T., Strykowski, P., Tamma, K., Bar-Cohen, A., Heberlein, J., Davidson, J., Bischof, J., Kulacki, F., Kortshagen, U., Garrick, S. and Srinivasan, V. (2005). Heat transfer-a review of 2002 literature. *Int. J. Heat Mass Transf.*, **48**, 819 – 927.

Goldstein, R., Ibele, W., Patankar, S., Simon, T., Kuehn, T., Strykowski, P., Tamma, K., Heberlein, J., Davidson, J., Bischof, J., Kulacki, F., Kortshagen, U., Garrick, S. and Srinivasan, V. (2006). Heat transfer-a review of 2003 literature. *Int. J. Heat Mass Transf.*, **49**, 451 – 534.

Goyal, K. and Mehra, M. (2011). Wavelets and inverse probl. In *Mathematics In Science And Technology: Mathematical Methods, Models and Algorithms in Science and Technology*, 430–447, World Scientific.

Goyal, K. and Mehra, M. (2012). *Wavelets and Inverse Probl.*, 430–447. WORLD SCIENTIFIC.

Goyal, K. and Singhal, M. (2018). Adomian decomposition method for thermal analysis of a furnace. In *International Conference on Engineering Research and Applications*, 141–148, Springer.

Grossmann, A. and Morlet, J. (1984). Decomposition of hardy functions into square integrable wavelets of constant shape. *SIAM J. Math. Anal.*, **15**, 723–736.

Habibian, S., Abolmaali, A.M. and Afshin, H. (2018). Numerical investigation of the effects

of fin shape, antifreeze and nanoparticles on the performance of compact finned-tube heat exchangers for automobile radiator. *Appl. Therm. Eng.*, **133**, 248–260.

Hadamard, J. (1902). Sur les problèmes aux dérivées partielles et leur signification physique. *Princeton university bulletin*, 49–52.

Hadamard, J. (1923). *Lectures on Cauchy's Problem in Linear Partial Differential Equations*. Yale University Press, H. Milford, Oxford University Press.

Hafid, M. and Lacroix, M. (2018). Inverse method for simultaneously estimating multi-parameters of heat flux and of temperature-dependent thermal conductivities inside melting furnaces. *Appl. Therm. Eng.*, **141**, 981 – 989.

Haghighi, M.G., Malekzadeh, P. and Afshari, M. (2015). Inverse estimation of heat flux and pressure in functionally graded cylinders with finite length. *Compos. Struct.*, **121**, 1 – 15.

Hahn, D.W. and Özışık, M.N. (2012). *Heat Conduction*. John Wiley & Sons INC.

Hansen, P.C. (1994). Regularization tools: A matlab package for analysis and solution of discrete ill-posed problems. *Numer. Algorithms*, **6**, 1–35.

Hào, D.N. and Reinhardt, H.J. (1998). Gradient methods for inverse heat conduction problems. *Inverse Probl. in Engineering*, **6**, 177–211.

Hào, D.N., Thành, N.T. and Sahli, H. (2009). Splitting-based conjugate gradient method for a multi-dimensional linear inverse heat conduction problem. *J. Comput. Appl.*, **232**, 361–377.

Hazanee, A., Lesnic, D., Ismailov, M. and Kerimov, N. (2019). Inverse time-dependent source problems for the heat equation with nonlocal boundary conditions. *Appl. Math. Comput.*, **346**, 800 – 815.

He, H., He, C. and Chen, G. (2015). Inverse determination of temperature-dependent thermophysical parameters using multiobjective optimization methods. *Int. J. Heat Mass Transf.*, **85**, 694 – 702.

Heidari, M. and Garshasbi, M. (2015). Using artificial neural networks in solving heat conduction problems. *Int. J. Oper. Res.*, **12**, 16–20.

Heidari, M., Mortazavi, M. and Rufer, A. (2017). Design, modeling and experimental validation of a novel finned reciprocating compressor for isothermal compressed air energy storage applications. *Energy*, **140**, 1252–1266.

Hematiyan, M., Khosravifard, A. and Shiah, Y. (2015). A novel inverse method for identification of 3d thermal conductivity coefficients of anisotropic media by the boundary element

analysis. *Int. J. Heat Mass Transf.*, **89**, 685 – 693.

Herrando, M., Pantaleo, A.M., Wang, K. and Markides, C.N. (2019). Solar combined cooling, heating and power systems based on hybrid pvt, pv or solar-thermal collectors for building applications. *Renew. Energy*, **143**, 637–647.

Hetmaniok, E., Słota, D., Zielonka, A. and Wituła, R. (2012). Comparison of abc and aco algorithms applied for solving the inverse heat conduction problem. In *Swarm Evol. Comput.*, 249–257, Springer.

Hikavyy, A., Rosseel, E., Kubicek, S., Mannaert, G., Favia, P., Bender, H., Loo, R. and Horiguchi, N. (2016). Properties and growth peculiarities of si0.30ge0.70 stressor integrated in 14 nm fin-based p-type metal-oxide-semiconductor field-effect transistors. *Thin Solid Films*, **602**, 72–77.

Holland, J.H. (1992). *Adaptation in natural and artificial systems: an introductory analysis with applications to biology, control, and artificial intelligence*. MIT press.

Holschneider, M. (1991). Inverse radon transforms through inverse wavelet transforms. *Inverse Probl.*, **7**, 853.

Hon, Y. and Wei, T. (2004). A fundamental solution method for inverse heat conduction problem. *Eng Anal Bound Elem*, **28**, 489 – 495.

Hsieh, C. and Kassab, A.J. (1986). A general method for the solution of inverse heat conduction problems with partially unknown system geometries. *Int. J. Heat Mass Transf.*, **29**, 47–58.

Huang, C. and Tsai, C. (1998). An inverse heat conduction problem of estimating boundary fluxes in an irregular domain with conjugate gradient method. *Heat Mass Transf*, **34**, 47–54.

Huang, C. and Yan, J. (1996). An inverse problem in predicting temperature dependent heat capacity per unit volume without internal measurements. *Int J Numer Methods Eng*, **39**, 605–618.

Huang, C.H. and Jan-Yuan, Y. (1995). An inverse problem in simultaneously measuring temperature-dependent thermal conductivity and heat capacity. *Int. J. Heat Mass Transf.*, **38**, 3433–3441.

Huang, C.H. and Wang, S.P. (1999). A three-dimensional inverse heat conduction problem in estimating surface heat flux by conjugate gradient method. *Int. J. Heat Mass Transf.*, **42**, 3387 – 3403.

Huang, C.H. and Wu, H.H. (2006). An inverse hyperbolic heat conduction problem in estimating surface heat flux by the conjugate gradient method. *J Phys Appl Phys*, **39**, 4087.

Huang, C.H., Yan, J.Y. and Chen, H.T. (1995). Function estimation in predicting temperature-dependent thermal conductivity without internal measurements. *J Thermophys Heat Trans*, **9**, 667–673.

Huang, C.H., Yuan, I.C. and Ay, H. (2003). A three-dimensional inverse problem in imaging the local heat transfer coefficients for plate finned-tube heat exchangers. *Int. J. Heat Mass Transf.*, **46**, 3629 – 3638.

Huang, C.H., Liu, Y.C. and Ay, H. (2015). The design of optimum perforation diameters for pin fin array for heat transfer enhancement. *Int. J. Heat Mass Transf.*, **84**, 752–765.

Imber, M. and Khan, J. (1972). Prediction of transient temperature distributions with embedded thermocouples. *AIAA J.*, **10**, 784–789.

Inc, M. and Akgül, A. (2014). Numerical solution of seventh-order bound. value probl. by a novel method. In *Abstract and Applied Analysis*, vol. 2014.

Ivanov, V.K. (1962). On linear problems which are not well-posed. *Dokl. Akad. Nauk SSSR (in Russian)*, **145**, 270–272.

Iwan, M., Akmeliawati, R., Faisal, T. and Al-Assadi, H.M.A.A. (2012). Performance comparison of differential evolution and particle swarm optimization in constrained optimization. *Procedia Eng.*, **41**, 323 – 1328.

Jaluria, Y. (1998). *Design and Optimization of Thermal Systems*. McGraw Hill.

Janno, J. and Tautenhahn, U. (2003). On lavrentiev regularization for ill-posed problems in hilbert scales. *Numer Funct Anal Optim*, **24**, 531–555.

Jarny, Y., Özışık, M. and Bardon, J. (1991). A general optimization method using adjoint equation for solving multidimensional inverse heat conduction. *Int. J. Heat Mass Transf.*, **34**, 2911 – 2919.

Ji, C.C. and Jang, H.Y. (1998). Experimental investigation in inverse heat conduction problem. *Numer. Heat Transf. , Part A: Applications*, **34**, 75–91.

Ji, C.C., Tuan, P.C. and Jang, H.Y. (1997). A recursive least-squares algorithm for on-line 1-d inverse heat conduction estimation. *Int. J. Heat Mass Transf.*, **40**, 2081–2096.

Jiang, H.J. and Dai, H.L. (2015). Analytical solutions for three-dimensional steady and transient heat conduction problems of a double-layer plate with a local heat source. *Int. J. Heat Mass Transfer*, **89**, 652–666.

Jiao, Y., Yamamoto, Y., Dang, C. and Hao, Y. (2002). An aftertreatment technique for improving

the accuracy of adomian's decomposition method. *Comput. Math. with Appl.*, **43**, 783–798.

Jiji, L.M. (2009). *Heat Conduction*. Springer Berlin Heidelberg.

Jolly, J.C. and Autrique, L. (2016). Semi-analytic conjugate gradient method applied to a simple inverse heat conduction problem. *IFAC-PapersOnLine*, **49**, 156 – 161.

Kabanikhin, S.I. (2008). Definitions and examples of inverse and ill-posed problems. *J. Inv. Ill-Posed Problems*, **16**, 317–357.

Kaipio, J.P. and Fox, C. (2011). The bayesian framework for inverse probl. in heat transfer. *Heat Transf. Eng.*, **32**, 718–753.

Kamble, L., Pangavhane, D. and Singh, T. (2014). Heat transfer studies using artificial neural network-a review. *Int. Energy J.*, **14**.

Kang, C., hong Meng, Z. and qiang He, G. (2010). Newton-type methods and their modifications for inverse heat conduction problems. *Journal of Shanghai University (English Edition)*, **14**, 196–200.

Kang, S. and Zabaras, N. (1995). Control of the freezing interface motion in two-dimensional solidification processes using the adjoint method. *Int J Numer Methods Eng*, **38**, 63–80.

Kaska, O. and Yumrutas, R. (2008). Comparision of experimental and theoretical results for the transient heat flow through multilayer walls and flat roofs. *Energy*, **33**, 1816–1823.

Katheder, N.S., Khezri, R., O'Farrell, F., Schultz, S.W., Jain, A., Rahman, M.M., Schink, K.O., Theodossiou, T.A., Johansen, T., Juhász, G. *et al.* (2017). Microenvironmental autophagy promotes tumour growth. *Nature*, **541**, 417–420.

Keller, W. (1999). Wavelet-vaguelette decomposition as a tool in local geoid determination. *Phys Chem Earth (A)*, **24**, 15–18.

Kennedy, J. and Eberhart, R.C. (1995). Particle swarm optimization. In *Proceedings of the 1995 IEEE International Conference on Neural Networks*, vol. 4, 1942–1948.

Kern, D. and Kraus, A. (1972). *Extended surface heat transfer*. McGraw-Hill.

Khachfe, R.A. and Jarny, Y. (2000). Numerical solution of 2-d nonlinear inverse heat conduction problems using finite-element techniques. *Numer. Heat Transf. : Part B: Fundamentals*, **37**, 45–67.

Kiefer, J. (1953). Sequential minimax search for a maximum. *Proc Am Math Soc*, **4**, 502–506.

Kim, S.K. and Daniel, I.M. (2004). Gradient method for inverse heat conduction problem in

nanoscale. *Int J Numer Methods Eng*, **60**, 2165–2181.

Kirsch, A. (1996). *An Introduction to the Mathematical Theory of Inverse Probl.*. Applied Mathematical Sciences, Springer, NY, USA.

Kiwan, S. and Al-Nimr, M. (2000). Using porous fins for heat transfer enhancement. *J. Heat Transfer*, **123**, 790–795.

Klann, E. (2006). *Regularization of linear ill-posed problems in two steps: combination of data smoothing and reconstruction methods*. Ph.D. thesis, Universität Bremen.

Klann, E. and Ramlau, R. (2008). Regularization by fractional filter methods and data smoothing. *Inverse Probl.*, **24**, 025018.

Klann, E., Maass, P. and Ramlau, R. (2006). Two-step regularization methods for linear inverse probl. *J Inverse Ill Posed Probl*, **14**, 583–607.

Kolaczyk, E.D. (1994). *Wavelet method for the inversion of certain homogeneous linear operators in the presence of noisy data*. Ph.D. thesis, Citeseer, Stanford University, California.

Koveryanov, V. (1967). Inverse problem of nonsteady-state thermal conductivity. *High Temp.*, **5**.

Krejsa, J., Slama, L., Horsky, J., Raudensky, M. and Patikova, B. (1996). A comparison of traditional and non-classical methods for solving inverse heat conduction problem. *Trans. Engg. Sci.*, **12**.

Krejsa, J., Woodbury, K., Ratliff, J. and Raudensky, M. (1999). Assessment of strategies and potential for neural networks in the inverse heat conduction problem. *Inverse Probl. in Engineering*, **7**, 197–213.

Kryzhanivskyy, V., Bushlya, V., Gutnichenko, O., M'Saoubi, R. and Ståhl, J.E. (2017). Computational and experimental inverse problem approach for determination of time dependency of heat flux in metal cutting. *Procedia CIRP*, **58**, 122–127.

Kumar, D., Kumar, P. and Rai, K.N. (2017). Numerical solution of non-linear dual-phase-lag bioheat transfer equation within skin tissues. *Math. Biosci.*, **293**, 56–63.

Kumar, V., Dixit, U.S. and Zhang, J. (2019). Determination of thermal conductivity, absorptivity and heat transfer coefficient during laser-based manufacturing. *Measurement*, **131**, 319 – 328.

Kumari, T., S. K. Singh, D.K. and Rai, K.N. (2020). A numerical solution of heat transfer problem of dpl model in living biological tissues amidst hyperthermia treatment. *Comput. Therm. Sci.*, **12**.

Lagier, G., Lemonnier, H. and Coutris, N. (2004). A numerical solution of the linear multidimensional unsteady inverse heat conduction problem with the boundary element method and the singular value decomposition. *Int. J. Therm. Sci.*, **43**, 145 – 155.

Lamm, P.K. (1995). Future-sequential regularization methods for iii-posed volterra equations: Applications to the inverse heat conduction problem. *J. Math. Anal. Appl.*, **195**, 469–494.

Langford, D. (1967). New analytic solutions of the one-dimensional heat equation for temperature and heat flow rate both prescribed at the same fixed boundary (with applications to the phase change problem). *Q Appl Math.*, **24**, 315–322.

Lavrentiev, M.M. (1959). Integral equations of the first kind. *Dokl. Akad. Nauk SSSR (in Russian)*, **127**, 31–33.

Lee, H.L. and Yang, Y.C. (2003). Function estimation in predicting time-dependent heat flux of an annular fin. *J. Therm. Stresses*, **26**, 799–813.

Lee, H.L., Chou, H.M. and Yang, Y.C. (2004). The function estimation in predicting heat flux of pin fins with variable heat transfer coefficients. *Energy Convers. Manag.*, **45**, 1749–1758.

Lee, H.L., Chang, W.J., Chen, W.L. and Yang, Y.C. (2012). Inverse heat transfer analysis of a functionally graded fin to estimate time-dependent base heat flux and temperature distributions. *Energy Convers. Manag.*, **57**, 1–7.

Lee, K.H. and Kim, K.W. (2015). Performance comparison of particle swarm optimization and genetic algorithm for inverse surface radiation problem. *Int. J. Heat Mass Transf.*, **88**, 330 – 337.

Lesnic, D. and Elliott, L. (1999). The decomposition approach to inverse heat conduction. *J. Math. Anal. Appl.*, **232**, 82–98.

Lesnic, D. and Mohsin, B.B. (2012). Inverse shape and surface heat transfer coefficient identification. *J. Comp. Appl. Math.*, **236**, 1876–1891.

Levenberg, K. (1944). A method for the solution of certain non-linear problems in least squares. *Quart. Appl. Math.*, **2**, 164–168.

Lewpiriyawong, N., Khoo, K.L., Sun, C. and Lee, P.S. (2019). Thermal and hydraulic analysis of aluminium oblique-tube condenser coils with plain fins manufactured by controlled atmosphere brazing. *Int. J. Refrig.*, **101**, 81–89.

Li, H., Lei, J. and Liu, Q. (2012). An inversion approach for the inverse heat conduction problems. *Int. J. Heat Mass Transf.*, **55**, 4442 – 4452.

Li, M. and Lai, A.C.K. (2013). Analytical solution to heat conduction in finite hollow composite cylinders with a general boundary condition. *Int. J. Heat Mass Transfer*, **60**, 549–556.

Li, Z.Y., Shao, L.L. and Zhang, C.L. (2015). Fin and tube condenser performance modeling with neural network and response surface methodology. *Int. J. Refrig.*, **59**, 124–134.

Lilla, A.D., Khan, M.A. and Barendse, P. (2013). Comparison of differential evolution and genetic algorithm in the design of permanent magnet generators. In *2013 IEEE International Conference on Industrial Technology (ICIT)*, 266–271.

Lin, D.T., Yang, C.y., Li, J.C. and Wang, C.C. (2011). Inverse estimation of the unknown heat flux boundary with irregular shape fins. *Int. J. Heat Mass Transf.*, **54**, 5275–5285.

Ling, X., Keanini, R.G. and Cherukuri, H.P. (2003). A non-iterative finite element method for inverse heat conduction problems. *Int J Numer Methods Eng*, **56**, 1315–1334.

Ling, X., Cherukuri, H.P. and Horstemeyer, M.F. (2006). A hybrid regularization method for inverse heat conduction problems. *Int J Numer Methods Eng*, **65**, 2246–2264.

Liu, F.B. (2008). A modified genetic algorithm for solving the inverse heat transfer problem of estimating plan heat source. *Int. J. Heat Mass Transf.*, **51**, 3745 – 3752.

Liu, F.B. (2012). Inverse estimation of wall heat flux by using particle swarm optimization algorithm with gaussian mutation. *Int. J. Therm. Sci.*, **54**, 62 – 69.

Lu, S., Heng, Y. and Mhamdi, A. (2012). A robust and fast algorithm for three-dimensional transient inverse heat conduction problems. *Int. J. Heat Mass Transf.*, **55**, 7865 – 7872.

Lu, X., Tervolab, P. and Viljanen, M. (2006). Transient analytical solution to heat conduction in multi-dimensional composite cylinder slab. *Int. J. Heat Mass Transfer*, **49**, 1107–1114.

Luchesi, V.M. and Coelho, R.T. (2012). An inverse method to estimate the moving heat source in machining process. *Appl. Therm. Eng.*, **45**, 64–78.

Maillet, D., Batsale, J.C. and Degiovanni, A. (1994). Thermal characterization of opaque composite walls: Homogeneation problems. In *International Heat Transfer Conference Digital Library*, Begel House Inc.

Malan, A.G., Ahmadi-Noubari, H., Pourshaghaghy, A., Kowsary, F. and Hakkaki-Fard, A. (2008). Wavelet application for reduction of measurement noise effects in inverse boundary heat conduction problems. *Int J Numer Method H*, **18**.

Mallat, S. (2008). *A Wavelet Tour of Signal Processing, 3rd Edition*. Academic Press, Elsevier.

Malyshev, I. (1989). An inverse source problem for heat equation. *J. Math. Anal. Appl.*, **142**,

206 – 218.

Maniatty, A.M. and Zabaras, N.J. (1994). Investigation of regularization parameters and error estimating in inverse elasticity problems. *Int J Numer Methods Eng*, **37**, 1039–1052.

Marcos, B., Boulet, M., Ousegui, A. and Moresoli, C. (2011). Comparison of global and sequential methods for an inverse heat transfer problem. *Inverse Probl Sci En.*, **19**, 793–814.

Mariam, I., N. Ghaddar, K.G. and Laouadi, A. (2020). Bioheat modeling of elderly and young for prediction of physiological and thermal responses in heat-stressful conditions. *J. Therm. Biol.*, **88**, 102533.

Marquardt, D.W. (1963). An algorithm for least squares estimation of nonlinear parameters. *J. Soc. Ind. Appl. Math*, **11**, 431–441.

Martin, T.J. and Dulikravich, G.S. (1996). Inverse determination of boundary conditions and sources in steady heat conduction with heat generation. *J Heat Transfer*, **118**.

McCormick, N.J. (1992). Inverse radiative transfer problems: A review. *Nucl Sci Eng*, **112**, 185–198.

McMasters, R.L. (2014). Using derivative regularization to solve inverse heat conduction problems. *Inverse Probl Sci En.*, **22**, 591–601.

Mehta, R.C. (1984). Numerical solution of nonlinear inverse heat conduction problem with a radiation boundary condition. *Int J Numer Methods Eng*, **20**, 1057–1066.

Melo, A.R., Loureiro, M.M.S. and Loureiro, F. (2017). Blood perfusion parameter estimation in tumors by means of a genetic algorithm. *Procedia Comput. Sci.*, **108**, 1384–1393.

Mierzwiczak, M. and Kołodziej, J. (2011). The determination temperature-dependent thermal conductivity as inverse steady heat conduction problem. *Int. J. Heat Mass Transf.*, **54**, 790 – 796.

Mirjalili, S. and Lewis, A. (2016). The whale optimization algorithm. *Adv. Eng. Softw.*, **95**, 51–67.

Mirjalili, S., Mirjalili, S.M. and Lewis, A. (2014). Grey wolf optimizer. *Adv Eng Softw*, **69**, 46–61.

Mirsepahi, A. (2017). *An intelligent approach to inverse heat transfer analysis of irradiative enclosures*. Ph.D. thesis, School of Chemical Engineering.

Mobtil, M., Bougeard, D. and Russeil, S. (2018). Experimental study of inverse identification of unsteady heat transfer coefficient in a fin and tube heat exchanger assembly. *Int. J. Heat*

Mass Transfer, **125**, 17–31.

Moftakhari, A., Aghanajafi, C. and Ghazvin, A.M.C. (2017). Inverse heat transfer analysis of radiator central heating systems inside residential buildings using sensitivity analysis. *Inverse Probl Sci En.*, **25**, 580–607.

Mohamad, R., Ghaddar, N., Ghali, K. and Hoballah, J. (2014). Elderly bioheat modeling: changes in physiology, thermoregulation, and blood flow circulation. *Int. J. Biometeorol.*, **58**, 1825–1843.

Mohammadiun, M. and Rahimi, A. (2011). Estimation of time-dependent heat flux using temperature distribution at a point in a two layer system. *Sci Iran*, **18**, 966–973.

Mohammadiun, M., Rahimi, A. and Khazaee, I. (2011). Estimation of the time-dependent heat flux using the temperature distribution at a point by conjugate gradient method. *Int. J. Therm. Sci.*, **50**, 2443–2450.

Mohanty, R. (2007). An implicit high accuracy variable mesh scheme for 1-d non-linear singular parabolic partial differential equations. *Appl. Math. Comput.*, **186**, 219–229.

Mohanty, R. and Singh, S. (2006). A new highly accurate discretization for three-dimensional singularly perturbed nonlinear elliptic partial differential equations. *Numer Meth Part D E*, **22**, 1379–1395.

Mohanty, R.K. and Sharma, S. (2020). Fourth-order accurate method based on half-step cubic spline approximations for the 1d time-dependent quasilinear parabolic partial differential equations. *TWMS J. of Apl. & Eng. Math.*, **10**, 415–427.

Mohasseb, S., Moradi, M., Sokhansefat, T., kowsari, F., Kasaeian, A. and Mahian, O. (2017). A novel approach to solve inverse heat conduction problems: Coupling scaled boundary finite element method to a hybrid optimization algorithm. *Eng Anal Bound Elem*, **84**, 206 – 212.

Mohebbi, F., Sellier, M. and Rabczuk, T. (2017). Estimation of linearly temperature-dependent thermal conductivity using an inverse analysis. *Int. J. Therm. Sci.*, **117**, 68 – 76.

Monde, M., Arima, H., Liu, W., Mitsutake, Y. and Hammad, J. (2003). Analytical method of two-dimensional inverse heat conduction problem using laplace transformation: Effect of number of measurement points. *Heat Tran Asian Res*, **32**, 618–629.

Morozov, V.A. (1984). *Methods for Solving Incorrectly Posed Problems*. Springer Verlag, New York.

Mosayebidorcheh, S., Ganji, D. and Farzinpoor, M. (2014). Approximate solution of the nonlinear heat transfer equation of a fin with the power-law temperature-dependent thermal con-

ductivity and heat transfer coefficient. *Propuls. Power Res.*, **3**, 41–47.

Mousseau, P., Delaunay, D. and Jarny, Y. (2001). Temperature profiles within a moving plate in a cooling fluid using a heat flux clamp associated to an inverse algorithm. *Exp. Heat Transf.*, **14**, 75–88.

Mueller, J.L. and Siltanen, S. (2012). *Linear and Nonlinear Inverse Probl. with Practical Applications*. Society of Industrial and Applied mathematics(SIAM).

Muniz, W.B., de C. Velho, H.F. and Ramos, F.M. (1999). A comparison of some inverse methods for estimating the initial condition of the heat equation. *J. Comput. Appl.*, **103**, 45 – 163.

Mzad, H. (2015). A simple mathematical procedure to estimate heat flux in machining using measured surface temperature with infrared laser. *Case Stud Therm Eng*, **6**, 128–135.

Nagham, I., Ghaddar, N. and Ghali, K. (2014). Predicting segmental and overall ventilation of ensembles using an integrated bioheat and clothed cylinder ventilation models. *Text. Res. J.*, **84**, 2198–2213.

Naka, S., Yura, T.G. and Fukuyama, T. (2001). Practical distribution state estimation using hybrid particle swarm optimization. In *Proceedings IEEE Power Engineering Society, Winter Meeting*, Columbus, Ohio.

Nazari, M., Farahani, S.D. and Kowsary, F. (2012). Comparison of the mollification and wavelet prefiltering of temperature data in an ill-posed inverse heat conduction problem, application: Nonthermal equilibrium porous medium. *Heat Transf. Eng.*, **33**, 704–711.

Nenarokomov, A., Alifanov, O. and Titov, D. (2012). Estimating thermal and radiative properties of insulating materials. *Inverse Probl Sci En.*, **20**, 639–649.

Nenarokomov, A., Alifanov, O., Budnik, S. and Netelev, A. (2016). Research and development of heat flux sensor for ablative thermal protection of spacecrafts. *Int. J. Heat Mass Transf.*, **97**, 990–1000.

Nenarokomov, A., Alifanov, O., Nenarokomov, K., Titov, D. and Finchenko, V. (2018). Study of defects of elastic thermal protection by inverse methods of nonlinear acoustics. In *Journal of Physics: Conference Series*, vol. 1047, 012011.

Nenarokomov, A., Chebakov, E., Krainova, I., Morzhukhina, A., Reviznikov, D. and Titov, D. (2019). Geometric inverse problem of radiative heat transfer as applied to the development of alternate spacecraft orientation systems. *J. Eng. Phys. Thermophys.*, **92**, 948–955.

Nenarokomov, A.V., Alifanov, O.M., Artioukhine, E. and Repin, I.V. (2004). A study of convective heat fluxes for materials interacting with dust-loaded flows by inverse probl. method.

Int. J. Therm. Sci., **43**, 825–831.

Nenarokomov, A.V., Dombrovsky, L.A., Krainova, I.V., Alifanov, O.M. and Budnik, S.A. (2017). Identification of radiative heat transfer parameters in multilayer thermal insulation of spacecraft. *Int J Numer Method H*, **27**, 598–614.

Neto, A.S. and Özişik, M. (1992). Two-dimensional inverse heat conduction problem of estimating the time-varying strength of a line heat source. *J. Appl. Phys*, **71**, 5357–5362.

Neto, A.S. and Soeiro, F. (2003). Solution of implicitly formulated inverse heat transfer problems with hybrid methods. In K. Bathe, ed., *Computational Fluid and Solid Mechanics 2003*, 2369 – 2372, Elsevier Science Ltd, Oxford.

Ngo, T.T., Huang, J.H. and Wang, C.C. (2015). The bfgs method for estimating the interface temperature and convection coefficient in ultrasonic welding. *Int Commun Heat Mass*, **69**, 66 – 75.

Norouzi, M., Delouei, A.A. and Seilsepour, M. (2013). A general exact solution for heat conduction in multilayer spherical composite laminates. *Compos. Struct.*, **106**, 288–295.

Nowak, A.J., Bialecki, R.A., Erhart, K., Divo, E. and Kassab, A. (2008). An evolutionary-based inverse approach for the identification of non-linear heat generation rates in living tissues using a localized meshless method. *Int J Numer Method H*.

Nowakowska, O. and Buliński, Z. (2017). Mathematical modelling of heat transport in a section of human forearm. *CAMES*, **22**, 347–363.

Okamoto, K. (2005). *Optimal numerical methods for inverse heat conduction and inverse design solidification problems*. Ph.D. thesis, Washington state University, United States.

Orlande, H.R.B. (2012). Inverse probl. in heat transfer: New trends on solution methodologies and applications. *J Heat Transfer*, **134**.

Osman, A.M., Dowding, K.J. and Beck, J.V. (1997). Numerical solution of the general two-dimensional inverse heat conduction problem (ihcp). *J Heat Transfer*, **119**.

Ozel, M. (2013a). Determination of optimum insulation thickness based on cooling transmission load for building walls in hot climate. *Energy Convers Manage*, **66**, 106–114.

Ozel, M. (2013b). Thermal, economical and environmental analysis of insulated building walls in cold climate. *Energy Convers Manage*, **76**, 674–684.

Ozel, M. (2014). Effect of insulation location on dynamic heat transfer characteristics of building external walls and optimization of insulation thickness. *Energy Build*, **72**, 288–295.

Özısık, M. (1993). *Heat Conduction*. Wiley.

Özışık, M.N. (1994). *Heat Conduction (Chapter-14)*. Wiley.

Özışık, M.N. and Orlande, H.R.B. (2000). *Inverse Heat Transfer: Fundamentals and Applications*. Taylor and Francis, New York.

Pakrouh, R., Hosseini, M., Ranjbar, A. and Bahrampoury, R. (2015). A numerical method for pcm-based pin fin heat sinks optimization. *Energy Convers. Manag.*, **103**, 542–552.

Panda, S. and Das, R. (2015). Inverse analysis of a radial porous fin using genetic algorithm. In *Eighth International Conference on Contemporary Computing (IC3)*, 167–170.

Panda, S. and Das, R. (2018). A golden section search method for the identification of skin subsurface abnormalities. *Inverse Probl Sci En.*, **26**, 183–202.

Panda, S., Bhowmik, A., Das, R., Repaka, R. and Martha, S.C. (2014). Application of homotopy analysis method and inverse solution of a rectangular wet fin. *Energy Convers. Manag.*, **80**, 305–318.

Papiol, G.C., Gracia, L.O. and Oosterlee, C.W. (2017). Two-dimensional shannon wavelet inverse fourier technique for pricing european options. *Appl. Num. Math.*, **117**, 115–138.

Park, H.M. and Chung, O.Y. (1999). Comparison of various conjugate gradient methods for inverse heat transfer problems. *Chem Eng Commun*, **176**, 201–228.

Park, S.J., Jeon, D.Y. and Kim, G.T. (2019). Impact of fin shapes and channel doping concentrations on the operation of junctionless transistors. *Microelectron. Eng.*, **207**, 50–54.

Parthasarathy, S. and Balaji, C. (2008). Estimation of parameters in multi-mode heat transfer problems using bayesian inference–effect of noise and a priori. *Int. J. Heat Mass Transf.*, **51**, 2313–2334.

Péneau, S., Humeau, J., Jarny, Y. and Sarda, A. (1995). Shape identification and boundary heat flux determination. application to a phase change apparatus. *IFAC Proceedings Volumes*, **28**, 515–520.

Pennes, H.H. (1948). Analysis of tissue and arterial blood temperatures in the resting human forearm. *J. Appl. Physiol.*, **1**, 93–122.

Polak, E. (1971). *Computational Methods in Optimization*. Academic Press, New York.

Pourgholi, R., Dana, H. and Tabasi, S.H. (2014). Solving an inverse heat conduction problem using genetic algorithm: Sequential and multi-core parallelization approach. *Appl. Math. Model.*, **38**, 1948 – 1958.

Powell, M.J.D. (1977). Restart procedures for the conjugate gradient method. *Math. Program.*, **12**, 241–254.

Prud'homme, M. and Nguyen, T. (1998). On the iterative regularization of inverse heat conduction problems by conjugate gradient method. *Int Commun Heat Mass*, **25**, 999 – 1008.

Raeisian, L., Niazmand, H., Ebrahimnia Bajestan, E. and Werle, P. (2019). Thermal management of a distribution transformer: an optimization study of the cooling system using cfd and response surface methodology. *Int. J. Elec. Power*, **104**, 443–455.

Ramadan, K. (2009). Semi analytical solutions for the dual phase lag heat conduction in multilayered media. *Int. J. Therm. Sci*, **48**, 14–25.

Rana, P.S., Jain, S.K., Bhattacharya, M. and Shukla, A. (2013). Structure stability analysis of ni n (n= 2–22) using nature inspired algorithms: a performance study. *Int. J. Adv. Intell. Paradig.*, **5**, 16–30.

Raudenský, M., Woodbury, K.A., Kral, J. and Brezina, T. (1995). Genetic algorithm in solution of inverse heat conduction problems. *Numer. Heat Transf. , Part B: Fundamentals*, **28**, 293–306.

Raynaud, M. and Beck, J. (1988). Methodology for comparison of inverse heat conduction methods. *J Heat Transfer*, **110**, 30–37.

Reddy, S.R. and Dulikravich, G.S. (2017). Inverse design of cooling arrays of micro pin-fins subject to specified coolant inlet temperature and hot spot temperature. *Heat Transf. Eng.*, **38**, 1147–1156.

Reddy, Y.P., Kumar, B.J., Srinivasulu, D. and Rao, C.S. (2015). Temperature distribution analysis of composite pin fin by experimental and finite element method. *Int J Innov Res Sci Eng Technol*, **4**.

Reeve, T. and Johansson, B.T. (2013). The method of fundamental solutions for a time-dependent two-dimensional cauchy heat conduction problem. *Eng Anal Bound Elem*, **37**, 569 – 578.

Reinhardt, H. (1991). A numerical method for the solution of two-dimensional inverse heat conduction problems. *Int J Numer Methods Eng*, **32**, 363–383.

Rudin, L.I., Osher, S. and Fatemi, E. (1992). Nonlinear total variation based noise removal algorithms. *Physica D*, **60**, 259–268.

Ruiz-Medina, M.D., Angulo, J.M. and Fernandez-Pascual, R. (2007). Wavelet-vaguelette decomposition of spatiotemporal random fields. *Stoch Environ Res Risk Assess*, **21**, 273–281.

Ruperti, N.J., Raynaud, M. and Sacadura, J.F. (1996). A method for the solution of the coupled inverse heat conduction-radiation problem. *J Heat Transfer*, **118**.

Sabatier, P.C. (1978). *Applied Inverse Probl.*. Springer Verlag, Hamburg.

Sagar, P., Teotia, P., Sahlot, A.D. and Thakur, H. (2017a). Heat transfer analysis and optimization of engine fins of varying geometry. *Mater Today*, **4**, 8558–8564.

Sagar, P., Teotia, P., Sahlot, A.D. and Thakur, H. (2017b). Heat transfer analysis and optimization of engine fins of varying surface roughness. *Mater Today*, **4**, 8565–8570.

Saker, L.F. and Orlande, H.R. (2004). Simultaneous estimation of spatially-dependent mass and heat transfer coefficients of drying bodies. *Inverse Probl Sci En.*, **12**, 549–561.

Saleh, A.A., Mohamed, A.A.A., Hemeida, A.M. and Ibrahim, A.A. (2018). Comparison of different optimization techniques for optimal allocation of multiple distribution generation. In *2018 International Conference on Innovative Trends in Computer Engineering (ITCE)*, 317–323.

Salloum, M., Ghaddar, N. and Ghali, K. (2007). A new transient bioheat model of the human body and its integration to clothing models. *Int. J. Therm. Sci.*, **46**, 371–384.

Samai, M., Jarny, Y. and Delaunay, D. (1993). An optimization method using an adjoint equation to identify solidification front location. *Numer. Heat Transf.*, **23**, 67–89.

Sankar, G., Rao, A.C., Seshadri, P. and Balasubramanian, K. (2016). Techniques for measurement of heat flux in furnace waterwalls of boilers and prediction of heat flux–a review. *Appl. Therm. Eng.*, **103**, 1470–1479.

Sarabadan, S., Rashedi, K. and Adibi, H. (2018). Boundary determination of the inverse heat conduction problem in one and two dimensions via the collocation method based on the satisfier functions. *Iranian Journal of Science and Technology, Transactions A: Science*, **42**, 827–840.

Sawaf, B., Özışık, M. and Jarny, Y. (1995). An inverse analysis to estimate linearly temperature dependent thermal conductivity components and heat capacity of an orthotropic medium. *Int. J. Heat Mass Transf.*, **38**, 3005–3010.

Scherzer, O., Grasmair, M., Grossauer, H., Haltmeier, M. and Lenzen, F. (2009). *Variational Methods in Imaging*. Springer, New York.

Scott, E.P. and Beck, J.V. (1989). Analysis of order of the sequential regularization solutions of inverse heat conduction problems. *J Heat Transfer*, **111**, 218–224.

Sevilgen, G. (2017). A numerical analysis of a convective straight fin with temperature-dependent thermal conductivity. *Therm Sci*, **21**, 939–952.

Sharma, D., Parwani, A.K. and Shrivastava, C. (2014). A review on solution of inverse heat conduction problems. *IJERT*, **3**, 1955–1958.

Shen, S.Y. (1999). A numerical study of inverse heat conduction problems. *Comput. Math. with Appl.*, **38**, 173 – 188.

Shenefelt, J., Luck, R., Taylor, R. and Berry, J. (2002). Solution to inverse heat conduction problems employing singular value decomposition and model-reduction. *Int. J. Heat Mass Transf.*, **45**, 67 – 74.

Shidfar, A. and Karamali, G. (2005). Numerical solution of inverse heat conduction problem with nonstationary measurements. *Appl. Math. Comput.*, **168**, 540 – 548.

Shiguemori, É.H., Da Silva, J.D.S. and de Campos Velho, H.F. (2004). Estimation of initial condition in heat conduction by neural network. *Inverse Probl Sci En.*, **12**, 317–328.

Shojaeefard, M., Molaeimanesh, G., Yarmohammadi, A. and Changizian, S. (2017). Multi-objective optimization of an automotive louvered fin-flat tube condenser for enhancing hvac system cooling performance. *Appl. Therm. Eng.*, **125**, 546–558.

Singh, J., Gupta, P.K. and Rai, K.N. (2011). Solution of fractional bioheat equations by finite difference method and hpm. *Math Comput Model*, **54**, 2316–2325.

Singh, K., Das, R. and Singla, R.K. (2016). Closed-form solution for a rectangular stepped fin involving all variable thermal parameters and nonlinear boundary conditions. *J Process Mech. Engg.*, 1–19.

Singh, S. (2019). *Parameters Retrieval of Heat Transfer systems using Inverse Optimization*. Master's thesis, Thapar Institute of Engineering & Technology.

Singh, S. and Melnik, R. (2020). Thermal ablation of biological tissues in disease treatment: A review of computational models and future directions. *Electromagn Biol Med.*, 1–40.

Singh, S. and Singla, R.K. (2019). Experimental and numerical analysis of a nonlinear pin fin with temperature dependent properties and disparate boundary conditions. *Int Commun Heat Mass*, **108**, 104313.

Singh, S., Singhal, M. and Singla, R.K. (2019). Inverse problem to retrieve heat flux and heat transfer coefficient for a solid pin fin. In *Proceedings of the 25th National and 3rd International ISHMT-ASTFE Heat and Mass Transfer Conference (IHMTC-2019)*, Begel House Inc.

Singh, S.K., Yadav, M.K., Sonawane, R., Khandekar, S. and Muralidhar, K. (2017). Estimation of time-dependent wall heat flux from single thermocouple data. *Int. J. Therm. Sci.*, **115**, 1–15.

Singh, V., Kumar, V. and Kumar, D. (2008). Numerical solution of diffusion model of brown stock washing beds of finite length using matlab. In *Second UKSIM European Symposium on Computer Modeling and Simulation*, 295–300.

Singhal, M., Singh, S., Singla, R.K., Goyal, K. and Jain, D. (2019). Experimental and computational inverse thermal analysis of transient, non-linear heat flux in circular pin fin with temperature-dependent thermal properties. *Appl. Therm. Eng.*, 114721.

Singhal, M., Singla, R.K. and Goyal, K. (2020). A novel comparative approach on inverse heat transfer analysis of an experimental setup of an extended surface. *Int Commun Heat Mass*, **118**, 104822.

Singla, R.K. and Das, R. (2014). Application of decomposition method and inverse prediction of parameters in a moving fin. *Energy Convers. Manag.*, **84**, 268–281.

Singla, R.K. and Das, R. (2017). A differential evolution algorithm for maximizing heat dissipation in stepped fins. *Neural. Comput. Appl.*.

Singla, R.K. and Das, R. (2018). A differential evolution algorithm for maximizing heat dissipation in stepped fins. *Neural. Comput. Appl.*, **30**, 3081–3093.

Singla, R.K., Singh, K. and Das, R. (2016). Tower characteristics correlation and parameter retrieval in wet-cooling tower with expanded wire mesh packing. *Appl. Therm. Eng.*, **96**, 240–249.

Skeel, R.D. and Berzins, M. (1990). A method for the spatial discretization of parabolic equations in one space variable. *SIAM J Sci Stat Comp*, **11**, 1–32.

Slodička, M., Lesnic, D. and Onyango, T. (2010). Determination of a time-dependent heat transfer coefficient in a nonlinear inverse heat conduction problem. *Inverse Probl Sci En.*, **18**, 65–81.

Sriram, S.B., Sravan, S. and Gnanasekaran, N. (2016). Numerical estimation of heat flux and convective heat transfer coefficient in a one dimensional rectangular plate by levenberg-marquardt method. *Indian J. Sci. Technol*, **9**, 1–7.

Stoecker, W.F. (1989). *Design of Thermal Systems*. McGraw Hill.

Stolz, G. (1960). Numerical solutions to an inverse problem of heat conduction for simple shapes. *ASME J. Heat Transfer*, **82**, 20–26.

Storn, R. and Price, K. (1997). Differential evolution-a simple and efficient heuristic for global optimization over continuous spaces. *J. of global optimization*, **11**, 341–359.

Su, J. and Hewitt, G.F. (2004). Inverse heat conduction problem of estimating time-varying heat transfer coefficient. *Numer. Heat Transf. , Part A: Applications*, **45**, 777–789.

Sun, S., Qi, H., Sun, J., Ren, Y. and Ruan, L. (2017a). Estimation of thermophysical properties of phase change material by the hybrid sso algorithms. *Int. J. Therm. Sci.*, **120**, 121 – 135.

Sun, S.C., Qi, H., Ren, Y.T., Yu, X.Y. and Ruan, L.M. (2017b). Improved social spider optimization algorithms for solving inverse radiation and coupled radiation–conduction heat transfer problems. *Int Commun Heat Mass*, **87**, 132 – 146.

Sundén, B. (1986). Transient heat conduction in a composite slab by a time-varying incident heat flux combined with convective and radiative cooling. *Int. Comm. Heat Mass Transfer*, **13**, 515–522.

Suram, S. and Bryden, K.M. (2004). Solution of a two-dimensional inverse radiation problem using evolutionary algorithms. In *Heat Transfer Summer Conference*, vol. 46938, 819–823.

Taler, J. (1996). A semi-numerical method for solving inverse heat conduction problems. *Heat Mass Transf*, **31**.

Taler, J. (2007). Determination of local heat transfer coefficient from the solution of the inverse heat conduction problem. *Forschung im Ingenieurwesen*, **71**, 69–78.

Tapaswini, S., Chakraverty, S. and Behera, D. (2015). Numerical solution of the imprecisely defined inverse heat conduction problem. *Chin. Phys. B*, **24**, 050203.

Tarantola, A. (2005). *Inverse problem theory and methods for model parameter estimation*. Society for Industrial and Applied Mathematics (SIAM).

Tervola, P. (1989). A method to determine the thermal conductivity from measured temperature profiles. *Int. J. Heat Mass Transfer*, **32**, 1425 – 1430.

Thomas, M., Boyard, N., Lefèvre, N., Jarny, Y. and Delaunay, D. (2010). An experimental device for the simultaneous estimation of the thermal conductivity 3-d tensor and the specific heat of orthotropic composite materials. *Int. J. Heat Mass Transf.*, **53**, 5487–5498.

Thoti, N. and Lakshmi, B. (2017). Rf performance enhancement in multi-fin tfets by scaling inter fin separation. *Mater. Sci. Semicond. Process.*, **71**, 304–309.

Throne, R. and Olson, L. (2001). The steady inverse heat conduction problem: a comparison of methods with parameter selection. *J Heat Transfer*, **123**, 633–644.

Tian, N., Sun, J., Xu, W. and Lai, C.H. (2011). Estimation of unknown heat source function in inverse heat conduction problems using quantum-behaved particle swarm optimization. *Int. J. Heat Mass Transf.*, **54**, 4110 – 4116.

Tikhonov, A. and Arsenin, V. (1977a). *Solutions of ill-posed problems*. Winston.

Tikhonov, A.N. (1943). On the stability of inverse probl. *Dokl. Akad. Nauk SSSR (in Russian)*, **39**, 176–179.

Tikhonov, A.N. and Arsenin, V.Y. (1977b). *Solution of Ill-Posed Problems*. Winston & Sons, Washington, DC.

Torabi, M. and Zhang, K. (2014a). Classical entropy generation analysis in cooled homogenous and functionally graded material slabs with variation of internal heat generation with temperature, and convective-radiative boundary conditions. *Energy*, **65**, 387–397.

Torabi, M. and Zhang, K. (2014b). Entropy generation analysis in convective-radiative cooling composite walls with temperature-dependent thermal conductivity and internal heat generation. In *Energy Procedia*, 463–467, The 6th International Conference on Applied Energy ICAE2014.

Torabi, M. and Zhang, K. (2014c). Temperature distribution and classical entropy generation analyses in an asymmetric cooling composite hollow cylinder with temperature-dependent thermal conductivity and internal heat generation. *Energy*, **73**, 484–496.

Torabi, M. and Zhang, K. (2015). Heat transfer and thermodynamic performance of convective-radiative cooling double layer walls with temperature dependent thermal conductivity and internal heat generation. *Energy Convers Manage*, **89**, 12–23.

Torabi, M. and Zhang, K. (2016). Analytical solution for transient temperature and thermal stresses within convective multilayer disks with time-dependent internal heat generation, part i: Methodology. *J. Therm. stresses*, **39**, 398–413.

Trinks, W., Mawhinney, M.H., Shannon, R., Reed, R. and Garvey, J. (2003). *Industrial furnaces*, vol. 1. John Wiley & Sons.

Udayraj, Mulani, K., Talukdar, P., Das, A. and Alagirusamy, R. (2015). Performance analysis and feasibility study of ant colony optimization, particle swarm optimization and cuckoo search algorithms for inverse heat transfer problems. *Int. J. Heat Mass Transf.*, **89**, 359 – 378.

Vakili, S. and Gadala, M. (2013). Low cost surrogate model based evolutionary optimization solvers for inverse heat conduction problem. *Int. J. Heat Mass Transf.*, **56**, 263 – 273.

Vasconcellos, C.A.B., Reis, M.M., Mansur, W., Tadeu, A., Simões, N. and Simões, I. (2012).

Experimental validation of numerical solutions using the explicit green's approach to simulate transient heat conduction in multilayer systems. *Int. J. Comp. Methodo.*, **61**, 651–668.

Vikulov, A. and Nenarokomov, A. (2019). Intensification of mathematical models of the heat exchange in space vehicles. *J. Eng. Phys. Thermophys.*, **92**, 29–42.

Vogel, C. (2002). *Computational methods for Inverse Probl.*. Society of Industrial and Applied mathematics(SIAM), Philadelphia, PA.

Wan, W., Deng, D., Huang, Q., Zeng, T. and Huang, Y. (2017). Experimental study and optimization of pin fin shapes in flow boiling of micro pin fin heat sinks. *Appl. Therm. Eng.*, **114**, 436–449.

Wang, C.C. and Yang, C.Y. (2010). Inverse method in simultaneously estimate internal heat generation and root temperature of the t-shaped fin. *Int Commun Heat Mass*, **37**, 1312–1320.

Wang, G., Zhang, L., Wang, X. and Tai, B.L. (2016). An inverse method to reconstruct the heat flux produced by bone grinding tools. *Int. J. Therm. Sci.*, **101**, 85–92.

Wang, J. and Zabaras, N. (2004). A bayesian inference approach to the inverse heat conduction problem. *Int. J. Heat Mass Transf.*, **47**, 3927–3941.

Wang, J. and Zabaras, N. (2005). Using bayesian statistics in the estimation of heat source in radiation. *Int. J. Heat Mass Transf.*, **48**, 15–29.

Wang, L. (2004). A new algorithm for solving classical blasius equation. *Appl. Math. Comput.*, **157**, 1–9.

Wang, X., Wang, Z., Zeng, T., Cheng, S. and Yang, F. (2018a). Exact analytical solution for steady-state heat transfer in functionally graded sandwich slabs with convective-radiative boundary conditions. *Compos. Struct.*, **192**, 379–386.

Wang, Y., Luo, X., Yu, Y. and Yin, Q. (2017). Evaluation of heat transfer coefficients in continuous casting under large disturbance by weighted least squares levenberg-marquardt method. *Appl. Therm. Eng.*, **111**, 989 – 996.

Wang, Y., Shin, J.H., Woodcock, C., Yu, X. and Peles, Y. (2018b). Experimental and numerical study about local heat transfer in a microchannel with a pin fin. *Int. J. Heat Mass Transf.*, **121**, 534–546.

Wazwaz, A.M. (2005). Adomian decomposition method for a reliable treatment of the emden–fowler equation. *Appl. Math. Comput.*, **161**, 543–560.

Weiland, E. and Babary, J.P. (1988). Comparative study for a new solution to the inverse heat

conduction problem. *Commun. Appl. Anal.*, **4**, 687–689.

Weisz-Patrault, D., Ehrlacher, A. and Legrand, N. (2014). Temperature and heat flux fast estimation during rolling process. *Int. J. Therm. Sci.*, **75**, 1–20.

Wen, P., Hon, Y. and Xu, Y. (2011). Inverse heat conduction problems by using particular solutions. *Heat Tran Asian Res*, **40**, 171–186.

Wen, S., Qi, H., Yu, X.Y., Ren, Y.T., Wei, L.Y. and Ruan, L.M. (2019). Real-time estimation of time-dependent imposed heat flux in graded index media by kf-rlse algorithm. *Appl. Therm. Eng.*, **150**, 1–10.

Weres, J., Olek, W. and Kujawa, S. (2009). Comparison of optimization algorithms for inverse fea of heat and mass transport in biomaterials. *J Theor App Mech-Pol*, **47**, 701–716.

Wolpert, D.H. and Macready, W.G. (1997). No free lunch theorems for optimization. *IEEE Trans. Evol. Comput.*, **1**, 67–82.

Woodbury, K.A. (2002). *Inverse engineering handbook*. Crc press.

Wróblewska, A., Frąckowiak, A. and Ciałkowski, M. (2016). Regularization of the inverse heat conduction problem by the discrete fourier transform. *Inverse Probl Sci En.*, **24**, 195–212.

Wu, Z.C. (2009). Variational-based finite element method for inverse shape design of heat conduction. *Communications in Numerical Methods in Engineering*, **25**, 1107–1119.

Xu, J. and Chen, T. (1998). A nonlinear solution of inverse heat conduction problem for obtaining the inner heat transfer coefficient. *Heat Transf. Eng.*, **19**, 45–53.

Yan, L., Haji-Sheikh, A. and Beck, J. (1993). Thermal characteristics of two-layered bodies with embedded thin-film heat source. *J Electron Packag.*, **115**, 276–283.

Yan, L., Fu, C.L. and Yang, F.L. (2008). The method of fundamental solutions for the inverse heat source problem. *Eng Anal Bound Elem*, **32**, 216 – 222.

Yang, C.Y. (1998). Solving the two-dimensional inverse heat source problem through the linear least squares error method. *Int. J. Heat Mass Transf.*, **41**, 393 – 398.

Yang, F. and Fu, C.L. (2010). The method of simplified tikhonov regularization for dealing with the inverse time-dependent heat source problem. *Comput. Math. with Appl.*, **60**, 1228 – 1236.

Yang, F. and Fu, C.L. (2014). A mollification regularization method for the inverse spatial-dependent heat source problem. *J. Comput. Appl.*, **255**, 555–567.

Yang, S. and Xiong, X. (2018). A tikhonov regularization method for solving an inverse heat

source problem. *Bull. Malaysian Math. Sci. Soc.*.

Yang, X.S. and Deb, S. (2009). Cuckoo search via lévy flights. In *2009 World congress on nature & biologically inspired computing (NaBIC)*, 210–214.

Yang, Y.C. and Chen, W.L. (2011). A nonlinear inverse problem in estimating the heat flux of the disc in a disc brake system. *Appl. Therm. Eng.*, **31**, 2439–2448.

Yang, Y.C., Chen, W.L., Chou, H.M. and Salazar, J.L.L. (2013). Inverse hyperbolic thermoelastic analysis of a functionally graded hollow circular cylinder in estimating surface heat flux and thermal stresses. *Int. J. Heat Mass Transf.*, **60**, 125–133.

Yen, R., Nguyen, V., Fedorczak, N., Brochard, F., Bonhomme, G., Schneider, K., Farge, M. and Monier-Garbet, P. (2012). Tomographic reconstruction of tokamak plasma light emission from single image using wavelet-vaguelette decomposition. *Nucl. Fusion*, **52**.

Yildiz, A.R. (2013). Comparison of evolutionary-based optimization algorithms for structural design optimization. *Eng. Appl. Artif. Intell.*, **26**, 327–333.

Yoshida, M., Ishihara, S., Murakami, Y., Nakashima, K. and Yamamoto, M. (2006). Air-cooling effects of fins on a motorcycle engine. *JSME Int. J. Ser. B Fluids Therm. Eng.*, **49**, 869–875.

Yu, B., Yao, W., Gao, Q., Zhou, H. and Xu, C. (2017). A novel non-iterative inverse method for estimating boundary condition of the furnace inner wall. *Int Commun Heat Mass*, **87**, 91 – 97.

Zabaras, N. and Mukherjee, S. (1987). An analysis of solidification problems by the boundary element method. *Int J Numer Methods Eng*, **24**, 1879–1900.

Zabaras, N., Mukherjee, S. and Richmond, O. (1988). An analysis of inverse heat transfer problems with phase changes using an integral method. *J Heat Transfer*, **110**, 554–561.

Zhang, B., Qi, H., Ren, Y.T., Sun, S.C. and Ruan, L.M. (2013). Application of homogenous continuous ant colony optimization algorithm to inverse problem of one-dimensional coupled radiation and conduction heat transfer. *Int. J. Heat Mass Transf.*, **66**, 507 – 516.

Zhang, J. and Delichatsios, M. (2009). Determination of the convective heat transfer coefficient in three-dimensional inverse heat conduction problems. *Fire Saf J*, **44**, 681 – 690.

Zhang, K.L., Chou, S.K. and Ang, S.S. (2007). Fabrication, modeling and testing of a thin film au/ti microheater. *Int. J. Therm. Sci*, **46**, 580–588.

Zhang, Q., Lippmann, S., Grasemann, A., Zhu, M. and Rettenmayr, M. (2016). Determination of temperature dependent thermophysical properties using an inverse method and an infrared

line camera. *Int. J. Heat Mass Transf.*, **96**, 242 – 248.

Zhang, Q., Xu, L., Li, J. and Ouyang, M. (2017). Performance prediction of plate-fin radiator for low temperature preheating system of proton exchange membrane fuel cells using cfd simulation. *Int. J. Hydrog. Energy*, **42**, 24504–24516.

Zhao, W., Wang, L. and Zhang, Z. (2019). Atom search optimization and its application to solve a hydrogeologic parameter estimation problem. *Knowl-Based Syst*, **163**, 283–304.

Zhu, L. and Diao, C. (2001). Theoretical simulation of temperature distribution in the brain during mild hypothermia treatment for brain injury. *Med Biol Eng Comput.*, **39**, 681–687.

List of Publications

International Journal Papers

1. **Singhal M.**, Singla, R. K.and Goyal K. (2019). "Convective and radiative thermal analysis of composite wall with non-linear, temperature-dependent properties", *Heat Transfer Research*, 51 (3), 275-296,
doi: 10.1615/HeatTransRes.2019031349 **(Impact Factor: 1.155)**.

2. **Singhal, M.**, Singh, S., Singla, R. K., Goyal, K., & Jain, D. (2019). "Experimental and computational inverse thermal analysis of transient, non-linear heat flux in circular pin fin with temperature-dependent thermal properties", *Applied Thermal Engineering*, 168, 114721, doi: 10.1016/j.applthermaleng.2019.114721 **(Impact Factor: 4.725)**.

3. **Singhal M.**, Singla, R. K.and Goyal K. (2020). "A novel comparative approach on inverse heat transfer analysis of an experimental setup of an extended surface", *International Communications in Heat and Mass Transfer*, 118, 104822,
doi: 10.1016/j.icheatmasstransfer.2020.104822 **(Impact Factor: 3.971)**.

4. **Singhal M.**, Singla, R. K.and Goyal K. "A review of regularization strategies and solution techniques for ill-posed inverse problems, with application to inverse heat transfer problems", *Journal of Inverse and Ill-posed problems* (Revised Manuscript communicated).

5. **Singhal M.**, Singla, R. K.and Goyal K. "Swarm based regularized inversion algorithms PDEPE-WOA and PDEPE-GWOCS to detect multiple tumors in a human brain tissue", *International Communications in Heat and Mass Transfer* (Communicated).

International Conferences Papers

1. Singh S., **Singhal M.**, Singla R. K. (2019). "Inverse problem to retrieve heat flux and heat transfer coefficient for a solid pin fin", The 25th National and 3rd International ISHMT-

ASTFE Heat and Mass Transfer Conference (IHMTC-2019), December 28-31, 2019, IIT Roorkee, Roorkee, India, doi: 10.1615/IHMTC-2019.480.

2. Goyal, K & **Singhal, M**. (2018). "Adomian Decomposition Method for Thermal Analysis of a Furnace," Proceedings of the International Conference, ICERA 2018, Dec 1, (pp. 141-148). Springer, Cham., doi: 10.1007/978-3-030-04792-4_20.

3. Singh S., **Singhal M.**, Singla R. K. "Estimation of multiple tumor parameters in a human brain tissue using inverse optimization", in 2nd International Conference on Mathematical Modelling, Applied Analysis and Computation–2019 (ICMMAAC-19), from August 8-10, 2019. (Presented)